Dynamics and Specificity of Influenza A Virus-Receptor Interactions

Hongbo Guo

Cover art: https://www.cdc.gov/flu/images.htm

Cover art acknowledgement: Centers for Disease Control and Prevention, National Center for Immunization and Respiratory Diseases (NCIRD), United States

Layout and design: Hongbo Guo

Print: Proefschrift-aio.nl

Printing of this thesis was sponsored in part by Infection & Immunity Utrecht

ISBN: 978-90-393-6958-6

Dynamics and specificity of influenza A virus-receptor interactions

Dynamiek en specificiteit van influenza A virus-receptor interacties

(met een samenvatting in het Nederlands)

Proefschrift

ter verkrijging van de graad van doctor aan de Universiteit Utrecht op gezag van de rector magnificus, prof.dr. G.J. van der Zwaan, ingevolge het besluit van het college voor promoties in het openbaar te verdedigen op dinsdag 20 maart 2018 des middags te 2.30 uur

door

Hongbo Guo

geboren op 2 februari 1988 te Shandong, China

Promotor: Prof.dr. F.J.M. van Kuppeveld

Copromotoren: Dr. C.A.M. de Haan

Dr. E. de Vries

Hongbo Guo was financially supported by Chinese Scholarship Council (CSC).

Contents

Chapter 1

General Introduction

Influenza A viruses (IAVs) are pathogens of birds and mammals, including humans. They cause a huge economic burden and major public health problems. In humans, IAVs cause seasonal epidemics and occasional pandemics. The pandemics are caused by animal viruses that managed to cross the host species barrier and to adapt to humans. Pandemic viruses infect a large proportion of the world population and can have devastating effects (1, 2).

Influenza viruses belong to the *Orthomyxoviridae* family (3). They are enveloped viruses containing negative-sense, segmented RNA genomes (4). Influenza viruses are classified according to antigenic differences in their nucleoprotein and matrix protein into four genera: IAV, influenza B virus (IBV), influenza C virus (ICV) and influenza D virus (IDV) (5). While IAVs infect many different animal species besides humans, IBVs only circulate among humans (6). ICVs can infect both humans and pigs but infections are generally mild and are rarely reported (7). IDVs, which are closely related to ICVs, infect cattle and pigs (8). IAVs are classified further into different subtypes according to the particular combination of hemagglutinin (HA) and neuraminidase (NA) surface glycoproteins that they contain. Sixteen HA (H1-16) and nine NA (N1-9) subtypes have been identified (9), all of which are found in viruses from aquatic birds (4). In addition, two HA- and NA-like proteins have been found in bat IAVs (10, 11). Aquatic birds are considered the natural IAV reservoir (4). IAVs from aquatic birds may adapt to other host species, including domestic poultry and different mammals (Figure 1) (2, 12).

I. IAV host species

I.a. IAV in avian species

So far, IAVs have been isolated from more than 100 different species of wild birds (2). Infected birds can shed IAVs in their saliva, nasal secretions, and feces. Susceptible birds become infected when they have contact with infected birds or through contact with virus-contaminated surfaces or water. Also domesticated birds (chickens, turkeys, etc.) may become infected with IAVs (2, 13). Disease signs associated with IAV infections in avian species vary considerably with the strain of virus. Infections with most strains are asymptomatic or only cause mild disease. These viruses are considered low pathogenic (LP) IAVs (14). In contrast, some IAVs of the H5 and H7 subtype are considered highly pathogenic (HP) as they cause an extremely contagious and aggressive disease that causes rapid systemic illness and high mortality, particularly in poultry (15). Both HP AIVs and LP AIVs can spread rapidly through flocks of poultry. HP AIV infection in poultry can cause disease that affects multiple internal organs with mortality up to 90% to 100%, often within 48 hours (15). HPAI viruses are not normally present in wild bird host reservoirs (16). The first reported cases of HPAI were reported in 1878 in chickens in northern Italy, which were followed by geographically dispersed outbreaks in Europe, Asia, Africa, and

North and South America (17). Most previous HPAI virus epizootics have been geographically limited, and the HPAI virus did not circulate in wild birds. However, an H5N1 HPAI virus was detected in 1996 in a domestic goose in Guangdong China causing deaths in wild birds, poultry, and humans and has spread to over 80 countries in Asia, Europe, Africa, and North America. (18, 19) This virus has evolved into distinct virus clades and multiple subclades (20). Since 2008, HPAI subtypes H5N2, H5N5, and H5N8 bearing the genetic backbone of the goose lineage H5 clade 2.3.4 have been identified in domestic ducks and poultry in live markets in China, and those subtypes have subsequently evolved into different subclades including 2.3.4.4 (21-23). Since then, clade 2.3.4.4 HPAI viruses have undergone genetic reassortments at an unprecedented scale with other LP and HP avian viruses. In early 2014, outbreaks of novel reassortant H5N2, H5N6 and H5N8 viruses were reported in poultry and wild birds in China and Vietnam (24) and in Japan and Korea (25), respectively. Since late 2014, a rapid spread from East Asia to North America, West Asia, and Europe has occurred (26) causing extensive damage to the poultry industry.

I.b. IAV in mammals

IAVs have been isolated from numerous mammalian host species, including humans, domestic pigs, horses and dogs, as well as such diverse hosts as pinnipeds (seals), cetaceans (toothed whales), mink and anteaters, among others (Figure 1) (1). Phylogenetic evidence indicates that all mammalian IAV strains ultimately derive from the avian IAV pool (2).

I.b.1. IAV in humans

The annual epidemics caused by IAVs result in about three to five million cases of severe illness, and about 250,000 to 500,000 deaths worldwide (27). Influenza infection may result in pneumonia and acute respiratory failure, frequently complicated by bacterial coinfection (28). Pandemics, caused by zoonotic IAVs, are rare events that cause increased morbidity and mortality resulting from very rapid virus spread in the immunologically naive population.

In the last hundred years, four human IAVs have emerged that caused pandemics. The Spanish H1N1 pandemic (1918) is known as the deadliest influenza outbreak recorded in human history, killing approximately 50 million people worldwide (29). It probably sprang from North American and domestic and wild birds (30) although another report concluded that several genome segments circulated in a mammalian host as early as 1911 (31). The ‘Asian’ pandemic H2N2 virus of 1957 was responsible for approximately 2 million deaths globally (32). This virus resulted from reassortment, i.e. exchange of genome segments between human H1N1 and avian H2N2 influenza viruses (33, 34) and replaced the H1N1 virus. In 1968, the circulating H2N2 virus was replaced by the ‘Hong Kong’ H3N2 virus,

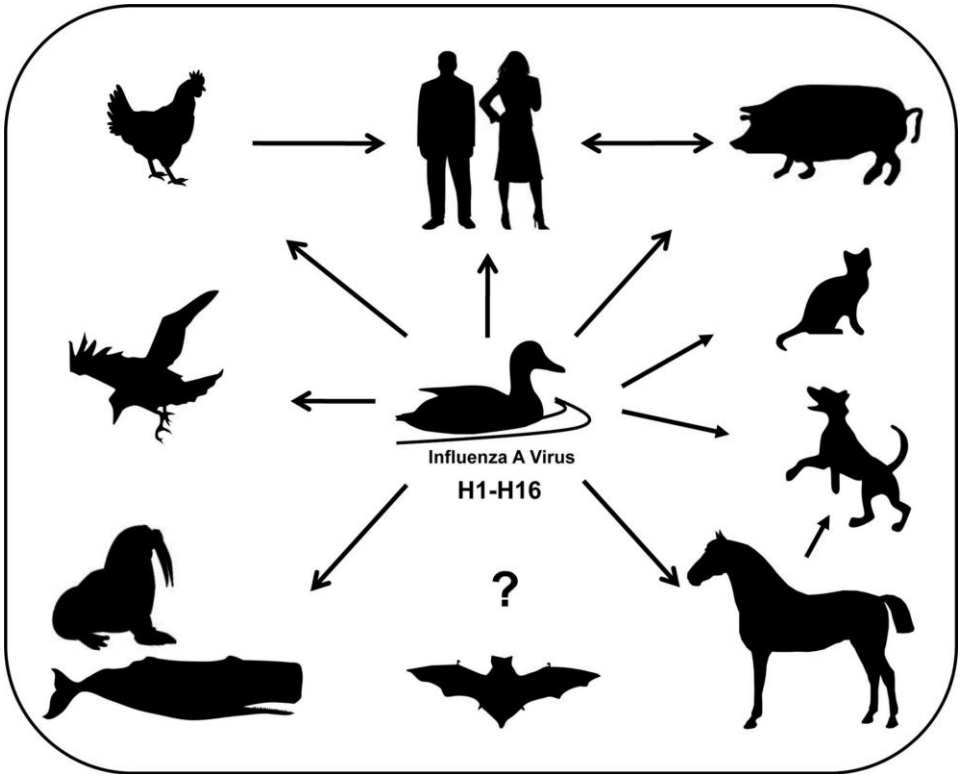

Figure 1. IAV host species. Host range of influenza A viruses. Wild water birds represent the natural reservoir of influenza A viruses, from which they can be transmitted to a wide variety of other hosts, including horses, cats, dogs, whales, seals, wild flying birds, chicken, pigs, and humans. Only recently, IAV has also been detected in bats. The figure was taken from (167).

which has continued to circulate in humans to date. The 1968 pandemic was mild compared to the earlier pandemics with approximately one million people succumbing to the infection (32). Also the pandemic H3N2 virus was the result of reassortment between avian and human influenza viruses, in which the H2 gene of H2N2 was replaced by an H3 gene from an avian virus (33, 34). In 1977, the H1N1 virus reappeared in the human population, probably resulting from the release of a laboratory strain (35). In spring 2009, a new pandemic H1N1 virus (H1N1pdm09) emerged in Mexico, after which it spread around the world in only a few months. The H1N1pdm09 virus emerged after a complicated series of reassortment events between different swine viruses (36).

I.b.2. IAV in swine

Swine IAV was for the first time clinically detected in 1918 in association with the 1918 IAV pandemic (37). Since then, swine IAVs of several different subtypes have been recognized, causing disease of major economic and public health importance (1). Swine

IAVs currently circulating appear descendants of avian as well as human viruses. Since swine have been shown to be susceptible to infection with both avian and human IAV strains, this host species has been proposed to be a prime `mixing vessel' or intermediate host for the generation of IAV of pandemic potential to humans (4). However, only for the H1N1pdm09 virus, it is clear that reassortment between different IAVs in swine preceded the emergence of this virus in the human population (38).

I.b.3. IAV in horses and dogs

Horses have become natural hosts for sustained IAV transmission on at least three occasions, with an outbreak of an unknown equine IAV subtype occurring in 1872 (39), an H7N7 IAV that emerged around 1956 (40), and an H3N8 IAV that was recognized around 1963 (41). The equine H3N8 IAV appears to have emerged from an avian IAV that spread to horses (42). Around 2004, the horse virus transmitted to dogs, resulting in H3N8 canine IAV (43). An avian H3N2 virus-like strain jumped to dogs in Asia around 2005 or 2006 (44-46). The epidemiology of the canine H3N2 IAV is still poorly understood, but some reports indicate moderate seroprevalence (up to 11 %) in some household dog populations, and the virus has been transferred over long distances both within and between the three Asian countries in which it has been detected (47). In 2015, canine H3N2 IAV was first detected in the USA. Both H3N2 and H3N8 canine IAVs have circulated in the dog population since their emergence, creating many opportunities for exposure to humans and other species (12).

II. IAV genome and particle

IAV particles contain 8 negative-sense RNA segments, the sizes of which range from 890 to 2341 nucleotides (Figure 2A). Each segment encodes for at least 1 viral protein. The coding sequences are flanked by highly conserved untranslated regions (UTR) (48). The viral RNA genome (vRNA) is fully covered with multiple copies of a nucleoprotein (NP) and associated at its UTRs with the polymerase complex, which consists of single copies of the basic polymerase 1 and 2 proteins (PB1 and PB2) and the acidic polymerase protein (PA). vRNAs together with NP, PB1, PB2 and PA form the viral ribonucleoprotein complex (vRNP). The vRNPs are enveloped by a lipid bilayer derived from the host cell in which the virus multiplied. The matrix (M1) protein, which interacts with the vRNPs, underlies the envelope. The non-structural protein 1 (NS1), besides many other functions, interferes with the splicing and nuclear export of cellular mRNA in the nucleus and stimulates translation in the cytoplasm. The NS2 protein binds to the nucleoporins yRip1 and Rab/hRip and to the M1 protein and plays an important role in the nuclear export of the vRNPs (49). The envelope contains three integral membrane proteins: HA, which is responsible for virus-cell attachment and fusion; NA, which has receptor-destroying activity; and matrix protein 2 (M2), which functions as an ion channel. IAV virions appear

either as spherical or filamentous particles. Spherical particles are typically found in the case of laboratory-adapted strains (50). Field strains on the other hand often occur in both shapes. IAV virion pleiomorphy and the number of HA and NA glycoproteins has been characterized by cryoelectron tomography (Figure 2B)(51). The amount of HA and NA appears to differ between virus particles depending on the particle shape and the particular strain studied. On average, there are approximately 300 HAs and 40-50 NA

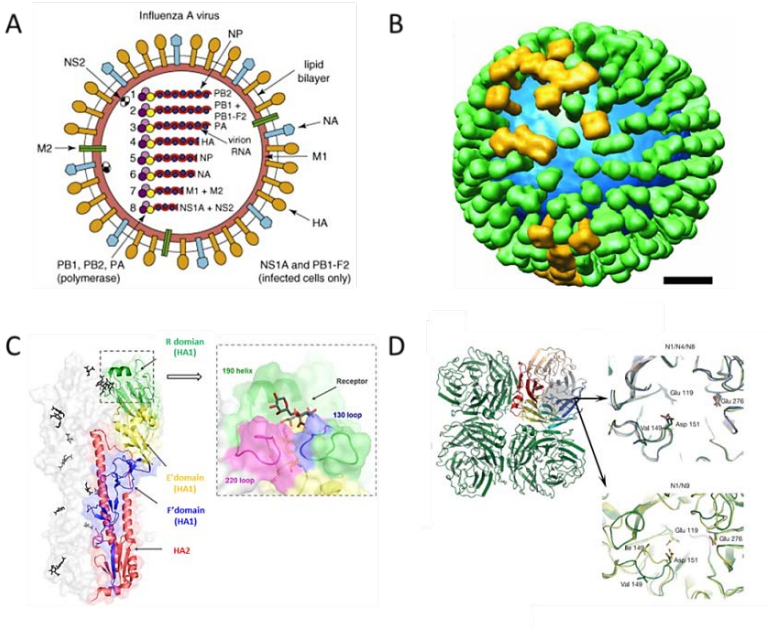

Figure 2. IAV particle and protein structure. A) Schematic representation of an IAV particle. IAV particles contain 8 segments that encode at least 11 proteins. NP molecules are bound at regular intervals along the entire length of each of the genomic RNAs to form vRNPs. Each vRNP is bound by a single polymerase complex consisting of PA, PB1 and PB2. The M1 protein underlies the viral lipid membrane and interacts with the genomic vRNPs and with the inner (cytoplasmic) tails of the envelope glycoproteins HA and NA. The envelope also contains the M2 protein, an ion channel protein that is essential for the uncoating of the virus. The smallest segment encodes two proteins, NS1A and NS2. The NS2 protein, also called NEP, mediates the export of newly synthesized viral RNPs from the nucleus to the cytoplasm. The NS1A protein, which is not incorporated into virions, is a multi-functional protein that has an integral role in suppressing host antiviral responses. The figure was taken from (168). B) A tomographic model showing the distribution of HA (green) and NA (gold) spikes on the surface of a single virion. The lipid bilayer is shown in blue (Scale bar, 20 nm). The figure was taken from (51). C) Crystal structure of an HA trimer. One protomer is shown in cartoon representation with subdomains of HA1 labeled in green (receptor binding domain, R), yellow (vestigial esterase domain, E') and blue (fusion domain, F') and the HA2 subunit in red. The other monomers are displayed in surface representation with carbohydrate moieties in black. The magnification of the R subdomain of HA1 shows the structural elements of HA1 forming the receptor binding site (130-loop in blue, 190-helix in green, 220-loop in pink) in complex with a human-type receptor analog (dark gray). Conserved residues forming hydrogen bonds with sialic acid are displayed in stick representation (yellow transparent). The figure was taken from (169). D) Crystal structure of a NA tetramer. One protomer is colored to emphasize the molecules' canonical six-bladed β-propeller structure. The active site region at the center of the six-bladed β-propeller structure is highlighted and also shown enlarged for different NA subtypes. The upper enlargement shows a superposition of the active sites of N1, N4 and N8. Lower enlargement is superposition of the active site of N1 (green) and N9 (yellow). The figure was taken from (170).

proteins per virion.

III. IAV life cycle

The IAV life cycle can be divided into several steps, as illustrated in Figure 3.

1. **Virus attachment, entry and uncoating.** The virus life cycle starts with the attachment of HA to its sialic acid (SIA) receptor (52). SIA is a generic term for the N- or O-substituted derivatives of neuraminic acid, including N-acetylneuraminic acid (Neu5Ac) and N-glycolylneuraminic acid (Neu5Gc). SIAs are terminal carbohydrate residues found on N- and O-glycosylated proteins and glycolipids. SIAs attached to the penultimate galactose (Gal) via a α2,3 or α2,6 linkages may serve as receptors for IAV. Avian IAVs prefer binding to α2,3-linked SIAs, while human viruses prefer binding to α2,6-linked SIAs. Upon HA binding to receptors, the virus particle is endocytosed into the target cell. Besides clathrin-mediated endocytosis (53, 54), also a macropinocytosis-like pathway has been identified as an IAV entry route (55, 56). This latter route seems particularly important for the uptake of filamentous IAV particles (56). After internalization, IAVs are transported to late endosomes, where the acidic environment (pH=5~6) triggers HA conformational changes that mediate fusion of viral and cellular membranes. The low pH in the endosomes is also transferred to the virion interior via the proton-selective M2 ion channel protein thereby promoting conformational changes in the M1 proteins that facilitate release of vRNPs devoid of M1 in the cytoplasm after membrane fusion (57).
2. **Genome replication and transcription.** After release into the cytoplasm, the vRNPs are transported to the nucleus, where IAV genome replication and transcription takes place. vRNA genomes are the templates for subgenomic messenger RNA (mRNA) and full-length copy RNA (cRNA) synthesis (58). Capped RNA fragments, cleaved from the 5'end of cellular RNAs, serve as primers for mRNA synthesis. When the 5' end of the vRNA is approached, the polymerase stutters on a poly-U stretch, resulting in the formation of a poly-A tail (59, 60). Some mRNAs undergo alternative splicing resulting in the generation of M2 and NS2-encoding mRNAs (61). cRNAs are an exact full length transcript of the vRNA and serve as a template for the synthesis of new vRNAs. Synthesis of vRNA and cRNA is a primer-independent process, but requires NP (62).
3. **Virus assembly and release.** During vRNA synthesis, vRNPs are formed by the association of vRNAs with multiple copies of NP and the polymerase complex. In the nucleus, vRNPs associate with M1, which in turn allows binding of the NS2 protein and nuclear export. vRNP-M1 complexes are subsequently transported to the plasma membrane on Rab11-positive vesicles (63). The envelope proteins HA, NA and M2 are co-translationally inserted into the membrane of the endoplasmic

reticulum (ER), after which they are processed by enzymes of the ER and Golgi and transported to the apical plasma membrane. vRNP-M1 complexes bud through plasma membrane domains containing HA, NA and M2 (64). The NA protein cleaves SIA from glycoproteins and glycolipids, thereby creating a desialylated cell surface which is required for release of the progeny virions (65).

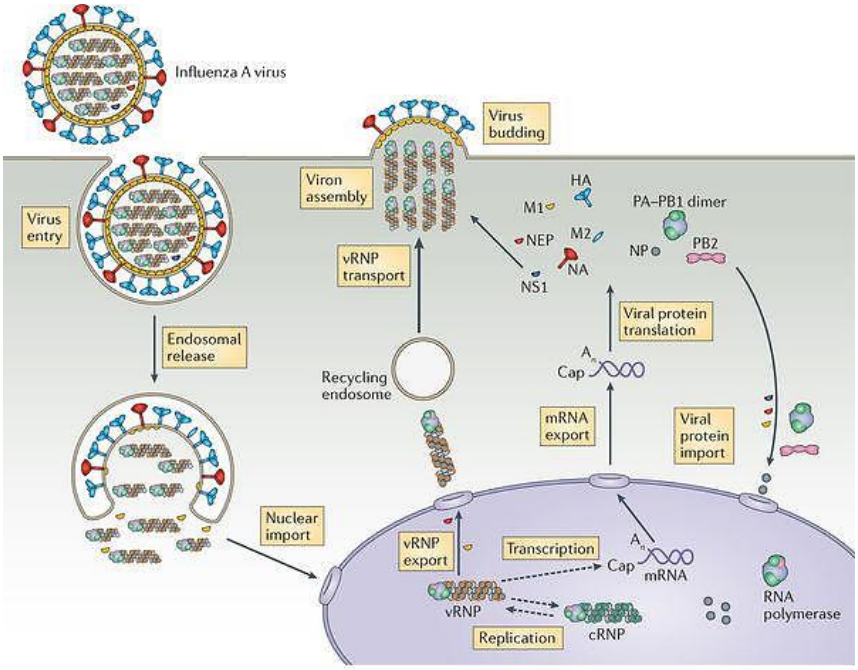

Figure 3. IAV life cycle. Viral infection is initiated when a virion binds to cell surface receptors that contain sialic acid, followed by endocytosis of the virion. After fusion of the viral and endosomal membranes, the vRNPs are released into the cytoplasm and then transported into the nucleus. In the nucleus, the viral RNA-dependent RNA polymerase replicates the single-stranded negative-sense vRNAgenome segments by copying them into complementary, positive-sense RNAs (cRNAs), which serve as templates for the production of vRNAs. The viral RNA polymerase also carries out transcription of the vRNA segments to produce mRNAs. Viral mRNA is exported to the cytoplasm for translation by cellular mechanisms. Newly synthesized viral RNA polymerase subunits (PB1, PB2 and PA) and NP are imported into the nucleus and bind to vRNA genomic segments and cRNAs to assemble vRNPs and cRNPs, respectively. Following nuclear export, progeny vRNPs are transported across the cytoplasm on recycling endosomes in a RAB11-dependent manner to the cell membrane, where the assembly of progeny virions takes place. Mature virions incorporate a substantial amount of host proteins and are released by budding. The figure was taken from (59).

IV. Hemaglutinin and Neuraminidase

The two major IAV envelope glycoproteins, HA and NA, both recognize SIAs. Host cell infection by IAV requires binding of multiple HAs to SIAs on carbohydrate side chains of cell-surface glycoproteins and/or glycolipids. Following virus replication, the receptor-destroying enzyme NA removes SIAs from the surface of infected cells, so that newly

made viruses do not remain associated with the cell surface and to each other (66). The NA is also important in early stages of the virus live cycle. NA activity helps the virus to approach the target cells by cleavage of SIAs from respiratory tract mucins that are present in the mucus layer that cover epithelial cells (67). In addition, its activity has been proposed to enhance fusion of viral and cell membranes (66). In view of the different receptor usage of avian and human IAVs, HA and NA are important determinants of host tropism and pathogenesis. In addition, both HA and NA are main targets of the host immune system, while NA is the target of the currently used antiviral drugs.

IV.a. HA protein

The HA attachment and fusion protein is a type I transmembrane glycoprotein that after synthesis and folding will interact to form homotrimers (Figure 2C). The precursor HA0 protein is cleaved into HA1 and HA2 subunits by trypsin-like proteases; HA proteins containing a multibasic cleavage site (H5 and H7 proteins of HP AIVs) are additionally recognized by furin-like proteases (68). HA1, which mostly forms the globular head of the protein, contains the receptor-binding site (RBS). HA2, which forms most of the stem, contains the fusion peptide at its N-terminus and two heptad repeat regions, which are central to the complex conformational changes leading to fusion between the virus and host cell membranes (69, 70). These conformational changes are triggered by low pH. The pH-threshold for conformational changes may differ between human and avian viruses (71-73).

In 1983 the first X-ray crystal structure of HA was solved for H3 of A/Hong Kong/68/H3N2 (70). Since then, the X-ray crystal structure of several other HA subtypes has been solved as well, some of them in complex with SIA-containing receptors (69, 74-78). These structures provided detailed insights into the RBS of HA. The RBS has at its base four conserved amino acids (Y98, W153, H183, and Y195; H3 numbering), while the edges are formed by three structural elements, an α-helix composed by residues 190-198 (the 190-helix) and two loop structures formed by residues 133-138 (the 130-loop) and 220-229 (the 220-loop) (52). A subset of amino acids mediates binding to either α2,3- or α2,6-linked SIAs. For H1, glutamic acid and glycine residues at position 190 and 225, respectively, will confer binding to α2,3 sialosides (avian-type receptors). Aspartic acids at these positions will shift binding preference to α2,6-linked SIAs (human-type receptors) (79, 80). For H2 and H3, glutamine and glycine residue at position 226 and 228, respectively, result in binding to avian-type receptors. Mutation of these residues to a leucine (position 226) and serine (position 228) will mediate a shift from avian to human specificity (77, 81). Receptor binding may also be affected by glycosylation in the head domain (82), with increased numbers of N-glycan side chains generally resulting in reduced receptor-binding avidity (82, 83).

Interactions between individual HA and SIAs are very weak, with dissociation constants in the millimolar range as detected by different methods (52, 84, 85). However, multivalent interactions between multiple HA proteins in a virus particles and a surface decorated with sialosides result in a very tight binding with an estimated dissociation constant in the picomolar range (85). These tight multivalent interactions are probably required for efficient endocytic uptake and infection.

IV.b. NA protein

NA is an exosialidase (ec 3.2.1.18) which cleaves the α-ketosidic linkage between SIA and an adjacent sugar residue (86). It is a type II transmembrane protein of approximately 470 amino acid residues (87) that forms homo-tetramers (88) (Figure 2D). The three-dimensional structure of NA consists of a very short cytoplasmic domain and a transmembrane domain, which are connected to the active site-containing "head" domain by an elongated "stem" region (86).

Only the 3D structure of the NA head domain has been solved (89). The head region consists of a single domain, which is formed by six identical antiparallel β-sheets organized in the form of a propeller-like structure. The head domain contains the active site. Residues which directly interact with SIA and account for the catalytic function of the enzyme (Arg118, Asp151, Arg152, Arg224, Glu276, Arg292, Arg371 and Tyr406, N2 numbering Figure 2D), are highly conserved in all NA genotypes of IAV. The NA head domain contains several calcium binding sites affecting temperature and low pH stability (89, 90). The NA proteins of several avian IAVs (e.g. N1, N2, and N9) have been shown to display hemadsorption activity independent of their enzyme active sites, indicating the presence of a 2nd SIA-binding site (91-94). This 2nd SIA-binding site was confirmed by X-ray crystallography for the N9 protein and by saturation transfer difference (STD) nuclear magnetic resonance (NMR) spectroscopy for N1 (95). The 2nd SIA-binding site was shown to enhance NA enzymatic activity of N2 and N9 proteins for multivalent substrates (94, 96). The significance of the 2nd SIA binding site for replication in vivo remains to be elucidated. Interestingly, the conservation of the SIA contact residues in the 2nd SIA-binding site is lost in human IAVs (86, 97).

The NA protein inhibitors (NAIs) zanamivir, oseltamivir and peramivir are the only antiviral drugs that are being used against IAVs. They are SIA analogues that bind to the active site of NA. NAIs interfere with the release of (progeny) influenza virus particles from infected cells or decoy receptors. In this way, NAIs prevent infection of new host cells and thereby halt the spread of infection in the respiratory tract (98). Decreased susceptibility to NAIs can occur as a result of mutations at the conserved residues in the active site of NA that limit the interaction of the drug with the SIA-binding pocket of NA (99).

IV.c. Antigenic shift and drift.

IAV pandemics are caused by animal IAVs that have managed to cross the host species barrier. They are immunologically novel for the human population (100, 101). These pandemic viruses may be directly introduced from an animal host species into the human population, or alternatively, may be generated by antigenic shift (102). Antigenic shift refers to reassortment, i.e. the mixing of genome segments from two (or more) animal and human IAVs, that gives rise to antigenically different viruses by replacement of HA and/or NA genome segments. Reassortment resulting in antigenic shift gave rise to the pandemic H3N2 virus that replaced the H2N2 virus in 1968 by replacement of the HA segment of H2N2 by that of an avian H3 virus (33, 34).

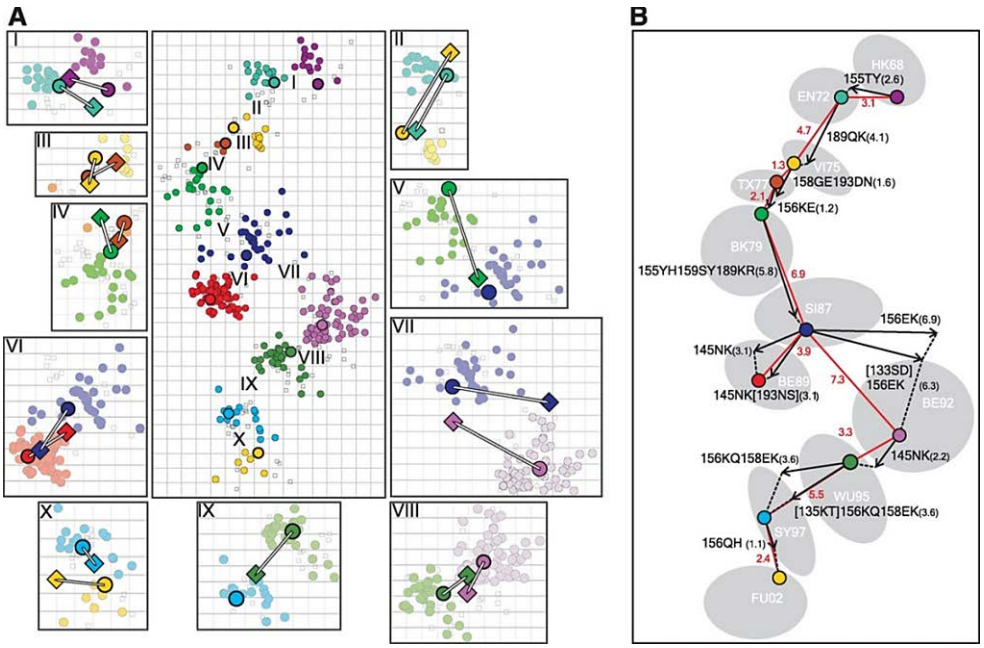

Figure 4. A. Antigenic maps of A/H3N2 virus evolution and cluster transition mutants. The central map provides an overview in which antisera and epidemic strains are indicated by open squares and colored circles, respectively, and consensus viruses by larger colored circles. Both vertical and horizontal axes represent antigenic distance. The spacing between gridlines is one antigenic unit distance, corresponding to a factor of 2 difference in the HI assay. Cluster names are as indicated in (B). Maps I through X show each cluster transition in more detail. Diamonds indicate the position of viruses with cluster-transition substitutions. B. Overview of cluster-transition substitutions. The clusters are named after the first vaccine strain in the cluster, with letters and digits referring to location and year of isolation (HK, Hong Kong; EN, England; VI, Victoria; TX, Texas; BK, Bangkok; SI, Sichuan; BE, Beijing; WU, Wuhan; SY, Sydney; FU, Fujian). Colored circles indicate the consensus viruses. The gray background shapes indicate the cloud of strains that make up an antigenic cluster. The red line represents the evolutionary path from the HK68 to the FU02 consensus virus. Antigenic distances between consensus viruses are shown in red. Arrows indicate antigenic distance and direction of the cluster-transition amino acid substitutions. Antigenic distance between the mutant and consensus virus is indicated in parentheses. Substitutions between square brackets are accessory substitutions, which changed direction toward the subsequent cluster and did not significantly add to the antigenic distance. The figure was taken from (106).

Infection with IAV results in protective immunity directed against the viral surface glycoproteins HA and NA. However, the accumulation of point mutations in HA and NA allows the virus to escape from the pre-existing host immune response (103). This phenomenon, known as antigenic drift, explains in part the occurrence of seasonal influenza epidemics. As a result of this antigenic drift, the vaccine composition has to be updated on average every 3-4 years (104, 105). After its introduction in 1968, the H3N2 virus has displayed a continuous genetic and antigenic evolution, which has been analyzed in detail for its HA protein. Antigenic evolution from 1968 to 2003 was shown to be more punctuated than genetic evolution. Viruses grouped in distinct antigenic clusters as visualized on two-dimensional antigenic cartography maps. From these maps it appeared that some genetic changes had disproportionately large antigenic effects (105) (Figure 4). Subsequently, it was shown that antigenic changes (referred to as cluster transitions) particularly resulted from one to three amino acid substitutions at only seven positions around the RBS (Figure 5) (106), despite the presence of several other antigenic sites in the HA head domain (107). Substitutions at similar positions in other HA subtypes also had relatively large effects on HA antigenicity (108, 109). In view of the low fidelity of the IAV RNA polymerase, cluster transition-determining mutations occur relatively infrequent. This suggests that additional mutations in HA are required in order to compensate for potential negative selective effects of the antigenic cluster transition mutations (106, 110). Analysis of antigenicity of HP H5N1 viruses indicated that, in addition to positions surrounding the RBS, mutations at other positions also significantly contribute to antigenic differences between H5 proteins (111). Furthermore, replication in immunized mice was shown to select for mutations that increased HA-receptor binding affinity. Using a mouse-model, antigenic change was shown to result from repeated cycles of alternating replication of viruses in immune and non-immune hosts (112). This resulted in the selection of mutations that enhance binding avidity followed by compensatory mutations at other positions in HA that restore binding avidity to the original level. Collectively these mutations resulted in antigenic drift.

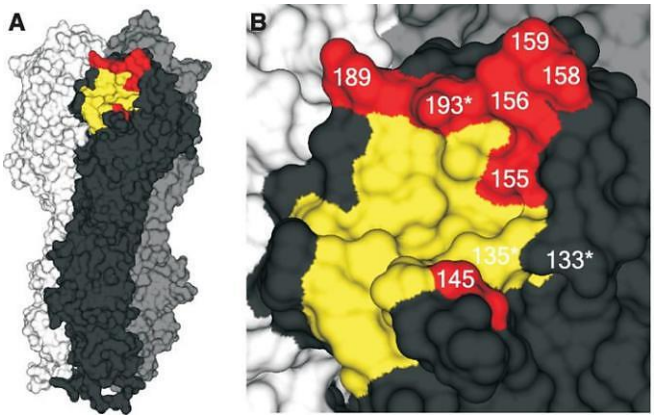

Figure 5. Positions of the cluster-transition amino acid substitutions indicated on an A/Aichi/2/1968 HA trimer. The three monomers are shown in black, white, and gray; the RBS is in yellow. (A and B) The positions responsible for A/H3N2 cluster transitions are shown in red. An asterisk indicates accessory substitutions. Position 193 is both a cluster-transition substitution and an accessory substitution. The figure was taken from (106)

V. Influenza A virus (decoy) receptors

Sialosides, omnipresent on host cells and in mucus, constitute the IAV receptors. SIAs are abundantly present on the cell surface of all types of eukaryotic cells, allowing virus infection of multiple cell types and species (113). In the host, SIAs have many different functions and are involved, among others, in cell–cell adhesion and in cell signaling (114). SIAs are generally α-linked via their C2 carbon to carbohydrate chains on glycoproteins and glycolipids (115). They are most commonly linked to a penultimate Gal via an α2,3 or α2,6 linkage.

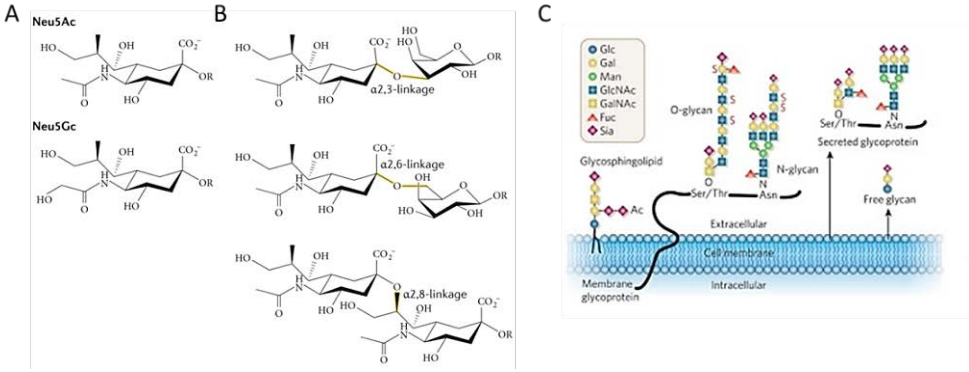

Figure 6. Structures and predominant types of SIAs. A. SIAs are nine-carbon monosaccharide derivatives of neuraminic acid. The two most common SIAs are Neu5Ac and Neu5Gc. The C5 carbon in Neu5Ac is modified with an N-acetyl group, which can be further hydroxylated to form Neu5Gc. The hydroxyl groups at C4, C7, C8 and C9 are subject to various modifications (not shown). Common constituents include O-acetyl, O-sulphate, O-lactyl, O-methyl and O-phosphate groups. B. SIAs are attached to carbohydrate chains on glycoproteins and glycolipids via different glycosidic linkages. The most common linkage types are α2,3-linkage to a galactose residue, α2,6-linkage to a galactose moiety or to an N-acetylgalactosamine moiety, and α2,8-linkage to another SIA moiety on a glycan. The figures A and B were taken from (171). SIAs are terminating units of N- and O-linked glycoproteins and glycosphingolipids that can be found on the cell surface as part of the glycocalyx, as well as on secreted glycoproteins. Ac, O-acetyl ester; Fuc, fucose; Gal, galactose; GalNAc, N-acetyl galactosamine; Glc, glucose; GlcNAc, N-acetylglucosamine; Man, mannose; Sia, sialic acid, type unspecified; S, sulfate ester. The figure was taken from (172).

Glycan chains are attached to lipids or to proteins. The variety of internal saccharides as well as their linkages, their branching patterns and their modifications result in hundreds of different SIA-containing oligosaccharides (115). Glycans attached to proteins occur as N- or O-linked glycans (Figure 6). N-linked oligosaccharides have a common pentsaccharide ‘core’ Man3GlcNAc2 which is extended by many different types of linear and branching oligosaccharide chains of variable length, thereby forming 3 different classes of N-linked oligosaccharides: high mannose-, complex- and hybrid-type oligosaccharides. The structures of O-linked oligosaccharides have been classified into 8 core structures. Generally, O-glycans are shorter and less branched than N-glycans. A selection of sialylated glycan structures that are most commonly detected on glycoproteins in epithelial tisues is shown in Figure 7. Glycolipids are sphingolipids with a

carbohydrate attached via a glycosidic bond. Gangliosides are the most complex animal glycolipids containing short negatively charged oligosaccharides with one or more SIA residues attached to Gal (116).

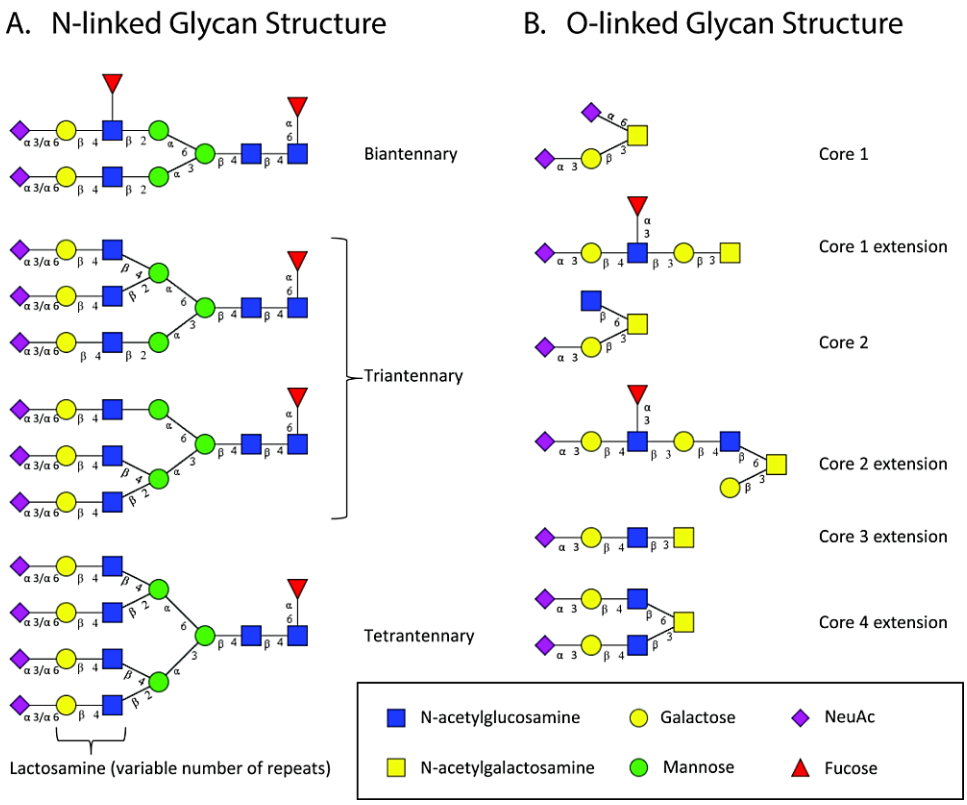

Figure 7. N and O linked glycan structure. A. Complex type of N-linked glycan. Glycans can be classified into biantennary, triantennary or tetrantennary structures. There are variable number of repeats of lactosamine. Fucose can be added to N-acetylglucosamine. B. Major core structures of O-linked glycans. Blue square: N-acetylglucosamine; yellow square: N-acetygalactosamine; yellow circle: galactose; green circle: mannose; purple diamond: NeuAc; red triangle: fucose.

Glycosyltransferases are enzymes that establish natural glycosidic linkages. Sialyltransferases specifically add SIAs to the glycans attached to glycolipids (gangliosides) or to the N- or O-linked sugar chains of glycoproteins. There are six different α2,3 sialyltransferases (ST3GALI-VI) and two α2,6 sialytransferases (ST6GALI-II). ST3GAL I and ST3GAL II almost exclusively modify a type III disaccharide (Galβ1-3GalNAc) found in glycoproteins (core 1 of O-glycoproteins) and glycolipids. ST3Gal III, ST3Gal IV and ST3Gal VI show similar enzymatic specificity and catalyze the transfer of SIA to the Gal moiety of type I (Galβ1-3GlcNAc) or type II (Galβ1-4GlcNAc) disaccharides found on glycoproteins. ST6Gal I and ST6Gal II catalyze the transfer of SIA to type II disaccharides via an α2,6 linkage leading to the synthesis of the Neu5Acα2-6Galβ1-4GlcNAc. Type-II disaccharides

are abundantly present on N-glycoproteins but, to a lesser extent, also on O-glycoproteins, glycolipids and free oligosaccharides (117).

Influenza viruses engage α2,3-linked and α2,6-linked SIAs attached to a penultimate Gal of a glycan chain. Avian IAVs preferably bind to α2,3-linked sialosides, whereas human IAVs prefer binding to α2,6-linked SIA (Figure 6)(118, 119). The subtle switch from α2,3 SIA to α2,6 SIA receptor specificity is thought to be a critical step in the adaptation of avian viruses to a human host, and appears to limit most avian influenza viruses from directly crossing the species barrier into the human population (120). Receptor binding specificity of IAV HA is not only determined by the α2,3 or α2,6 SIA linkage type, but also by the sub-terminal residues and their linkages (121-123). For instance, H2 from an avian IAV preferred binding to α2-3-sialylated type I glycans , except when these glycans were fucosylated, while an H7 preferred binding to α2,3-sialylated type II glycans. IAV strains may also differ in their binding preferences with respect to the length of the glycan chain. Human H3N2 IAVs prefer binding to elongated branches of N-linked sugar chain, which potentially bind simultaneously to two subunits of a single HA trimer (124). Besides, the N- and O-linked glycan cores may also differentially impact the ability of individual HAs to recognize sialosides (125). For instance, while the H1 (A/SC/1/18) and the H2 (A/Japan/305/57) HAs bound strongly to a linear sialoside with a di-LacNAc extension on Core 1, they bound poorly to the same sequence presented on Core 3 and Core 4 O-glycans.

It is not known whether specific sialylated protein receptors play a role in IAV entry. Chu and coworkers (126) demonstrated that IAVs need to attach to N-linked glycoproteins in order for productive entry to occur. However, further study (127) showed that sialylated N-glycans are not required for IAV entry *per se* as binding of IAVs to O-linked glycans and/or glycolipids is sufficient for entry to occur. Interestingly, in the absence of sialylated N-glycans, the macropinocytic uptake route of IAV particles, which is induced by serum factors in combination with IAV particles, was negatively affected (127). This is in agreement with other results indicating that IAV entry involves the activation of tyrosine kinase growth factor receptor signaling upon virus binding (128) and that specifically the macropinocytosis-like entry route is sensitive to inhibitors of tyrosine kinase growth factor receptors (55).

Interestingly, in the absence of sialylated N-glycans, binding of HA to cells as well as entry of IAV was reduced by the presence of serum (127). These results indicate that decoy receptors on soluble proteins may compete with cell surface receptors for binding to HA. Likewise, IAV infection may be inhibited by the presence of mucus (129). The inhibitory effect of soluble decoy receptors on virus infection was much enhanced by inhibition of the receptor-destroying activity of the NA protein (127, 129). Mucins, the major macromolecular components of respiratory mucus, are produced mainly by goblet

epithelial cells and by mucous cells of submucosal glands. (130). Mucins are encoded by different MUC genes (131) and exist as multimers linked by disulphide bonds. Characteristic features of mucins are a high molecular weight (up to several thousand kDa) and a high content of O-linked oligosaccharide chains (up to 80% sugars by weight) that are clustered in sugar-rich domains giving the mucin molecule a 'bottle-brush' appearance (132-134). The sugar chains of mucins are rich in SIAs. It is estimated that mucins secreted by a single individual may contain several hundreds of structurally different carbohydrate chains (135) with distinct length, branching and sugar composition. Given their extreme heterogeneity and ability to attach to various carbohydrate-binding microorganisms, airway mucins can be regarded as a combinatorial library of carbohydrate epitopes that have evolved to serve as decoys for pathogenic bacteria and viruses (135, 136).

VI. HA and NA balance

Intuitively, it makes sense that the HA and NA proteins need to be carefully balanced in order to traverse the mucus layer, to attach to host cells for endocytic uptake and to be released from host cells after assembly. Several studies have shown that balanced HA and NA proteins are crucial for virus replication and transmission (137-139).

It seems obvious that the substrate specificity of NA must be correlated to some extent with the receptor binding specificity of the HA. For example, H2N2 and H3N2 viruses isolated from 1957 to 1987 were all shown to preferentially bind to α2,6-linked SIA receptors. While the NAs of the earliest human H2N2 isolates exhibited strict enzymatic specificity for α2,3-linked SIAs in correlation with the receptor specificity of an ancestor avian virus, later H2N2 and H3N2 isolates had acquired increased activity on α2,6 linked SIAs although they still display higher activity on α2,3 sialosides (140). Similarly, although NA proteins from human IAVs generally prefer cleavage of α2,3 linked SIAs, they are relatively better in cleaving α2,6 linked sialosides, which are bound by their HA proteins, than the NA proteins of avian isolates (141). A correlation between HA and NA specificity has also been detected at the level of the molecular species of SIA recognized. As indicated above, human IAVs prefer binding to the Neu5Ac SIA form. However, some swine IAV recognize both Neu5Ac and Neu5Gc (142). Correspondingly, these swine isolates were able to hydrolyse sialosides carrying either SIA species, whereas the majority of human viruses lacked appreciable activity against Neu5Gc.

The cleavage activity of NA also needs to match the receptor binding affinity of HA. Mismatched IAV with HA from avian and NA from human isolates replicated poorly in embryonated chicken eggs as the human IAV NA was not able to fully desialylate progeny virions, leading to the formation of virus aggregates (143). Non-aggregating viruses were selected after serial passage of these low yield reassortants. The HA molecule of the selected variant had acquired compensatory mutations, which resulted in a decreased

affinity for SIA receptors and thereby lowered tendency for virus self-aggregation (144). Likewise, the use of NA inhibitors to block IAV infection may lead to the selection mutations in HA that reduce receptor binding avidity. The use of NA inhibitors can lead to inhibitor-resistant IAV, resulting from amino acid substitutions in the NA catalytic site (145-147). These NA substitutions generally significantly reduce the enzymatic activity of NA and subsequently result in the selection of HA variants that display reduced receptor binding avidity resulting from mutations in the RBS (148-150). Even the complete loss of NA in NA-deficient viruses can be partially compensated for by decreased HA receptor-binding affinity (151).

VII. Existing methods for studying HA, NA and HA/NA balance

A variety of different methods have been developed to study HA and NA protein specificity and activity independently, as well to a limited extent in the context of the virus particle.

VII.a. Methods for HA binding activity and specificity

Hemagglutination assays, developed in 1942 (152), measure the agglutination of red blood cells (RBC) by virus particles and allow to estimate the number of virus particles and to study virus binding properties. Hemagglutination inhibition assays are used to determine antibody titers or to analyze receptor analogues that inhibit agglutination of RBCs. These widely used assays are fast and require little instrumentation. Reproducibility depends on controlled experimental conditions, such as temperature, incubation time, and type of RBC. Hemagglutination assays have been used for determining specificity of receptor binding, as RBCs from different species are biased in their expression of either α2,3- or α2,6-linked SIAs. However, structural diversity and distribution of glycans on RBCs is poorly understood. The specificity can be improved by removal of endogenous SIAs followed by specific resialylation of the RBCs with either α2,3- or α2,6-linked SIAs (153). Unfortunately, desialylation and resialylation of glycans are highly selective processes, which may bias the outcome of such experiments. Furthermore, hemaglutination-based assays are endpoint assays that cannot be used to elucidate binding kinetics of IAVs.

Enzyme-linked immunosorbent assays (ELISA) have been developed to study IAV-receptors interactions (154, 155). Viruses can be immobilized on microtiter plates and evaluated for binding to soluble (multivalent) sialylated glycans (81, 155). Alternatively, glycans or glycoproteins are immobilized on the plates, after which viruses or HA proteins (pre-complexed by antibodies) can be used for analysis binding detection. While ELISA-based assays are well suited to studying binding specificity towards α2,3- or α2,6-linked glycan structures, the necessity to use antibody-complexed HAs in solid phase endpoint binding assays to increase binding avidity, is highly artificial and little informative about the binding of virus particles.

More recently, glycan microarray technology has been developed, which is used to profile the glycan specificity of glycan binding proteins (156). Binding of lectins is monitored by using fluorescently labelled antibodies, followed by image acquisition by confocal scanners (156). The glycan arrays of the Consortium for Functional Glycomics (CFG) display a continuously increasing number of structurally defined glycans. Similar to ELISA assay, the glycan array technology is useful for the analysis of receptor binding of both viruses and recombinant HA proteins (157). The use of viruses has similar disadvantages as mentioned above for solid phase binding assays and the binding of virus particles may be influenced by the activity of the viral NA. Furthermore, a surface that is densely coated with a unique synthetic glycan is not representative for the glycan-coated surfaces encountered in vivo.

VII.b. Methods for NA activity and specificity

The most employed substrate for NA activity determination is (4-Methylumbelliferyl)-α-D-N-acetylneuraminic acid (MU-Neu5Ac or MU-NANA). Its use was first explored by Potier et al in 1979 (158) as an alternative to colorimetric or radioactive methods. Cleavage results in the generation of a fluorophore that can be quantified using a fluorescence plate reader (159). While the MUNANA assay can be used to determine NA enzyme kinetics, this substrate hardly mimics the substrates that NA encounters in vivo and MUNANA cleavage does not reveal a preference of NA for cleaving α2,3- or α2,6-linked SIAs.

Other assays are based on the cleavage of SIAs from high molecular weight substrates, such as the serum glycoprotein fetuin or sialosides present on RBCs. Released SIAs can be determined by reacting with resorcinol (160) allowing to conduct measurements in the presence of the sialylated substrate (161). Alternatively, enzyme-linked lectin assays (ELLAs) have been developed to study NA activity (162). In ELLAs, lectins are used that specifically recognize sialylated or non-sialylated glycotopes. Decreased or increased binding of these lectins is used to quantify NA enzymatic activity, and may also be used to quantify NA cleavage specificity by using lectins specifically recognizing either α2,3- or α2,6-linked SIAs. However, these assay are performed as endpoint assays and do not easily reveal NA cleavage kinetics.

VII.c. Current methods to study HA/NA balance

IAVs need to maintain a delicate balance between HA and NA for efficient replication and transmission. Little is known about what this HA/NA balance entails at the molecular level. Most studies on HA and NA balance focused on virus infection or transmission experiments, in which “mismatched” viruses were used that were obtained by reverse genetics or by the acquisition of NA inhibitor resistance mutations (144). The HA/NA balance has also been investigated by analyzing the HA and NA protein activities in separation by using recombinant proteins in combination with the assays described above

(140). It was concluded that HA and NA proteins of human viruses, but not of swine viruses have balanced activities. However, the HA/NA balance present in virus particles is probably not only determined by the activity of the HA and NA proteins *per se*, but also by their level of incorporation into virus particles. In addition, NA substrate accessibility in the context of virus particles is, in contrast to soluble NA, also determined by the length of the NA stalk domain (163). The HA/NA balance has also been inferred form the ability of a virus to elute itself after virus binding to RBCs (164). However, just as for the hemagglutination assays, the results are hard to interpret due to poorly defined receptor repertoire on RBCs.

VII.d. Kinetic analysis of HA and NA activities

Surface plasmon resonance (SPR) is a label-free and real-time assay for studying receptor-ligand interactions. Synthetic glycans or glycoproteins were immobilized on a surface in a flow-cell, after which IAV binding and release was studied in a real-time (165). However, this method is relatively expensive and does not appear to be amendable for the study of large numbers of HA proteins or viruses particles. Biolayer-interferometry (BLI) provides a recently developed alternative for real-time interaction studies and has been used extensively throughout the studies described in this thesis. Like SPR, BLI is a label-free technology for measuring biomolecular interactions. It is an optical analytical technique that analyzes the interference pattern of white light reflected from two surfaces: a layer of immobilized protein on the biosensor tip and an internal reference layer. Any change in the number of molecules bound to the biosensor tip causes a shift in the interference

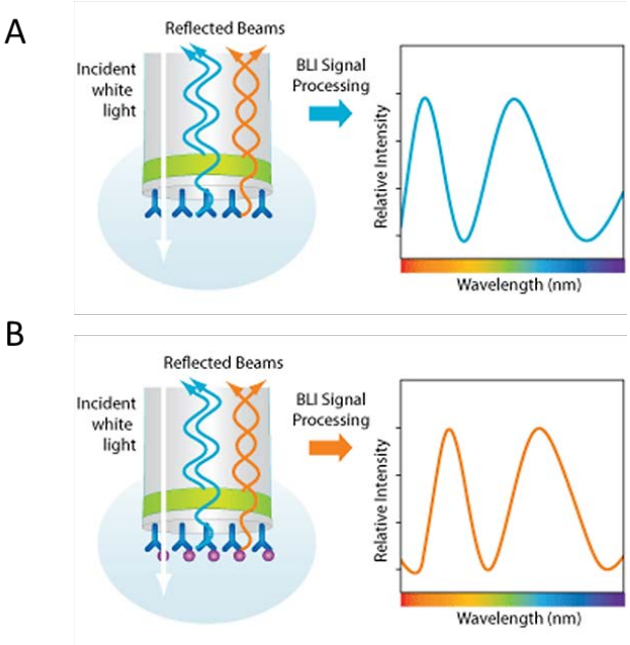

Figure 8. BLI is a label-free technology for measuring biomolecular interactions. It is an optical analytical technique that analyzes the interference pattern of white light reflected from two surfaces: a layer of immobilized protein on the biosensor tip, and an internal reference layer (Figure A). Any change in the number of molecules bound to the biosensor tip causes a shift in the interference pattern that can be measured in real-time (Figures A and B). The figure was taken from (https://www.fortebio.com/bli-technology.html).

pattern that can be measured in real-time (Figure 8). BLI provides the ability to monitor rates of association and dissociation using simple dip and read assays using crude samples without the need for complicated microfluidics used in SPR. During the research described in this thesis, Benton et al (166) also showed the potential of BLI to study HA/NA balance using a limited number of viruses in combination with synthetic glycans.

VIII. Aim and outline of this thesis

HA binding, NA cleavage and the HA/NA balance are of great importance in IAV entry, replication, release and transmission. Most existing methods for studying HA and NA activity and specificity are based on end-point assays which do not easily reveal kinetic parameters of the interactions between virus and receptor. There is a clear need for efficient and well-defined methods for studying HA and NA activities and their balance, particularly in virus particles in combination with physiologically relevant receptors. Therefore, in **Chapter 2**, kinetic and label free methodology based on BLI was established, which was used for investigating the dynamic interactions between IAV and its receptors, including HA- and NA-dependent activities and the balance between the two proteins. In addition, we demonstrated rolling of virus particles on a receptor-coated surface. In **Chapter 3**, we used the BLI technology to study the dynamics of IAV-receptor interactions in more detail by using different recombinant soluble glycoproteins and analyzing the ability of antibodies and mucus decoy receptors to interfere with these interactions. Among others, we showed that virus binding to receptors may become tighter in time, which we refer to as maturation of virus binding. As a further application of BLI, in **Chapter 4**, we analyzed the correlation between antigenic drift and virus-receptor binding of H3N2 viruses from 1968 to 2002.

In 2014 novel HPAI H5 viruses emerged that contained different NA subtypes (referred to as H5Nx viruses) and that displayed unprecedented intercontinental spread. In **Chapter 5**, we determined the evolutionary history of the HA proteins of these novel HP subtypes and showed that these H5 genes form a monophyletic group that evolved from a clade 2.3.4 H5N1 variant. In **Chapter 6**, we subsequently studied to what extent the emergence of novel HP H5Nx viruses was accompanied with changes in virus receptor binding properties using among others BLI.

REFERENCES

1. Landolt GA, Olsen CW. Up to new tricks - a review of cross-species transmission of influenza A viruses. Animal health research reviews. 2007 Jun;8(1):1-21.
2. Taubenberger JK, Kash JC. Influenza virus evolution, host adaptation, and pandemic formation. Cell host & microbe. 2010 Jun 25;7(6):440-51.
3. ICTV. Virus Taxonomy; 2009.
4. Webster RG, Bean WJ, Gorman OT, Chambers TM, Kawaoka Y. Evolution and ecology of influenza A viruses. Microbiological reviews. 1992 Mar;56(1):152-79.
5. Longo DL. 187: Influenza. Harrison's principles of internal medicine. New York: McGraw-Hill; 2012.
6. Hay AJ, Gregory V, Douglas AR, Lin YP. The evolution of human influenza viruses. Philosophical transactions of the Royal Society of London Series B, Biological sciences. 2001 Dec 29;356(1416):1861-70.
7. Taubenberger JK, Morens DM. The pathology of influenza virus infections. Annual review of pathology. 2008;3:499-522.
8. Collin EA, Sheng Z, Lang Y, Ma W, Hause BM, Li F. Cocirculation of two distinct genetic and antigenic lineages of proposed influenza D virus in cattle. Journal of virology. 2015 Jan 15;89(2):1036-42.
9. Fouchier RA, Munster V, Wallensten A, Bestebroer TM, Herfst S, Smith D, et al. Characterization of a novel influenza A virus hemagglutinin subtype (H16) obtained from black-headed gulls. Journal of virology. 2005 Mar;79(5):2814-22.
10. Ma W, Garcia-Sastre A, Schwemmle M. Expected and Unexpected Features of the Newly Discovered Bat Influenza A-like Viruses. PLoS pathogens. 2015 Jun;11(6):e1004819.
11. Ciminski K, Thamamongood T, Zimmer G, Schwemmle M. Novel insights into bat influenza A viruses. The Journal of general virology. 2017 Sep 14.
12. Parrish CR, Murcia PR, Holmes EC. Influenza virus reservoirs and intermediate hosts: dogs, horses, and new possibilities for influenza virus exposure of humans. Journal of virology. 2015 Mar;89(6):2990-4.
13. Fergus R, Fry M, Karesh WB, Marra PP, Newman S, Paul E. Migratory birds and avian flu. Science. 2006 May 12;312(5775):845-6.
14. Böttcher-Friebertshäuser E. The Hemagglutinin: A Determinant of Pathogenicity. In: Compans RW, Oldstone, Michael B. A, editor. Influenza Pathogenesis and Control Switzerland: Springer International Publishing; 2014. p. 3-34.
15. Swayne DE, Suarez DL. Highly pathogenic avian influenza. Rev Sci Tech. 2000 Aug;19(2):463-82.
16. Rohm C, Horimoto T, Kawaoka Y, Suss J, Webster RG. Do hemagglutinin genes of highly pathogenic avian influenza viruses constitute unique phylogenetic lineages? Virology. 1995 Jun 01;209(2):664-70.
17. Swayne DE. The global nature of avian influenza. In: Swayne DE, editor. Avian Influenza: Wiley-Blackwell; 2008. p. 123-43.
18. Saito T, Tanikawa T, Uchida Y, Takemae N, Kanehira K, Tsunekuni R. Intracontinental and intercontinental dissemination of Asian H5 highly pathogenic avian influenza virus (clade 2.3.4.4) in the winter of 2014-2015. Reviews in medical virology. 2015 Nov;25(6):388-405.
19. Ip HS, Torchetti MK, Crespo R, Kohrs P, DeBruyn P, Mansfield KG, et al. Novel Eurasian highly pathogenic avian influenza A H5 viruses in wild birds, Washington, USA, 2014. Emerging infectious diseases. 2015 May;21(5):886-90.
20. Toward a unified nomenclature system for highly pathogenic avian influenza virus (H5N1). Emerging infectious diseases. 2008 Jul;14(7):e1.
21. Gu M, Liu W, Cao Y, Peng D, Wang X, Wan H, et al. Novel reassortant highly pathogenic avian influenza (H5N5) viruses in domestic ducks, China. Emerging infectious diseases.

2011 Jun;17(6):1060-3.
22. Wu H, Peng X, Xu L, Jin C, Cheng L, Lu X, et al. Novel reassortant influenza A(H5N8) viruses in domestic ducks, eastern China. Emerging infectious diseases. 2014 Aug;20(8):1315-8.
23. Zhao G, Gu X, Lu X, Pan J, Duan Z, Zhao K, et al. Novel reassortant highly pathogenic H5N2 avian influenza viruses in poultry in China. PloS one. 2012;7(9):e46183.
24. Wong FY, Phommachanh P, Kalpravidh W, Chanthavisouk C, Gilbert J, Bingham J, et al. Reassortant highly pathogenic influenza A(H5N6) virus in Laos. Emerging infectious diseases. 2015 Mar;21(3):511-6.
25. Lee YJ, Kang HM, Lee EK, Song BM, Jeong J, Kwon YK, et al. Novel reassortant influenza A(H5N8) viruses, South Korea, 2014. Emerging infectious diseases. 2014 Jun;20(6):1087-9.
26. Lee DH, Torchetti MK, Winker K, Ip HS, Song CS, Swayne DE. Intercontinental Spread of Asian-Origin H5N8 to North America through Beringia by Migratory Birds. Journal of virology. 2015 Jun;89(12):6521-4.
27. Global, regional, and national incidence, prevalence, and years lived with disability for 301 acute and chronic diseases and injuries in 188 countries, 1990-2013: a systematic analysis for the Global Burden of Disease Study 2013. Lancet. 2015 Aug 22;386(9995):743-800.
28. Peteranderl C, Herold S, Schmoldt C. Human Influenza Virus Infections. Seminars in respiratory and critical care medicine. 2016 Aug;37(4):487-500.
29. Taubenberger JK, Morens DM. 1918 Influenza: the mother of all pandemics. Emerging infectious diseases. 2006 Jan;12(1):15-22.
30. Smith GJ, Bahl J, Vijaykrishna D, Zhang J, Poon LL, Chen H, et al. Dating the emergence of pandemic influenza viruses. Proceedings of the National Academy of Sciences of the United States of America. 2009 Jul 14;106(28):11709-12.
31. Worobey M, Han GZ, Rambaut A. A synchronized global sweep of the internal genes of modern avian influenza virus. Nature. 2014 Apr 10;508(7495):254-7.
32. Kilbourne ED. Influenza pandemics of the 20th century. Emerging infectious diseases. 2006 Jan;12(1):9-14.
33. Scholtissek C, Rohde W, Von Hoyningen V, Rott R. On the origin of the human influenza virus subtypes H2N2 and H3N2. Virology. 1978 Jun 01;87(1):13-20.
34. Kawaoka Y, Krauss S, Webster RG. Avian-to-human transmission of the PB1 gene of influenza A viruses in the 1957 and 1968 pandemics. Journal of virology. 1989 Nov;63(11):4603-8.
35. Nakajima K, Desselberger U, Palese P. Recent human influenza A (H1N1) viruses are closely related genetically to strains isolated in 1950. Nature. 1978 Jul 27;274(5669):334-9.
36. Garten RJ, Davis CT, Russell CA, Shu B, Lindstrom S, Balish A, et al. Antigenic and genetic characteristics of swine-origin 2009 A(H1N1) influenza viruses circulating in humans. Science. 2009 Jul 10;325(5937):197-201.
37. Taubenberger JK, Reid AH, Janczewski TA, Fanning TG. Integrating historical, clinical and molecular genetic data in order to explain the origin and virulence of the 1918 Spanish influenza virus. Philosophical transactions of the Royal Society of London Series B, Biological sciences. 2001 Dec 29;356(1416):1829-39.
38. Ma W, Kahn RE, Richt JA. The pig as a mixing vessel for influenza viruses: Human and veterinary implications. Journal of molecular and genetic medicine : an international journal of biomedical research. 2008 Nov 27;3(1):158-66.
39. Coady JH. The 1872 epizootic. Journal of the American Veterinary Medical Association. 1977 Apr 01;170(7):668.
40. Sovinova O, Tumova B, Pouska F, Nemec J. Isolation of a virus causing respiratory disease in horses. Acta virologica. 1958 Jan-Mar;2(1):52-61.
41. Waddell GH, Teigland MB, Sigel MM. A New Influenza Virus Associated with Equine Respiratory Disease. Journal of the American Veterinary Medical Association. 1963 Sep 15;143:587-90.

42. Murcia PR, Wood JL, Holmes EC. Genome-scale evolution and phylodynamics of equine H3N8 influenza A virus. Journal of virology. 2011 Jun;85(11):5312-22.
43. Crawford PC, Dubovi EJ, Castleman WL, Stephenson I, Gibbs EP, Chen L, et al. Transmission of equine influenza virus to dogs. Science. 2005 Oct 21;310(5747):482-5.
44. Song D, Kang B, Lee C, Jung K, Ha G, Kang D, et al. Transmission of avian influenza virus (H3N2) to dogs. Emerging infectious diseases. 2008 May;14(5):741-6.
45. Bunpapong N, Nonthabenjawan N, Chaiwong S, Tangwangvivat R, Boonyapisitsopa S, Jairak W, et al. Genetic characterization of canine influenza A virus (H3N2) in Thailand. Virus genes. 2014 Feb;48(1):56-63.
46. Wang H, Jia K, Qi W, Zhang M, Sun L, Liang H, et al. Genetic characterization of avian-origin H3N2 canine influenza viruses isolated from Guangdong during 2006-2012. Virus genes. 2013 Jun;46(3):558-62.
47. Yang X, Liu C, Liu F, Liu D, Chen Y, Zhang H, et al. Identification and genetic characterization of avian-origin H3N2 canine influenza viruses isolated from the Liaoning province of China in 2012. Virus genes. 2014 Oct;49(2):342-7.
48. Steinhauer DA, Skehel JJ. Genetics of influenza viruses. Annual review of genetics. 2002;36:305-32.
49. Enami M. [Structure and function of influenza virus NS1 and NS2 proteins]. Nihon rinsho Japanese journal of clinical medicine. 1997 Oct;55(10):2605-9.
50. Calder LJ, Wasilewski S, Berriman JA, Rosenthal PB. Structural organization of a filamentous influenza A virus. Proceedings of the National Academy of Sciences of the United States of America. 2010 Jun 08;107(23):10685-90.
51. Harris A, Cardone G, Winkler DC, Heymann JB, Brecher M, White JM, et al. Influenza virus pleiomorphy characterized by cryoelectron tomography. Proceedings of the National Academy of Sciences of the United States of America. 2006 Dec 12;103(50):19123-7.
52. Skehel JJ, Wiley DC. Receptor binding and membrane fusion in virus entry: the influenza hemagglutinin. Annual review of biochemistry. 2000;69:531-69.
53. Matlin KS, Reggio H, Helenius A, Simons K. Infectious entry pathway of influenza virus in a canine kidney cell line. The Journal of cell biology. 1981 Dec;91(3 Pt 1):601-13.
54. Rust MJ, Lakadamyali M, Zhang F, Zhuang X. Assembly of endocytic machinery around individual influenza viruses during viral entry. Nature structural & molecular biology. 2004 Jun;11(6):567-73.
55. de Vries E, Tscherne DM, Wienholts MJ, Cobos-Jimenez V, Scholte F, Garcia-Sastre A, et al. Dissection of the influenza A virus endocytic routes reveals macropinocytosis as an alternative entry pathway. PLoS pathogens. 2011 Mar;7(3):e1001329.
56. Rossman JS, Leser GP, Lamb RA. Filamentous influenza virus enters cells via macropinocytosis. Journal of virology. 2012 Oct;86(20):10950-60.
57. Skehel JJ, Cross K, Steinhauer D, Wiley DC. Influenza fusion peptides. Biochemical Society transactions. 2001 Aug;29(Pt 4):623-6.
58. Neumann G, Brownlee GG, Fodor E, Kawaoka Y. Orthomyxovirus replication, transcription, and polyadenylation. Current topics in microbiology and immunology. 2004;283:121-43.
59. Te Velthuis AJ, Fodor E. Influenza virus RNA polymerase: insights into the mechanisms of viral RNA synthesis. Nat Rev Microbiol. 2016 Aug;14(8):479-93.
60. Zheng H, Lee HA, Palese P, Garcia-Sastre A. Influenza A virus RNA polymerase has the ability to stutter at the polyadenylation site of a viral RNA template during RNA replication. Journal of virology. 1999 Jun;73(6):5240-3.
61. Larsen S, Bui S, Perez V, Mohammad A, Medina-Ramirez H, Newcomb LL. Influenza polymerase encoding mRNAs utilize atypical mRNA nuclear export. Virology journal. 2014 Aug 28;11:154.
62. Resa-Infante P, Jorba N, Coloma R, Ortin J. The influenza virus RNA synthesis machine: advances in its structure and function. RNA biology. 2011 Mar-Apr;8(2):207-15.

63. Eisfeld AJ, Neumann G, Kawaoka Y. At the centre: influenza A virus ribonucleoproteins. Nat Rev Microbiol. 2015 Jan;13(1):28-41.
64. Chen BJ, Leser GP, Morita E, Lamb RA. Influenza virus hemagglutinin and neuraminidase, but not the matrix protein, are required for assembly and budding of plasmid-derived virus-like particles. Journal of virology. 2007 Jul;81(13):7111-23.
65. Rossman JS, Lamb RA. Influenza virus assembly and budding. Virology. 2011 Mar 15;411(2):229-36.
66. Wagner R, Wolff T, Herwig A, Pleschka S, Klenk HD. Interdependence of hemagglutinin glycosylation and neuraminidase as regulators of influenza virus growth: a study by reverse genetics. Journal of virology. 2000 Jul;74(14):6316-23.
67. Matrosovich MN, Matrosovich TY, Gray T, Roberts NA, Klenk HD. Neuraminidase is important for the initiation of influenza virus infection in human airway epithelium. Journal of virology. 2004 Nov;78(22):12665-7.
68. Steinhauer DA. Role of hemagglutinin cleavage for the pathogenicity of influenza virus. Virology. 1999 May 25;258(1):1-20.
69. Ha Y, Stevens DJ, Skehel JJ, Wiley DC. X-ray structures of H5 avian and H9 swine influenza virus hemagglutinins bound to avian and human receptor analogs. Proceedings of the National Academy of Sciences of the United States of America. 2001 Sep 25;98(20):11181-6.
70. Wilson IA, Skehel JJ, Wiley DC. Structure of the haemagglutinin membrane glycoprotein of influenza virus at 3 A resolution. Nature. 1981 Jan 29;289(5796):366-73.
71. DuBois RM, Zaraket H, Reddivari M, Heath RJ, White SW, Russell CJ. Acid stability of the hemagglutinin protein regulates H5N1 influenza virus pathogenicity. PLoS pathogens. 2011 Dec;7(12):e1002398.
72. Zaraket H, Bridges OA, Russell CJ. The pH of activation of the hemagglutinin protein regulates H5N1 influenza virus replication and pathogenesis in mice. Journal of virology. 2013 May;87(9):4826-34.
73. Reed ML, Bridges OA, Seiler P, Kim JK, Yen HL, Salomon R, et al. The pH of activation of the hemagglutinin protein regulates H5N1 influenza virus pathogenicity and transmissibility in ducks. Journal of virology. 2010 Feb;84(3):1527-35.
74. Eisen MB, Sabesan S, Skehel JJ, Wiley DC. Binding of the influenza A virus to cell-surface receptors: structures of five hemagglutinin-sialyloligosaccharide complexes determined by X-ray crystallography. Virology. 1997 May 26;232(1):19-31.
75. Ha Y, Stevens DJ, Skehel JJ, Wiley DC. X-ray structure of the hemagglutinin of a potential H3 avian progenitor of the 1968 Hong Kong pandemic influenza virus. Virology. 2003 May 10;309(2):209-18.
76. Russell RJ, Gamblin SJ, Haire LF, Stevens DJ, Xiao B, Ha Y, et al. H1 and H7 influenza haemagglutinin structures extend a structural classification of haemagglutinin subtypes. Virology. 2004 Aug 01;325(2):287-96.
77. Stevens J, Blixt O, Tumpey TM, Taubenberger JK, Paulson JC, Wilson IA. Structure and receptor specificity of the hemagglutinin from an H5N1 influenza virus. Science. 2006 Apr 21;312(5772):404-10.
78. Yang H, Chen LM, Carney PJ, Donis RO, Stevens J. Structures of receptor complexes of a North American H7N2 influenza hemagglutinin with a loop deletion in the receptor binding site. PLoS pathogens. 2010 Sep 02;6(9):e1001081.
79. Glaser L, Stevens J, Zamarin D, Wilson IA, Garcia-Sastre A, Tumpey TM, et al. A single amino acid substitution in 1918 influenza virus hemagglutinin changes receptor binding specificity. Journal of virology. 2005 Sep;79(17):11533-6.
80. Tumpey TM, Maines TR, Van Hoeven N, Glaser L, Solorzano A, Pappas C, et al. A two-amino acid change in the hemagglutinin of the 1918 influenza virus abolishes transmission. Science. 2007 Feb 02;315(5812):655-9.

81. Matrosovich M, Tuzikov A, Bovin N, Gambaryan A, Klimov A, Castrucci MR, et al. Early alterations of the receptor-binding properties of H1, H2, and H3 avian influenza virus hemagglutinins after their introduction into mammals. Journal of virology. 2000 Sep;74(18):8502-12.
82. Wang CC, Chen JR, Tseng YC, Hsu CH, Hung YF, Chen SW, et al. Glycans on influenza hemagglutinin affect receptor binding and immune response. Proceedings of the National Academy of Sciences of the United States of America. 2009 Oct 27;106(43):18137-42.
83. Ohuchi M, Ohuchi R, Feldmann A, Klenk HD. Regulation of receptor binding affinity of influenza virus hemagglutinin by its carbohydrate moiety. Journal of virology. 1997 Nov;71(11):8377-84.
84. Sauter NK, Hanson JE, Glick GD, Brown JH, Crowther RL, Park SJ, et al. Binding of influenza virus hemagglutinin to analogs of its cell-surface receptor, sialic acid: analysis by proton nuclear magnetic resonance spectroscopy and X-ray crystallography. Biochemistry. 1992 Oct 13;31(40):9609-21.
85. Sieben C, Kappel C, Zhu R, Wozniak A, Rankl C, Hinterdorfer P, et al. Influenza virus binds its host cell using multiple dynamic interactions. Proceedings of the National Academy of Sciences of the United States of America. 2012 Aug 21;109(34):13626-31.
86. Shtyrya YA, Mochalova LV, Bovin NV. Influenza virus neuraminidase: structure and function. Acta naturae. 2009 Jul;1(2):26-32.
87. Air GM. Influenza neuraminidase. Influenza Other Respir Viruses. 2012 Jul;6(4):245-56.
88. Kundu A, Avalos RT, Sanderson CM, Nayak DP. Transmembrane domain of influenza virus neuraminidase, a type II protein, possesses an apical sorting signal in polarized MDCK cells. Journal of virology. 1996 Sep;70(9):6508-15.
89. Varghese JN, Colman PM. Three-dimensional structure of the neuraminidase of influenza virus A/Tokyo/3/67 at 2.2 A resolution. Journal of molecular biology. 1991 Sep 20;221(2):473-86.
90. Bossart-Whitaker P, Carson M, Babu YS, Smith CD, Laver WG, Air GM. Three-dimensional structure of influenza A N9 neuraminidase and its complex with the inhibitor 2-deoxy 2,3-dehydro-N-acetyl neuraminic acid. Journal of molecular biology. 1993 Aug 20;232(4):1069-83.
91. Laver WG, Colman PM, Webster RG, Hinshaw VS, Air GM. Influenza virus neuraminidase with hemagglutinin activity. Virology. 1984 Sep;137(2):314-23.
92. Webster RG, Air GM, Metzger DW, Colman PM, Varghese JN, Baker AT, et al. Antigenic structure and variation in an influenza virus N9 neuraminidase. Journal of virology. 1987 Sep;61(9):2910-6.
93. Air GM, Laver WG. Red cells bound to influenza virus N9 neuraminidase are not released by the N9 neuraminidase activity. Virology. 1995 Aug 01;211(1):278-84.
94. Uhlendorff J, Matrosovich T, Klenk HD, Matrosovich M. Functional significance of the hemadsorption activity of influenza virus neuraminidase and its alteration in pandemic viruses. Archives of virology. 2009;154(6):945-57.
95. Lai JC, Garcia JM, Dyason JC, Bohm R, Madge PD, Rose FJ, et al. A secondary sialic acid binding site on influenza virus neuraminidase: fact or fiction? Angewandte Chemie. 2012 Feb 27;51(9):2221-4.
96. Dai M, McBride R, Dortmans JC, Peng W, Bakkers MJ, de Groot RJ, et al. Mutation of the Second Sialic Acid-Binding Site, Resulting in Reduced Neuraminidase Activity, Preceded the Emergence of H7N9 Influenza A Virus. Journal of virology. 2017 May 01;91(9).
97. Varghese JN, Colman PM, van Donkelaar A, Blick TJ, Sahasrabudhe A, McKimm-Breschkin JL. Structural evidence for a second sialic acid binding site in avian influenza virus neuraminidases. Proceedings of the National Academy of Sciences of the United States of America. 1997 Oct 28;94(22):11808-12.

98. Moscona A. Neuraminidase inhibitors for influenza. The New England journal of medicine. 2005 Sep 29;353(13):1363-73.
99. Gubareva LV, Kaiser L, Hayden FG. Influenza virus neuraminidase inhibitors. Lancet. 2000 Mar 04;355(9206):827-35.
100. Parrish CR, Holmes EC, Morens DM, Park EC, Burke DS, Calisher CH, et al. Cross-species virus transmission and the emergence of new epidemic diseases. Microbiology and molecular biology reviews : MMBR. 2008 Sep;72(3):457-70.
101. Taubenberger JK, Morens DM. Pandemic influenza--including a risk assessment of H5N1. Revue scientifique et technique. 2009 Apr;28(1):187-202.
102. Stower H. Viral evolution: Flu host evasion. Nature reviews Genetics. 2014 Jan;15(1):4.
103. Wikramaratna PS, Sandeman M, Recker M, Gupta S. The antigenic evolution of influenza: drift or thrift? Philosophical transactions of the Royal Society of London Series B, Biological sciences. 2013 Mar 19;368(1614):20120200.
104. Smith DJ, Lapedes AS, de Jong JC, Bestebroer TM, Jones TC, Rimmelzwaan GF, et al. Mutations, drift, and the influenza archipelago. Discovery medicine. 2004 Dec;4(24):371-7.
105. Smith DJ, Lapedes AS, de Jong JC, Bestebroer TM, Rimmelzwaan GF, Osterhaus AD, et al. Mapping the antigenic and genetic evolution of influenza virus. Science. 2004 Jul 16;305(5682):371-6.
106. Koel BF, Burke DF, Bestebroer TM, van der Vliet S, Zondag GC, Vervaet G, et al. Substitutions near the receptor binding site determine major antigenic change during influenza virus evolution. Science. 2013 Nov 22;342(6161):976-9.
107. Isin B, Doruker P, Bahar I. Functional motions of influenza virus hemagglutinin: a structure-based analytical approach. Biophysical journal. 2002 Feb;82(2):569-81.
108. Koel BF, Mogling R, Chutinimitkul S, Fraaij PL, Burke DF, van der Vliet S, et al. Identification of amino acid substitutions supporting antigenic change of influenza A(H1N1)pdm09 viruses. Journal of virology. 2015 Apr;89(7):3763-75.
109. Lewis NS, Anderson TK, Kitikoon P, Skepner E, Burke DF, Vincent AL. Substitutions near the hemagglutinin receptor-binding site determine the antigenic evolution of influenza A H3N2 viruses in U.S. swine. Journal of virology. 2014 May;88(9):4752-63.
110. Stubbs TM, Te Velthuis AJ. The RNA-dependent RNA polymerase of the influenza A virus. Future virology. 2014 Sep;9(9):863-76.
111. Peeters B, Reemers S, Dortmans J, de Vries E, de Jong M, van de Zande S, et al. Genetic versus antigenic differences among highly pathogenic H5N1 avian influenza A viruses: Consequences for vaccine strain selection. Virology. 2017 Mar;503:83-93.
112. Hensley SE, Das SR, Bailey AL, Schmidt LM, Hickman HD, Jayaraman A, et al. Hemagglutinin receptor binding avidity drives influenza A virus antigenic drift. Science. 2009 Oct 30;326(5953):734-6.
113. Garcia-Sastre A. Influenza virus receptor specificity: disease and transmission. The American journal of pathology. 2010 Apr;176(4):1584-5.
114. Varki NM, Varki A. Diversity in cell surface sialic acid presentations: implications for biology and disease. Laboratory investigation; a journal of technical methods and pathology. 2007 Sep;87(9):851-7.
115. S.A. Brooks MVD, U. Schumacher. Functional and Molecular Glycobiology: BIOS Scientific Publishers; 2002.
116. Kinoshita. RLSaT. Chapter 11, Glycosphingolipids. In: Varki A, editor. Essentials of Glycobiology: Cold Spring Harbor Laboratory Press; 2015.
117. Tiralongo IM-D. Sialobiology: Structure, Biosynthesis and Function Sialic Acid Glycoconjugates in Health and Disease; 2013.
118. Rogers GN, Paulson JC. Receptor determinants of human and animal influenza virus isolates: differences in receptor specificity of the H3 hemagglutinin based on species of origin. Virology. 1983 Jun;127(2):361-73.

119. Rogers GN, Pritchett TJ, Lane JL, Paulson JC. Differential sensitivity of human, avian, and equine influenza A viruses to a glycoprotein inhibitor of infection: selection of receptor specific variants. Virology. 1983 Dec;131(2):394-408.
120. Stevens J, Blixt O, Glaser L, Taubenberger JK, Palese P, Paulson JC, et al. Glycan microarray analysis of the hemagglutinins from modern and pandemic influenza viruses reveals different receptor specificities. Journal of molecular biology. 2006 Feb 3;355(5):1143-55.
121. de Graaf M, Fouchier RA. Role of receptor binding specificity in influenza A virus transmission and pathogenesis. The EMBO journal. 2014 Apr 16;33(8):823-41.
122. Air GM. Influenza virus-glycan interactions. Current opinion in virology. 2014 Aug;7:128-33.
123. de Vries RP, Zhu X, McBride R, Rigter A, Hanson A, Zhong G, et al. Hemagglutinin receptor specificity and structural analyses of respiratory droplet-transmissible H5N1 viruses. Journal of virology. 2014 Jan;88(1):768-73.
124. Peng W, de Vries RP, Grant OC, Thompson AJ, McBride R, Tsogtbaatar B, et al. Recent H3N2 Viruses Have Evolved Specificity for Extended, Branched Human-type Receptors, Conferring Potential for Increased Avidity. Cell host & microbe. 2017 Jan 11;21(1):23-34.
125. Nycholat CM, McBride R, Ekiert DC, Xu R, Rangarajan J, Peng W, et al. Recognition of sialylated poly-N-acetyllactosamine chains on N- and O-linked glycans by human and avian influenza A virus hemagglutinins. Angew Chem Int Ed Engl. 2012 May 14;51(20):4860-3.
126. Chu VC, Whittaker GR. Influenza virus entry and infection require host cell N-linked glycoprotein. Proceedings of the National Academy of Sciences of the United States of America. 2004 Dec 28;101(52):18153-8.
127. de Vries E, de Vries RP, Wienholts MJ, Floris CE, Jacobs MS, van den Heuvel A, et al. Influenza A virus entry into cells lacking sialylated N-glycans. Proceedings of the National Academy of Sciences of the United States of America. 2012 May 08;109(19):7457-62.
128. Eierhoff T, Hrincius ER, Rescher U, Ludwig S, Ehrhardt C. The epidermal growth factor receptor (EGFR) promotes uptake of influenza A viruses (IAV) into host cells. PLoS pathogens. 2010 Sep 09;6(9):e1001099.
129. Cohen M, Zhang XQ, Senaati HP, Chen HW, Varki NM, Schooley RT, et al. Influenza A penetrates host mucus by cleaving sialic acids with neuraminidase. Virology journal. 2013 Nov 22;10:321.
130. Jeffery PK, Li D. Airway mucosa: secretory cells, mucus and mucin genes. The European respiratory journal : official journal of the European Society for Clinical Respiratory Physiology. 1997 Jul;10(7):1655-62.
131. Moniaux N, Escande F, Porchet N, Aubert JP, Batra SK. Structural organization and classification of the human mucin genes. Frontiers in bioscience : a journal and virtual library. 2001 Oct 01;6:D1192-206.
132. Button B, Cai LH, Ehre C, Kesimer M, Hill DB, Sheehan JK, et al. A periciliary brush promotes the lung health by separating the mucus layer from airway epithelia. Science. 2012 Aug 24;337(6097):937-41.
133. Rose MC, Voynow JA. Respiratory tract mucin genes and mucin glycoproteins in health and disease. Physiological reviews. 2006 Jan;86(1):245-78.
134. Hattrup CL, Gendler SJ. Structure and function of the cell surface (tethered) mucins. Annual review of physiology. 2008;70:431-57.
135. Lamblin G, Roussel P. Airway mucins and their role in defence against micro-organisms. Respiratory medicine. 1993 Aug;87(6):421-6.
136. Scharfman A, Lamblin G, Roussel P. Interactions between human respiratory mucins and pathogens. Biochemical Society transactions. 1995 Nov;23(4):836-9.
137. Wagner R, Matrosovich M, Klenk HD. Functional balance between haemagglutinin and neuraminidase in influenza virus infections. Reviews in medical virology. 2002 May-Jun;12(3):159-66.

138. Xu R, Zhu X, McBride R, Nycholat CM, Yu W, Paulson JC, et al. Functional balance of the hemagglutinin and neuraminidase activities accompanies the emergence of the 2009 H1N1 influenza pandemic. Journal of virology. 2012 Sep;86(17):9221-32.
139. Schrauwen EJ, Fouchier RA. Host adaptation and transmission of influenza A viruses in mammals. Emerging microbes & infections. 2014 Feb;3(2):e9.
140. Baum LG, Paulson JC. The N2 neuraminidase of human influenza virus has acquired a substrate specificity complementary to the hemagglutinin receptor specificity. Virology. 1991 Jan;180(1):10-5.
141. Mochalova L, Kurova V, Shtyrya Y, Korchagina E, Gambaryan A, Belyanchikov I, et al. Oligosaccharide specificity of influenza H1N1 virus neuraminidases. Archives of virology. 2007;152(11):2047-57.
142. Suzuki T, Horiike G, Yamazaki Y, Kawabe K, Masuda H, Miyamoto D, et al. Swine influenza virus strains recognize sialylsugar chains containing the molecular species of sialic acid predominantly present in the swine tracheal epithelium. FEBS letters. 1997 Mar 10;404(2-3):192-6.
143. Rudneva IA, Sklyanskaya EI, Barulina OS, Yamnikova SS, Kovaleva VP, Tsvetkova IV, et al. Phenotypic expression of HA-NA combinations in human-avian influenza A virus reassortants. Archives of virology. 1996;141(6):1091-9.
144. Kaverin NV, Gambaryan AS, Bovin NV, Rudneva IA, Shilov AA, Khodova OM, et al. Postreassortment changes in influenza A virus hemagglutinin restoring HA-NA functional match. Virology. 1998 May 10;244(2):315-21.
145. Gubareva LV, Robinson MJ, Bethell RC, Webster RG. Catalytic and framework mutations in the neuraminidase active site of influenza viruses that are resistant to 4-guanidino-Neu5Ac2en. Journal of virology. 1997 May;71(5):3385-90.
146. McKimm-Breschkin JL, Sahasrabudhe A, Blick TJ, McDonald M, Colman PM, Hart GJ, et al. Mutations in a conserved residue in the influenza virus neuraminidase active site decreases sensitivity to Neu5Ac2en-derived inhibitors. Journal of virology. 1998 Mar;72(3):2456-62.
147. Tai CY, Escarpe PA, Sidwell RW, Williams MA, Lew W, Wu H, et al. Characterization of human influenza virus variants selected in vitro in the presence of the neuraminidase inhibitor GS 4071. Antimicrobial agents and chemotherapy. 1998 Dec;42(12):3234-41.
148. McKimm-Breschkin JL, Blick TJ, Sahasrabudhe A, Tiong T, Marshall D, Hart GJ, et al. Generation and characterization of variants of NWS/G70C influenza virus after in vitro passage in 4-amino-Neu5Ac2en and 4-guanidino-Neu5Ac2en. Antimicrobial agents and chemotherapy. 1996 Jan;40(1):40-6.
149. Bantia S, Ghate AA, Ananth SL, Babu YS, Air GM, Walsh GM. Generation and characterization of a mutant of influenza A virus selected with the neuraminidase inhibitor BCX-140. Antimicrobial agents and chemotherapy. 1998 Apr;42(4):801-7.
150. Blick TJ, Sahasrabudhe A, McDonald M, Owens IJ, Morley PJ, Fenton RJ, et al. The interaction of neuraminidase and hemagglutinin mutations in influenza virus in resistance to 4-guanidino-Neu5Ac2en. Virology. 1998 Jun 20;246(1):95-103.
151. Hughes MT, Matrosovich M, Rodgers ME, McGregor M, Kawaoka Y. Influenza A viruses lacking sialidase activity can undergo multiple cycles of replication in cell culture, eggs, or mice. Journal of virology. 2000 Jun;74(11):5206-12.
152. Hirst GK. The Quantitative Determination Of Influenza Virus And Antibodies by Means Of Red Cell Agglutination. The Journal of experimental medicine. 1942 Jan 01;75(1):49-64.
153. Paulson JC, Rogers GN. Resialylated erythrocytes for assessment of the specificity of sialyloligosaccharide binding proteins. Methods in enzymology. 1987;138:162-8.
154. Baenziger JU, Fiete D. Structure of the complex oligosaccharides of fetuin. The Journal of biological chemistry. 1979 Feb 10;254(3):789-95.

155. Gambaryan AS, Matrosovich MN. A solid-phase enzyme-linked assay for influenza virus receptor-binding activity. Journal of virological methods. 1992 Sep;39(1-2):111-23.
156. Blixt O, Head S, Mondala T, Scanlan C, Huflejt ME, Alvarez R, et al. Printed covalent glycan array for ligand profiling of diverse glycan binding proteins. Proceedings of the National Academy of Sciences of the United States of America. 2004 Dec 07;101(49):17033-8.
157. Stevens J, Blixt O, Paulson JC, Wilson IA. Glycan microarray technologies: tools to survey host specificity of influenza viruses. Nat Rev Microbiol. 2006 Nov;4(11):857-64.
158. Potier M, Mameli L, Belisle M, Dallaire L, Melancon SB. Fluorometric assay of neuraminidase with a sodium (4-methylumbelliferyl-alpha-D-N-acetylneuraminate) substrate. Analytical biochemistry. 1979 Apr 15;94(2):287-96.
159. Engstler M, Talhouk JW, Smith RE, Schauer R. Chemical synthesis of 4-trifluoromethylumbelliferyl-alpha-D-N-acetylneuraminic acid glycoside and its use for the fluorometric detection of poorly expressed natural and recombinant sialidases. Analytical biochemistry. 1997 Aug 01;250(2):176-80.
160. Jourdian GW, Dean L, Roseman S. The sialic acids. XI. A periodate-resorcinol method for the quantitative estimation of free sialic acids and their glycosides. The Journal of biological chemistry. 1971 Jan 25;246(2):430-5.
161. Warren L. The thiobarbituric acid assay of sialic acids. The Journal of biological chemistry. 1959 Aug;234(8):1971-5.
162. Lambre CR, Terzidis H, Greffard A, Webster RG. Measurement of anti-influenza neuraminidase antibody using a peroxidase-linked lectin and microtitre plates coated with natural substrates. Journal of immunological methods. 1990 Dec 31;135(1-2):49-57.
163. Blumenkrantz D, Roberts KL, Shelton H, Lycett S, Barclay WS. The short stalk length of highly pathogenic avian influenza H5N1 virus neuraminidase limits transmission of pandemic H1N1 virus in ferrets. Journal of virology. 2013 Oct;87(19):10539-51.
164. Brown J, Laver WG. The effect of antineuraminidase antibody on the elution of influenza virus from cells. The Journal of general virology. 1968 Mar;2(2):291-5.
165. Wang W, Wolff MW, Reichl U, Sundmacher K. Avidity of influenza virus: model-based identification of adsorption kinetics from surface plasmon resonance experiments. Journal of chromatography A. 2014 Jan 24;1326:125-9.
166. Benton DJ, Martin SR, Wharton SA, McCauley JW. Biophysical measurement of the balance of influenza a hemagglutinin and neuraminidase activities. The Journal of biological chemistry. 2015 Mar 06;290(10):6516-21.
167. Manz B, Schwemmle M, Brunotte L. Adaptation of avian influenza A virus polymerase in mammals to overcome the host species barrier. Journal of virology. 2013 Jul;87(13):7200-9.
168. Krug RM, Aramini JM. Emerging antiviral targets for influenza A virus. Trends in pharmacological sciences. 2009 Jun;30(6):269-77.
169. Mair CM, Ludwig K, Herrmann A, Sieben C. Receptor binding and pH stability - how influenza A virus hemagglutinin affects host-specific virus infection. Biochimica et biophysica acta. 2014 Apr;1838(4):1153-68.
170. Russell RJ, Haire LF, Stevens DJ, Collins PJ, Lin YP, Blackburn GM, et al. The structure of H5N1 avian influenza neuraminidase suggests new opportunities for drug design. Nature. 2006 Sep 07;443(7107):45-9.
171. Stencel-Baerenwald JE, Reiss K, Reiter DM, Stehle T, Dermody TS. The sweet spot: defining virus-sialic acid interactions. Nat Rev Microbiol. 2014 Nov;12(11):739-49.
172. Samraj AN, Laubli H, Varki N, Varki A. Involvement of a non-human sialic Acid in human cancer. Frontiers in oncology. 2014;4:33.

Chapter 2

Kinetic analysis of influenza A virus HA/NA balance reveals contribution of NA to virus binding and NA-dependent rolling on receptor-containing surfaces

Hongbo Guo[1], Huib Rabouw[1], Anne Slomp[1], Meiling Dai[1], Floor van der Vegt[1], Ryan McBride[2], James C. Paulson[2], Raoul J. de Groot[1], Frank J. van Kuppeveld[1], Erik de Vries[1]*, Cornelis A. de Haan[1]*.

1 Virology Division, Department of Infectious Diseases and Immunology, Faculty of Veterinary Medicine, Utrecht University, Utrecht, the Netherlands.
2 Departments of Cell and Molecular Biology, Chemical Physiology, and Immunology and Microbial Science, Scripps Research Institute, La Jolla, California, USA.
(*co-coresponding author)

Manucsript in preparation

ABSTRACT

Influenza A virus (IAV) binding to, and release from functional host cells receptors and mucus decoy receptors, which is essential for host tropism and viral fitness, is largely determined by the hemagglutinin (HA) and neuraminidase (NA) envelope glycoproteins. The dynamics of these multivalent virus-receptor interactions cannot be properly analyzed using equilibrium binding models and endpoint binding assays. We therefore applied biolayer interferometry (BLI), using synthetic sialoglycans as well as specifically engineered glycoproteins, to quantitatively determine virus binding and release in real time, HA/NA balance and the individual and combined contributions of HA and NA thereto. Virus binding in absence of NA activity, which is virtually irreversible due to multivalent interactions, proceeded at an initial binding rate, which is linear with virus concentration and depending on receptor density. The initial binding rate therefore allows for a virus concentration-independent quantitative comparison of relative binding strength to different receptor-coated surfaces. Whereas virus-binding is largely driven by HA we could identify a contribution of NA with low enzymatic activity to the initial binding rate. In turn, NA activity was critically dependent on the ability of virion-associated HA proteins to associate with a receptor-coated surface. Virus dissociation from the receptor-coated surface strictly depended on NA activity. Prior to dissociation, virus particles were rolling over the receptor-coated surface, thereby removing sialic acid receptors from the complete sensor surface, and to undergo morphological changes driven by NA activity. These novel aspects of virus binding and release, that can now be analyzed in detail and quantified, are expected to be crucial elements of the viral fitness properties required for efficient infection of an organism.

INTRODUCTION

Specificity, avidity and dynamics of virus-receptor interactions are crucial factors in host-, tissue- and cell-selectivity, determining virus spread and pathogenesis. Of pivotal importance for IAV infection and transmission is the requirement for a precisely tuned functional balance of the virus envelope proteins hemagglutinin (HA) and neuraminidase (NA) (1-3). This balance governs the interaction of virions with the sialic acid (SIA) receptors on the host cell surface and with decoy receptors in the extracellular environment. Virus attachment to SIA receptors is mediated by HA, a homotrimeric type I transmembrane protein (4-6), while NA, a homotetrameric type II transmembrane protein, acts as a receptor-destroying enzyme by cleaving sialic acids (7-9).

SIA moieties that function as IAV receptor are attached to the penultimate residue by either an α2,3 or an α2,6 linkage (10-12). Linkage-type has been shown to be an important determinant of host- and cell-specificity. IAVs that infect humans bind preferentially to SIAs in an α2,6 conFigureuration, whereas avian IAVs prefer binding to α2,3-linked SIAs (12-14). In addition, binding affinity is strongly affected by the composition, branching, modifications and linkage-types of the internal carbohydrate chain residues (15). This is important as the cell surface glycan composition is highly variable between host and cell type. Just as for binding affinity and specificity of HA, NA specificity and activity depends on the viral isolate examined: NAs of avian IAVs are highly active and exhibit a substrate preference for α2,3 sialoglycans, while human virus NAs have lower activity and cleave both α2,3 and α2,6 sialylated glycans (16-18). Whereas the fine-specificity of HA proteins and implications thereof have been studied in considerable detail, little is known about NA fine-specificity (19), mainly because of the relative lack of accurate assays.

Multivalent interactions of several HA trimers and sialosides at the contact surface between virus and host cell allow IAVs to adhere to the host cell with high avidity. Nevertheless, the low affinity (KD of ~0.3-3 mM) (20-22) of the monovalent interaction between a single HA binding site and a SIA molecule enables a dynamic binding mode in which individual HA-SIA interactions are rapidly formed and broken without causing dissociation of the virus but providing access of NA to temporarily free SIAs. Ongoing SIA cleavage by NA will reduce surface receptor density and result in virus dissociation. The rate of this process depends on the individual kinetic parameters of HA and NA for their interaction with individual sialosides, which are present in an extensive structural variety and variable density and membrane distribution. These factors determine what is referred to as the HA/NA balance.

This balance is important at several stages of the infection cycle. First, epithelial cells of the airways and intestinal tract are covered with a thick layer of mucus containing a range of abundantly sialylated mucins. These SIAs function as decoy receptors specifically

binding to HA, thereby inhibiting IAV penetration of the mucus layer and blocking access to the epithelial cell surface (23, 24) which needs to be counteracted by NA activity. Second, NA activity is also required to prevent the virus to become permanently trapped at HA binding sites on the cell surface that do not support efficient endocytosis (25, 26). Third, NA activity facilitates budding and release of new virus particles by de-sialylation of the surface of the infected cell. Finally, de-sialylation of the virus envelope glycoproteins HA and NA also prevents virus aggregation (27).

Viral fitness depends on continuous fine-tuning of the HA/NA balance during virus evolution within a host or upon transfer to a novel host. Adaptation of a non-optimal HA–NA balance, for instance when a virus is confronted with mucus decoy receptors of a novel host species, has been shown to involve increased NA activity as well as decreased binding by HA to the novel decoy receptors (28-30). Replication of viruses, harboring mismatched pairs of HA and NA or propagated in the presence of inhibitory decoy receptors or NA inhibitors, can be rescued by adaptive mutations in the HA, NA or both proteins (1, 31, 32). Cross-species transmission events, leading to human pandemics in the past, require adaptions in both HA and NA (33, 34) that are necessary to deal efficiently with the novel decoy and functional receptor repertoire while maintaining a proper HA/NA balance.

There is no straightforward method to determine the highly dynamic functional HA/NA balance of different IAV strains and the receptors they encounter. Classical approaches are often based on hemagglutination of erythrocytes that harbor poorly defined receptor repertoires and do not well reflect binding avidity, let alone binding dynamics. Solid phase binding assays (e.g. ELISAs, glycan arrays), mostly performed as an endpoint assay, are highly artificial in their setup and do not handle well the polyvalency aspects of virus binding. NA activity assays often use soluble substrates poorly reflecting natural sialosides (35), and consequently ignore the effects of the context of a virus particle on NA activity. Thus, methods that determine the dynamic effects of HA and NA activity urgently need improvement to allow integration into a model that accurately provides a quantitative description of the dynamic interaction between IAV particles and receptor-coated surfaces. Ultimately, such a model should be able to deal with IAV binding to host cell surfaces in the presence of a natural mucus barrier.

Here we have used biolayer interferometry (BLI) as a label-free, real-time method for studying the dynamics of IAV-receptor interaction and to demonstrate novel aspects thereof. Our results indicate that the initial virus binding rate is the prime, and physiologically most important, kinetic parameter of HA-dependent IAV particle binding to synthetic as well as natural glycoprotein receptors. It can be determined by BLI. NA was shown to contribute to virus binding and to be absolutely required for virus elution. In turn, NA activity was critically dependent on the ability of virions to bind to a receptor-

coated surface. The HA/NA balance of different virus-receptor combinations could be determined by measuring empirical virus binding and elution parameters. BLI allowed us to demonstrate that virus particles roll over a receptor-coated surface in a NA activity-dependent manner. BLI also allowed to deduce morphological chances in receptor-bound virus particles due to NA activity.

MATERIALS AND METHODS

Cells and Viruses. HEK293T**,** Madin–Darby canine kidney (MDCK)-II, CHO K1 and CHO 15B cells were maintained as described previously (30, 52). Influenza A/Puerto Rico/8/34/Mount Sinai ($PR8_{MtSIN}$), A/WSN/33 (H1N1) (WSN) and reassortant virus strains $WSN_{HAMtSIN}$, $PR8_{CAM2,6}$, $PR8_{CAM2,3}$ were grown in MDCK-II cells as described previously (52) and stored at −80 °C. Reassortant virus strains $WSN_{HAMtSIN}$, $PR8_{CAM2,6}$ and $PR8_{CAM2,3}$ were made by standard reverse genetic procedures (53) creating viruses with different HA-encoding genome segments (from PR8 Sinai [Accession No. ADX99484.1], PR8 Cambridge [Accession No. NP_040980.1], and PR8 Cambridge with substitution E190D introduced by sited-directed mutagenesis according standard procedures. See Supplementary Figure S2 for a schematic outline) in the background of the other seven WSN genome segments. Virus titers were determined by measuring the TCID50 on MDCK-II cells. Accession numbers are P03454.1 for WSN HA, ACF54601.1 for WSN NA, and P03468.2 for PR8 NA. TX77 is a recombinant virus carrying the HA of A/Bilthoven/1761/76 in the background $PR8_{MtSIN}$ (54).

Virus particle, HA and NA quantification. For quantification, virus samples were concentrated by TCA precipitation (55) and applied to standard 10% SDS/PAGE gels for separation of viral proteins followed by silver staining. Silver-stained polymerase bands were quantified by densitometry on silver staining gels as outlined and shown in supplementary Figure S3. HA and NA amounts were quantified by western blotting of SDS/PAGE gels as described above. Monoclonal antibodies used for detection and quantification by densitometry were FI6 (56) and N1-7D3 (provided by Xavier Saelens) and GT288-GTX629696 (GeneTex).

Genes, Expression Vectors, and Protein Expression and Purification. Codon-optimized H1-encoding and N1-encoding cDNAs (GenScript, Piscataway, NJ, USA) of A/Puerto Rico/8/34/Mount Sinai (H1N1) and A/WSN/33 (H1N1) (WSN_{WT}) were cloned in pCD5 expression vectors flanked by signal peptide-, GCN4- isoleucine-zipper trimerization (HA) or tetramerization (NA) motif-, and Strep-tag II-encoding sequences, expressed, and purified as described (57). Codon-optimized human fetuin-encoding cDNAs (GenScript, Piscataway, NJ, USA) were cloned in pCAGGs vector fused to a Fc-tag and a Bap-tag for binding to octet sensors and a strep-tag II for purification.

Chemicals. OC was a gift from Roche, dissolved in DMSO at 100 Mm concentration, aliquoted and stored at -20^{o}C. Mal I, Mal II, SNA, and ECA were obtained from VectorLabs.

Neuraminidase enzyme acitivity assay. The activity of IAV virus particles as well as recombinant soluble NAs was determined by using a fluorimetric assay similarly as described previously (19). In this assay, the substrate 2'-(4-methylumbelliferyl)-α-D-N-acetylneuraminic acid (MUNANA; Sigma-Aldrich) is hydrolyzed by neuraminidase, resulting in fluorescent 4-methylumbelliferone (4-MU).

Glycan array assay. Microarrays were printed as described previously (58). The glycan array analysis of the HA proteins was performed as previously described (59). Briefly, 200 µg/ml recombinant HA was precomplexed with a horseradish peroxidase-linked anti-streptavidin tag antibody and an Alexa Fluor 488 antimouse antibody (4:2:1 molar ratio) for 30 min at 0°C, prior to incubation for 90 min on the microarray slide under a microscope cover glass in a humidified chamber at room temperature. After repeated washes with phosphate-buffered saline (PBS) with 0.05% Tween, PBS, and deionized water, the slides were immediately subjected to imaging.

Receptor probes for BLI experiments. Biotinylated synthetic glycan 3'SLN and 3'SLE^{X} were obtained from the consortium for glycomics (CFG). Biotinylated transferrin was obtained from Sigma.

Biolayer interferometry. BLI analysis was performed on an Octet QK machine using standard streptavidin (SA) or protein A bio-sensors (all from Pall-FortBio). PBS with calcium and magnesium (PBS+/+) was used as standard assay buffer. Receptor loading was performed by loading biotinylated receptors (synthetic glycans or proteins) to SA sensors or Fc-tagged glycoprotein receptors to protein A sensors. Unless otherwise specified, sensor were loaded with receptor to maximum levels (no further increase in reflection) using 100 nM synthetic glycan or 4 µg/ml glycoprotein as loading sample concentration. After loading sensors were washed in PBS+/+ until a stable baseline was obtained. Virus binding was performed by moving receptor-loaded sensors to wells containing 100 µl virus sample at the indicated concentrations (the use and concentration of OC is indicated where applicable). Then virus-loaded sensors are usually moved to PBS+/+ in presence of 10 µM OC to examine virus dissociation (usually producing a flat line), washed 3 times for 3 seconds in PBS+/+ to remove OC and next transferred to PBS+/+ without OC to measure NA activity-driven self-elution. Alternatively, in order to determine simultaneous action of HA and NA virus binding was analyzed from the start in PBS+/+. Regeneration of sensors, preserving the binding of biotinylated receptors but removing all bound virus, was performed by dipping sensors briefly in 10 mM Tris/Glycine buffer pH 2.

Statistical analysis. Each BLI experiment was repeated at least twice. Representative experiments were graphed. The correlation between virus particle number and the initial binding rate was determined by linear regression and Pearson r analysis using the GraphPad Prism 7.04 software. Significant differences between curves were analyzed by IBM SPSS statistic 24. Fractional receptor densities correlating with half maximum initial binding rates were determined by non-linear regression analysis using Graphpad Prism 7.04 software. Significance analysis was based on two tailed unpaired t test or one way ANOVA (GraphPad Prism 7.04).

RESULTS

BLI provides real time quantitative recording of virion binding to and release from a receptor-coated surface and is therefore expected to provide direct quantification of the dynamics of virus binding as occurring *in vitro* and *in vivo*. Before studying these highly dynamic interactions, we evaluated our experimental set-up by describing the geometric properties of the BLI sensor surface and IAV virions, and by analyzing virus binding in the absence of NA activity using different receptors and densities thereof.

Geometry of sensors and virions

Most experiments described in this paper were performed using BLI sensors coated with streptavidin (SA, Fortebio), to which biotinylated glycans or glycoproteins can be irreversibly attached ($K_d = 10^{-14}$), thereby providing a well-defined receptor-coated surface at maximal loading levels. Tetrameric SA carries four biotin binding sites, which are ordered two by two at opposing planes of the cubic structure of the tetramer (36) (Figure 1A). Only two biotin binding sites (spaced at 2.5nm distance) at the surface exposed plane of SA are expected to be available for receptor binding (37). Thus, maximally 2 synthetic glycans, bound to the same SA , can bind to a single HA trimer. Synthetic glycans bound to neighboring SAs (at 25 nm distance) are too short to bind to the same HA trimer. Information on the number of monovalent HA-receptor interactions contributing to polyvalent binding in most currently employed IAV binding assays is lacking. We estimate that 10% of the virion surface can interact with the sensor surface (Figure. S1A), resulting in maximally ~7 HA trimers on the viral envelope to interact simultaneously with ~7 receptor-loaded streptavidins (Figure. 1B).

Virion binding kinetics in the absence of NA activity

We continued our analysis by quantification of virus binding in absence of NA activity, by the addition of the NA inhibitor oseltamivir carboxylate (OC). Viruses carrying different HA/NA pairs in the background of the internal gene segments of IAV lab strains PR8 or WSN were generated by reverse genetics. Figure S2 provides an overview of the viruses and receptors used in this paper. At first, we determined the binding kinetics of IAVs carrying the HA of two different PR8 variants ($PR8_{MtSIN}$ and $PR8_{CAM2,3}$) to a SA biosensor

loaded to saturation with the sialoglycan 3'SLN (Neu5Acα2-3Galβ1-4GlcNAcβ) (Figure. 2). Viruses were adjusted to equal particle numbers on basis of quantitation by silverstaining of the polymerase complex (PB1/PB2/PA). Based on the assumption that 8 copies of the polymerase complex are present per virion a molar concentration could be calculated (see Figure S3). Figure 2A and B display the binding kinetics of a concentration series of virus particles. Clearly, $PR8_{MtSIN}$ was a more efficient binder than $PR8_{CAM2,3}$. Maximum binding levels of approximately 10 nm (see Figure S4A and B for elongated binding times) were estimated to represent sensors fully loaded with virus. Theoretically, a sensor can accommodate 3.3E+07 spherical particles of 100nm diameter (hexagonal packaging) (Figure. S1B). Quantification of bound virus particles using a neuraminidase activity assay was in agreement with these estimates (Figure S4C). Virus binding curves could be reproduced upon regeneration of sensors and re-binding of virus using the same solutions for at least 6 times. This indicates that decay of virus, or selection of a limited subset of virus particles with particular properties, does not occur and therefore does not affect the shape of the curves during the course of binding. We conclude that the BLI results faithfully reflect the binding properties of a given virus strain and therefore can be used to directly compare different strains.

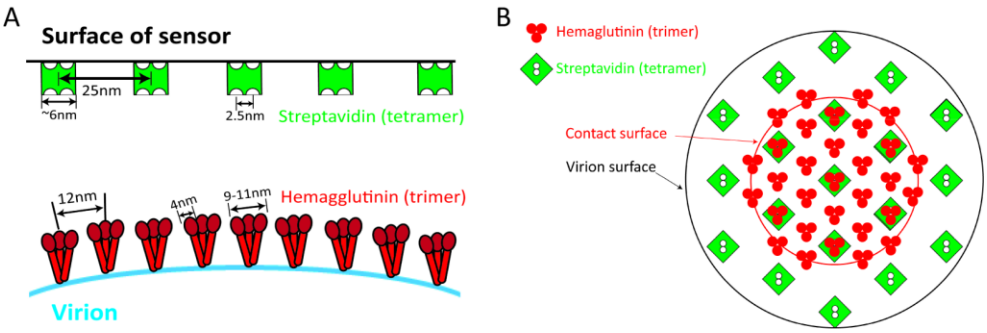

Figure 1. Geometric model of IAV virus – SA sensor interaction. (A) Streptavidin-coated (SA) biosensors contain 109 biotin binding sites according to the manufacturer (Pall-BioForte). The distance between the centers of SA tetramers can be calculated at 25 nm assuming regular hexagonal packaging. Tetrameric SA molecules coated to a surface are assumed to have on average two surface exposed biotin binding sites (37). The distance between two binding sites on one side of the cubic SA tetramer has been shown to be 2.5 nm by X-ray crystallography (37). HA trimers are closely packaged on the virus surface and the center to center distance has been determined at 12nm whereas the distance between SIA binding sites in a HA trimer was determined at 4 nm (60). (B) Following the assumption that labstrains PR8 and WSN are spherical with a diameter of ~ 100 nm [refs] and that 10% of the virus surface is in contact with the sensor (Fig. S1), ~7 HA trimers can interact with receptor-loaded SA molecules at the virus-sensor contact interface (inner red circle). In principle two receptor molecules can be loaded on a SA molecule but whether both can interact simultaneously with an HA trimer will probably depend on the exact geometry of the specific glycan that was loaded.

Lack of virus dissociation in the absence of NA activity

Negligible virus dissociation form the sensors was observed after transfer of the sensors to buffer containing OC (Figure 2A and B; Dissociation). The K_D of monovalent HA-sialic

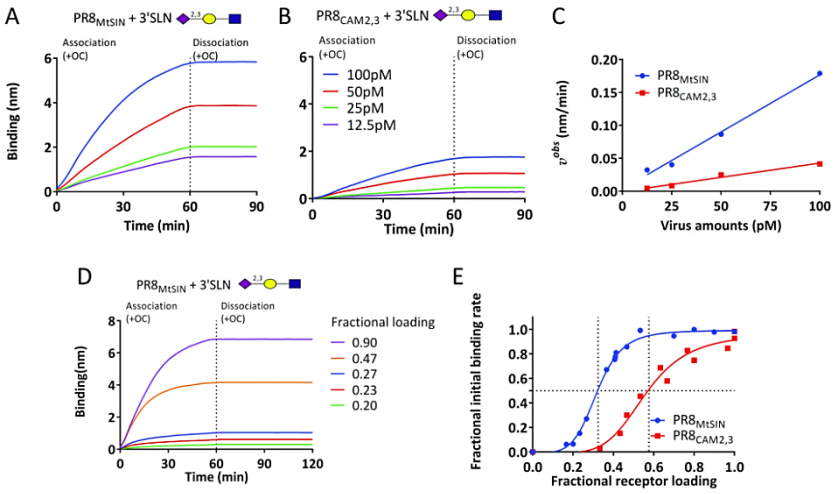

Figure 2. Determination of IAV binding rates by BLI. Streptavidin sensors were fully loaded with biotinylated Neu5Acα2-3Galβ1-4GlcNAcβ-Sp8 (3'SLN). $PR8_{MtSIN}$ (A) and $PR8_{CAM2,3}$ (B) virus particles were bound at four concentrations (12.5 pM to 100 pM, corresponding to 0.75E+09 to 6E+09 particles in 100 µl) in the presence of 10 µM OC. After 60 minutes sensors were washed three times in PBS and virus dissociation in PBS was monitored for another 30 minutes. (C) The observed initial binding rate (v^{obs}) of both viruses was plotted against virus concentration. A significant difference between the two curves was observed based on univariate analysis of variance model by IBM SPSS statistic 24 (P<0.001). Also when normalized for particle number, the v^{obs} (mean ± standard deviation [SD]; 0.19285 ± 0.044309 and 0.03985 ± 0.007378 nm/min per 100pM virus particles for $PR8_{MtSIN}$ and $PR8_{CAM2,3}$, respectively) significantly differed using two-tailed unpaired t test (P=0.0005). (D) 3'SLN receptor was loaded to a range of densities and allowed to bind to 100 pM virus ($PR8_{MtSIN}$) in the presence of OC. After 60 minutes sensors were washed three times in PBS and virus dissociation in PBS was monitored for another 60 minutes. (E) The v^{obs} was calculated for all individual binding curves (shown in Fig S4) of $PR8_{MtSIN}$ and $PR8_{CAM2,3}$ and different densities of 3'SLN and plotted as fractional binding rate (y-axis) against fractional receptor loading density (x-axis). The receptor density corresponding to 50% maximum fractional initial binding rate was 0.332 ± 0.00364 and 0.593 ± 0.01752 for $PR8_{MtSIN}$ and $PR8_{CAM2,3}$, respectively, as determined by nonlinear regression analysis. These values significantly differed (P<0.001) by using two tailed unpaired t test.

acid interactions is typically in the range of ~0.3-3 mM)(20-22, 38). The lack of dissociation is explained by the occurrence of highly polyvalent interactions between viruses and the multivalent receptor-coated solid phase. The observed off-rate constant ($k_{off} \approx 0$) prohibits the quantification of the resulting dissociation constant ($K_D = k_{off}/k_{on} \approx 0$) of virus particles. In view of the extremely low k_{off}, the equation of the binding rate (v^{obs}) for an equilibrium binding model (v^{obs} = d[R.virus]/dt = k_{on}[virus][R] - k_{off}[R.virus]) can be simplified to v^{obs} = d[R.virus]/dt = k_{on}[virus][R] where [virus] is constant (as shown by repeated binding experiments) and receptor concentration [R] = [R_{max}] - [R.virus]. During the initial binding phase, [R] can be regarded as a constant resulting in a linear binding curve (Figure 2A and B). Consequently, a linear correlation is obtained between the observed initial binding rate (v^{obs} = dB/dt) and the virus concentrations for both the fast ($PR8_{MtSIN}$; r=0.997, P=0.0002) and the slow binding ($PR8_{CAM2,3}$; r=0.9915, P=0.0009) viruses (Figure 2C). We conclude that the observed initial binding provides a quantifiable parameter for comparison of the binding properties of different viruses.

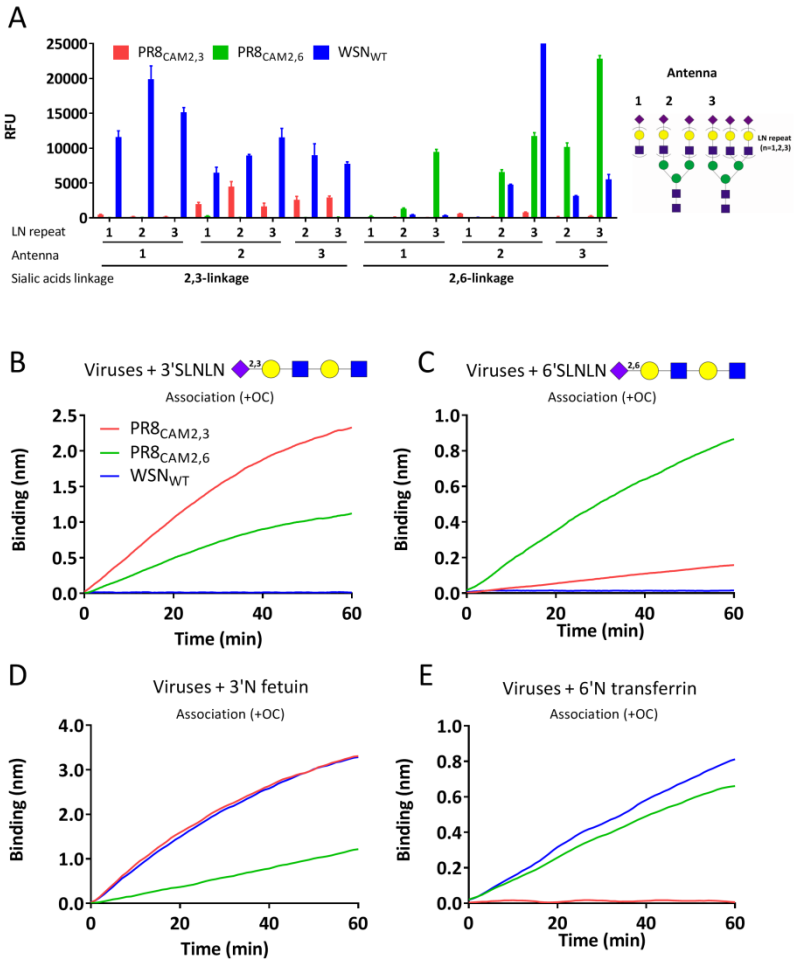

Figure 3. Quantification of virus binding specificity by BLI. (A) Specificity of recombinant soluble HA trimers of $PR8_{CAM2,3}$, $PR8_{CAM2,6}$ or WSN was determined by glycan array analysis. Binding to mono-, bi- and tri-antennary glycans carrying one, two or three LacNAc repeats terminated with a α2,3- or α2,6-linked SIA is indicated. Means of 6 independent replicates are graphed, standard errors of the means are indicated. Biotinylated 3'SLNLN or 6'SLNLN (B, C) or Fc-tagged 3'N fetuin (D) or biotinylated 6'N transferrin (E) were loaded to maximum levels to SA or Protein A biosensors after which binding of 100 pM $PR8_{CAM2,3}$, $PR8_{CAM2,6}$ or WSN virus was monitored for 60 minutes in the presence of 10 µM OC.

The maximal binding level and the initial binding rate are affected by receptor density

To further validate our experimental set up, we studied the effect of receptor density on IAV binding. The receptor density on the sensor surface affected maximal virion binding levels (Figure. 2D and Figure. S5) and the initial binding rate (Figure. 2E). Importantly, also at low receptor-density virus dissociation was negligible (Figure 2D). Apparently,

polyvalent interaction of a few HA-trimers with receptor-loaded streptavidin molecules is sufficient for virtually irreversible virus binding ($k_{off} \approx 0$) again indicating that calculation of the dissociation constant ($K_D = k_{off}/k_{on} \approx 0$) is a poor method for quantifying virus binding strength. Plotting the fractional initial binding-rate v^{obs} against fractional receptor density (Figure 2E) shows that $PR8_{MtSIN}$ reached a maximum binding rate at ~55% receptor density whereas the weaker binder $PR8_{CAM2\text{-}3}$ required 100% receptor density for reaching a maximum binding rate. A 3-fold reduction in receptor density was sufficient to reduce the initial binding rate from maximal to zero for both viruses. In principle, an HA-trimer, in which the SIA-binding sites are spaced at 4nm distance, can form a bivalent interaction with a streptavidin loaded with 2 receptor molecules (Figure 1A). This might contribute differently to the binding avidity than two interactions between neighboring HA-streptavidin pairs. It should therefore be noted that lowering the receptor-density results in a sensor surface coated with streptavidin loaded with 0, 1 or 2 receptor molecules, the distribution of which will change with receptor loading concentration. As a result, a non-homogenous receptor-coated surface with increasing amounts of surface-area having a receptor density too low to bind virus will occur at decreasing receptor concentrations. This phenomenon is likely to contribute to the observed decrease in maximum binding levels and initial binding rate when lowering receptor density (Figure. 2D and E).

Determination of relative receptor-specificity by BLI.

Quantitative comparison of the binding rate of different viruses requires quantification of virion numbers. However, in view of the negligibly low dissociation rate ($k_{off} \approx 0$) and an apparent constant receptor concentration [R] during the early binding phase, the relative specificity of a virus for two receptors can be quantified independently of virus concentration using the relative binding rate ($v^{rel} = v^{obs1} / v^{obs2}$) measured with receptors 1 and 2. This circumvents the need for highly precise, but elaborate, virus quantitation procedures (see e.g. Figure S3). To validate the use of BLI in determining relative receptor specificity, we quantified the effect on receptor-specificity of amino acid substitution E190D in H1. This substitution is known to cause a shift in binding from α2,3- to α2,6-linked SIA receptors (39). We analyzed lab strains $PR8_{CAM2,3}$ and $PR8_{CAM2,6}$, which contain an E or D at position 190, respectively, and the slightly different strain WSN, which carries 190E. Virion-binding results obtained with BLI were compared with a glycan array analysis of the corresponding HA proteins (Figure 3A). The glycan array assays, in which HA proteins were multimerized by antibody complexation to enable polyvalent binding, showed an absolute specificity shift caused by the E190D mutation when comparing $PR8_{CAM2,3}$ and $PR8_{CAM2,6}$. Comparison of the BLI-derived binding rates of the corresponding viruses, showed a relative specificity for α2,3 over α2,6 sialosides ($v^{rel} = v^{3'SLNLN}/v^{6'SLNLN}$) of 22.9 (SD=0.11; N=3) for $PR8_{CAM2,3}$ and 1.6 (SD=0.18; N=3) for $PR8_{CAM2,6}$ (Figure 3B and C). Remarkably, WSN virus did not bind to synthetic glycans in the BLI assay in contrast to efficient binding of WSN HA to α2,3- as well as α2,6-linked synthetic glycans on the

microarray. Apparently, differences exist in accessibility to short glycans of HA proteins used on glycan arrays and of envelope- embedded HAs in virus particles. We therefore also examined binding to receptors presented in the natural context of glycoproteins carrying α2,3- or α2,6-linked sialosides (3'N fetuin and 6'N transferrin, respectively; Figure 3D and E). For $PR8_{CAM2,3}$ an absolute specificity for α2,3-linked SIAs attached to fetuin was observed whereas mutation E190D present in $PR8_{CAM2,6}$ led to a much lower relative specificity for 3'N fetuin (v^{rel}= $v^{3'N\ fetuin}/v^{6'N\ transferrin}$=1.4; SD=0.21; N=3). WSN, which was not able to bind the synthetic glycans, displayed dual specificity for the N-linked glycoproteins (v^{rel}=4.9; SD=0.15; N=3). The results obtained with WSN are in agreement with the binding of WSN HA to multi-antennary α2,3- as well as α2,6-linked N-glycans on the glycan array. However, an absolute shift in IAV receptor specificity, as determined by glycan array for the $PR8_{CAM2,3}$/$PR8_{CAM2,6}$ HA protein pair, is not observed for the cognate unmodified virus particles using BLI. Multivalency differences between virus particles on the one hand, and HA proteins that are artificially complexed by antibodies to reach a degree of multivalency sufficient for receptor binding on the other hand, probably account for this. In conclusion, BLI allowed quantification of the relative receptor specificity shift resulting from a mutation (E190D) in the receptor binding site.

We further exploited the use of heterologously expressed glycoproteins as a more natural, and possibly more specific receptors, by assessing the contribution of sialylated O-linked and N-linked glycans to IAV binding. Genetically engineered fetuin variants containing either N-linked, O-linked or N-linked and O-linked glycosylation sites were produced (Figure S2) and confirmed to display the expected lectin binding profiles (Figure S6). Whereas both $PR8_{MtSIN}$ and $PR8_{CAM2,3}$ bound to fetuin containing N-glycans (Figure S7A and B), only $PR8_{CAM2,3}$ was able to bind fetuin containing O-glycans, albeit at a 6-fold lower initial binding rate than to N-glycosylated fetuin (Figure S7C). When N- and O-linked glycans are both present (Figure S7A), the initial binding rate seems to be determined by the stronger binding to N-linked glycans as binding of $PR8_{Cam2,3}$ is not accelerated despite its ability to bind 2,3 O-linked glycans. These results demonstrate that BLI in combination with tailor-made glycoproteins is suitable to elucidate quantitative differences in IAV receptor-binding fine specificity.

NA activity on a receptor-coated surface requires virion binding.

As a next step in understanding the dynamic interactions between virions and receptor-coated surfaces, we analyzed the contribution of bound and non-bound virions to receptor cleavage. We therefore compared two viruses with identical NAs in combination with HAs with different specificity. $TX77_{NAMtSIN}$, which contains a α2,6-linked SIA-specific HA from a human H3N2 virus in the background of $PR8_{MtSIN}$ was efficiently bound to 6'N transferrin, whereas the α2,3-linked SIA-specific $PR8_{MtSIN}$ could not bind this receptor. The experimental set-up of the is shown in Figure 4A. In absence of NA inhibitor the initial

lower binding rate of $TX77_{NAMtSIN}$ was lower than in the presence of OC (Figure. 4B). This binding rate became negative in time. We interpret this as the release of virus particles due to ongoing depletion of receptors by NA activity. The high K_D for individual HA-receptor interactions will result in a dynamic binding-mode in which individual HA-SIA interactions are continuously formed and broken. This allows access of NA to the receptors, resulting in their cleavage and ultimately leading to release of bound particles. After regeneration, which removes the bound virus particles but leaves the biotinylated glycans on the sensors, we probed the de-sialylation of the receptor-coated surfaces by determining the degree of binding of $TX77_{NAMtSIN}$ in presence of OC (Figure 4C). Only the sensor previously bound with $TX77_{NAMtSIN}$ with an active NA (i.e. in the absence of OC) displayed highly reduced re-binding of $TX77_{NAMtSIN}$ and was hence de-sialylated. In contrast, $PR8_{MtSIN,}$ which could not bind to the sensor in the first round in the absence of OC due to its α2,3 sialoside specificity, did not remove SIAs, as after regeneration the sensor was capable of binding of $TX77_{NAMtSIN}$ as efficiently as the sensors that were prior incubated with the two viruses in presence of the NA inhibitor OC. We conclude that IAV binding to a receptor-coated surface is required for sialidase activity by bringing NA in close proximity to its substrate. Non-bound virions did not contribute to sialidase activity. Our results also indicate that the effect of virion-associated NA activity on IAV receptor binding dynamics can be determined by BLI.

Effect of NA on the dynamics of IAV-receptor interactions

We obtained quantitative insight into the contribution of NA on the dynamics of IAV-receptor interactions by comparing the binding dynamics of two different viruses carrying the same HA, but different NA proteins ($WSN_{HAMtSIN}$ and $PR8_{MtSIN}$; Figure S2). In a NA activity assay using soluble substrates and recombinantly-expressed NA, the activity of WSN NA was 5.4-fold lower than of $PR8_{MtSinai}$ NA, whereas the NA activity of the cognate virus particles showed a 31.4-fold lower activity for WSN particles (Figure S2J). This difference was explained by the 6.4-fold higher incorporation level of NA in $PR8_{MtSIN}$ particles as determined by Western blotting (Figure S2G-I). The HA content of both viruses was identical (Figure S2D-E). Both viruses, having the same HA, displayed similar curves when bound to 3'N fetuin or 3'SLN (Figure 5A and D) when NA was inhibited by OC. When NA was not inhibited, the high activity of $PR8_{MtSIN}$ NA resulted in minor and short-lived binding of $PR8_{MtSIN}$ whereas binding of $WSN_{HAMtSIN}$, containing little NA activity, was only moderately affected (Figure 5B and E). We conclude that having a lower specific NA activity results in a drastically increased binding of the virus in the absence of NA inhibitors. This binding, which reflects the HA/NA balance, is quantifiable by determining empirical parameters like initial binding rate, the area under the curve (unit is min.nm) and x,y coordinates of the peak (time and binding level).

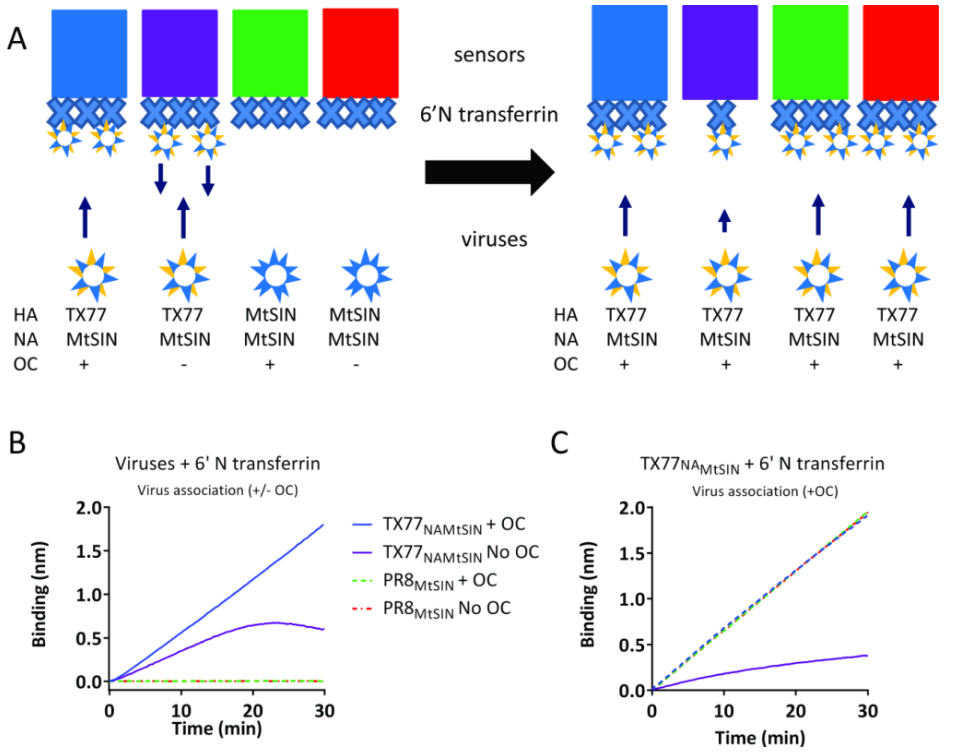

Figure 4. Receptor cleavage by virus particle-associated NA requires HA-dependent virus binding. (A) Schematic representation of the experimental set-up. Colours of the sensors correspond with the colours of the lines in (B) and (C). 6'N transferrin is indicated by the large Xs. Origin of the HA and NA proteins of the viruses used is indicated as well as the absence of presence of OC during the incubation of the sensors with the viruses. The left and right panels correspond with the graphs shown in (B) and (C), respectively. (B) Biotinylated 6'N transferrin was loaded to maximum levels on Streptavidin sensors and bound with 100 pM $PR8_{MtSIN}$ or $TX77_{NAMtSIN}$ in absence or presence of 10 µM OC as indicated. (C) Sensors bound in (B) with virus were regenerated at pH2, removing all virus particles, and subsequently bound again with 100 pM $TX77_{NAMtSIN}$ to assess the extent of desialytion that occurred in (B) by neuraminidase activity.

A second method for quantifying the effect of NA on receptor binding dynamics is by determination of NA activity-dependent self-elution (Figure 5C and F) of viruses bound in presence of OC (Figure 5A and D). As expected, $PR8_{MtSIN}$ displayed much faster self-elution than $WSN_{HAMtSIN}$ from both receptors analyzed. Of note, re-binding of released particles will not occur as the concentration of free virus particles is far too low. Furthermore, NA-dependent self-elution will critically depend on NA-activity in relation to the K_D of monovalent HA-receptor interactions as receptor cleavage by NA is in competition with receptor binding by HA. In conclusion, BLI can be used to quantify changes in the dynamics of receptor binding due to changes in NA activity by using virus binding assays in the absence of NA inhibitor and by analyzing NA activity-dependent self-elution after prior virus binding in the presence of NA inhibitor.

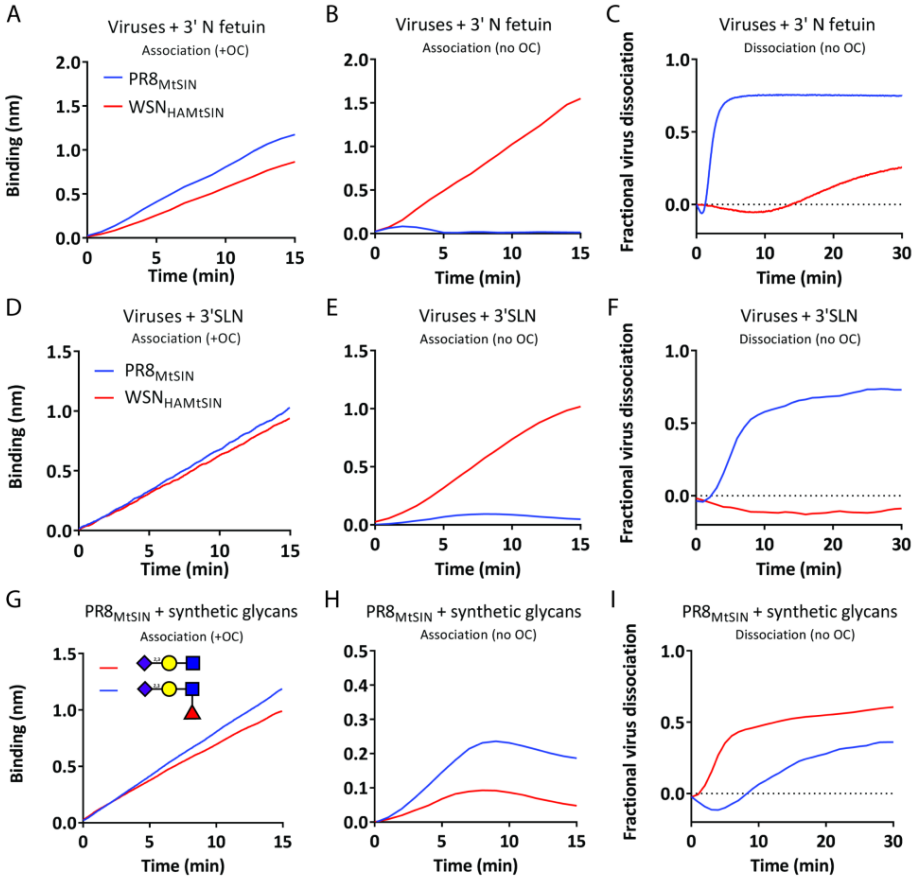

Figure 5. NA specificity affects the HA/NA balance. $PR8_{MtSIN}$ and $WSN_{HAMtSIN}$, both carrying the same HAMtSIN but either NAMtSIN (high NA activity) or NAWSN (low NA activity), respectively, were bound at 30 pM concentration to biotinylated 3'SLN or Fc-tagged 3'N Fetuin loaded to maximum level in the presence (A, D) or absence (B, E) of 10 µM OC. Viruses bound to sensors in presence of OC (A, D) were washed three times in PBS and subsequently examined for NA activity-dependent self-elution in absence of OC (C, F). Virus dissociation in panel C and F is plotted on the positive Y-axis as fraction of virus released relative to the binding level reached in panel A and D respectively. Biotinylated 3'SLN or its fucosylated derivative (SLe^X, NeuNAcα2,3Galβ1,4(Fucα1,3)GlcNAc) were loaded to maximum levels on SA sensors and bound with 30 pM $PR8_{MtSIN}$ in the presence (G) or absence (H) of 10 µM OC for 15 minutes. After three washes in PBS the sensors loaded with virus in (G) were incubated in PBS without OC to allow determination of virus self-elution due to NA activity (I).

Although initial binding rates to 3'SLN and 3'N fetuin are similar for both viruses, self-elution rates from 3'N-fetuin are higher than from 3'SLN indicating that the NA proteins display differences in specific activity for these receptors, which critically affects the HA/NA balance. Figure 5G-I shows more clearly how a simple glycan modification (in this case fucosylation of the synthetic glycan 3'SLN, giving Sialyl-Lewis^X; SLe^X) can specifically affect the contribution of NA to the receptor-interaction dynamics of $PR8_{MtSIN}$. The initial binding rate to SLe^X and to 3'SLN is similar in absence of NA activity (Figure 5G). With an

active NA, the initial binding rate to SLe^X is 2.24-fold higher than to 3'SLN and the maximum binding level to SLe^X is higher, resulting in a 2.61-fold larger area under the curve (0-15 min). These results show that the NA of $PR8_{MtSIN}$ is much more active on 3'SLN than on SLe^X. In agreement herewith, also self-elution from SLe^X proceeded much slower than from 3'SLN (Figure 5I). We conclude that BLI can be used to quantify a shift in the HA/NA balance due to a change in receptor or in NA receptor-specificity.

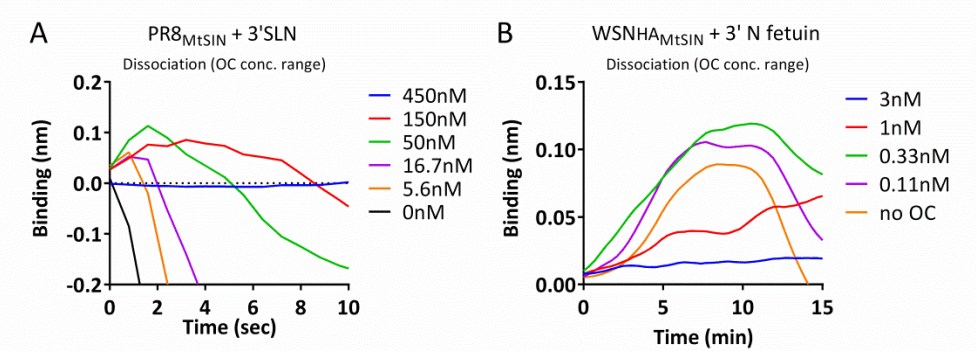

Figure 6. NA activity-driven virus dissociation is preceded by an increase in binding signal. NA activity-dependent virus self-elution was examined for the first seconds (for $PR8_{MtSIN}$; panel. A) or minutes (for $WSN_{HAMtSIN}$; panel B) of the dissociation phase. Viruses were loaded at 100 pM concentration to 3'SLN ($PR8_{MtSIN}$) or 3'N Fetuin ($WSN_{HAMtSIN}$) for 30 minutes in presence of 10 µM OC after which the sensors were washed in PBS and dissociation was examined at a range of OC concentrations as indicated in the panels.

Virus morphology is affected by the number of virus-receptor contacts.

In the self-elution experiments (e.g. Figure 5C, F and I), we consistently observed a small increase in the apparent binding level on the BLI sensor during the initial phase of self-elution. The effect was more prominent with $WSN_{HAMtSIN}$, harboring a low-activity WSN NA, suggesting a causal relationship with NA activity. To study this in more detail, $PR8_{MtSIN}$ and $WSN_{HAMtSIN}$ were bound to 3'SLN or 3'N-fetuin, respectively, in the presence of OC and subsequently allowed to self-elute in the presence of a range of oseltamivir concentrations. This allowed us to investigate the effect at different levels of NA activity (Figure 6). For $WSN_{HAMtSIN}$ 3'N fetuin was used as receptor as hardly any self-elution was observed with the synthetic glycans. Clearly, the height (maximally ~0.12nm) and duration of the increase in the apparent binding level depended on the degree of NA inhibition. The peak was absent ($PR8_{MtSIN}$) or smaller ($WSN_{HAMtSIN}$) in the absence of OC, while no peak was observed for both viruses at the highest OC concentration. As the effect took place in absence of free virus particles that can bind to the sensor, it must reflect a neuraminidase activity-dependent change in the receptor-bound virus particles. Cleavage of SIAs by NA is expected to gradually decrease the number of HA-SIA contacts between the receptor-coated surface and virus. At the maximal number of contacts, a virion might by slightly squeezed against the receptor surface. Possibly, a looser binding of a virus

particle resulting from fewer contacts could allow a more relaxed conformation thereof. This effect is probably even more prominent when the virus is not perfectly spherical enabling the virus to bind at different orientations to the surface. We hypothesize that the observed changes in the apparent binding level are due to a morphological change in and/or a reorientation of bound virus particles as a consequence of the gradual reduction of the number of HA-SIA interactions.

Contribution of NA to receptor binding.

Remarkably, the initial binding rate of $WSN_{HAMtSIN}$ to 3'N-fetuin was higher in absence than in presence of a high concentration of OC (compare Figure 5A and B). Several avian NA genotypes have been shown to possess a 2^{nd} SIA-binding site, alternatively referred to as hemadsorption site (40, 41), but such a site is not conserved in WSN NA and OC binding to this site has never been demonstrated. However, active site mutations in NA that completely abolish catalytic activity have been shown to enable NA-dependent hemagglutination, which could be inhibited with OC (42, 43). We therefore examined the concentration-dependent effect of OC on 3'SLN and 3'N-fetuin binding by $WSN_{HAMtSIN}$ and $PR8_{MtSIN}$ virus particles to obtain further evidence for a contribution of WSN NA to virus binding. At the highest concentration of OC, giving strong NA inhibition, the curves displayed a continuous increase of virus binding (Figure 7, blue lines). However, whereas the initial binding rate of $PR8_{MtSIN}$ decreased strongly at lower concentrations of OC (Figure 7A and C), the initial binding rates of $WSN_{HAMtSIN}$ were increased in a concentration-dependent way (Figure 7B and D). In time these latter curves bent down resulting from removal of SIA receptors by the remaining NA activity. These results imply that NAs with a relatively low cleavage rate (low k_{cat}), like WSN NA, contribute to the initial binding rate by binding with their active site to the SIA receptor.

To confirm and extend the contribution of the NA protein to the initial binding rate and the HA/NA balance by receptor binding via the active site, we next quantified the enhancement of the initial binding rate by WSN viruses carrying four different HAs. As a quantitative parameter for NA-enhanced binding rate, the ratio of the initial binding rate in absence or presence of OC of four recombinant viruses, all carrying a different HA in combination with the same NA, was plotted in Figure 7E. The individual binding curves are shown in Figure S8. NA contributed to the initial binding rate in the context of all four HAs. The virus with the lowest HA-dependent initial binding rate ($PR8_{CAM2,6}$, Figure S8E) was relatively most enhanced in initial binding rate by NA-dependent binding (Figure 7E). However, in absence of OC, ongoing receptor cleavage also reduces receptor density in time and thus the binding rate of additional virus particles, resulting in bending of the curves. As receptor cleavage by NA is in competition with receptor binding by HA, the weakest binder ($PR8_{CAM2,6}$), which is assisted most in initial binding rate by NA, will also

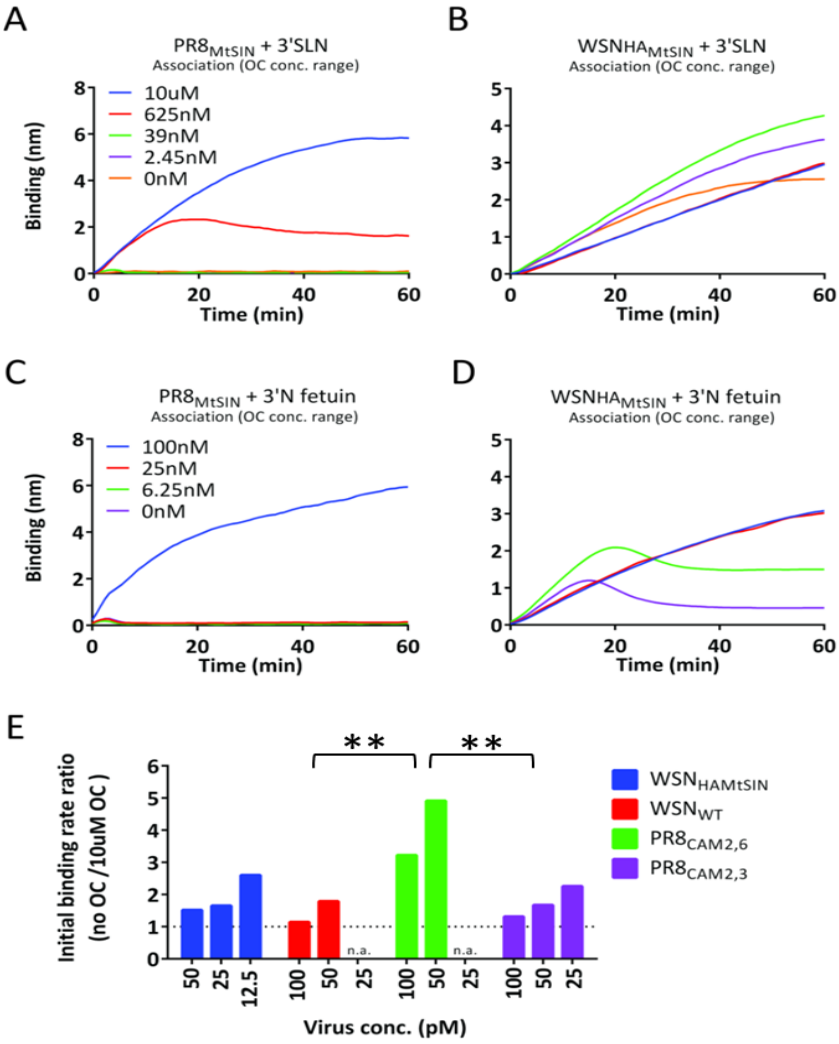

Figure 7. NA contributes to the initial virus binding rate. $PR8_{MtSIN}$ (A, C) and $WSN_{HAMtSIN}$ (B, D), both carrying the same HAMtSIN but either NAMtSIN (high NA activity) or NAWSN (low NA activity), respectively, were bound at 100 pM concentration to biotinylated 3'SLN (A, B) or Fc-tagged 3'N Fetuin (C, D) loaded to maximum level. Binding was performed in absence (red lines) or in the presence of a range of OC concentrations as indicated in the panels. (E) The ratio (initial virus binding rate v^{obs} in absence of OC)/(initial virus binding rate v^{obs} in presence of 10 µM OC) of four viruses carrying the WSN NA in the background four different HAs was plotted for each virus concentration tested (the individual binding curves are shown in fig S8). Experimental conditions that resulted in binding levels too low to allow reliable determination of v^{obs} are indicated by n.a. (not applicable). Singnificant differences between curves were determined based on univariate analysis of variance model by IBM SPSS statistic 24. In panel A, there is no significant difference between curves with 10µM OC and 625nM OC (P>0.1), whereas the curves of 10µM OC and 625nM OC were significantly different from 39nM, 2.45nM and 0nM (P<0.001). In panel B, the curves of 10µM OC and 625nM are also significantly different from 39nM, 2.45nM and 0nM. There is also significant difference between 39nM and 2.45nM. In panel C, the 100nM curves significantly differs from other three OC concentrations. In panel D, there are significant differences between 100nM (and 25nM) and 6.25nM and 0nM. In panel E, significant differences between the mean initial binding rate ratios for each virus were determined by one way ANOVA followed by Sidak's multiple comparisons test. * indicates P<0.05.

suffer most from receptor destruction by its NA and as a consequence display a binding curve that bends down fastest in absence of OC (Figure S8F). In conclusion, these results demonstrate that the NA protein may contribute to the initial binding rate and the HA/NA balance by binding with its active site to SIA receptors, which can be quantified using BLI.

NA activity enables virus rolling over a receptor-coated surface

The NA-dependent dissociation (self-elution) after virus particle binding in the absence of NA activity of the four WSN viruses carrying different HAs that are used above is shown in Figure 8A to D. Virus particles bound to a fixed position on a receptor-coated surface are expected to display NA activity-driven self-elution independently of other bound virus particles. However, all viruses showed a faster release when more virus was loaded, indicating that there is positive cooperativity between viruses in respect to self-elution rate. The only plausible mechanism by which viruses can assist each other in self-elution is by exerting NA activity on a larger surface area than their contact area, implicating that virus particles move over the receptor-coated surface. To test this hypothesis a concentration series (12.5 pM to 100 pM) of $PR8_{MtSIN}$ was bound to 3'N fetuin in presence of OC resulting in binding saturation of the sensor surface ranging from ~5% to ~ 60% (Figure. 8E), based on a maximal binding level of 10 nm after prolonged binding (Figure S4A). Virus particles were then allowed to self-elute by NA activity in absence of OC (Figure 8F). Again, sensors loaded with more virus particles displayed faster self-elution. After regeneration, which removes any small amounts of remaining virus, sensors were re-bound with a high concentration (100 pM) of virus (Figure 8G). This step is used to determine the extent to which self-elution in the previous step resulted in de-sialylation of the receptor by NA activity. Clearly, even at a level where only ~5% of the surface was bound with virus, self-elution created a surface to which only very limited re-binding of virus particles could take place. Thus, virus covering only ~5% of the surface can clear the complete surface extensively of SIAs. As the concentration of virus released from the surface is too low for re-association (see above) and non-bound virus does not contribute to receptor cleavage (Figure 4), we conclude that virus particles exert NA activity while moving over the receptor-coated surface.

Migration of attached IAV particles over a receptor surface necessarily depends on the very high K_D of monovalent HA-SIA interactions resulting in their rapid formation and dissociation. Upon dissociation HA must move away from the SIA to allow access for NA and subsequent receptor cleavage. We hypothesize that removal of SIAs by NA drives rolling of the virus as a non-bound HA cannot bind anymore to the, due to NA activity, receptor-free position but only to a receptor located further away. Rolling of virus particles is predicted to be faster for virus particles with higher NA activity. This was investigated by comparing the binding and dissociation dynamics of $PR8_{MtSIN}$ and $WSN_{HAMtSIN}$, which have the same HA but have high and low NA activity, respectively. The

experimental set-up is shown in Figure. 9A. First, $WSN_{HAMtSIN}$ was bound in the presence of OC to a ~15% saturation level on 3'N-fetuin-coated sensors (Figure 9B, blue and red line). Subsequently, these sensors were incubated with $PR8_{MtSIN}$ in presence or in absence of OC. In presence of OC efficient binding of $PR8_{MtSIN}$ to the large virus-free area takes place (Figure 9B, blue line). In absence of OC, long lasting binding of $PR8_{MtSIN}$ does not take place (Figure 9B, red line and green line) due to its high NA activity. Only minor dissociation of $WSN_{HAMtSIN}$ was observed in absence of OC (Figure 9B, red line) as expected on basis of its low NA activity. This also implicates that $WSN_{HAMtSIN}$ elution is not appreciably assisted by $PR8_{MtSIN}$. In the last step of the experiment the sensors were regenerated to remove all bound viruses and examined for residual SIA content by probing the association of $WSN_{HAMtSIN}$ in the presence of OC. The sensor, to which both viruses were bound in presence of OC, was as efficiently bound by $WSN_{HAMtSIN}$ as in the first round (Figure 9C, blue line). Hardly any binding of $WSN_{HAMtSIN}$ was observed to the sensor to which no virus was bound in the first step and $PR8_{MtSIN}$ in absence of OC in the second step (Figure 9C, green line). In contrast, significantly increased binding of $WSN_{HAMtSIN}$ was observed to the sensor of which ~15% of sensor surface was bound in the first step by $WSN_{HAMtSIN}$ (Figure. 9C, red line).This implies that $WSN_{HAMtSIN}$,, by not rolling over the surface because of its low NA activity, protects its contact surface with the sensor against the NA activity of $PR8_{MtSIN}$, which cleaves SIAs of all the non-protected surface area.

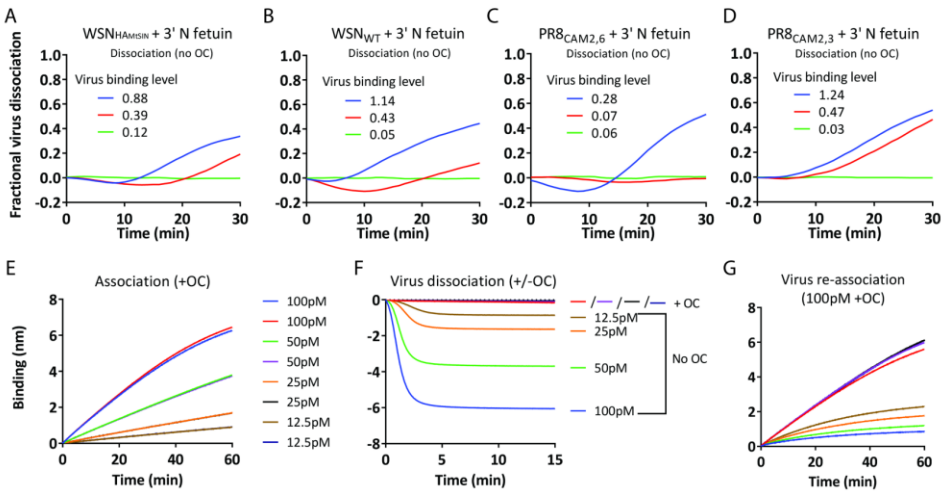

Figure 8. Viruses are rolling over the receptor surface before NA activity-driven dissociation takes place. (A-D) Virus dissociation of the indicated viruses in the absence of OC is plotted on the positive Y-axis as fraction of virus released relative to the binding level reached in the presence of OC (indicated in nm and shown in Fig S8). (E) $PR8_{MtSIN}$ was bound in duplicate at four virus concentrations to eight SA sensors containing biotinylated 3'N fetuin in presence of 10 µM OC. (F) Viruses bound to the sensors in (E) were allowed to dissociate at each concentration in absence or presence of OC for 15 minutes. (G) After the dissociation step (F), sensors were regenerated at pH2, thereby removing all bound viruses but leaving the 3'N fetuin bound to the sensor. All regenerated sensors were subsequently allowed to re-bind $PR8_{MtSIN}$ at a concentration of 100 pM to determine the degree of de-sialylation that occurred in (F).

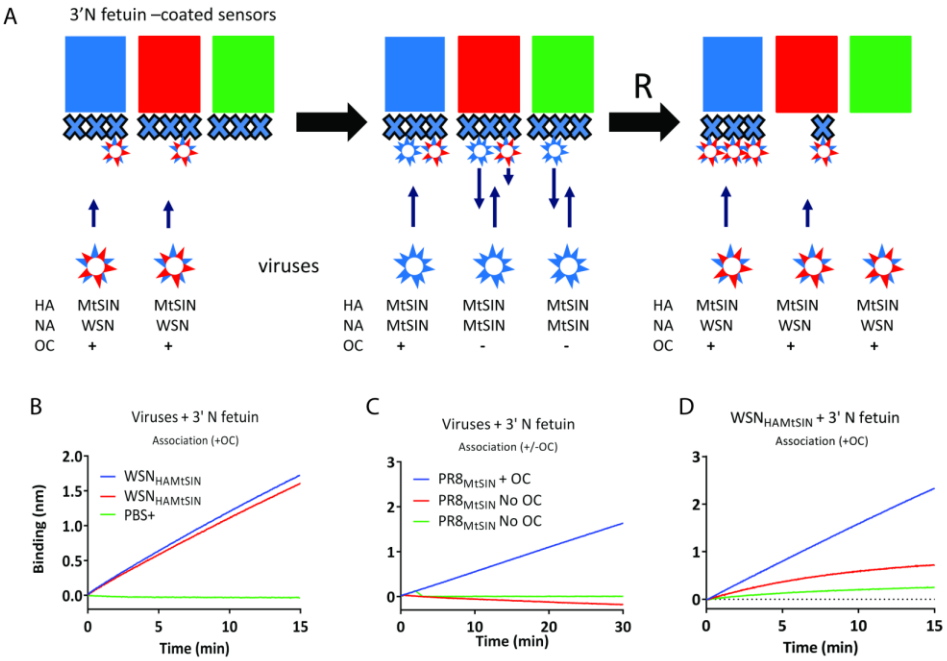

Figure 9. Virus rolling is driven by NA activity I. (A) Schematic representation of the experimental set-up. Colours of the sensors correspond with the colours of the lines in (B)(C) and (D). 3'N fetuin is indicated by the large Xs. Origin of the HA and NA proteins of the viruses used is indicated, as well as the absence of presence of OC during the incubation of the sensors with the viruses. The left, middle and right panels correspond with the graphs shown in (B),(C), and (D), respectively. The capital R indicates the regeneration of the sensors. (B) 75 pM $WSN_{HAMtSIN}$ (with low NA activity) was bound to two sensors in presence of 10 µM OC to biotinylated 3'N fetuin (loaded to maximum level) for 15 minutes reaching ~15% of the maximum binding level. A control sensor was dipped in PBS. (C) The $WSN_{HAMtSIN}$-loaded sensors were allowed to bind 30 pM $PR8_{MtSIN}$, one in presence and one in absence of 10 µM OC. The control sensor was bound by $PR8_{MtSIN}$ in absence of OC. (D) Sensors were regenerated at pH2 removing all bound viruses but leaving the 3'N fetuin bound to the sensor. The regenerated sensors were subsequently allowed to re-bind $WSN_{HAMtSIN}$ at a concentration of 100 pM to determine the degree of de-sialylation that occurred in (C).

To provide additional evidence for the capacity of $WSN_{HAMtSIN}$ to protect receptors from cleavage by $PR8_{MtSIN}$, an additional experiment was performed (Figure. 10A-D). In this experiment, both sensors were first bound by a small amount of $PR8_{MtSIN}$ (~8% loading level; Figure. 10B), which can clear the complete surface extensively of SIAs (Figure. 8E-G). In the second step, the sensors were incubated with $WSN_{HAMtSIN}$ with or without OC (Figure. 10C). Clearly, receptors not bound by $PR8_{MtSIN}$ were rapidly bound by $WSN_{HAMtSIN}$, both in the presence and absence of OC. Binding in the absence of OC was somewhat lower, probably resulting from the sensor being partly occupied by $PR8_{MtSIN}$ and by cleavage of part of the receptor-coated sensor by $PR8_{MtSIN}$. In the final step (Figure. 10D), the sensors were examined after regeneration for residual SIA content by probing the association of $WSN_{HAMtSIN}$ in the presence of OC. Both sensors were efficiently bound by $WSN_{HAMtSIN}$. These results indicate that the SIAs on the sensor were protected against cleavage by rolling $PR8_{MtSIN}$ viruses in the absence of OC by binding of $WSN_{HAMtSIN}$, which

has low NA activity. We conclude that NA activity is the driver of virus rolling on a receptor-coated surface.

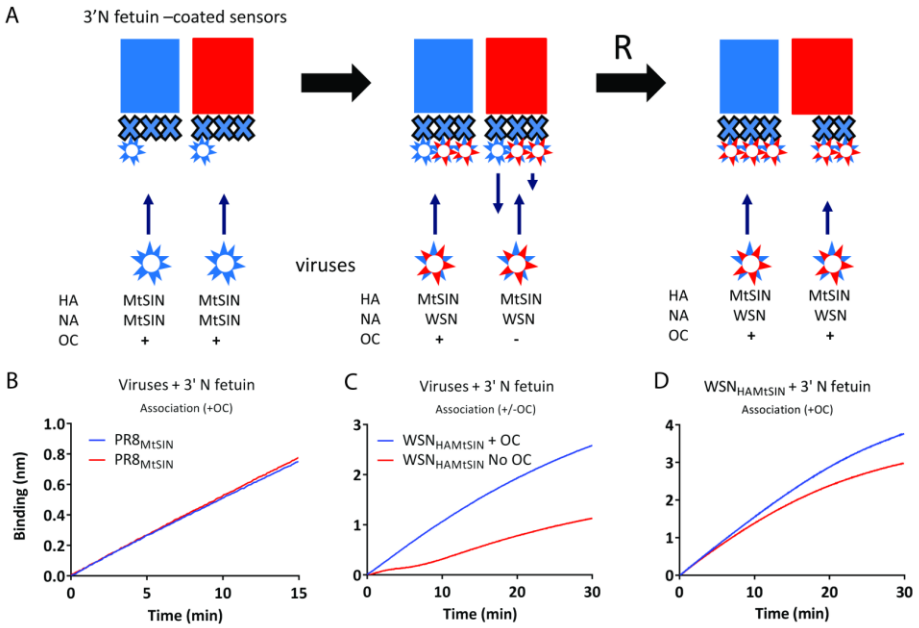

Figure 10. Virus rolling is driven by NA activity II. (A) Schematic representation of the experimental set-up. Colours of the sensors correspond with the colours of the lines in (B)(C) and (D). 3'N fetuin is indicated by the large Xs. Origin of the HA and NA proteins of the viruses used is indicated, as well as the absence of presence of OC during the incubation of the sensors with the viruses. The left, middle and right panels correspond with the graphs shown in (B),(C), and (D), respectively. The capital R indicates the regeneration of the sensors. (B) 30 pM $PR8_{MtSIN}$ (with high NA activity) was bound in duplo in presence of 10 µM OC to biotinylated 3'N fetuin (loaded to maximum level) for 15 minutes reaching ~8% of the maximum binding level. (C) $PR8_{MtSIN}$ loaded sensors were allowed to bind 75 pM $WSN_{HAMtSIN}$, one in presence and one in absence of OC. (D) Sensors were regenerated at pH2 removing all bound viruses but leaving the 3'N fetuin bound to the sensor. The regenerated sensors were subsequently allowed to re-bind $WSN_{HAMtSIN}$ at a concentration of 100 pM to determine the degree of de-sialylation that occurred in (C).

IAV-receptor interaction model

Based on literature and our results, we generated a model for the dynamics of IAV-receptor interactions (Figure. 11). A key feature of the multivalent interaction between a virus and a receptor-coated surface is the presence of the kinetically different elementary steps. The first HA-dependent binding event is a virus concentration-dependent intermolecular process governed by a binding rate constant k_{on} with the unit M^{-1} s^{-1} and a dissociation constant k_{off} with the unit s^{-1} (Figure 11, binding event 1). Subsequent HA binding steps are intramolecular with a k_{on} (not necessarily the same as in the first step) and k_{off} both with the unit s^{-1} For IAV, having a K_D (k_{off}/k_{on}) of ~0.3 to ~3mM for a monovalent HA-receptor interaction, binding at pM concentrations inevitably results in a low binding rate, which is presumably determined by the first binding event. In Figure 7

we obtained evidence that NA with a low catalytic activity also contributes to the initial binding rate. This contributory effect could be inhibited by OC and therefore was attributed to binding of receptor to a NA catalytic site.

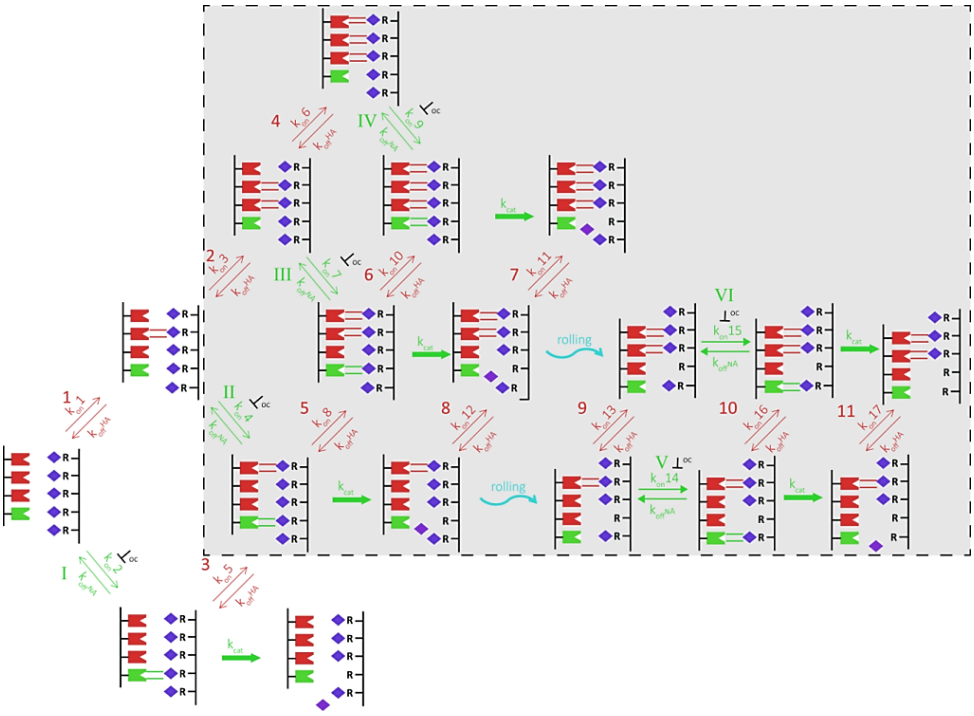

Figure 11. Kinetic model showing the basic flow of events taking place during virus particle binding. IAV binding to a receptor-coated surface (purple diamonds represent SIA) is initiated by a virus concentration-dependent step 1 (red, HA) or step I (green, NA), the equilibrium of which is governed by their respective kon and koff constants and for NA also by kcat (bold green). Enzymatic cleavage of the sialosides may cause virus dissociation. Binding via the NA active site can be inhibited by oseltamivir carboxylate. Koff/kon for NA is lower than for HA implicating that NAs with a low kcat have the potential to contribute to binding considerably. Longer lasting binding requires the formation of additional HA- and/or NA–SIA bonds (depicted in the grey shaded area actually recorded by BLI which will hardly detect the low levels of equilibrium binding in step 1 and I). During this phase HA- and NA–SIA interactions are formed and broken in a virus concentration independent mode with the result that all binding states shown here as an example, can rapidly interconvert via binding/dissociation events 2 to 11 and II to IV. The number of simultaneous interactions that can occur is logically dependent on receptor density and koff/kon ratios but how many simultaneous interactions suffice to keep a virus particle bound to the surface remains unknown although the experiments shown in Fig 2 suggest the number of interactions required is very low. Theoretically, the dynamics of HA-SIA interactions allow a virus to roll over the surface but experiments shown in Fig 9 and 10 show that NA activity strongly stimulates rolling (and eventually leads to virus dissociation). This is schematically indicated by the curled arrows where NA cleavage activity creates receptor-free positions on the surface. The receptor gradient caused in this way is probably the driving force for virus rolling but the direction in which the virus rolls (away from the empty position or "reaching over" the empty position) still needs further research.

The contribution of NA to receptor binding is determined by a dissociation constant (K_D = k_{off}/k_{off}) for the substrate and a catalytic rate constant (k_{cat}) determining the receptor cleavage rate. A lower k_{cat} will result in prolonged receptor binding before cleavage or

dissociation takes place. This will enhance the chance for additional binding events (mostly by HA), thereby promoting the cascade of multivalent interactions responsible for tight virus binding. Given the lower K_D (30μM~600μM) (44) of NA, in comparison to HA, for interaction with sialosides, the contribution to the initial binding rate by NA could be considerable even whereas the NA/HA ratio of a virus particle is generally quite low. The model also illustrates the role of NA activity in rolling by producing receptor-free spots that drive virus movement as is discussed below.

DISCUSSION

The *ménage a trois* between IAV HA, NA and (decoy) receptors is largely responsible for virus tropism and viral fitness but the interplay between these factors is still poorly understood. Here, BLI was implemented to develop highly versatile methods for quantitative and mechanistic analysis of the dynamics of IAV-receptor interactions. The results indicate that the initial binding rate is the best quantifiable parameter for comparison of receptor binding of different viruses and allows for a virus concentration-independent quantitative comparison of relative binding strength to different receptor-coated surfaces. The use of BLI revealed a contribution of NA to the initial binding rate and a critical role for HA in supporting cleavage of SIAs from a receptor-coated surface by its accompanying virion-associated NA. Analysis of virion binding in the absence of NA inhibitors enabled quantification of the HA/NA balance using empirical parameters. Dissociation of virus particles from a receptor-coated sensor was critically dependent on NA activity. Prior to dissociation, we observed NA-dependent morphological changes in receptor-associated virus particles. Strikingly, virus particles were shown to roll on a receptor-coated surface by a NA activity-driven mechanism, thereby removing SIAs from the complete sensor surface. Thus, detailed analysis of the dynamics of IAV-receptor interactions using BLI revealed novel virion phenotypes, which are likely to be of crucial importance for virus replication and host tropism *in vivo*.

The initial binding rate is the most relevant quantifiable parameter for IAV binding

A low initial binding rate, in combination with extremely high avidity resulting from concentration-independent subsequent binding events, leads to binding curves dominated by avidity effects. Over a range of virus concentrations binding slowly proceeds to a binding plateau at a level that is close to saturation of the binding surface. Importantly, these virus binding curves cannot be fitted well to 1:1 or 1:2 binding models. This probably reflects complexities related to polyvalent binding and the mechanisms by which a surface becomes fully occupied at high binding levels. Current kinetic models for polyvalent binding are inherently complex and lack general applicability (45, 46). They will therefore not assist in accurate determination of the binding constants of the different binding steps, even more so when falsely based on equilibrium binding models. Instead of

plotting initial binding rates, Benton et al (47) have used BLI as an endpoint binding assay by plotting the fractional saturation (f) of virus binding after a fixed time at a range of receptor densities (shown for our data in Figure S5C) and derived an apparent K_D for IAV-receptor interaction (K_D = ([virus](1-f))/f). This approach, like derivation of K_D values from other endpoint assays (e.g. ELISAs), assumes a simple equilibrium binding model which is discredited by the irreversible IAV binding, even at low receptor densities. Moreover, for low virus concentrations or low-avidity virus-receptor interactions, maximum binding will not be reached within the fixed time (60 min) of measurement (Figure S4A and B), thereby introducing additional errors into apparent K_D determinations.

Infection of cells requires the binding of only a few virus particles. In view of the poor reversibility of IAV binding to cells at physiological pH 7.4 (48), it is of high avidity, as was also observed in the BLI assays. We therefore consider the initial binding rate v^{obs} as the prime and most relevant quantifiable parameter for IAV binding. Determination of v^{obs} is possible by BLI, but not by endpoint assays, like glycan arrays or receptor-coated 96-well plate based assays. Virus concentration and v^{obs} displayed a strictly linear correlation and during the initial binding phase the receptor concentration behaved as an apparent constant. This provides an accurate method for comparing viruses of unknown concentration by determination of the relative binding rate constants for different receptor pairs, including synthetic glycans and recombinant proteins. The use of recombinant protein receptors enables attachment to the sensor in a homogeneous orientation by virtue of their unique tag (e.g. Fc-tag, biotinylated Bap-tag) and allows for genetic engineering resulting in the expression of specific glycosylation patterns. This will support a better systematic analysis of glycan-type (N-linked, O-linked) and glycan-density in a natural glycoprotein context than, for instance, the often used biotinylated polyacrylamide molecules carrying randomly distributed glycans and adopting a spherical conFigureuration with a ~15nm diameter (49).

Contribution of HA and NA to virion binding, receptor destruction and release

As a major advantage, real time analysis of IAV binding offers the unique opportunity to study the role of NA and the interplay between the HA and NA (HA/NA balance) in IAV-receptor binding dynamics. The results show that NA with a low catalytic activity contributes to the initial binding rate. This effect is exerted by binding of the receptor to the catalytic site as demonstrated by the inhibitory effect of OC. These findings are of relevance in view of the recent emergence of seasonal H3N2 strains displaying NA-dependent hemagglutination (42).

Whereas the NA protein can contribute to virus binding, the HA protein provides crucial support to NA in receptor destruction. Cleavage of SIAs from a receptor-coated surface was shown to be critically dependent on the ability of the HA protein to bind to this

surface. This is in agreement with the observation that antibodies targeting the HA protein can interfere with cleavage of fetuin by virus particles (50). BLI also provides us with a quantitative view on the HA/NA balance by recording virus binding/dissociation profiles in the absence of NA inhibitor. These profiles, for which no mathematical model yet exists, are affected by multiple parameters, including viruses particle number and receptor specificity of NA and HA, and are quantifiable by determining empirical parameters like initial binding rate, the area under the curve and x,y (time, binding level) coordinates of the binding peak.

NA-dependent rolling and morphological changes of virus particles

Our observations provide the mechanistic insight that IAV particles role over a receptor-coated surface driven by NA activity. The rolling phase is characterized by an initial, NA-dependent, minor increase in the apparent binding level. We propose this to represent a morphological change in the virus by adopting a "more relaxed binding mode" due to ongoing reduction of the number virus particle-receptor interactions by NA activity. The model in Figure 11 illustrates the role of NA activity in rolling by producing receptor-free spots that drive virus movement. A virus may "take a large step" by binding of virus-associated HAs to a site beyond the de-sialylated receptor. Alternatively, the virus may move away from the receptor-free spot in the direction of immediately neighboring sites with higher receptor density. Sakai *et al.* have recently studied virion movement using total internal reflection microscopy and fetuin-coated glass slides (51). Directional movement of virus particles at two different velocities, both dependent on NA activity, was reported. Earlier, others have already proposed *in vivo* functionality for IAVs having a receptor-binding and a receptor-destroying enzyme. This would enable virus movement through a mucus layer or over a cell surface by a mechanism of repeated cycles of receptor binding, receptor release and receptor cleavage (23, 24). We propose that rolling is also important for cell-to-cell virus spread. By rolling over the cell surface to the neighboring cells, viruses prevent diffusion into the extracellular milieu and avoid the first, rate-limiting, binding event for cell binding by a virus in solution. Nascent virus particles, budding from de-sialylated cells resulting from NA activity, may also benefit from virus rolling. Sialylated mucus proteins covering the epithelial cell layer prevent virus release into the extracellular milieu and may assist the virus in rolling to neighboring cells by functioning as the rolling substrate.

In conclusion, we have established a BLI-based methodology that allows quantitative determination and comparison of virus binding rates to a highly versatile, modifiable and controllable receptor repertoire. In addition, the HA/NA balance can be quantified by empirical parameters that are the resultant of different processes. Most interesting, the technique has allowed the identification of potentially highly relevant mechanistic principles of IAV-receptor binding dynamics that govern host and cell infection.

REFERENCES

1. Mitnaul LJ, Matrosovich MN, Castrucci MR, Tuzikov AB, Bovin NV, Kobasa D, et al. Balanced hemagglutinin and neuraminidase activities are critical for efficient replication of influenza A virus. Journal of virology. 2000 Jul;74(13):6015-20.
2. Rudneva IA, Kovaleva VP, Varich NL, Farashyan VR, Gubareva LV, Yamnikova SS, et al. Influenza A virus reassortants with surface glycoprotein genes of the avian parent viruses: effects of HA and NA gene combinations on virus aggregation. Archives of virology. 1993;133(3-4):437-50.
3. Rudneva IA, Sklyanskaya EI, Barulina OS, Yamnikova SS, Kovaleva VP, Tsvetkova IV, et al. Phenotypic expression of HA-NA combinations in human-avian influenza A virus reassortants. Archives of virology. 1996;141(6):1091-9.
4. Skehel JJ, Wiley DC. Receptor binding and membrane fusion in virus entry: the influenza hemagglutinin. Annual review of biochemistry. 2000;69:531-69.
5. Wilson IA, Skehel JJ, Wiley DC. Structure of the haemagglutinin membrane glycoprotein of influenza virus at 3 A resolution. Nature. 1981 Jan 29;289(5796):366-73.
6. Wiley DC, Skehel JJ. The structure and function of the hemagglutinin membrane glycoprotein of influenza virus. Annual review of biochemistry. 1987;56:365-94.
7. Shtyrya YA, Mochalova LV, Bovin NV. Influenza virus neuraminidase: structure and function. Acta naturae. 2009 Jul;1(2):26-32.
8. Air GM. Influenza neuraminidase. Influenza Other Respir Viruses. 2012 Jul;6(4):245-56.
9. Varghese JN, Laver WG, Colman PM. Structure of the influenza virus glycoprotein antigen neuraminidase at 2.9 A resolution. Nature. 1983 May 5-11;303(5912):35-40.
10. Weis W, Brown JH, Cusack S, Paulson JC, Skehel JJ, Wiley DC. Structure of the influenza virus haemagglutinin complexed with its receptor, sialic acid. Nature. 1988 Jun 2;333(6172):426-31.
11. Shinya K, Ebina M, Yamada S, Ono M, Kasai N, Kawaoka Y. Avian flu: influenza virus receptors in the human airway. Nature. 2006 Mar 23;440(7083):435-6.
12. Connor RJ, Kawaoka Y, Webster RG, Paulson JC. Receptor specificity in human, avian, and equine H2 and H3 influenza virus isolates. Virology. 1994 Nov 15;205(1):17-23.
13. Rogers GN, D'Souza BL. Receptor binding properties of human and animal H1 influenza virus isolates. Virology. 1989 Nov;173(1):317-22.
14. Rogers GN, Paulson JC. Receptor determinants of human and animal influenza virus isolates: differences in receptor specificity of the H3 hemagglutinin based on species of origin. Virology. 1983 Jun;127(2):361-73.
15. Raman R, Tharakaraman K, Shriver Z, Jayaraman A, Sasisekharan V, Sasisekharan R. Glycan receptor specificity as a useful tool for characterization and surveillance of influenza A virus. Trends in microbiology. 2014 Nov;22(11):632-41.
16. Kobasa D, Kodihalli S, Luo M, Castrucci MR, Donatelli I, Suzuki Y, et al. Amino acid residues contributing to the substrate specificity of the influenza A virus neuraminidase. Journal of virology. 1999 Aug;73(8):6743-51.
17. Franca de Barros J, Jr., Sales Alviano D, da Silva MH, Dutra Wigg M, Sales Alviano C, Schauer R, et al. Characterization of sialidase from an influenza A (H3N2) virus strain: kinetic parameters and substrate specificity. Intervirology. 2003;46(4):199-206.
18. Mochalova L, Kurova V, Shtyrya Y, Korchagina E, Gambaryan A, Belyanchikov I, et al. Oligosaccharide specificity of influenza H1N1 virus neuraminidases. Archives of virology. 2007;152(11):2047-57.
19. Dai M, Guo H, Dortmans JC, Dekkers J, Nordholm J, Daniels R, et al. Identification of Residues That Affect Oligomerization and/or Enzymatic Activity of Influenza Virus H5N1 Neuraminidase Proteins. Journal of virology. 2016 Oct 15;90(20):9457-70.

20. Sauter NK, Bednarski MD, Wurzburg BA, Hanson JE, Whitesides GM, Skehel JJ, et al. Hemagglutinins from two influenza virus variants bind to sialic acid derivatives with millimolar dissociation constants: a 500-MHz proton nuclear magnetic resonance study. Biochemistry. 1989 Oct 17;28(21):8388-96.
21. Takemoto DK, Skehel JJ, Wiley DC. A surface plasmon resonance assay for the binding of influenza virus hemagglutinin to its sialic acid receptor. Virology. 1996 Mar 15;217(2):452-8.
22. Wang CC, Chen JR, Tseng YC, Hsu CH, Hung YF, Chen SW, et al. Glycans on influenza hemagglutinin affect receptor binding and immune response. Proceedings of the National Academy of Sciences of the United States of America. 2009 Oct 27;106(43):18137-42.
23. Yang X, Steukers L, Forier K, Xiong R, Braeckmans K, Van Reeth K, et al. A beneficiary role for neuraminidase in influenza virus penetration through the respiratory mucus. PloS one. 2014;9(10):e110026.
24. Cohen M, Zhang XQ, Senaati HP, Chen HW, Varki NM, Schooley RT, et al. Influenza A penetrates host mucus by cleaving sialic acids with neuraminidase. Virology journal. 2013 Nov 22;10:321.
25. Ohuchi M, Asaoka N, Sakai T, Ohuchi R. Roles of neuraminidase in the initial stage of influenza virus infection. Microbes and infection / Institut Pasteur. 2006 Apr;8(5):1287-93.
26. Matrosovich MN, Matrosovich TY, Gray T, Roberts NA, Klenk HD. Neuraminidase is important for the initiation of influenza virus infection in human airway epithelium. Journal of virology. 2004 Nov;78(22):12665-7.
27. Wagner R, Wolff T, Herwig A, Pleschka S, Klenk HD. Interdependence of hemagglutinin glycosylation and neuraminidase as regulators of influenza virus growth: a study by reverse genetics. Journal of virology. 2000 Jul;74(14):6316-23.
28. Matrosovich M, Gao P, Kawaoka Y. Molecular mechanisms of serum resistance of human influenza H3N2 virus and their involvement in virus adaptation in a new host. Journal of virology. 1998 Aug;72(8):6373-80.
29. Pritchett TJ, Paulson JC. Basis for the potent inhibition of influenza virus infection by equine and guinea pig alpha 2-macroglobulin. The Journal of biological chemistry. 1989 Jun 15;264(17):9850-8.
30. de Vries E, de Vries RP, Wienholts MJ, Floris CE, Jacobs MS, van den Heuvel A, et al. Influenza A virus entry into cells lacking sialylated N-glycans. Proceedings of the National Academy of Sciences of the United States of America. 2012 May 08;109(19):7457-62.
31. Kaverin NV, Gambaryan AS, Bovin NV, Rudneva IA, Shilov AA, Khodova OM, et al. Postreassortment changes in influenza A virus hemagglutinin restoring HA-NA functional match. Virology. 1998 May 10;244(2):315-21.
32. Zanin M, Marathe B, Wong SS, Yoon SW, Collin E, Oshansky C, et al. Pandemic Swine H1N1 Influenza Viruses with Almost Undetectable Neuraminidase Activity Are Not Transmitted via Aerosols in Ferrets and Are Inhibited by Human Mucus but Not Swine Mucus. Journal of virology. 2015 Jun;89(11):5935-48.
33. Xu R, Zhu X, McBride R, Nycholat CM, Yu W, Paulson JC, et al. Functional balance of the hemagglutinin and neuraminidase activities accompanies the emergence of the 2009 H1N1 influenza pandemic. Journal of virology. 2012 Sep;86(17):9221-32.
34. Gambaryan AS, Matrosovich MN. What adaptive changes in hemagglutinin and neuraminidase are necessary for emergence of pandemic influenza virus from its avian precursor? Biochemistry Biokhimiia. 2015 Jul;80(7):872-80.
35. Thomas JJ, Folger EC, Nist DL, Thomas BJ, Jones RH. Km values of influenza virus neuraminidases for a new fluorogenic substrate, 4-methylumbelliferone N-acetyl neuraminic acid ketoside. Analytical biochemistry. 1978 Aug 1;88(2):461-7.
36. Weber PC, Ohlendorf DH, Wendoloski JJ, Salemme FR. Structural origins of high-affinity biotin binding to streptavidin. Science. 1989 Jan 06;243(4887):85-8.

37. Ren CL, Carvajal D, Shull KR, Szleifer I. Streptavidin-biotin binding in the presence of a polymer spacer. A theoretical description. Langmuir : the ACS journal of surfaces and colloids. 2009 Oct 20;25(20):12283-92.
38. Gambaryan AS, Matrosovich MN. A solid-phase enzyme-linked assay for influenza virus receptor-binding activity. Journal of virological methods. 1992 Sep;39(1-2):111-23.
39. Stevens J, Corper AL, Basler CF, Taubenberger JK, Palese P, Wilson IA. Structure of the uncleaved human H1 hemagglutinin from the extinct 1918 influenza virus. Science. 2004 Mar 19;303(5665):1866-70.
40. Uhlendorff J, Matrosovich T, Klenk HD, Matrosovich M. Functional significance of the hemadsorption activity of influenza virus neuraminidase and its alteration in pandemic viruses. Archives of virology. 2009;154(6):945-57.
41. Kobasa D, Rodgers ME, Wells K, Kawaoka Y. Neuraminidase hemadsorption activity, conserved in avian influenza A viruses, does not influence viral replication in ducks. Journal of virology. 1997 Sep;71(9):6706-13.
42. Lin YP, Gregory V, Collins P, Kloess J, Wharton S, Cattle N, et al. Neuraminidase receptor binding variants of human influenza A(H3N2) viruses resulting from substitution of aspartic acid 151 in the catalytic site: a role in virus attachment? Journal of virology. 2010 Jul;84(13):6769-81.
43. Hooper KA, Bloom JD. A mutant influenza virus that uses an N1 neuraminidase as the receptor-binding protein. Journal of virology. 2013 Dec;87(23):12531-40.
44. Zhu X, McBride R, Nycholat CM, Yu W, Paulson JC, Wilson IA. Influenza virus neuraminidases with reduced enzymatic activity that avidly bind sialic Acid receptors. Journal of virology. 2012 Dec;86(24):13371-83.
45. Xu H, Shaw DE. A Simple Model of Multivalent Adhesion and Its Application to Influenza Infection. Biophysical journal. 2016 Jan 05;110(1):218-33.
46. Huskens J, Mulder A, Auletta T, Nijhuis CA, Ludden MJ, Reinhoudt DN. A model for describing the thermodynamics of multivalent host-guest interactions at interfaces. Journal of the American Chemical Society. 2004 Jun 02;126(21):6784-97.
47. Benton DJ, Martin SR, Wharton SA, McCauley JW. Biophysical measurement of the balance of influenza a hemagglutinin and neuraminidase activities. The Journal of biological chemistry. 2015 Mar 06;290(10):6516-21.
48. Matlin KS, Reggio H, Helenius A, Simons K. Infectious entry pathway of influenza virus in a canine kidney cell line. The Journal of cell biology. 1981 Dec;91(3 Pt 1):601-13.
49. Bovin NV. Polyacrylamide-based glycoconjugates as tools in glycobiology. Glycoconjugate journal. 1998 May;15(5):431-46.
50. Kosik I, Yewdell JW. Influenza A virus hemagglutinin specific antibodies interfere with virion neuraminidase activity via two distinct mechanisms. Virology. 2017 Jan;500:178-83.
51. Sakai T, Nishimura SI, Naito T, Saito M. Influenza A virus hemagglutinin and neuraminidase act as novel motile machinery. Scientific reports. 2017 Mar 27;7:45043.
52. de Vries E, Tscherne DM, Wienholts MJ, Cobos-Jimenez V, Scholte F, Garcia-Sastre A, et al. Dissection of the influenza A virus endocytic routes reveals macropinocytosis as an alternative entry pathway. PLoS pathogens. 2011 Mar;7(3):e1001329.
53. Fodor E, Devenish L, Engelhardt OG, Palese P, Brownlee GG, Garcia-Sastre A. Rescue of influenza A virus from recombinant DNA. Journal of virology. 1999 Nov;73(11):9679-82.
54. Koel BF, Burke DF, Bestebroer TM, van der Vliet S, Zondag GC, Vervaet G, et al. Substitutions near the receptor binding site determine major antigenic change during influenza virus evolution. Science. 2013 Nov 22;342(6161):976-9.
55. Link AJ, LaBaer J. Trichloroacetic acid (TCA) precipitation of proteins. Cold Spring Harbor protocols. 2011 Aug 01;2011(8):993-4.

56. Corti D, Voss J, Gamblin SJ, Codoni G, Macagno A, Jarrossay D, et al. A neutralizing antibody selected from plasma cells that binds to group 1 and group 2 influenza A hemagglutinins. Science. 2011 Aug 12;333(6044):850-6.
57. de Vries RP, de Vries E, Bosch BJ, de Groot RJ, Rottier PJ, de Haan CA. The influenza A virus hemagglutinin glycosylation state affects receptor-binding specificity. Virology. 2010 Jul 20;403(1):17-25.
58. Blixt O, Westerlind U. Arraying the post-translational glycoproteome (PTG). Current opinion in chemical biology. 2014 Feb;18:62-9.
59. de Vries RP, de Vries E, Moore KS, Rigter A, Rottier PJ, de Haan CA. Only two residues are responsible for the dramatic difference in receptor binding between swine and new pandemic H1 hemagglutinin. The Journal of biological chemistry. 2011 Feb 18;286(7):5868-75.
60. Imai M, Mizuno T, Kawasaki K. Membrane fusion by single influenza hemagglutinin trimers. Kinetic evidence from image analysis of hemagglutinin-reconstituted vesicles. The Journal of biological chemistry. 2006 May 05;281(18):12729-35.
61. Harris A, Cardone G, Winkler DC, Heymann JB, Brecher M, White JM, et al. Influenza virus pleiomorphy characterized by cryoelectron tomography. Proceedings of the National Academy of Sciences of the United States of America. 2006 Dec 12;103(50):19123-7.
62. Inglis SC, Carroll AR, Lamb RA, Mahy BW. Polypeptides specified by the influenza virus genome I. Evidence for eight distinct gene products specified by fowl plague virus. Virology. 1976 Oct 15;74(2):489-503.
63. Dai M, McBride R, Dortmans JC, Peng W, Bakkers MJ, de Groot RJ, et al. Mutation of the Second Sialic Acid-Binding Site, Resulting in Reduced Neuraminidase Activity, Preceded the Emergence of H7N9 Influenza A Virus. Journal of virology. 2017 May 01;91(9).

SUPPLEMENTARY FIGURES

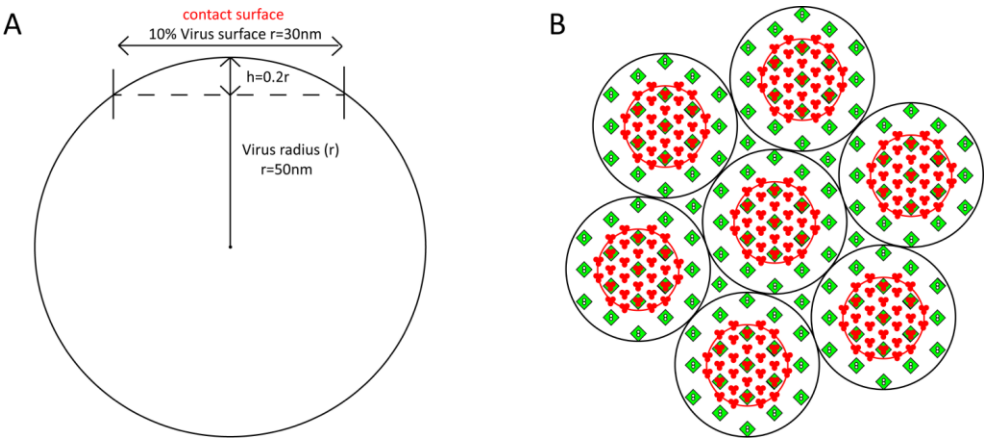

Figure. S1. Additional information on geometry of IAV virus particles and SA sensor loading
(A) Labstrains PR8 and WSN have repeatedly been reported to be spherical viruses with a diameter of ~ 100 nm in close agreement with our own quantitative analysis of HA and NA content (Figure. S2). For our model we assume that virus particles can be flattened during binding for 0.2 times the radius allowing 10% of the virus surface to be in contact with the sensor. (B) Representation of a sensor fully loaded with virus particles (hexagonal packaging) showing the large fraction of SA molecules that are not present at the contact interface and therefore cannot interact with HA and NA without virus movement.

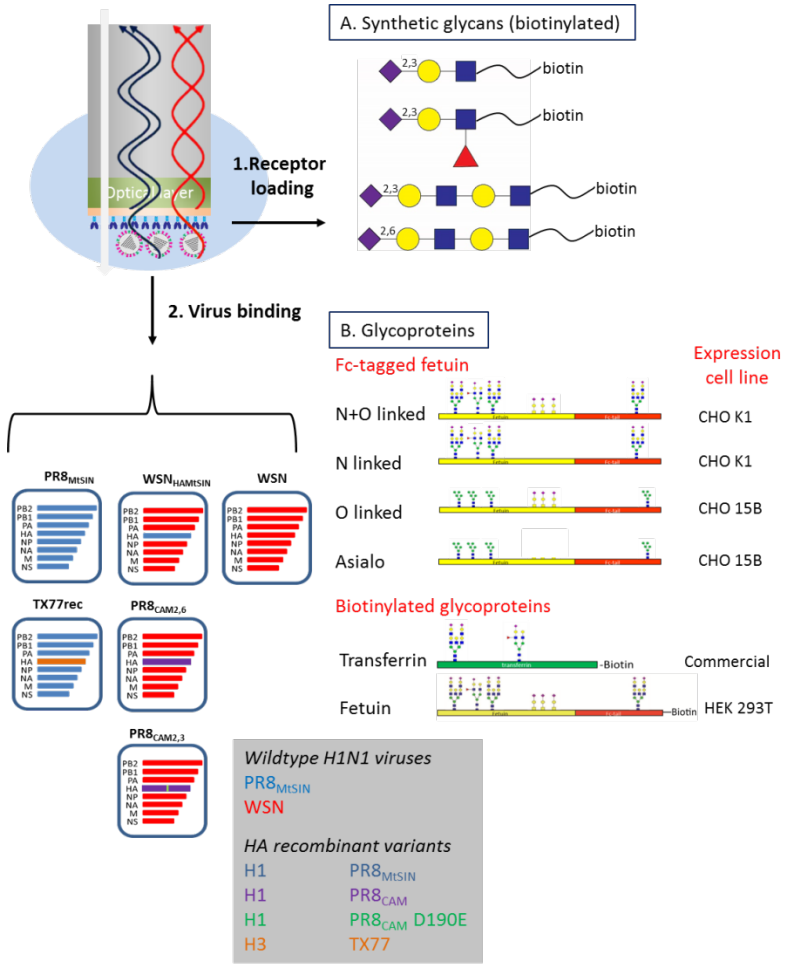

Figure S2. Schematic overview of receptors and viruses used for BLI in this report. Biotinylated receptors (synthetic glycans or glycoproteins) were bound to SA sensors whereas Fc-tagged glycoproteins were bound to Protein A sensors. Expression of fetuin in CHO k1 cells yields 3'N+O fetuin carrying exclusively α2,3-linked sialic acids (both on N-linked and O-linked glycans). Expression of fetuin in CHO 15B cells (deficient in N-acetylglucosamine transferase I) yields 3'O fetuin with sialylated O-linked glycans but immature N-linked glycans that are not sialylated. Wild type fetuin carries 3 N-linked glycans and 3 O-linked glycans. Expression of a fetuin-encoding plasmid in which the O-linked glycosylation sites are removed by site-directed mutagenesis yields 3'N fetuin upon expression in CHO k1 cells and asialo fetuin upon expression in CHO 15B cells. Biotinylated transferin is commercially available and carries two α2,6 N-linked glycans. Biotinylated fetuin was made by expressing a construct encoding a Bap-tag fused to fetuin that, by co-transfection with a plasmid carrying a biotinylation enzyme, yields C-terminally biotinylated fetuin upon expression in CHO K1 cells. Viruses used for binding to receptor-loaded sensors are wild type $PR8_{MtSIN}$, wild type WSN and recombinant viruses carrying the HA encoding segments of $PR8_{MtSIN}$ ($WSN_{HAMtSIN}$) or $PR8_{CAM}$ ($PR8_{CAM2,6}$) in the background of seven WSN segments. $PR8_{CAM2,3}$ is identical to $PR8_{CAM2,6}$ except for a substitution (D190E) that was introduced in HA to obtain a shift from α2,6 to α2,3 linkage-type binding specificity. TX77 carries the HA encoding segment of A/Bilthoven/1761/76 (H3N2) in the background of seven $PR8_{MtSIN}$ segments (54)

Virus particle quantification

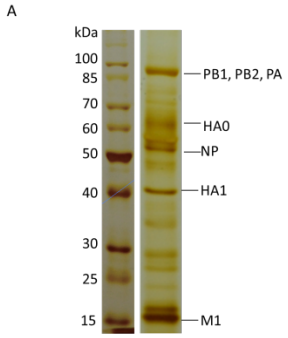

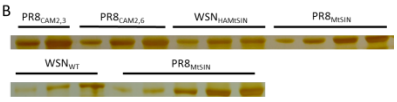

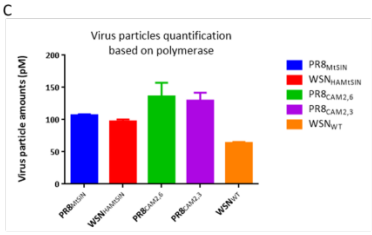

HA protein quantification

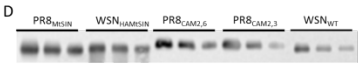

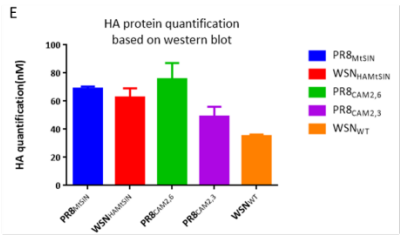

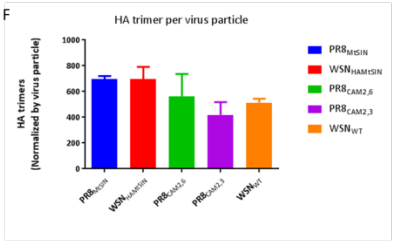

NA protein quantification

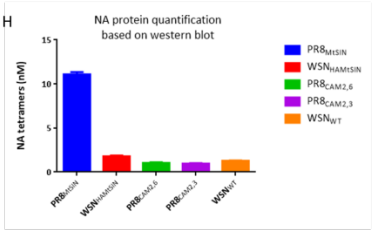

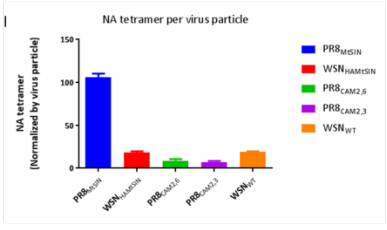

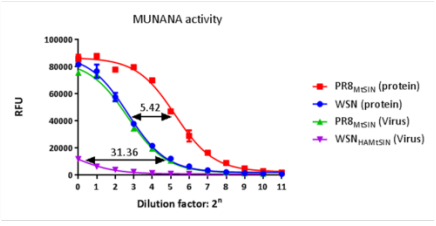

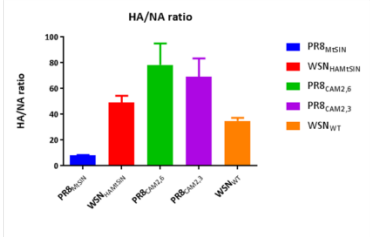

Figure S3. Quantification of virus particle number and HA and NA content. Highly precise determination of virus concentration is crucial for reliable determination of k_{on}. Hemagglutination titers or infectious titers have been used for this purpose but do not reveal actual particle numbers and are inadequate for determination of relative particle numbers of different viruses. Quantitative PCR or Western blotting (usually targeting NP) are sensitive to variation caused by RNA or protein contamination of virus preparations and, when comparing different viruses, to differences in specificity of probes or antibodies. Therefore, virus particle number was quantified by densitometric analysis of the polymerase content of a virus preparation assuming that every particle carries eight genome segments, each attached to a heterotrimeric complex of the three polymerase subunits PB1, PB2 and PA. (A) Silver-stained SDS-PAGE gel showing the separation of a MW marker and a $PR8_{MtSIN}$ virus stock. (B) Silver-stained region showing the polymerase complex (PB1, PB2 and PA appearing as a single band due to similar size) of a dilution series of five virus stocks. Densitometric scanning allowed absolute quantification using a dilution series of the molecular marker shown in (A) for calibration. (C) Estimated concentration of virus stocks in pM. For calculation a MW of 250 kDa for the the polymerase complex (PB1/PB2/PA) was taken. (D) Western blot showing the staining of the HA0 band of a concentration series of five viruses using monoclonal antibody FI6 recognizing a universally conserved epitope localized in the stem of HA. Quantification was performed by densitometric scanning (E) Absolute quantification of HA trimers in nM was performed by calibration using a Western blot in which a standard concentration series of $PR8_{MtSIN}$ and WSN HA proteins expressed in HEK293S cells (30) was included. (F) Number of HA trimers per virus particle as derived from (C) and (E). The obtained numbers/particle fit well to numbers reported in literature and obtained by different methods by others (61, 62) showing the accuracy of the method. (G, H, I) Quantification of NA by similar procedures as applied for HA in panel D-F. Antibodies GT288-GTX629696 (WSN) and N1-7D3 (PR8) were used and quantification was calibrated using a Western blot of a standard concentration series of NA of $PR8_{MtSIN}$ and WSN expressed in HEK293T cells. The NA proteins were expressed similarly are described previously (63) that was run in paralel. (J) NA activity of $PR8_{MtSIN}$ and WSN virus particles and expressed recombinant NA soluble tetramers was determined using a two-fold dilution series in a soluble substrate NA activity assay (MUNANA assay). (K) HA/NA ratio was determined from panels F and I. Error bars indicate standard deviations (N=2).

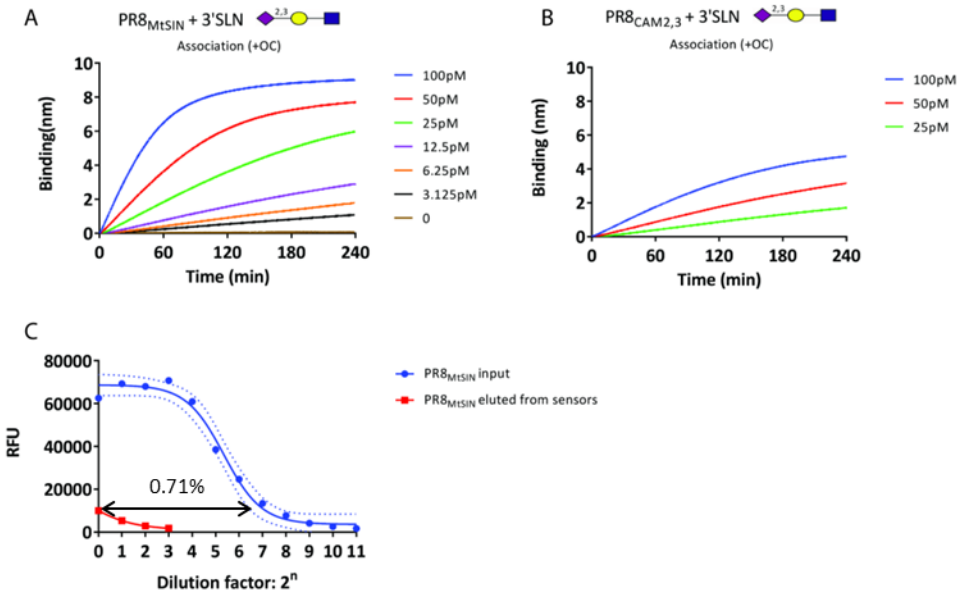

Figure S4. Prolonged binding of $PR8_{MtSIN}$ or $PR8_{CAM2,3}$ and virus fraction bound to sensor. $PR8_{MtSIN}$ (A) or $PR8_{CAM2,3}$ (B) were bound to 3'SLN for 240 min at the indicated concentrations. (C) NA activity of $PR8_{MtSIN}$ virus particles after complete dissociation from a maximally loaded sensor (3'SLN receptor) by self-elution in 100 µl PBS was determined in comparison to 100 µl 100 pM $PR8_{MtSIN}$ used for initial loading using two-fold dilutions in a MUNANA assay. The results indicate that approximately 0.71% of the virus particles present during the initial loading were associated to the sensor surface.

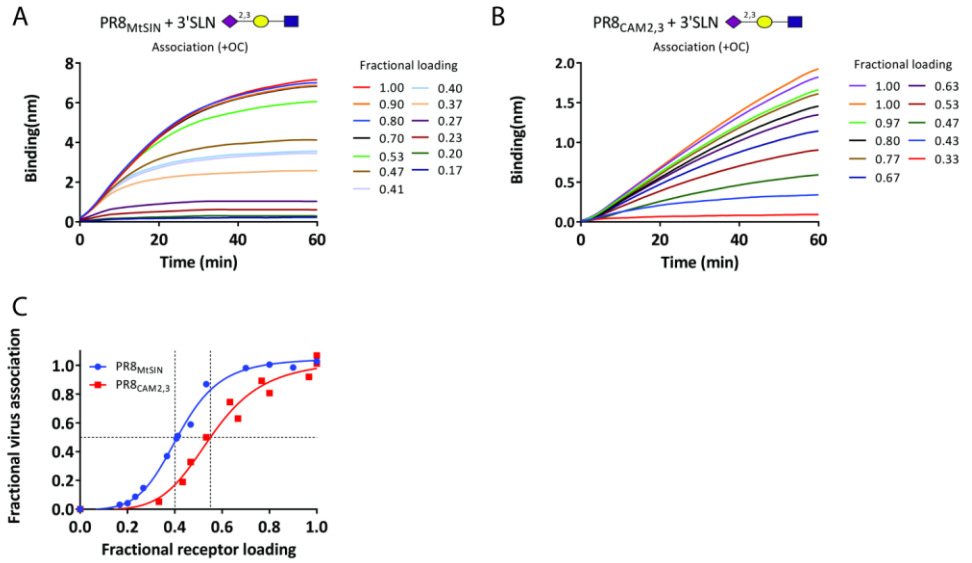

Figure S5. The effect of receptor density on virus binding. (A, B) Biotinylated 3'SLN was loaded to the sensors at a density range as indicated in the Figure (fractional loading of 1.0 corresponds to a sensor maximally loaded with receptor) followed by binding of 100 pM $PR8_{MtSIN}$ or $PR8_{CAM2,3}$ virus. (C) Relative virus association was plotted against fractional receptor loading.

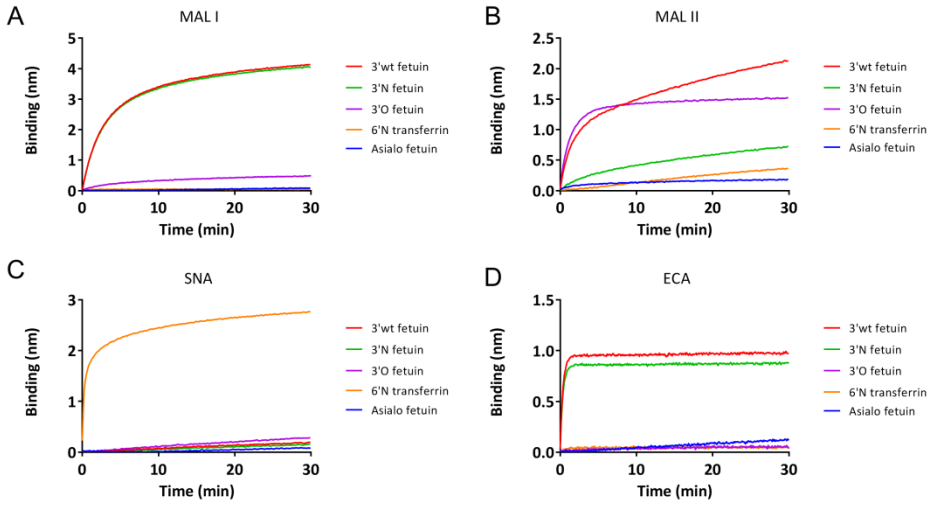

Figure S6. Analysis of SIA linkage-type specificity of glycoproteins using lectin binding. The glycoproteins used in the paper and outlined in Figure S1 were analyzed for linkage type specificity of their sialic acids using lectins MAL I (A; specific for SIAα2,3Galα1,4GlcNAc linkages abundantly present on N-linked glycans), MAL II (B; specific for SIAα2,3Galα1,3GalNAc linkages abundantly present on O-linked glycans) and SNA (C; specific for SIAα2,6Galα1,4GlcNAc linkages abundantly present on N-linked glycans). (D) ECA binding specific for terminal Galα1,4GlcNAc epitopes present on non-sialylated N-linked glycan antennae).

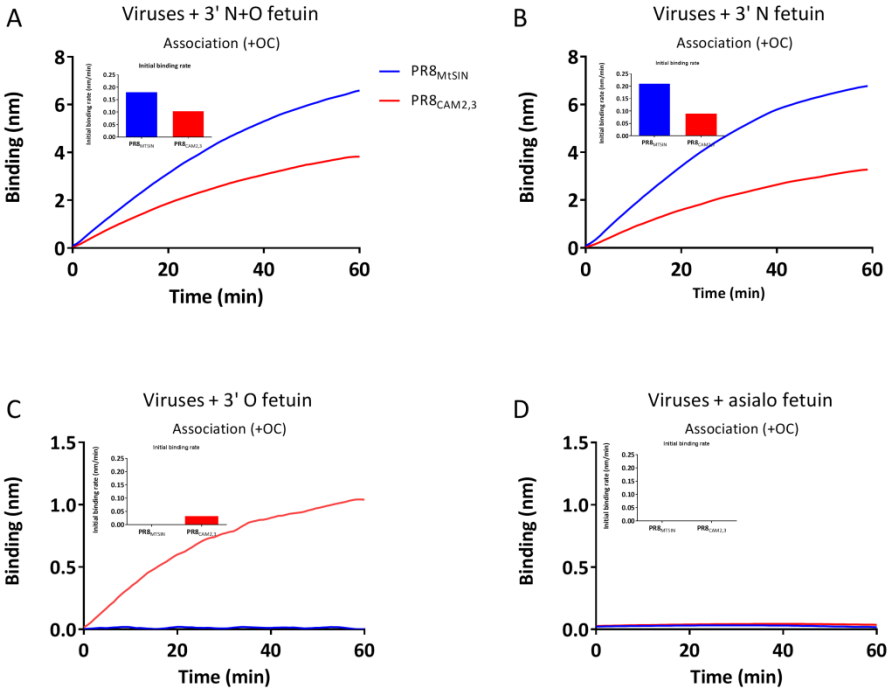

Figure S7. Quantification of binding specificity to N-linked or O-linked glycoproteins. (A-D) Fc-tagged fetuin specifically engineered and expressed to carry either exclusively N-linked or O-linked glycans, a mixture of both glycan types (N+O), or no sialylated glycans at all (asialo fetuin) was loaded to Protein A to maximum levels after which binding of 100 pM $PR8_{MtSIN}$ and $PR8_{CAM2,3}$ was performed. 10 µM OC was present during virion binding. The initial binding rates were calculated and plotted in the bar diagram inserts.

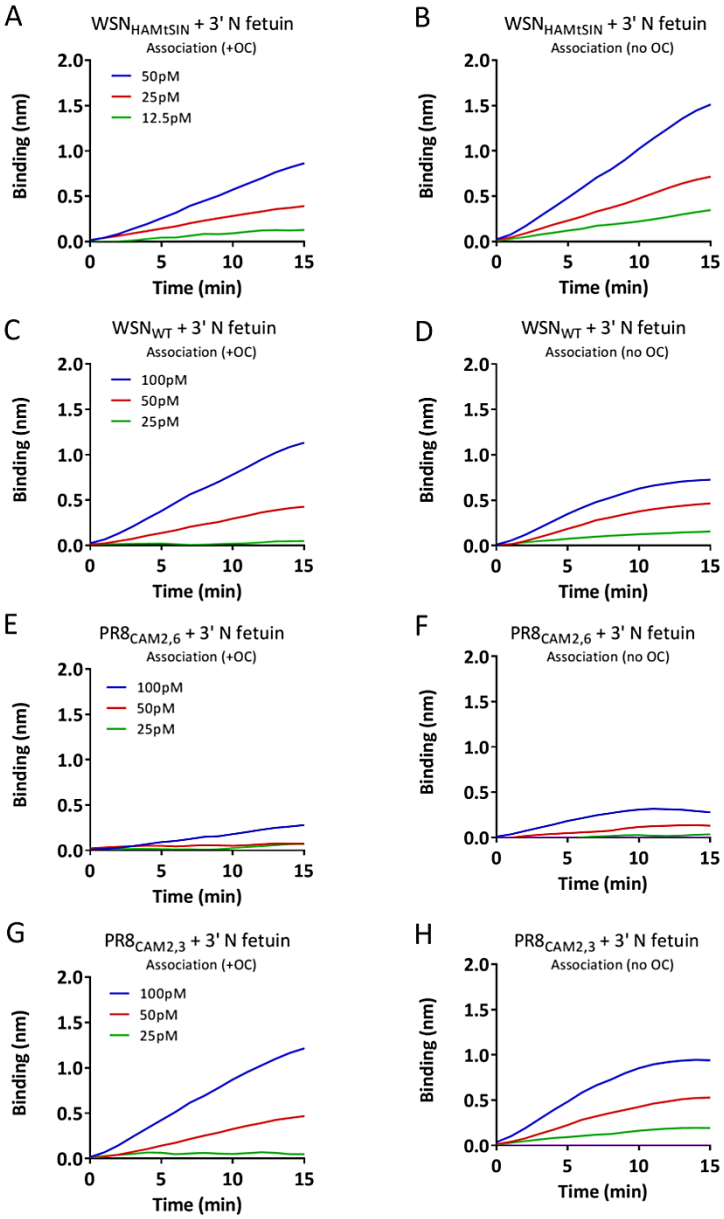

Figure S8. The NA activity-driven self elution rate depends on virus binding level. Four viruses (A-B, WSN$_{HAMtSIN}$; C-D, WSN$_{WT}$; E-F, PR8$_{CAM2,6}$; G-H, PR8$_{CAM2,3}$) all carrying the same NA (NA$_{WSN}$) but a different HA were bound to Fc-tagged 3'N fetuin loaded to maximum level at three virus concentrations as indicated in the panels. Viruses were bound for 15 min in presence (A, C, E, G) or absence (B, D, F, H) of 10 µM OC.

Chapter 3

Time-dependent maturation of influenza A virus-receptor interactions reduces disruption of virus-receptor complexes by antibodies or mucus

Hongbo Guo[1], Wenjuan Du[1], Floor van der Vegt[1], Jack Li[2], Geert Jan Boons[2], Frank J. van Kuppeveld[1], Erik de Vries[1]*, Cornelis A. de Haan[1]*.

1 Virology Division, Department of Infectious Diseases & Immunology, Faculty of Veterinary Medicine, Utrecht University, Yalelaan 1, 3584CL Utrecht, the Netherlands.

2 Department of Chemical Biology and Drug Discovery, Utrecht Institute for Pharmaceutical Sciences and Bijvoet Center for Biomolecular Research, Utrecht University, 3584 CG Utrecht, the Netherlands

(*co-coresponding author)

Manucsript in preparation

ABSTRACT

Influenza A virus (IAV)-receptor interactions determine the ability of IAV particles to traverse the mucus layer, to become endocytosed upon cell binding and to be transmitted to other cells and hosts. However, the dynamics of these virus-receptor interactions are still poorly understood. Here, we analyzed the dynamics of IAV-receptor interactions using different sialylated glycoproteins, mimicking potential receptors *in vivo*, with biolayer interferometry. The initial binding rate to, as well as neuraminidase (NA)-dependent virion rolling on, and self-elution from receptor-coated surfaces were shown to depend on receptor density and identity. Although virus dissociation is negligible in the absence of NA activity, the highly dynamic interactions between hemagglutinin (HA) and its receptor resulted in dissociation of virus particles from a receptor-coated surface in the presence of specific antibodies or mucus. Remarkably, reduced levels of virus self-elution and mucus- or antibody-driven dissociation could be observed after prolonged virus-receptor association times. We refer to this time-dependent increase in binding affinity as maturation of virus binding. Maturation of IAV-receptor binding presumably results from the simultaneous interaction of multiple HA protomers in HA trimer with a receptor-containing surface. This hitherto unrecognized feature is important for IAV biology and is proposed to also occur for other enveloped viruses.

INTRODUCTION

Influenza A virus (IAV) is an enveloped, negative-strand RNA virus that causes respiratory and/or intestinal infections in a variety of hosts, among which humans, swine, wild water fowl and poultry are the most important. IAV-receptor interaction is a crucial factor of host, tissue and cell specificity and a key determinant of the zoonotic potential of swine and avian IAVs. Upon infection of a host, IAV particles interact with a diverse repertoire of potential receptors in a highly dynamic fashion.

Upon IAV infection of a human host, IAV particles moves to their target cells in tissues of the respiratory tract by traveling over a considerable distance while encountering a diverse repertoire of potential sialic acid (SIA) receptors. They also need to traverse a thick mucus layer full of potential SIA decoy receptors, which may trap the IAV particles (1). Having arrived at the epithelial cell layer IAV needs to find receptors on permissive cells, binding to which results in endocytic uptake (2). Even during endosomal traffic and fusion of the viral envelope with the endosomal membrane virus-receptor interactions have been shown to be involved (3-5). New virus particles budding from the plasma membrane, again encounter the overlaying mucus layer, before they can infect neighboring or distantly located cells (1). Alternatively, they embark in aerosolic droplets or other secretions for transmission to a new host. To be able to move and to avoid getting trapped by the diverse repertoire of (decoy) receptors encountered, IAV-receptor interactions need to be highly dynamic and precisely tuned. These dynamic interactions are affected by the functional balance between the activities of the hemagglutinin (HA) attachment protein and the neuraminidase (NA) protein, which is a receptor-destroying enzyme (6-8).

IAV (decoy) receptors are SIAs present on the host cell surface and soluble molecules like mucins. SIA is a terminal monosaccharide attached to the penultimate glycan residue via either an α2,3- or α2,6-linkage that determines host-specificity (9-11). Fine specificity is determined by variation and/or modification of sub-terminal residues that also interact with HA (12-14). Cell surface glycan composition is complex and varies between host and cell type. Sialylated glycans are attached to glycoproteins proteins via asparagine (N-linked glycans) or serine/threonine (O-linked glycans) residues or to membrane phospholipids. Glycans belonging to these three groups are highly diverse and include group-specific glycan structures as well as structures shared between the three groups. These three types of glycans may, besides having a specific function in virus attachment, also specifically affect the efficiency of virus entry. Sialylated N-linked glycans are generally considered as IAV receptors (15). It has been shown, however, that IAV can enter into cells lacking sialylated N-glycans (16). Modifications (e.g. fucosylation or sulfation) at the sub-terminal glycans could also affect virus binding properties (**Chapter 2**)(17-19).

High receptor density at the cell surface and a high HA-receptor binding affinity are

considered to be prime requirements for an efficient primary interaction leading to productive infection (20). The binding between a single pair of HA and SIA molecules is weak (K_D ~ 0.3-3 mM) (3, 21, 22). Multivalent interactions between HA and SIA molecules at the contact surface collectively ensure that the virus adheres to the host cell with high avidity. It has been estimated that binding affinity between IAV and a receptor surface is approximately 10-25pM (22). We recently estimated by BLI that ~7 HAs can interact simultaneously with a sialylated receptor surface study (**Chapter 2**), which gives rise to virtually irreversible binding.

Despite the extremely high avidity binding, IAV is not expected to bind in a static mode upon initial cell contact but probably travels along cilia and over the cell surfaces to sites appropriate for endocytosis (2, 23, 24). We recently demonstrated by BLI that IAV particles, while remaining tightly associated with a receptor-coated surface, can move over such a surface in an NA activity dependent mode (**Chapter 2**). We concluded that the balance between the very weak binding affinity of a monomeric HA-SIA interaction and the specific activity of the NA is a key factor in the dynamics of IAV-receptor binding. Others have recently visualized NA dependent motion over fetuin-coated glass surfaces by microscopic methods (25). Single virus particle tracking by live microscopy with high spatio-temporal resolution has visualized IAV entry from the moment that virus particles become tightly stuck at a spot on the plasma membrane. There they induce unusually fast de novo formation of clathrin-coated pits, after which the virus particles are endocytosed by the host cells (2). However, tracking of virions prior to their immobilization at the cell surface is technically challenging and has not been shown thus far.

The initial interaction of IAVs infecting a new host occurs with respiratory tract mucus. This mucus layer is an important determinant of infectivity and transmissibility of respiratory pathogens (1). Mucins comprise a significant portion of airway mucus and contribute to the barrier function of mucus. Mucins are heavily glycosylated, mostly in an O-linked form, and have a high SIA content (26). Species-specific differences of the glycosylation pattern of mucins are known to exist (27). HA of IAV can bind to SIAs present on mucins, which therefore may potentially block infection. NA facilitates infection by cleaving SIAs on mucins, thereby preventing viruses from becoming trapped before they infect the epithelium (28-30). It is therefore essential to include the role of mucus in experimental assays aimed at unraveling the dynamics of IAV-receptor interactions.

We recently established BLI-based assays for studying IAV-receptor interactions in the presence of an active NA (**Chapter 2**), which enabled the identification of novel aspects of IAV binding dynamics. These aspects included particle rolling over receptor-coated surfaces, NA activity-dependent morphological changes of surface-bound particles and a contribution of NA to the initial binding rate. The initial binding rate of a virus particle is determined by the K_D of monovalent HA-SIA interactions, NA cleavage rate and receptor

density (**Chapter 2**). We consider the initial binding rate of a virus particle as the most relevant parameter for quantifying of IAV-receptor binding as it relates to a critical step during an in vivo infection. For binding of epithelial cell surfaces, speed is more relevant than equilibrium or maximum binding levels that are probably only reached long after the induction of endocytosis. Here we used different synthetic glycans as well as recombinant glycoproteins, presenting a biologically relevant glycan repertoire, to study the dynamics of IAV-receptor interactions using BLI. The highly dynamic IAV-receptor interactions were shown to become much tighter over time, the magnitude of the effect depending on the exact nature and density of the receptor. Importantly, this change directly interferes with the protective properties of specific antibodies and mucus, of which the effects could be quantified by BLI.

MATERIALS AND METHODS

Cells and Viruses. Madin–Darby canine kidney (MDCK)-II, HEK 293T cells were maintained as described previously (16, 51). Influenza A/Puerto Rico/8/34/Mount Sinai (PR8) was grown in MDCK-II cells as described previously (51) and stored at −80 °C. Virus titers were determined by measuring the TCID50 on MDCK-II cells. TX77 is recombinant virus on the background PR8 with HA from A/Bilthoven/1761/76, amino acid sequence of which was consensus in that cluster (52).

Genes, Expression Vectors, and Protein Expression and Purification. Codon-optimized human Fetuin, ICAM1, Glycophorin A and LAMP1 ectodomain-encoding cDNAs (GenScript, Piscataway, NJ, USA) were genetically fused to a Fc-tag, for protein-A based purification, and a Bap-tag (53), for binding to octet sensors, and cloned in a pCAGGs vector. The accession numbers of Fetuin, ICAM 1, Glycophorin A and LAMP1 are [P12763][P05362][P02724][P11279], respectively. Human ST3Gal1, ST3Gal4 and ST6Gal1 expression vectors were kindly provided by Dr. Raoul de Groot.

Chemicals. Oseltamivir Carboxylate (OC) was obtained from Roche, dissolved in DMSO at 100 Mm concentration, aliquoted and stored at -20°C. Mal I, Mal II, SNA, and ECA were obtained from VectorLabs. Mucus from primary human epithelial nasal cell air-to-liquid cultures is from Epithelix. PR8 HA antibody was obtained from NIBSC. Biotinylated synthetic glycans 3'SLN, 3'SLNLN, 3'SLNLN-PAA and 6'SLNLN were obtained from the Consortium for Functional Glycomics (CFG) or synthesized in house.

Biolayer interferometry. BLI analysis was performed on an Octet RED384 machine using standard streptavidin (SA) sensors (all from Pall-FortBio). PBS with calcium and magnesium (PBS+/+) was used as standard assay buffer. Receptor loading was performed by loading biotinylated receptors (synthetic glycans or proteins) to SA sensors. Receptor loading and virus association and dissociation steps were performed as described previously. (1st Octet paper). Virus-receptor association times are indicated in the text or

in the legends. When indicated, sensors were subjected to prolonged association times in the presence of OC in the absence of free virus particles. When indicated different dilutions of antibodies or mucus samples were added during or after virus association in presence of OC.

Hemaglutination elution assay. Hemaglutination assays (HA) were performed for one, two or four hours in V-shape 96-well plates. Two-fold dilutions of viruses were applied in this assay, with initial amount of 50µl of viruses. After dilution, 50µl 0.5% human erythrocytes was added to each dilution. After hemagglutination, plates were incubated at 37°C. The HA titers were checked for every 30 min.

Statistical analysis. Each virus-receptor interaction BLI experiment was repeated at least twice. Representative experiments were graphed. Significant differences between linear curves were analyzed by IBM SPSS statistic 24. Fractional receptor densities correlating with half maximum initial binding rates were determined by non-linear regression analysis using Graphpad Prism 7.04 software. Significance analysis was based on two tailed unpaired t test or one way ANOVA (GraphPad Prism 7.04).

RESULTS

Maturation of virus binding to synthetic glycans.

Previously, we showed that virus particles roll over a receptor-coated surface in a NA-dependent manner, thereby cleaving SIA receptors until the density thereof is too low to sustain virus particle binding (**Chapter 2**). In these experiments, the removal of SIAs from the receptor-coated surface was demonstrated by probing virus binding to the sensor after regeneration of the sensors by three washes in a buffer with a pH of 2. Regeneration resulted in efficient removal of receptor-bound virus particles and virus binding/regeneration cycles could be reproduced six times, using the same receptor-loaded sensor (**Chapter 2**). However, virus association times longer than 30 minutes reduced the reproducibility of virus binding when using regenerated sensors loaded with synthetic glycans. We therefore compared the effectivity of regeneration after 15 or 60 minutes of virus binding. H1N1 lab strain A/Puerto Rico/8/34/Mount Sinai (PR8) was associated for 15 min (Figure 1A, blue line) or 60 min (Figure 1B, blue line) to 3'SLNLN (Neu5Acα2-3Galβ1-4GlcNAcβ1-3Galβ1-4GlcNAc) after which the sensors were regenerated and re-associated with PR8. The re-association rate of PR8 to the sensors was not affected after 15 min of initial binding (Figure 1A, red line). However, binding was severely reduced after 60 min of initial binding (Figure 1B, red line). We also determined the efficiency of regeneration by detecting the amount virus particles that remain attached to the sensor after regeneration with an antiserum against PR8. The results only showed high residual levels of virus binding upon regenaration after 60 min of association

(Figure 1C). Thus, virus binding becomes tighter during prolonged binding, to such an extent that a large fraction of the virus particles even withstands sensor regeneration at pH 2. In Figure 1D, changes in binding strength were shown to be of functional importance by affecting NA-activity dependent self-elution. PR8 was bound for 15 min to two 3'SLNLN-coated sensors in the presence of the NA inhibitor oseltamivir carboxylate (OC). One sensor was directly subjected to NA-dependent self-elution (Figure 1D, blue line), while the other sensor was incubated for another 120 min in PBS containing OC (in the absence of free virus particles) prior to self-elution (Figure 1D, red line). 56% of the virus particles that were bound for 15 min, self-eluted in 20 min. In contrast, virus particles bound for 135 min did not self-elute from 3'SLNLN. The negative fractional dissociation that was observed after prolonged binding, was previously studied (**Chapter 2**) and may reflect a NA activity dependent change in virus association to the sensor surface (**Chapter 2**). We conclude that virus binding to a synthetic glycan-coated surface becomes tighter during prolonged binding, resulting in less efficient NA activity-dependent self-elution. We further refer to this process as maturation of virus binding.

Expression of tailor-made glycoproteins

Although synthetic glycans are abundantly applied in endpoint-binding assays (31), and occasionally in BLI assays (31, 32), they do not reflect the diversity of the natural N- or O-linked glycan chain receptor repertoire. Phenomena like binding maturation and virus rolling might depend on the regular, high density, distribution patterns of synthetic glycans on a coated surface and need to be confirmed using glycoproteins. Often used, and commercially available, transferrin and fetuin serum glycoproteins only have a limited number of glycan chains in contrast to the abundant glycosylation often found on cell surface proteins. We therefore expressed in HEK293T cells, in addition to fetuin (3 N- and 3 O-linked glycans), three human transmembrane glycoproteins with a different distribution of N- and/or O-linked glycans. These were selected to represent functional cell surface receptors (ICAM1, 9 N-linked glycans; LAMP1, 18 N- and 6 O-linked glycans) or mucin-like decoy receptors (Glycophorin A, 1 N- and 16 O-linked glycans) and were equipped with an Fc-tag and a BAP-tag for purification and biotinylation purposes (Figure. 2A). After Fc-tag mediated purification using protein A beads, these C-terminally biotinylated glycoproteins can be irreversibly (KD ~10-14 M) attached to streptavidin-coated (SA) sensors in a uniform orientation.

The glycan profiles of the four proteins were characterized by lectin binding (Figure 2B) and the binding levels observed after 15 minutes are listed in Table 1. The glycan profiles were also characterized after co-expression with the sialyltransferase ST6Gal1 in order to

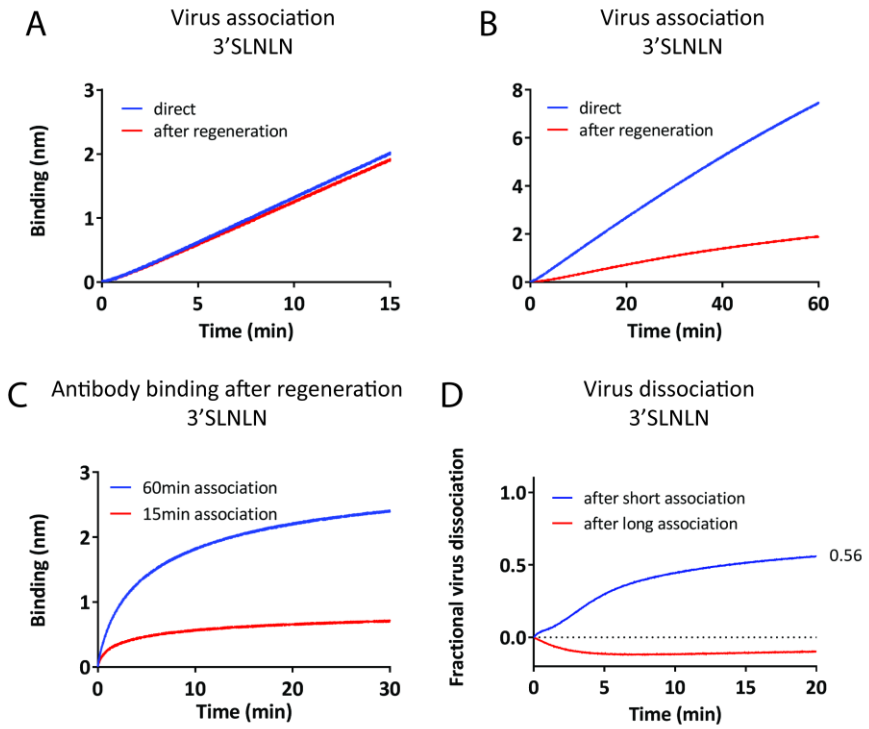

Figure. 1. Maturation of virus binding to synthetic glycans. A) PR8 (100 pM) binding to 3'SLNLN in the presence of OC was recorded for 15 min (blue line). Subsequently, virus particles were removed by regeneration at pH2 and the sensor was reassociated with PR8 for 15min (red line). B) The experiment shown in panel A was repeated but this time binding times were extended to 60 min. C) 3'SLNLN-coated sensors were subjected to virus binding in the presence of OC for 15 (red line) or 60 min (blue line), regenerated and incubated in the presence of PR8-specific antibodies. The curves show the antibody association step. D) 3'SLNLN-coated sensors were incubated with PR8 in the presence of OC for 15 min. After virus association, virus self-elution in the absence of OC was monitored immediately (blue line) or sensors were first transferred to PBS (containing 10 μM OC) for another 120 min of incubation prior to virus self-elution (red line). Dissociation was plotted as fractional dissociation by normalization to the original virus association level.

increase the amount of α2,6-linked SIAs. We detected sialylated glycans by MAL I (binding to SIAα2,3Gal1,4GlcNAc; abundant on N-linked glycans and more scarce on O-linked glycans), Mal II (SIAα2,3Galβ1,3GalNAc; O-linked) and SNA (SIAα2,6Gal1,4GlcNAc; N-linked, less on O-linked). Their non-sialylated counterparts were detected by ECA (terminal Gal1,4GlcNAc ; N-linked, less on O-linked) and PNA (terminal Galβ1,3GalNAc; O-linked). All four glycoproteins mostly contain α2,3-linked SIAs (indicated by MALI/II binding) , whereas co-expression with ST6Gal1 strongly increased the amount of α2,6-linked SIA (as indicated by SNA binding) on all glycoproteins. Remarkably, α2,3-linked SIAs that are characteristic for O-linked glycans (MAL II) were detected on fetuin and glycophorin A but not on LAMP1, which displayed a similar low level binding as ICAM1 (no

O-linked glycans). ECA binding identified considerable levels of non-sialylated Galβ1,4GlcNAc termini on all four glycoproteins (most abundantly on ICAM1) whereas non-sialylated Galβ1,3GalNAc termini (PNA) were restricted to Glycophorin A. We conclude that, by the expression of selected glycoproteins, a collection of glycoprotein receptors that carry a specific repertoire of N-linked and/or O-linked glycans at different glycan densities could be produced. The combination with further tuning of sialylation and glycosylation patterns, by the co-expression of specific glycosyltransferases, provides the basis **for** an expandable, well-defined, receptor toolkit.

Initial virus binding rate in relation to receptor density

We first analyzed the binding characteristics of IAV to the four glycoprotein receptors, three short synthetic glycans (Neu5Acα2-3Galβ1-4GlcNAc, 3'SLN; 3'SLNLN; Neu5Acα2-3Galβ1-4GlcNAcβ1-3Galβ1-4GlcNAcβ1-3Galβ1-4GlcNAc, 3'SLNLNLN) and a sialoglycopolymer bearing mono-antennary 3'SLNLN on a biotinylated polyacrylamide backbone (3'SLNLN-PAA). We determined the initial binding rate (v^{obs}) for PR8 to a range of receptor densities in the presence of OC. The relative v^{obs} was plotted against the relative receptor density (Figure 3A and B). We did not observe a linear correlation between the relative v^{obs} and the receptor density, which would be expected if a virus particle could efficiently bind to a single glycoprotein molecule. Instead, the relative v^{obs} dropped from 0.9 to 0.1 over a ~2 -fold receptor density range for all receptors. This indicates that multiple sialoglycans on a glycoprotein (up to 18 N-linked glycans on LAMP1 and 16 O-linked glycans on glycophorin A) do not support tight binding of PR8 to a single glycoprotein molecule. A similar maximal v^{obs} (listed in Table 2) was obtained for all receptors at maximum receptor density. In contrast the receptor density at which v^{obs} was half-maximal differed over a four-fold range for different receptors (Figure 3A and B; values listed in Table 2). The synthetic glycans were relatively best in binding virus at low receptor density except for the shortest glycan (3'SLN). For the glycoproteins, v^{obs} at low receptor density positively correlated with the number of glycans attached. We conclude that receptor density and identity are crucial parameters in determining the initial virus binding rate. Sialoglycoproteins, assumed to resemble genuine in vivo IAV receptors, better support virus binding at relatively low receptor density when carrying a higher intramolecular glycan density.

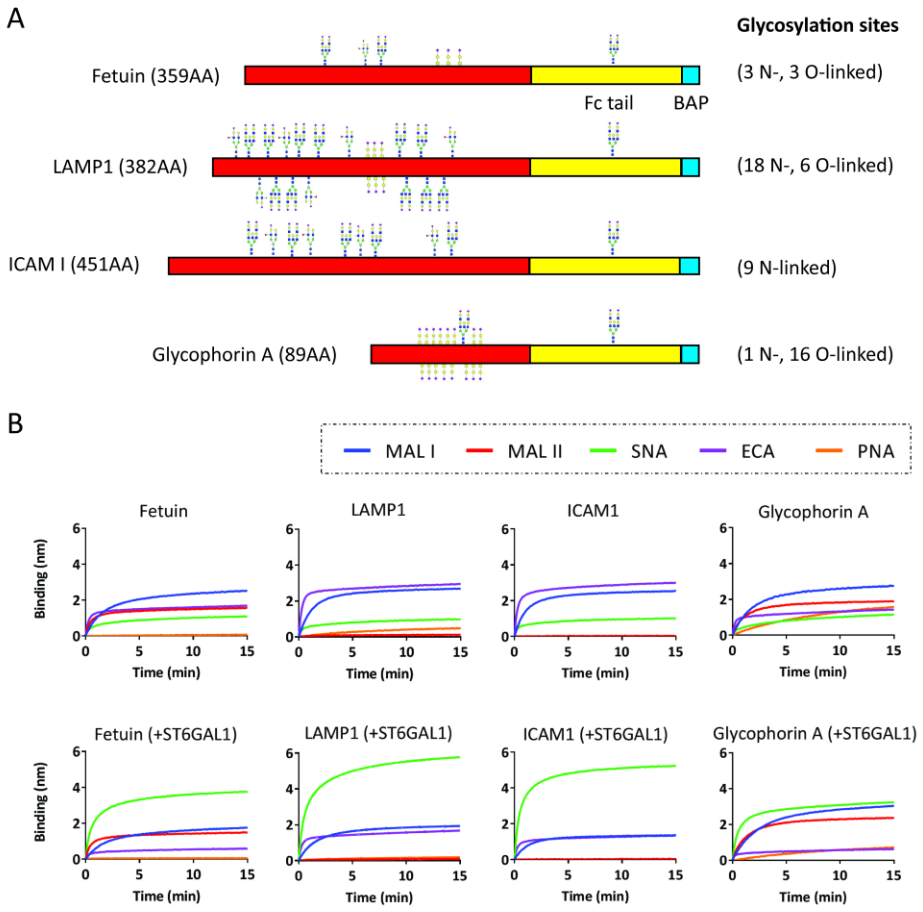

Figure 2. Recombinant glycoprotein receptors. A) Schematic representation of the recombinant soluble glycoproteins used. N- and/or O-linked glycans, as reported in the Uniprot database, are schematically indicated. To enable protein purification and coupling to BLI sensors, the constructs encode two affinity-tags at the C-terminus. An Fc-tag allows binding to protein A beads for purification as well as binding to protein A-coated sensors which can be re-used after removal of glycoproteins by regeneration. A Biotin Acceptor Peptide-tag (BAP-tag) becomes biotinylated when co-transfected with a plasmid encoding BirA (E. coli biotin ligase), which specifically recognizes the BAP-tag and is targeted to the endoplasmic reticulum by the N-terminal addition of a signal peptide (53). C-terminally biotinylated glycoproteins can be attached irreversibly to SA sensors. B) BLI analysis of lectin binding to the HEK293T-cell expressed glycoproteins immobilized on SA sensors. Where indicated, ST6Gal1 was co-expressed. MAL I prefers binding to SIAα2,3Gal1,4GlcNAc, which is abundant on N-linked glycans and more scarce on O-linked glycans. Mal II binds to SIAα2,3Galβ1,3GalNAc found on O-linked glycans. SNA binds to SIAα2,6Gal1,4GlcNAc present on N-linked, but less on O-linked, glycans. Non-sialylated glycans were detected using ECA (terminal Gal1,4GlcNAc ; N-linked, less on O-linked) and PNA (terminal Galβ1,3GalNAc; O-linked). The maximal lectin binding levels to the different glycoproteins are listed in Table 1. The standard deviations for maximal lectin binding levels range from 0.02 to 0.20 (N=2).

Table 1. Lectin binding to glycoproteins after 15min.

	MAL I (nm)	MAL II (nm)	SNA (nm)	ECA (nm)	PNA (nm)
Fetuin wt	2.51	1.55	1.09	1.69	0.08
Fetuin 2,6	1.74	1.48	3.79	0.57	0.07
ICAM 1 wt	2.53	0.04	1.00	2.99	0.00
ICAM 1 2,6	1.37	0.01	5.21	1.37	0.01
Glycophorin A wt	2.76	1.89	1.16	1.41	1.59
Glycophorin A 2,6	3.06	2.37	3.23	0.61	0.74
Lamp1 wt	2.67	0.10	0.99	2.96	0.47
Lamp 1 2,6	1.93	0.09	5.77	1.67	0.18

NA-driven rolling and self-elution of virus particles

Self-elution efficiency of a virus from a receptor-coated surface is one of the descriptive parameters of the HA/NA balance of a virion bound to a specific receptor and indicative of the ability of virions to roll on a receptor surface. We previously showed that the virus self-elution rate from a fetuin-coated sensor depends on receptor-clearance from the complete receptor-coated surface by virus rolling, and therefore correlates positively with the virus binding level (**Chapter 2**). Virus elution rates from LAMP1-coated sensors do not only positively correlate with the number of particles associated to the sensor, but are also faster at lower receptor densities (Figure S1). Thus, IAV rolls over receptor-coated surfaces at high and low receptor density until the sensors are no longer able to sustain virus binding. We subsequently compared the effect of receptor density on self-elution rates of PR8 from different sialoglycoproteins and synthetic glycans. Receptors were loaded to SA-sensors to a range of densities. PR8 virus was allowed to bind for 15 min in the presence of OC, after which NA activity-dependent self-elution (upon removal of OC by three washes) was measured and plotted as relative dissociation for each receptor density (Figure 4). Dissociation rates correlated negatively with receptor density for all six receptors, even when accompanied with decreased virion association levels, which has by itself a negative effect on self-elution efficiency. Whereas 90 to 100% dissociation was accomplished within 3 minutes for the glycoprotein receptors at all densities, dissociation from synthetic glycans is less than 50% after 5 min and proceeding at a very low rate by that time. To assist comparison of self-elution rates from the different receptors, the time required to reach 25% self-elution was plotted against receptor density (Figure 4G and H). Clearly, virus elution was least efficient for the synthetic glycans, while virus elution from the glycoprotein receptors was relatively fast. Elution from Glycophorin A, which contains a predicted number of 16 O-linked glycans, was less efficient than elution from the other glycoproteins (LAMP1, ICAM1, Fetuin) containing several N-linked glycans and only few or no O-glycans, as reported in the Uniprot database and based on MALII binding. These results indicate self-elution from O-linked glycans is slower than from N-linked glycans.

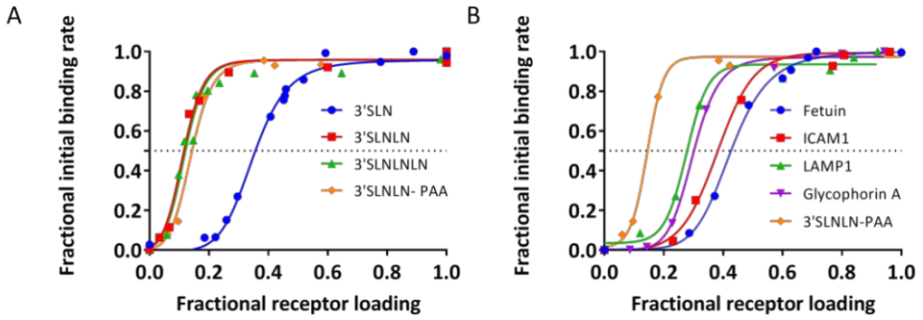

Figure 3. Receptor density- and identity-dependent initial binding rate.
A-B) BLI analysis of PR8 association to SA sensors coated with different densities of the indicated biotinylated receptors in the presence of OC. The fractional initial virus binding rate (v obs) is plotted against the fractional receptor loading. The maximum binding rates, binding levels and fractional density at half maximum binding rate are listed in Table 2. In panel A, there is significant difference between fractional receptor loading levels at half maximum binding rate between 3'SLN (blue curve) and other synthetic glycans (red, green and yellow curves)($P<0.001$). In panel B, fractional receptor loading levels at half maximum binding rate significantly differ between all five receptors ($P<0.001$)..

Table 2. Maximum initial binding rate, binding level after 60min and fractional density at half-maximum binding rate.

	Maximum binding rate (nm/min)	Maximum 60 min binding level (nm)	Fractional receptor loading at half maximum binding rate
3'SLN	0.24 (SD=0,0026)	6.3	0.37 (SD=0.0042)
3'SLNLN	0.28 (SD=0,0062)	8.2	0.12 (SD=0.0061)
3'SLNLNLN	0.27 (SD=0,0028)	8.0	0.12 (SD=0.0070)
3'SLNLN-PAA	0.30 (SD=0,0023)	8.9	0.15 (SD=0.0051)
Fetuin wt	0.22 (SD=0,0008)	7.2	0.43 (SD=0.0068)
ICAM 1 wt	0.25 (SD=0,0030)	9.3	0.38 (SD=0.0117)
Glycophorin A wt	0.30 (SD=0,0023)	7.2	0.28 (SD=0.0112)
Lamp1 wt	0.22 (SD=0,0047)	11.2	0.31 (SD=0.0059)

Virus binding maturation

As receptor identity clearly affects IAV self-elution rates, it might very well also affect virus binding maturation. We therefore analyzed the NA-activity driven self-elution after short (15 min) and prolonged (135 min) binding times to synthetic glycans and glycoproteins in a similar set up as described in Figure 1. To facilitate comparison, the results obtained with 3'SLNLN (Figure. 1) are shown again in Figure 5. In 20 min, 56% (3'SLNLN) or 64% (3'SLNLN-PAA) of the virus particles were self-eluted after binding for 15 min to synthetic glycans (Figure 5A and B; blue lines). Self-elution from glycoprotein receptors was highly efficient after 15 min of virus binding. Virus particles self-eluted within 4 minutes from all four glycoproteins, in agreement with the results shown in Figure. 4. In contrast, virus particles bound for 135 min did not self-elute from 3'SLNLN (Figure 5A; red line) and for

only 27% from 3'SLNLN-PAA (Figure 5B; red line). With the exception of Glycophorin A, initial virus self-elution rates from glycoprotein receptors (Figure 5C to F) were similar after 15 or 135 minutes of virus binding. However, self-elution generally proceeded to lower levels after 135 min of virus binding. Self-elution from glycophorin A (Figure 5F; red line) was most affected whereas hardly any decrease in self-elution from LAMP1 (Figure 5D) was observed. We conclude that virus binding to receptor-coated surfaces becomes tighter during prolonged binding, resulting in less efficient NA activity-dependent self-elution. The magnitude of the effect depends on the choice of receptor. Glycan linkage type, number and spatial arrangement on glycoproteins appear important parameters affecting maturation.

Maturation is not restricted to HA genotype or SIA-linkage type (Figure S2). An H3 HA with α2,6 linkage-type specificity, in a PR8 virus background, caused virus binding maturation on 6'SLNLN and LAMP1 co-expressed with ST6Gal1 to similar levels as PR8 virus itself on 3'SLNLN and LAMP1. Receptor density also affected virus binding maturation (Figure 6). Maturation on 3'SLNLN, loaded to a range of densities, was studied as before in Figure. 5. Comparison of virus self-elution after 15 min (Figure 6A) or 135 min (Figure 6B) of virus binding clearly shows that maturation of binding occurred at all receptor densities. However, a lower receptor density led to an elevated elution rate, while it reduced the negative fractional virus dissociation observed after long association. Overall, the largest maturation effect was observed at sensors with the maximum receptor density, where no self-elution at all was observed.

Analogous to the density-dependent binding maturation that we observed on a homogenous, synthetic glycan-coated surface, the specific structure and distribution of receptors on a glycoprotein might affect maturation of virus binding. To this end, we compared binding maturation on LAMP1 and Glycophorin A glycoproteins and, in addition, also examined the effect of a further increased sialylated glycan density by co-expression of ST3Gal1 or ST3Gal4 (Figure. 7). Co-expression of LAMP1 with ST3Gal4 resulted in increased sialylation at terminal Galβ1-4GlcNAc (abundant on N-linked glycans), as indicated by the increased MALI binding and reduced ECA binding (Figure 7B) and in agreement with the known specificity of this sialyltransferase (33). In contrast, co-expression of ST3Gal1 (targeting Galβ1,3GalNAc on O-linked glycans) had no effect on LAMP1 sialylation (Figure 7B, MALII). Increased sialylation at Galβ1,4GlcNAc termini on LAMP1 reduced virion self-elution rates, both after short and long association times (Figure 6C and D). Increased

sialylation did not reduce the eventual (after 20 min) fractional virus dissociation level after short association times (Figure 6C) but clearly lowered the eventual fractional dissociation level after long association (Figure 6D, blue line; Table 3). Co-expression of Glycophorin A with ST3Gal4 or with ST3Gal1, resulted in increased sialylation of terminal

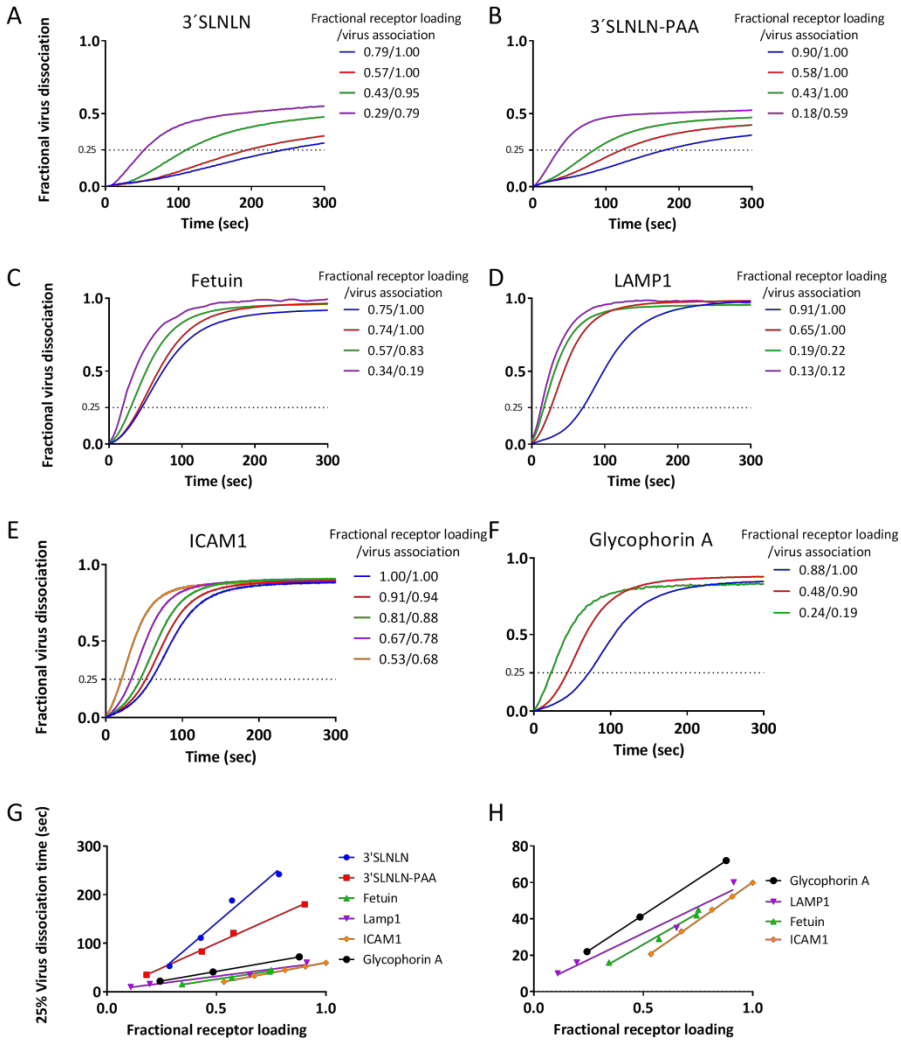

Figure 4. Receptor density- and identity-dependent virus self-elution.
A-F) The indicated receptors were loaded to SA-sensors to a range of densities (fractional receptor loading level is indicated), after which PR8 virus was allowed to bind for 15 min in the presence of OC (fractional virus association levels are also indicated in the panels). Subsequently, NA activity-dependent self-elution in the absence of OC was measured and plotted as dissociation normalized to the original virus association level (fractional virus dissociation) for each receptor density. G-H) Time required for 25% virus dissociation (dashed lines in panels A to F) were plotted against the fractional receptor loading levels by linear regression analysis (GraphPad Prism 7.04). There are significant differences between the slope of curves between 3'SLNLN and 3'SLNLN-PAA ($P<0.001$), between synthetic glycans (both 3'SLNLN and 3'SLNLN-PAA) and glycoproteins (Fetuin, Lamp1, ICAM1 and Glycophorin A) ($P<0.001$), and between Fetuin and Lamp1 ($P<0.01$), as well as between ICAM1 and LAMP1 ($P<0.01$). The intercepts of each these curves significantly differ from each other.

Galβ1,4GlcNAc (Figure 7A, MALI) or Galβ1,3GalNAc (Figure 7A, MALII), found on N-linked or short O-glycans respectively. Similar to what was observed for LAMPI, increased

sialylation of glycans on Glycophorin A reduced the rate of self-elution after long association as compared to short association. This was particularly the case upon co-expression of ST3Gal 1 (Figure 6E-F). It is also very clear that binding maturation occurs more extensively on Glycophorin A thaan on LAMPI (compare Figure 6D and 6F). We conclude that receptor identity (Glycophorin A versus LAMPI), as well as receptor density on a glycoprotein, affect maturation of virus binding.

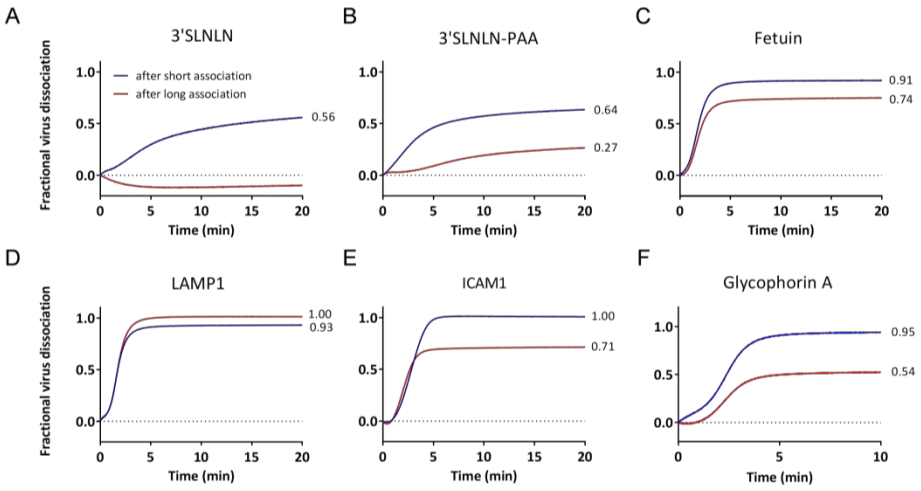

Figure 5. Maturation of virus binding to synthetic glycans and glycoproteins. A-F) Sensors coated with the indicated receptors were incubated with PR8 in the presence of OC for 15 min. After virus association, virus self-elution in the absence of OC was monitored immediately (blue lines) or sensors were first incubated in PBS in the presence of OC and in the absence of free virus particles for another 120 min prior to virus self-elution (red lines). Dissociation normalized to the virus association level (fractional dissociation) is graphed.

Table 3. Virus self-elution by NA activity

	After short association (15min)		After long association (135min)	
	Time for 25% self-elution (min)	Fractional elution (60min)	Time for 25% self-elution (min)	Fractional elution (60min)
LAMP1 wt	1.36	0.99	1.22	0.92
LAMP1 + ST3GAL4	1.62	0.99	2.51	0.81
LAMP1 + ST3GAL1	1.77	0.99	1.70	0.86
Glycophorin A wt	1.65	0.95	2.38	0.54
Glycophorin A + ST3GAL4	1.79	0.95	4.02	0.54
Glycophorin A + ST3GAL1	2.57	0.96	5.78	0.50

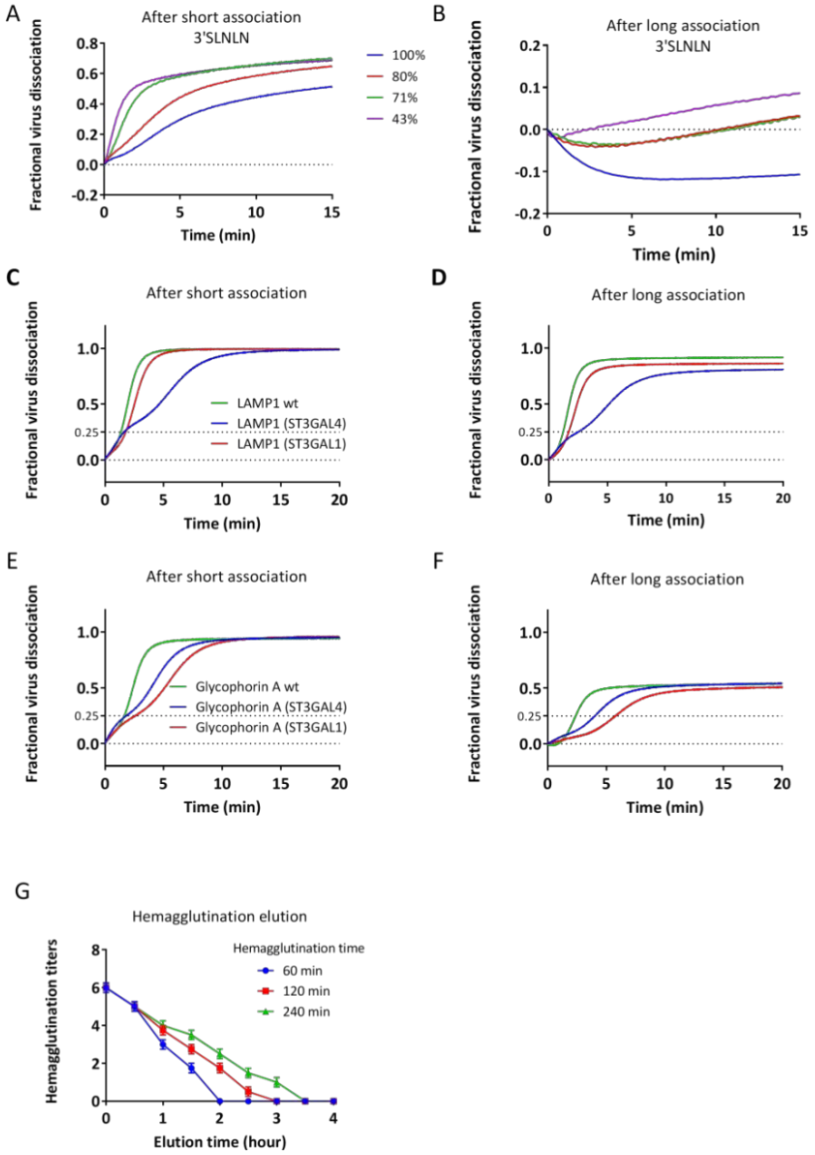

Figure 6. Receptor density-dependent maturation of virus binding. Sensors coated with the indicated receptors and densities were incubated with PR8 in the presence of OC for 15 min. After virus association, virus self-elution in the absence of OC was monitored immediately (A, C and E), or sensors were first incubated in PBS in the presence of OC and in the absence of free virus particles for another 120 min prior to virus self-elution (B, D and F). Dissociation normalized to the virus association level (fractional virus dissociation) is graphed. Time for 25% elution and fractional elution after 60 min is indicated in Table 3; G) Human erytrhrocytes were hemagglutinated for 1, 2 or 4 hours at 4°C by PR8. Subsequently, hemagglutination titers were determined every 30 minutes upon moving the plates to 37°C and graphed against the elution time. The curve after 60min hemagglutination significantly differs from the corresponding curve after 120 min ($P<0.01$) or 240 min ($P<0.001$) hemaglutination.

Having established a consistent effect of receptor density and identity on binding maturation, we investigated whether maturation of virus binding could be confirmed by an alternative method. As maturation was relatively efficient on glycophorin A, the most abundant sialoglycoprotein on human erythrocytes, we hereto used hemaglutination-elution. Human erytrhrocytes were hemagglutinated for 1, 2 or 4 hours at 4oC by PR8. Titers did not rise after 1 hour, suggesting that hemagglutination was completed within 1 hour. Subsequently, elution of the hemagglutination complexes was measured every 30 minutes upon moving the plates to 37oC, permitting NA activity (Figure 6G). The results show that longer hemagglutination times correlate with slower NA activity-dependent elution. This shows that virus binding to cellular membrane embedded sialoglycoproteins is also subject to maturation of binding.

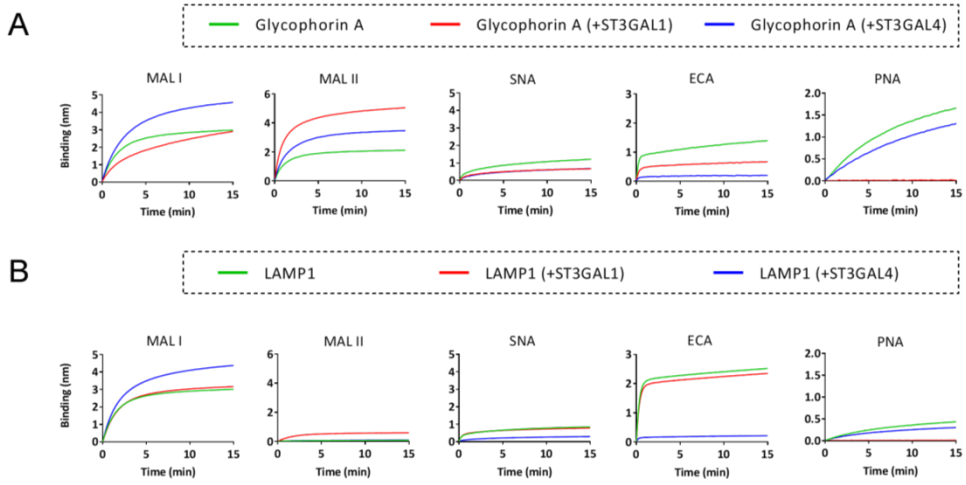

Figure 7. Manipulation of SIA content on glycoprotein receptors.
A-B) BLI analysis of lectin binding to Glycophorin A (A) or LAMP1 (B) co-expressed with or without with ST3Gal1 or ST3Gal4. For the specificity of the lectins used, see the legend to Fig 2. SA sensors were loaded to saturation with glycophorin A or LAMPI prior to lectin binding. The standard deviation for maximal lectin binding levels range from 0.02 to 0.20 (N=2).

Virus dissociation driven by antibodies and mucus

Host adaptive and innate immunity acts by interference with virus-receptor binding. HA-specific antibodies hinder HA-receptor interactions by blocking access to the receptor binding site. Likewise, SIAs attached to mucins act as a decoy receptors that block access of functional entry receptors to the binding site. The dynamic nature of IAV-receptor interactions results from multiple low affinity monovalent HA-receptor interactions (KD ≈ 0.3 to 3mM) which cooperatively cause a tight, virtually irreversible, polyvalent interaction. The low monovalent affinity enables a rapid exchange of SIA receptors between HA and NA resulting in virus rolling and release. Antibodies or mucins potentially

could interfere with this dynamic process. Current in vitro virus neutralization assays depend on pre-incubation of free virus particles with antisera but may not reflect the natural in vivo situation where IAV particles will be receptor-bound most of the time. We therefore compared the receptor-blocking properties of antibodies or mucus after pre-incubation with virus, with their capacity to interfere with already pre-formed virus-receptor interactions. First we checked whether PR8 HA antiserum can specifically block virus binding by pre-incubation. PR8-specific antiserum (50-fold diluted) completely blocked PR8 binding to LAMP1 (Figure 8A) whether it was de-sialylated (Anti-PR8 + AUNA) or not (Anti-PR8). H3N2-specific HA antiserum did not inhibit virus binding at 50-fold dilution (not shown). At a 12.5-fold dilution, H3N2 antiserum could block virus association for ~75% (Figure 8A, anti-H3N2). However, virus binding was inhibited much less by de-sialylated antiserum (Figure 8A, anti-H3N2 + AUNA), indicating that the inhibition by H3N2 antiserum is mostly due to its function as a sialylated decoy receptor. Pre-incubation of virus with an antiserum dilution series (Figure 8B) resulted in a concentration-dependent decrease of the virus binding rate. An 800-fold diluted anti-PR8 serum resulted in ~50% reduction of the binding rate. This was compared with an antibody-driven virus elution assay in which PR8 was first bound to LAMP1 after which the sensors with bound virus were transferred to a dilution series of antiserum. As a control, again the H3N2 antiserum was taken along. The results show that an 800-fold diluted anti-PR8 serum rapidly eluted LAMP1-associated PR8 (Figure 8C) whereas an 12.5-fold diluted H3-specific antiserum did not elute PR8 virus. Clearly, a higher antiserum specificity is obtained than in the pre-incubation assay where a 12.5-fold diluted H3-specific antiserum resulted in considerable inhibition of the binding rate.

The same methods were applied for determining the capacity of mucus, harvested from primary human airway epithelial cells, to interfere with virus binding. Pre-incubation of virus with mucus prohibited PR8 binding to LAMP1 in a SIA-dependent way (Figure 8D). A mucus dilution series showed that 1:25,000 mucus dilution is sufficient to reduce virus binding by ~70% (Figure 8E). Like specific antiserum, mucus could efficiently elute PR8 bound to LAMP1 (Figure 8F). The maximal dilution that drives self-elution (1:3,200) is higher than the maximal dilution that affects binding after pre-incubation (1:12,500). In Figure 8G the kinetics of antibody- and mucus-driven virus elution are compared. The time required for reaching 50% elution was plotted against the dilution factor of the antibody or the mucus preparation. Curve fitting resulted in curves with the equation $y=ax^{1.09}$ for both serum and mucus ($R^2 > 0.995$) showing almost direct proportionality between serum and mucus dilution and time needed for 50% virus elution. We conclude that virus-elution provides a flexible (e.g. choice of receptor and receptor density) and quantitative method for titration of antisera or binding competitors.

Maturation of virus binding shown by dissociation driven by antibodies and mucus

As is shown above, prolonged virus association could lead to virus binding maturation resulting in reduced NA activity-driven self-elution. Hence, we investigated how virus binding maturation affects antibody- or mucus-driven virus elution. Similar experiments as for NA activity-driven self-elution after elongated virus association (Figure 5) were performed. Antiserum- or mucus-driven elution was performed after 15 or 135 min of binding to synthetic glycans or glycoproteins (Figure 9). The results show that virus-elution by antibodies as well as by mucus is reduced after prolonged virus-receptor interaction providing further support for virus binding maturation. Tables 4 and 5 provide a summary of the maturation effect on the different receptors by listing the time required to reach 25% elution and the percentage of elution after 60 minutes. Clearly, the maturation effect is stronger for binding to synthetic glycans than to glycoproteins. A comparison of the glycoproteins shows the highest level of maturation on glycophorin A and the lowest level of maturation for LAMP1. Overall, the effects are very similar as to what was shown by NA activity-driven virus elution (Figure 5). Of note, the negative fractional dissociation particularly observed after maturation of virus binding (e.g. Figure. 9B and F) is most likely caused by binding of antibodies and mucins to the sensor-associated virions without resulting in their dissociation. The results indicate that virus binding maturation limits the accessibility for antibodies or mucins to the receptor binding sites of the HAs present at the contact area between virus and receptor surface.

Finally we analyzed whether virus binding maturation also limits the access of a soluble neuraminidase. We tested this by determining the capacity of the bacterial neuraminidase AUNA to release virus after different binding times (Figure S3). The results show a pattern that is remarkably similar to virus release driven by virion-associated NA, antibodies or mucus. Cleavage of SIAs by AUNA resulting in virus release is least efficient when bound to a synthetic glycan. Maturation is more pronounced on glycophorin A than on LAMP1. We conclude that binding maturation restricts virus motility, thereby limiting access of soluble proteins to the virus-receptor interface and prohibiting the elution of virus by viral envelope-embedded NA.

Table 4. Antisera elution

	After short association (15min)		After long association (135min)	
	Time for 25% antisera elution (min)	Fractional elution (60min)	Time for 25% antisera elution (min)	Fractional elution (60min)
3'SLNLN	47.66	0.28	n.d.	-0.96
3'SLNLN-PAA	0.93	0.73	n.d.	-0.43
Fetuin wt	0.60	0.92	0.57	0.66
ICAM 1 wt	0.41	0.90	0.30	0.80
Glycophorin A wt	0.85	0.95	1.40	0.38
Lamp1 wt	0.78	0.97	0.60	0.87

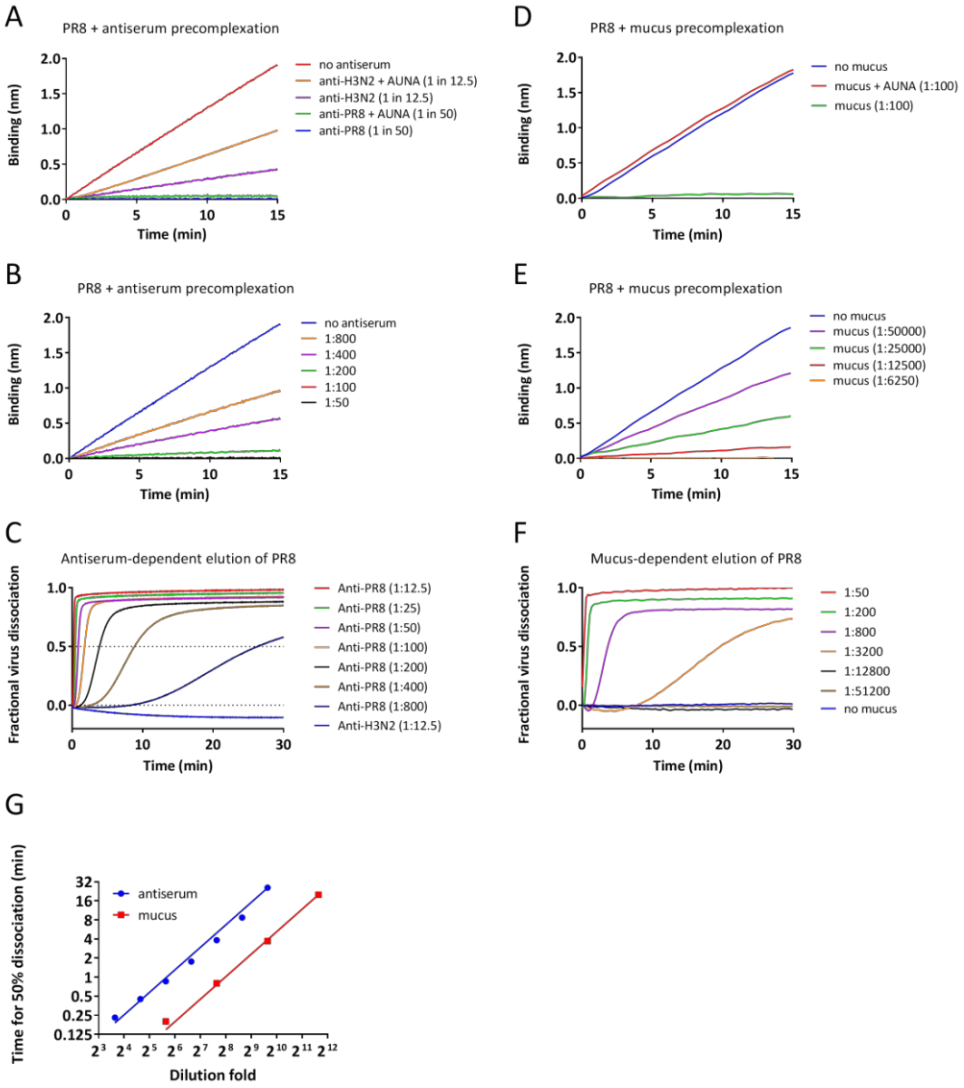

Figure 8. Dissociation of virus particles by antibodies and mucus. A and D) BLI analysis of virus association to LAMP1-coated sensors in the presence of OC and anti-PR8 or anti-H3N2 antiserum (A) or mucus (D). When indicated (AUNA), sera were treated with the bacterial neuraminidase AUNA prior to the analysis. Serum and mucus dilutions are indicated. B and E) BLI analysis of virus association to LAMP1-coated sensors in the presence of OC and different dilutions of desialylated anti-PR8 antiserum (B) or mucus (E). C and F) Virus was associated to LAMP1-coated sensors for 15 min in the presence of OC. Virus dissociation in the presence of OC and different dilutions of desialylated antiserum (C) or mucus (F) normalized to virus association levels (fractional virus dilution) is graphed. G) The time required for reaching 50% fractional virus elution as determined from graphs 8C and F is plotted against the dilution fold of the PR8 antiserum (blue line) or the mucus preparation (red line).The slope of two curves does not differ (P=0.943), whereas their intercept significantly differs (P<0.001).

Table 5. Mucus elution

	After short association(15min)		After long association(135min)	
	Time for 25% mucus elution (min)	Fractional elution (60min)	Time for 25% mucus elution (min)	Fractional elution (60min)
3'SLNLN	n.d.	0.14	n.d.	-0.39
3'SLNLN-PAA	n.d.	0.23	n.d.	-0.06
Fetuin wt	5.23	0.99	6.50	0.76
ICAM 1 wt	1.81	0.97	2.31	0.70
Glycophorin A wt	6.73	0.96	10.63	0.47
Lamp1 wt	7.06	0.96	7.09	0.93

DISCUSSION

IAV-receptor interactions determine how IAV particles traverse a mucus layer full of decoy receptors, become endocytosed upon cell binding and spread to other cells (3, 21, 34, 35). The dynamics of these events, determined by the interplay between HA and NA, are not well understood and mostly being studied by end-point assays (31, 36-38). Synthetic glycans and the serum glycoproteins fetuin and transferrin are commonly used to assess virus binding but poorly reflect the natural glycan diversity and density of membrane glycoproteins and mucins. We therefore produced soluble, C-terminally biotinylated, forms of membrane glycoproteins that are densely covered with N-linked glycans (ICAM-1, LAMP-1)(39-41) or have an O-linked glycan-rich, mucin-like, domain (glycophorin A) (42, 43) in HEK 293T cells. Manipulation of sialylation patterns by the co-expression of specific sialyltransferases, provided the basis for a toolkit of glycoproteins that mimic receptors encountered in vivo. BLI analysis of the dynamic interactions between IAV particles and glycoprotein receptors shows that the initial binding rate to, and NA activity-driven self-elution from, a receptor-coated surface depends on glycoprotein receptor density and identity. Virus particles that were pre-associated with the receptor-surface were efficiently eluted by mucus or HA-specific antibodies that compete with receptors for HA binding as a consequence of the highly dynamic interaction between individual HA receptor binding sites and SIAs. Thus, BLI assays provide novel ways to quantify virus-mucus interactions and antibody titers that block IAV-receptor interactions. Strikingly, prolonged virus-receptor association times reduced virus self-elution and mucus- or antibody-driven dissociation. Such maturation of IAV-receptor binding was hitherto unrecognized and has implications for the interpretation of results from endpoint binding assays. It could play a significant role in IAV biology and we expect that binding maturation could also occur for other enveloped viruses.

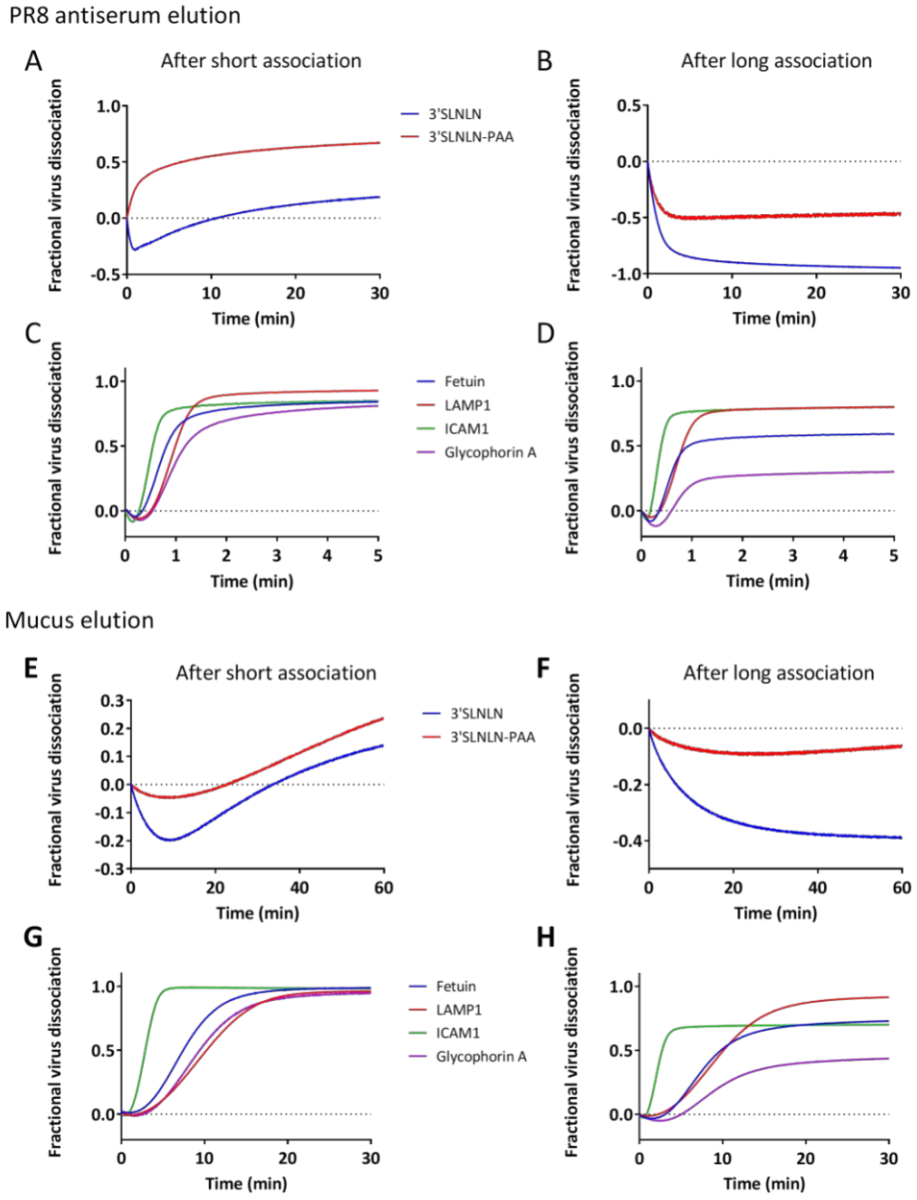

Figure 9. Effect of virus maturation on virus dissociation.
Sensors coated with the indicated receptors were incubated with PR8 in the presence of OC for 15 min. After virus association, virus dissociation was monitored immediately (A, C, E and G) or sensors were first incubated in PBS in the presence of OC and in the absence of free virus particles for another 120 min prior to virus dissociation (B, D, F and H). Virus dissociation was analyzed in the presence of PR8 antiserum (A-D) or mucus (E-H). Fractional virus dissociation is graphed against time. The time for 25% antiserum/mucus elution and fractional elution after short and long association is indicated in the Table 4 and 5, respectively.

Glycan density on glycoprotein receptors correlates with initial virus binding rate

IAV binding is, to unknown extents, affected by the structure, diversity, and local density of sialoglycans on the cell surface. Determination of a dissociation constant (KD) for virus binding is precluded as, in the absence of NA activity, virus dissociation is negligible due to multivalent HA-receptor interactions. Instead, we consider the initial binding rate as the most relevant parameter for quantifying of IAV-receptor binding (**Chapter 2**). While at maximal receptor density the initial binding rates to the different glycoprotein were similar (Table S2), the binding rate to the glycoproteins declined steeply at different receptor densities. The density supporting a half-maximum binding rate inversely correlated with the number of glycosylation sites present on a protein. This is relevant for in vivo virus binding to a specific host cell membrane glycoprotein, of which the density distribution might be variable and mostly lower as the maximum density in our experiments. A non-linear dependency of initial virus binding rate to receptor density is typical for multivalent particle-substrate interactions in combination with low affinity individual interactions. This results in an ultra-sensitive response to receptor density, referred to as super selectivity (44). We expect that heavily glycosylated glycoproteins will form the initial binding foci for IAV.

Virus self-elution depends on the interplay between HA, NA, receptor density and identity

After binding, virus particles roll over receptor-coated surfaces, removing SIAs until receptor density is low enough to cause virus particle dissociation. Rolling is driven by NA activity and requires weak, highly dynamic, HA-receptor interactions (**Chapter 2**). We showed that rolling is observed at any glycoprotein receptor density, but that self-elution is faster at low initial receptor density (Figure S1). The self-elution rate clearly depends on receptor identity, being the slowest from synthetic glycans (Figure. 4). From the glycoproteins, Glycophorin A, containing 17 O-linked glycans on a stretch of 50 amino acids, displayed the lowest dissociation rate indicating that the presence of high-density patches of sialoglycans decreases self-elution rates. This is confirmed by the observation that increased sialylation of glycoproteins, by co-expression of sialyl transferase ST3Gal4 or ST3Gal1, further decreases virus self-elution rates (Figure 6). Synthetic glycans are capable of binding IAV particles at lower densities than glycoproteins (Figure 2), fitting with the observation that virus particles elute at a lower rate from this substrate (Figure 6). On the other hand, differences in self-elution rates will reflect differences in NA cleavage rates per se for a specific receptor. Indeed, NA was reported to cleave N-linked sialosides (i.e. SIAα2,3Galβ1,4GlcNAc) more efficiently than O-linked sialosides (i.e. SIAα2,3Galβ1,3GalNAc) (45), in agreement with the observed faster elution from LAMP1 than from Glycophorin A (Figure. 2). We conclude that motility of IAV on a receptor-containing surface is determined by the activity of HA and NA as well as by receptor

density and identity. Our study provides a first analysis of the complex interplay between these different factors.

Mucus and antibodies are able to resolve virus-receptor complexes

IAV particles need to overcome the innate and adaptive defenses of a host. Innate defenses include the heavily sialylated mucus layer, which can trap microbes such as IAV. Most studies on IAV-mucus interaction focus either on inhibition of IAV infectivity by mucus (29) or on movement of particles in mucus (30). We now show that mucus can not only prevent virus-receptor interaction in a SIA-dependent manner but also efficiently resolves virus-receptor complexes (Figure. 8). Likewise, besides inhibiting receptor binding, antisera were shown to be able to dissociate virus particles from a receptor-coated surface. In the SIA-rich environment provided by a mucus-covered epithelial cell layer, IAV particles might be expected to be receptor-associated most of the time. Therefore, the ability of mucus and antibodies to dissociate viruses that are bound to a receptor-coated surface, in addition to receptor-binding blocking capacities as measured in a hemagglutination inhibition assay, is probably highly relevant. Mucus and antibodies will also interfere with virus rolling on cells, which expectedly precedes endocytic uptake and contributes to cell-to-cell spread. BLI-based assays can be used to quantify and characterize virus-mucus interactions and to determine HA-specific antibody titers. This is also attractive as BLI-based assays are amendable to high through-put analysis.

Maturation of virus binding

Prolonged incubation of preformed virus-receptor complexes resulted in tightened virus-receptor interaction. We refer to this as maturation of virus binding. Maturation was demonstrated by reduced rates of receptor-dissociation as driven by virion-associated NA activity, specific antibodies or mucus, soluble neuraminidases or low pH and was receptor density dependent. Maturation of virus binding to glycoproteins was most prominent with Glycophorin A. Increased sialylation of its 18 O-linked glycans further increased the maturation effect (Figure 6C). A likely mechanism for maturation is the increased binding of multiple SIAs by a single HA trimer. This was previously proposed to explain the tight interaction between soluble HA proteins of human H3N2 viruses and multi-antennary synthetic glycans with extended lactosamine chains as observed by glycan array analysis (46). Multiple interactions with a single HA trimer will reduce its rotational and translational freedom when only one interaction is broken. This will promote preferential re-association with the released SIA, thereby restricting accessibility for competitors and sialidases, as well as NA-dependent rolling. Multiple HA trimer-receptor interactions will most readily be formed at densely sialylated surfaces areas. It remains unknown whether the above-mentioned multi-antennary N-linked glycans with extended lactosamine chains [34], which have not been detected by glycomic analyses of human respiratory tissues (47,

48), function as attachment and uptake receptors in vivo. We now show that increased avidity, resulting in virus binding maturation, also can occur with short glycans and with glycoproteins containing patches of densely-packed O-linked glycans.

Maturation may assist efficient cell entry as exemplified by the finding that virus particles reside motionless at a spot on the cell surface where, prior to endocytic uptake, de novo assembly of clathrin-coated pits occurs (2). NA activity may slow down or prevent maturation which could thus be detrimental for cell entry efficiency. On the other hand it may prevent binding maturation to potential non-functional receptors at the heavily glycosylated cell surface and decoy receptors in the dense mucus. Adding to the complexity, soluble mucins that are commonly considered to act solely as decoy molecules could, like NA, also interfere with virus binding maturation to the cell surface as shown by their ability to efficiently elute virus particles from receptor-coated surface after short binding times (Figure 8). Thus, the extent of virus maturation will intrinsically depend on the precise HA/NA balance for every potential receptor molecule. Probably, virus maturation critically depends on the trimeric organization of HA on IAV particles. All enveloped viruses carry multiple oligomeric attachment proteins that provide them with a similar multilayered multivalency as IAVs. Such an arrangement not only allows super-selectivity (22, 49, 50), but also maturation of virus binding, even more so in the absence of receptor-destroying enzymes. We therefore propose that the maturation of virus binding may be a biologically important feature of enveloped viruses, for instance by mediating receptor-mediated uptake of virus particles.

REFERENCES

1. Zanin M, Baviskar P, Webster R, Webby R. The Interaction between Respiratory Pathogens and Mucus. Cell host & microbe. 2016 Feb 10;19(2):159-68.
2. Rust MJ, Lakadamyali M, Zhang F, Zhuang X. Assembly of endocytic machinery around individual influenza viruses during viral entry. Nature structural & molecular biology. 2004 Jun;11(6):567-73.
3. Skehel JJ, Wiley DC. Receptor binding and membrane fusion in virus entry: the influenza hemagglutinin. Annual review of biochemistry. 2000;69:531-69.
4. Suzuki T, Takahashi T, Guo CT, Hidari KI, Miyamoto D, Goto H, et al. Sialidase activity of influenza A virus in an endocytic pathway enhances viral replication. Journal of virology. 2005 Sep;79(18):11705-15.
5. Su B, Wurtzer S, Rameix-Welti MA, Dwyer D, van der Werf S, Naffakh N, et al. Enhancement of the influenza A hemagglutinin (HA)-mediated cell-cell fusion and virus entry by the viral neuraminidase (NA). PloS one. 2009 Dec 30;4(12):e8495.
6. Byrd-Leotis L, Cummings RD, Steinhauer DA. The Interplay between the Host Receptor and Influenza Virus Hemagglutinin and Neuraminidase. International journal of molecular sciences. 2017 Jul 17;18(7).
7. Wagner R, Matrosovich M, Klenk HD. Functional balance between haemagglutinin and neuraminidase in influenza virus infections. Reviews in medical virology. 2002 May-Jun;12(3):159-66.
8. Xu R, Zhu X, McBride R, Nycholat CM, Yu W, Paulson JC, et al. Functional balance of the hemagglutinin and neuraminidase activities accompanies the emergence of the 2009 H1N1 influenza pandemic. J Virol. 2012 Sep;86(17):9221-32.
9. Rogers GN, Paulson JC. Receptor determinants of human and animal influenza virus isolates: differences in receptor specificity of the H3 hemagglutinin based on species of origin. Virology. 1983 Jun;127(2):361-73.
10. Rogers GN, Pritchett TJ, Lane JL, Paulson JC. Differential sensitivity of human, avian, and equine influenza A viruses to a glycoprotein inhibitor of infection: selection of receptor specific variants. Virology. 1983 Dec;131(2):394-408.
11. Connor RJ, Kawaoka Y, Webster RG, Paulson JC. Receptor specificity in human, avian, and equine H2 and H3 influenza virus isolates. Virology. 1994 Nov 15;205(1):17-23.
12. de Graaf M, Fouchier RA. Role of receptor binding specificity in influenza A virus transmission and pathogenesis. The EMBO journal. 2014 Apr 16;33(8):823-41.
13. Childs RA, Palma AS, Wharton S, Matrosovich T, Liu Y, Chai W, et al. Receptor-binding specificity of pandemic influenza A (H1N1) 2009 virus determined by carbohydrate microarray. Nature biotechnology. 2009 Sep;27(9):797-9.
14. Gambaryan A, Yamnikova S, Lvov D, Tuzikov A, Chinarev A, Pazynina G, et al. Receptor specificity of influenza viruses from birds and mammals: new data on involvement of the inner fragments of the carbohydrate chain. Virology. 2005 Apr 10;334(2):276-83.
15. Chu VC, Whittaker GR. Influenza virus entry and infection require host cell N-linked glycoprotein. Proceedings of the National Academy of Sciences of the United States of America. 2004 Dec 28;101(52):18153-8.
16. de Vries E, de Vries RP, Wienholts MJ, Floris CE, Jacobs MS, van den Heuvel A, et al. Influenza A virus entry into cells lacking sialylated N-glycans. Proc Natl Acad Sci U S A. 2012 May 08;109(19):7457-62.
17. Xiong X, Tuzikov A, Coombs PJ, Martin SR, Walker PA, Gamblin SJ, et al. Recognition of sulphated and fucosylated receptor sialosides by A/Vietnam/1194/2004 (H5N1) influenza virus. Virus research. 2013 Dec 05;178(1):12-4.

18. Hiono T, Okamatsu M, Nishihara S, Takase-Yoden S, Sakoda Y, Kida H. A chicken influenza virus recognizes fucosylated alpha2,3 sialoglycan receptors on the epithelial cells lining upper respiratory tracts of chickens. Virology. 2014 May;456-457:131-8.
19. Guo H, de Vries E, McBride R, Dekkers J, Peng W, Bouwman KM, et al. Highly Pathogenic Influenza A(H5Nx) Viruses with Altered H5 Receptor-Binding Specificity. Emerg Infect Dis. 2017 Feb;23(2):220-31.
20. Boulant S, Stanifer M, Lozach PY. Dynamics of virus-receptor interactions in virus binding, signaling, and endocytosis. Viruses. 2015 Jun 02;7(6):2794-815.
21. Sauter NK, Hanson JE, Glick GD, Brown JH, Crowther RL, Park SJ, et al. Binding of influenza virus hemagglutinin to analogs of its cell-surface receptor, sialic acid: analysis by proton nuclear magnetic resonance spectroscopy and X-ray crystallography. Biochemistry. 1992 Oct 13;31(40):9609-21.
22. Sieben C, Kappel C, Zhu R, Wozniak A, Rankl C, Hinterdorfer P, et al. Influenza virus binds its host cell using multiple dynamic interactions. Proceedings of the National Academy of Sciences of the United States of America. 2012 Aug 21;109(34):13626-31.
23. Lakadamyali M, Rust MJ, Zhuang X. Endocytosis of influenza viruses. Microbes and infection. 2004 Aug;6(10):929-36.
24. Matlin KS, Reggio H, Helenius A, Simons K. Infectious entry pathway of influenza virus in a canine kidney cell line. The Journal of cell biology. 1981 Dec;91(3 Pt 1):601-13.
25. Sakai T, Nishimura SI, Naito T, Saito M. Influenza A virus hemagglutinin and neuraminidase act as novel motile machinery. Scientific reports. 2017 Mar 27;7:45043.
26. Shogren R, Gerken TA, Jentoft N. Role of glycosylation on the conformation and chain dimensions of O-linked glycoproteins: light-scattering studies of ovine submaxillary mucin. Biochemistry. 1989 Jun 27;28(13):5525-36.
27. Klein A, Carnoy C, Wieruszeski JM, Strecker G, Strang AM, van Halbeek H, et al. The broad diversity of neutral and sialylated oligosaccharides derived from human salivary mucins. Biochemistry. 1992 Jul 07;31(26):6152-65.
28. Matrosovich MN, Matrosovich TY, Gray T, Roberts NA, Klenk HD. Human and avian influenza viruses target different cell types in cultures of human airway epithelium. Proceedings of the National Academy of Sciences of the United States of America. 2004 Mar 30;101(13):4620-4.
29. Cohen M, Zhang XQ, Senaati HP, Chen HW, Varki NM, Schooley RT, et al. Influenza A penetrates host mucus by cleaving sialic acids with neuraminidase. Virology journal. 2013 Nov 22;10:321.
30. Yang X, Steukers L, Forier K, Xiong R, Braeckmans K, Van Reeth K, et al. A beneficiary role for neuraminidase in influenza virus penetration through the respiratory mucus. PloS one. 2014;9(10):e110026.
31. Blixt O, Head S, Mondala T, Scanlan C, Huflejt ME, Alvarez R, et al. Printed covalent glycan array for ligand profiling of diverse glycan binding proteins. Proceedings of the National Academy of Sciences of the United States of America. 2004 Dec 07;101(49):17033-8.
32. Benton DJ, Martin SR, Wharton SA, McCauley JW. Biophysical measurement of the balance of influenza a hemagglutinin and neuraminidase activities. J Biol Chem. 2015 Mar 06;290(10):6516-21.
33. Tiralongo J. Introduction to Sialic Acid Structure, Occurrence, Biosynthesis and Function. In: Joe Tiralongo IM-D, editor. Sialobiology: Structure, Biosynthesis and Function Sialic Acid Glycoconjugates in Health and Disease: Bentham Science Publishers; 2013. p. 76-114.
34. Air GM, Laver WG. The neuraminidase of influenza virus. Proteins. 1989;6(4):341-56.
35. Matrosovich MN, Matrosovich TY, Gray T, Roberts NA, Klenk HD. Neuraminidase is important for the initiation of influenza virus infection in human airway epithelium. Journal of virology. 2004 Nov;78(22):12665-7.

36. Hirst GK. The Quantitative Determination Of Influenza Virus And Antibodies by Means Of Red Cell Agglutination. The Journal of experimental medicine. 1942 Jan 01;75(1):49-64.
37. Baenziger JU, Fiete D. Structure of the complex oligosaccharides of fetuin. The Journal of biological chemistry. 1979 Feb 10;254(3):789-95.
38. Potier M, Mameli L, Belisle M, Dallaire L, Melancon SB. Fluorometric assay of neuraminidase with a sodium (4-methylumbelliferyl-alpha-D-N-acetylneuraminate) substrate. Analytical biochemistry. 1979 Apr 15;94(2):287-96.
39. Carlsson SR, Fukuda M. Structure of human lysosomal membrane glycoprotein 1. Assignment of disulfide bonds and visualization of its domain arrangement. The Journal of biological chemistry. 1989 Dec 5;264(34):20526-31.
40. Chen R, Jiang X, Sun D, Han G, Wang F, Ye M, et al. Glycoproteomics analysis of human liver tissue by combination of multiple enzyme digestion and hydrazide chemistry. Journal of proteome research. 2009 Feb;8(2):651-61.
41. Casasnovas JM, Stehle T, Liu JH, Wang JH, Springer TA. A dimeric crystal structure for the N-terminal two domains of intercellular adhesion molecule-1. Proceedings of the National Academy of Sciences of the United States of America. 1998 Apr 14;95(8):4134-9.
42. Hanisch FG, Jovanovic M, Peter-Katalinic J. Glycoprotein identification and localization of O-glycosylation sites by mass spectrometric analysis of deglycosylated/alkylaminylated peptide fragments. Analytical biochemistry. 2001 Mar 01;290(1):47-59.
43. Pisano A, Redmond JW, Williams KL, Gooley AA. Glycosylation sites identified by solid-phase Edman degradation: O-linked glycosylation motifs on human glycophorin A. Glycobiology. 1993 Oct;3(5):429-35.
44. Martinez-Veracoechea FJ, Frenkel D. Designing super selectivity in multivalent nano-particle binding. Proceedings of the National Academy of Sciences of the United States of America. 2011 Jul 05;108(27):10963-8.
45. Dai M, McBride R, Dortmans JC, Peng W, Bakkers MJ, de Groot RJ, et al. Mutation of the Second Sialic Acid-Binding Site, Resulting in Reduced Neuraminidase Activity, Preceded the Emergence of H7N9 Influenza A Virus. J Virol. 2017 May 01;91(9).
46. Peng W, de Vries RP, Grant OC, Thompson AJ, McBride R, Tsogtbaatar B, et al. Recent H3N2 Viruses Have Evolved Specificity for Extended, Branched Human-type Receptors, Conferring Potential for Increased Avidity. Cell host & microbe. 2017 Jan 11;21(1):23-34.
47. Walther T, Karamanska R, Chan RW, Chan MC, Jia N, Air G, et al. Glycomic analysis of human respiratory tract tissues and correlation with influenza virus infection. PLoS pathogens. 2013 Mar;9(3):e1003223.
48. Jia N, Barclay WS, Roberts K, Yen HL, Chan RW, Lam AK, et al. Glycomic characterization of respiratory tract tissues of ferrets: implications for its use in influenza virus infection studies. The Journal of biological chemistry. 2014 Oct 10;289(41):28489-504.
49. Wilen CB, Tilton JC, Doms RW. HIV: cell binding and entry. Cold Spring Harbor perspectives in medicine. 2012 Aug 1;2(8).
50. Jourdan N, Jobart-Malfait A, Dos Reis G, Quignon F, Piolot T, Klein C, et al. Live-cell imaging reveals multiple interactions between Epstein-Barr virus nuclear antigen 1 and cellular chromatin during interphase and mitosis. Journal of virology. 2012 May;86(9):5314-29.
51. de Vries E, Tscherne DM, Wienholts MJ, Cobos-Jimenez V, Scholte F, Garcia-Sastre A, et al. Dissection of the influenza A virus endocytic routes reveals macropinocytosis as an alternative entry pathway. PLoS Pathog. 2011 Mar;7(3):e1001329.
52. Koel BF, Burke DF, Bestebroer TM, van der Vliet S, Zondag GC, Vervaet G, et al. Substitutions near the receptor binding site determine major antigenic change during influenza virus evolution. Science. 2013 Nov 22;342(6161):976-9.
53. Predonzani A, Arnoldi F, Lopez-Requena A, Burrone OR. In vivo site-specific biotinylation of proteins within the secretory pathway using a single vector system. BMC biotechnology. 2008 Apr 18;8:41.

SUPPLEMENTARY FIGURES

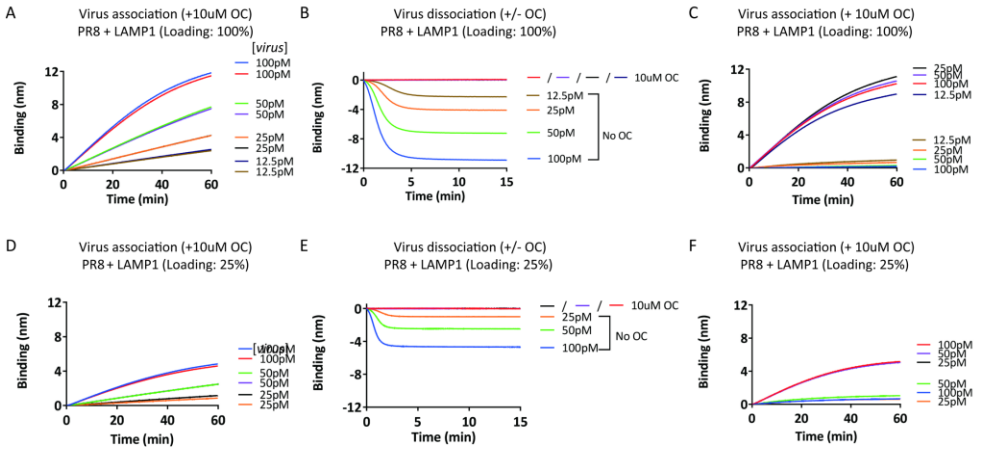

Figure. S1. Receptor density-dependent rolling of virus particles on LAMP1-coated sensors.
SA sensors were fully loaded with LAMP1 (100%; A) or to ~25% loading level (D), after which virus association was monitored in the presence of OC using different concentrations of virus (100-12.5 pM). For each virus concentration, 2 sensors were used. Subsequently, virus dissociation was analyzed either in the presence or the absence of OC (B and E). Finally, sensors were regenerated by incubation at pH2, after which virus association (100 pM) was monitored in the presence of OC (C and F). Virus concentrations used during binding shown in A and D, are also indicated in B, C, E and F. In panel C, virus association curves (black, purple, red and blue) are significantly different from brown, orange, green and light blue curves. In panel F, virus association curves (red, purple, black) significantly differ from green, blue and orane curves.

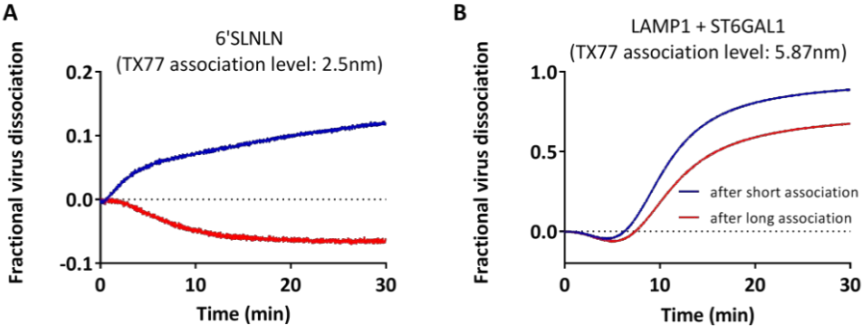

Figure. S2. Maturation of virus binding to α2,6-linked sialosides.
Sensors coated with 6'SLNLN (A) or with LAMP1 co-expressed with ST6Gal1 (B) were incubated with PR8 virus containing the H3 protein of the H3N2 virus (TX77) in the presence of OC for 15 min. After virus association, virus self-elution in the absence of OC was monitored immediately (blue line) or sensors were first incubated in PBS in the presence of OC and in the absence of free virus particles for another 120 min prior to virus self-elution (red line). Dissociation normalized to the virus association level (fractional dissociation) is graphed.

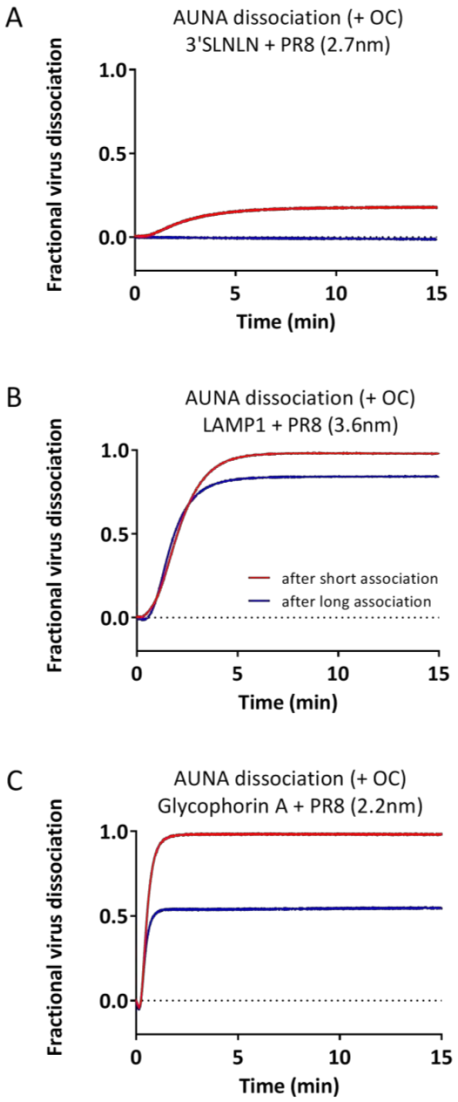

Figure S3. Maturation of virus binding shown by elution with bacterial NA. Sensors coated with 3'SLNLN (A) LAMP1 (B), or with Glycophorin A (C) were incubated with PR8 virus in the presence of OC for 15 min. After virus association, virus dissociation in the presence of OC and bacterial NA (AUNA) was monitored immediately (blue lines) or sensors were first incubated in PBS in the presence of OC and in the absence of free virus particles for another 120 min prior to AUNA-induced virus dissociation (red line). Dissociation normalized to the virus association level (fractional dissociation) is graphed. PR8 association level prior to virus dissociation is indicated.

Chapter 4

Human H3N2 influenza A viruses of consecutive antigenic clusters maintain similar receptor binding properties by the combined effects of individual amino acid substitutions

Hongbo Guo[1#], Wenjuan Du[1#], Floor van der Vegt[1], Jack Li[2], GeertJan Boons[2], Frank J. van Kuppeveld[1], Ron Fouchier[3], Erik de Vries[1]*, Cornelis A. de Haan[1]*

1 Virology Division, Department of Infectious Diseases & Immunology, Faculty of Veterinary Medicine, Utrecht University, Yalelaan 1, 3584CL Utrecht, the Netherlands.

2 Department of Chemical Biology and Drug Discovery, Utrecht Institute for Pharmaceutical Sciences and Bijvoet Center for Biomolecular Research, Utrecht University, 3584 CG Utrecht, the Netherlands.

3 Department of Viroscience, Erasmus MC, Rotterdam, The Netherlands.

#These authors contributed equally

(*co-coresponding author)

Manucsript in preparation

ABSTRACT

The influenza A virus (IAV) hemagglutinin (HA) protein is the prime target for antibody-mediated immunity. Antibody-driven immune pressure results in HA antigenic drift, which previously has been documented in detail for human H3N2 viruses from 1968 to 2003. Antigenic change has been shown to be caused by 1 to 3 amino acid substitutions in HA that occurred at only seven positions immediately adjacent to the receptor binding site, which are referred to as antigenic cluster transition mutations. To get more insight into the evolutionary pathways leading to the generation of novel antigenic clusters, we analyzed receptor-binding properties of viruses belonging to different antigenic clusters and quantified the effect of antigenic cluster transition mutations and antigenically neutral mutations on virus binding rate using biolayer interferometry. Viruses corresponding to eleven consecutive antigenic HA clusters of seasonal H3N2 IAVs from 1968 to 2002 were compared for their binding to different sialylated glycoproteins, showing that from 1972 to 1997 only limited changes in receptor binding kinetics to α2,6-linked SIAs have occurred. The binding rate to avian-type α2,3-linked SIA receptors gradually decreased to become undetectable after 1997. For three antigenic clusters, the effects of the individual antigenic cluster-transition mutations as well as of accessory (antigenically neutral) mutations were determined. Forward antigenic cluster transition mutations did not appear to have large effects on receptor binding. However, for one cluster transition the reciprocal backward mutation had a large negative effect. Accessory mutations that, according to phylogenetic analysis, preceded the corresponding forward antigenic cluster transition mutation clearly negatively affected receptor binding, suggesting that these mutations are crucial for creating a background in which introduction of a cluster transition mutation results in a virus with high fitness. Our study provides arguments against a previously proposed universal mechanism of IAV escape from immune pressure that is initiated with enhanced receptor binding.

INTRODUCTION

Annual epidemics of seasonal influenza caused by influenza A virus (IAV) H1N1 and H3N2 are a major cause of morbidity and mortality (1, 2). Each year, 5 to 15% of the human population becomes infected, resulting in up to half a million deaths per year (1). Yearly vaccination campaigns help to limit the burden of influenza but still provide only partial protection. Moreover, antigenic changes pose a huge challenge regarding the timely updating of IAV vaccine strains. Antigenic change is caused by genetic drift and results in the occurrence of novel antigenic clusters every 2 to 7 years (3, 4).

The major IAV envelope glycoprotein hemagglutinin (HA) is the prime target for antibody-mediated immunity. For a long time, accumulation of amino acid substitutions at five antigenic sites on the globular head domain of HA of H3N2 IAV was thought to be required for escape from a polyclonal antibody response (5). More recently it was shown that only one or two substitutions are required for an antigenic-cluster transition. These cluster-transition mutations are limited to only seven positions surrounding the receptor binding site (6). Transition from one antigenic cluster to the next evolves by relatively large steps in antigenicity resulting in a punctuated pattern as visualized by antigenic cartography (6). In contrast, HA phylogenetic trees show that genetic evolution proceeds by many small steps along a trunk with extended branches representing the different antigenic clusters (3). Many of the mutations along the trunk and the branches result in amino acid substitutions in the antigenic sites on the globular head but do not result in changes in antigenicity as determined by hemagglutination inhibition assays and antigenic cartography (3). Possibly, these substitutions are required for compensating potential negative effects of the cluster-transition mutations on viral fitness. In view of the close proximity of the cluster transition mutations to the receptor binding site, such negative effects may involve changes in receptor-binding avidity and specificity. According to this model, antigenic changes are caused by one or two antigenic cluster transition mutations, the selection of which requires or drives crucial compensatory mutations.

An alternative model for antigenic evolution has been proposed, in which IAV mutants with alternating high and low receptor-binding affinity are consecutively selected (7). High-avidity mutants are selected in immune individuals for their capacity to bind receptors fast enough to compete with neutralizing antibodies that block the receptor-binding sites. Low-avidity mutants are subsequently selected in naïve individuals as the high avidity comes at a viral fitness cost. This alternating process results in accumulation of mutations on the HA globular head which ultimately gives rise to sufficient antigenic change for escape from a polyclonal antibody response. The model is based on extensive experiments in mice (8), and alternating receptor-binding avidities have indeed been observed for new pandemic H1N1 IAV (9).

A detailed comparison of the effects of cluster-transition mutations as well as potential compensatory mutations on IAV-receptor binding has not been performed yet, but is crucial for obtaining further insight into the evolutionary pathways leading to the generation of novel antigenic clusters. IAV binds to terminal sialic acids (SIA) moieties of glycans attached to glycoproteins or glycolipids on the host cell membranes (10, 11). Seasonal IAV strains infecting humans preferentially bind to α2,6- over α2,3-linked SIAs (12). In addition, receptor fine-specificity, determined by the specific composition of different types of sub-terminal sugar moieties, linkage-types and branch points, can have large effects on IAV-binding kinetics. It is therefore necessary to study IAV-binding properties using a number of different receptors types.

We have recently developed biolayer interferometry (BLI) assays for quantitative kinetic analysis of IAV-receptor interactions (**Chapter 2&3**). Here, we used BLI to compare IAV binding to different arrangements of N- and O-linked glycans in their natural protein context by the production of soluble biotinylated forms of four selected glycoproteins (Fetuin, ICAM1, LAMP1 and Glycophorin A) in HEK293T cells. We also compared the binding to LAMP1 carrying either α2,3- or α,6-linked SIAs. Viruses derived from eleven consecutive antigenic HA clusters of seasonal H3N2 IAVs from 1968 to 2002 were compared, showing that from 1972 to 1997 only limited changes in receptor binding kinetics to α2,6-linked SIAs have occurred. In contrast, binding to α2,3-linked SIAs was gradually reduced to undetectable levels within these 29 years. For three clusters the effects of the individual cluster-transition mutations were determined. For one cluster-transition mutation, which resulted in increased receptor binding, the effect of potential compensatory was analyzed in detail and linked to the order in which these mutations appeared as revealed by phylogenetic analysis. Mutations preceding the cluster-transition mutation were shown to reduce the binding rate. Our study provides arguments against a universal mechanism of IAV escape from immune pressure that is initiated with enhanced receptor binding (7).

MATERIALS AND METHODS

Cells and Viruses. Madin–Darby canine kidney (MDCK)-II and HEK 293T cells were maintained as described previously (17, 25). All H3-containing recombinant PR8 viruses were generated previously at Erasmus MC as described [6]. Viruses were grown in MDCK-II cells as described previously (25) and stored at −80°C. Virus particle numbers were precisely determined by Nanoparticle Tracking Analysis (NTA). Virus samples were 20-fold diluted in PBS. Temperature for NTA was set at 19 °C, at which temperature the viscosity of PBS is 1.05. Each sample was loaded to NTA chambers for 5 times independently. For each loading, viruses were tracked for 1 min and virus particle numbers were determined as the average of 5 measurements.

Genes, Expression Vectors, and Protein Expression and Purification. Codon-optimized human Fetuin, ICAM 1, Glycophorin A and LAMP1-encoding cDNAs (GenScript, Piscataway, NJ, USA) were genetically fused to a Fc-tag, for protein-A based purification, and a Bap-tag, for binding to octet sensors, and cloned in a pCAGGs vector as described previously (2^{nd} Octet paper). Human ST3Gal4 and ST6Gal1 expression vectors were kindly provided by Dr. Raoul de Groot. Glycoprotein, sialyltransferase and BirA expression vectors were co-transfected in HEK293T cells. Glycoproteins were purified using protein A beads and concentrations were determined by densitometric scanning of bands visualized by coomassie blue staining of gels after SDS-PAGE.

Chemicals. Oseltamivir Carboxylate (OC) was obtained from Roche, dissolved in DMSO at 100 mM concentration, aliquoted and stored at -20°C. Mal I, Mal II, SNA, ECA and PNA were obtained from VectorLabs. Biotinylated synthetic glycans 3'SLNLN and 6'SLNLN were obtained from the Consortium for Functional Glycomics (CFG) or synthesized in house.

Hemagglutination assay and NA activity assay. Hemagglutinating titers were determined from a 2-fold dilutions series of 50µl of virus added to 50µl of 0.5% human erythrocytes in V-shape 96-well plates. Titers were read after 2 hours incubation at 4^{o}C. NA activity determination by using 2'-(4-Methylumbelliferyl)-α-D-N-acetylneuraminic acid (MUNANA) as a substrate was described previously (26).

Biolayer interferometry. BLI analysis was performed on an Octet RED384 (Pall-FortBio) using standard streptavidin (SA) sensors (Pall-ForteBio). PBS containing 0.9 mM calcium and 0.5 mM magnesium was used as standard assay buffer. Receptor loading was performed by loading biotinylated receptors (synthetic glycans or proteins) to SA sensors. Receptor loading and virus association were performed as described in **Chapter** 2. Virus-receptor association was performed for 15 min. Initial binding rates (v^{obs}) values were determined as described in **Chapter** 2. For most receptors, virus-receptor BLI interaction experiments were repeated at least once and representative results were graphed. Standard deviations of initial binding rates (10^{10}nm/(min×mol)) for binding of viruses to different receptors ranged from 0.00 to 0.39 with a mean of 0.06).

Phylogenetic analysis. 830 unique DNA sequences covering the HA1 domain of H3N2 viruses isolated from 1968 from humans from 1968 to 1998, downloaded from the NCBI database, were aligned using MUSCLE. A phylogenetic DNA tree was constructed by using the PHYLIP Neighbor Joining algorithm and the F84 distance matrix. 164 sequences representing the the full tree were subsequently selected to construct the tree shown in Figure 3 that still displays the same topology as the master tree.

RESULTS

After its introduction into the human population in 1968, eleven different antigenic clusters of H3N2 have evolved until 2002. Their antigenic distance was previously determined by using re-assortant H1N1 PR8 viruses harboring HA proteins from eleven H3N2 viruses that match the consensus sequence of the different antigenic clusters (6). Here we used BLI to determine the evolution of the binding kinetics from 1968 to 2003 using these eleven viruses. The cluster transition mutations and their effect on antigenic distance can be viewed in Figure 4B of **Chapter 3**. We have recently described the quantification of the initial binding rate as an ideal method for comparing the binding kinetics of IAV particles (**Chapter 2**). Here we compared binding to four glycoproteins (Fetuin, Glycophorin A, ICAM and LAMP1), selected for their different glycan profiles (**Chapter 3**), and a simple biotinylated mono-antennary synthetic glycan (**Chapter 3** Figure 1A). The erythrocyte membrane protein Glycophorin A contains 17 O-linked glycans on a stretch of 50 amino acids, thereby mimicking the densely O-glycosylated domains typical for mucins that are potential decoy receptors for IAVs (13-15). ICAM1 and LAMP1 are transmembrane proteins bearing a large number of N-linked glycans (**Chapter 3**), a feature that has been suggested to contribute to efficient cell entry by IAV (16-18). The four glycoproteins were produced in HEK293T cells and highly enriched in their 2,6-linked

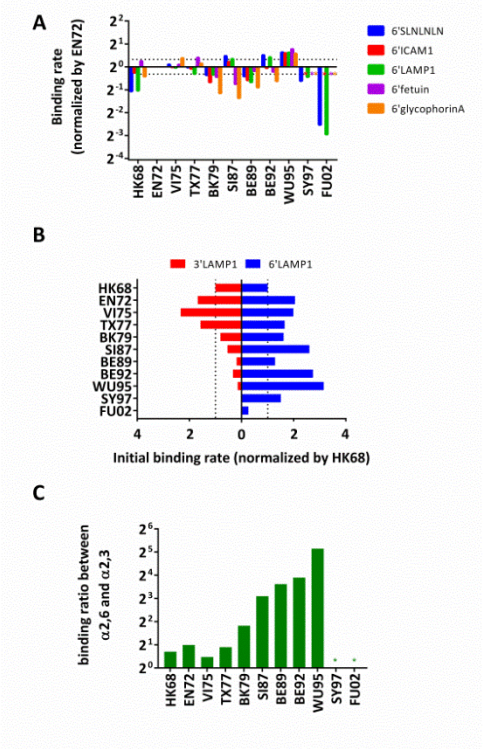

Figure 1. Binding rates of H3N1 viruses from 1968 to 2002 to different receptors. (A) Initial binding rates of H3N1 viruses, containing H3 genes derived from H3N2 viruses from 1968 until 2002, to synthetic glycan 6'SLNLNLN and glycoproteins co-expressed with ST6Gal1 (6'ICAM1, 6'LAMP1, 6'fetuin and 6'glycophorin A) are plotted ($log2^n$ scale) relative to the initial binding rates of EN72 (the absolute initial binding rates are indicated in Fig S1A). Dotted lines indicate 1.25-fold increase/decrease of initial binding rate. Asterisks indicate non-detectable binding. (B) Analysis of H3N1 virus binding to LAMP1 containing α2,3-linked SIAs (3'LAMP1; red bars) or α2,6-linked SIAs (6'LAMP1; blue bars). 3'LAMP1 was made by co-expression with ST3Gal4. Binding rates are normalized to binding rates of HK68 (the absolute binding rates are indicated in Fig S1B). (C) Ratio of absolute initial binding rates to 6'LAMP1 and 3'LAMP1 ($log2^n$ scale). Asterisks indicate non-detectable binding to 3'LAMP1.

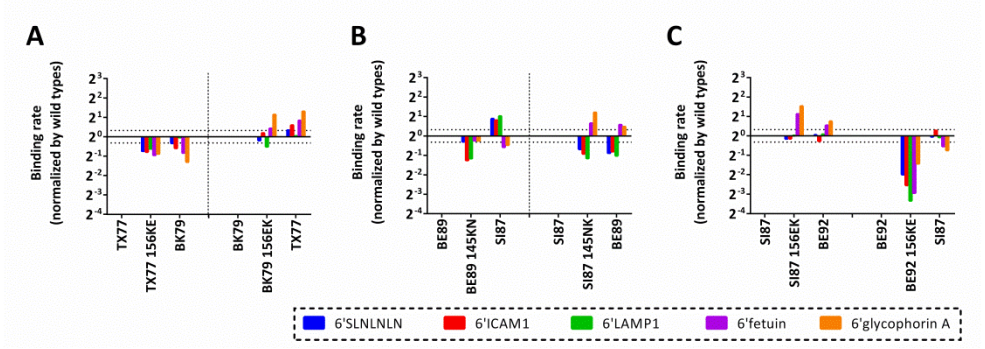

Figure 2. Effects of antigenic cluster transition mutations on virus binding. Initial binding rate effects of three cluster transition mutations are plotted relative to the initial binding rates that were obtained with the wildtype H3N1 viruses into which they were introduced. The effect of forward and backward mutations was examined. (A) TX77 156KE and BK79 156EK. (B) SI87 145NK and BE89 145KN. (C) SI187 156EK and BE92 156KE. (absolute binding rates are indicated in Fig S1A).

SIA content by co-expression of ST6Gal1 (**Chapter** 3). Virus binding curves were recorded for 15 minutes by BLI after which initial binding rates were determined as previously described (**Chapter** 2). In Figure 1A the results for the different receptors are plotted relative to the binding rates obtained with EN72 (absolute binding rates are indicated in Figure S1). The y-axis (2^n logarithmic scale) displays fold-up/fold-down factors relative to the binding rate of EN72. Whereas the preceding HK68 virus is a slower binder than EN72 (~2-fold down for 6'SLNLNLN and LAMP1), only small changes in binding rate were observed from EN72 up to WU95. The exception to this is the binding rate to glycophorin A which is considerably lower (up to ~2.3-fold) for BK79 to BE92. Remarkably, SY97 and FU02 are poor binders for which only a very low binding rate to LAMP1 and 6'SLNLNLN was observed. We also investigated whether a change in binding preference for 2,6-linked versus 2,3-linked SIA receptors had occurred over time by comparison of the binding rates to LAMP1 containing α,6- or α2,3-linked SIAs (referred to as 6'LAMP1 and 3'LAMP1). In Figure 1B, the fold-change in binding rate to 3'LAMP1 and 6'LAMP1 is plotted relative to the binding rates obtained for HK68. Clearly, the binding rate to an avian-type α2,3-linked SIA receptor gradually decreases to undetectable levels from VI75 to SY97. In Figure 1C the α2,6-SIA/α2,3-SIA binding rate ratio is plotted showing a ~30-fold increased binding α2,6-linked SIA binding from HK68 to WU95.

We next determined the effect on binding of three cluster transition mutations (Figure 2A) that had shifted the antigenicity of TX77 to BK79 (156KE), SI87 to BE89 (145NK) and SI87 to BE92 (156EK). Results are plotted relative, as in Figure 1, to the old cluster (TX77 or SI87). For TX77, the cluster transition mutation had a negative effect on the binding of all receptors analyzed. For SI87 the two cluster transition mutations have a negative (145NK)

or no effect (156EK) on the binding rate to N-linked type receptors (6'SLNLNLN, ICAM1 and LAMP1) and a positive effect on the O-linked type receptor Glycophorin A as well as fetuin which bears three N-linked and three O-linked glycans. The effect of the cluster transition mutations was also determined for the backward mutations which were introduced in the background of the "novel" antigenic clusters (BK79, BE89 and BE92).

Introduction of 156EK in BK79 resulted in increased binding to most receptors in agreement with the decreased binding resulting from the reciprocal mutation (156KE) in TX77. The other backward mutations in the new antigenic cluster context did not induce the opposite effect to the forward mutations (Figure 2B). This is most strikingly observed for the SI87 to BE92 transition. Thus, 156KE mutation had a large negative effect on binding, while the opposite effect was not observed for the reciprocal mutation in SI87. We conclude that antigenic cluster transitions from 1972 to 1995 are not associated with large (< 2-fold) differences in binding rates. Also the cluster transition determining mutations themselves do not have large effects. Introduction of a backward mutation in BE92 did result, however, in much decreased binding indicating an important role for the background in which the mutations are introduced.

Analysis of the virus binding effects of accessory, possibly compensatory, mutations will contribute to a further understanding of the mechanisms that drive antigenic evolution. Knowledge on the order in which substitutions have occurred is crucial. Therefore a phylogenetic analysis of the evolution of the H3N2 HA gene from 1968 to 1998 was performed using 830 HA DNA sequences present in the NCBI sequence database. Amino acid substitutions occurring along the trunk of the resulting phylogenetic tree were determined and are indicated on a summarizing tree (Figure 3). The different antigenic clusters are indicated and the viruses representing the cluster consensus sequence (6) are highlighted. Cluster transition mutations are indicated in red along the tree. Cluster transitions are mostly caused by single amino acid substitutions, which are expected to arise rapidly. Still, they do not seem to be selected frequently as revealed by a straightforward count of their appearance in other antigenic clusters (Table 1). The occurrence of most cluster transition mutations appears to be exclusively restricted to their own antigenic cluster. As an exception, cluster transition mutation 156EK (and to a lesser extent 145NK) frequently appears before the solid establishment of the new antigenic cluster. Its introduction has occurred repeatedly along many different side branches, however without ever leading to the generation of a sub-cluster of considerable size. Whereas substitution 156EK is likely selected for its immunity evading properties, the prior selection (see tree, Figure 2) of potential compensatory mutations 193NS, 190ED and 133SD in/close to the receptor binding site could have been crucial for creating a background in which the introduction of 156EK results in a virus with high fitness. Remarkably, the introduction of these mutations is a rather unique event (Table 1).

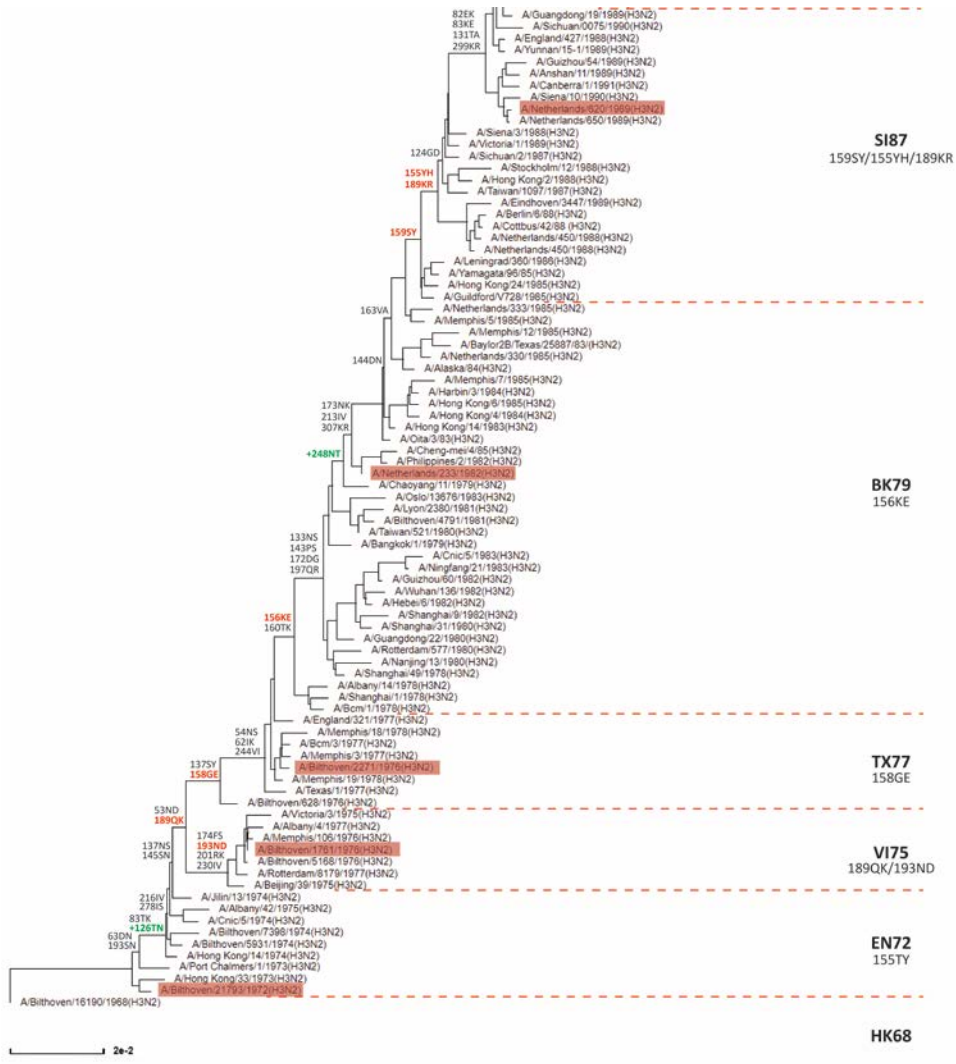

Figure 3. Phylogenetic analysis of H3 proteins from 1968 to 1997. A phylogenetic tree was constructed from 164 DNA sequences of human H3N2 viruses that were isolated between 1968 and 1997. Selection of sequences was guided by a master tree constructed from 830 sequences. Amino acid substitutions that were introduced, and maintained along the trunk of the tree are indicated. Mutations in red correspond to cluster transition mutations. Mutations in green ,preceded by '+' or '-', have led to the creation or deletion of potential N-linked glycosylation sites. The HA protein tree was rooted by HK68 (A/Bilthoven/16190/1968). Antigenic clusters are indicated and their borders are indicated by dashed lines. (HK68, A/Bilthoven/16190/68, EN72: A/Bilthoven/21793/72; VI75, A/Bilthoven/1761/76; TX77, A/Bilthoven/2271/76; BK79: A/Netherlands/233/82; SI87, A/Netherlands/620/89; BE89, A/Netherlands/823/92; BE92, A/Netherlands/179/93; WU95, A/Netherlands/178/95; SY97, A/Netherlands/427/98). Antigenic distances between the different clusters were visualized in Chapter 1, Fig 4).

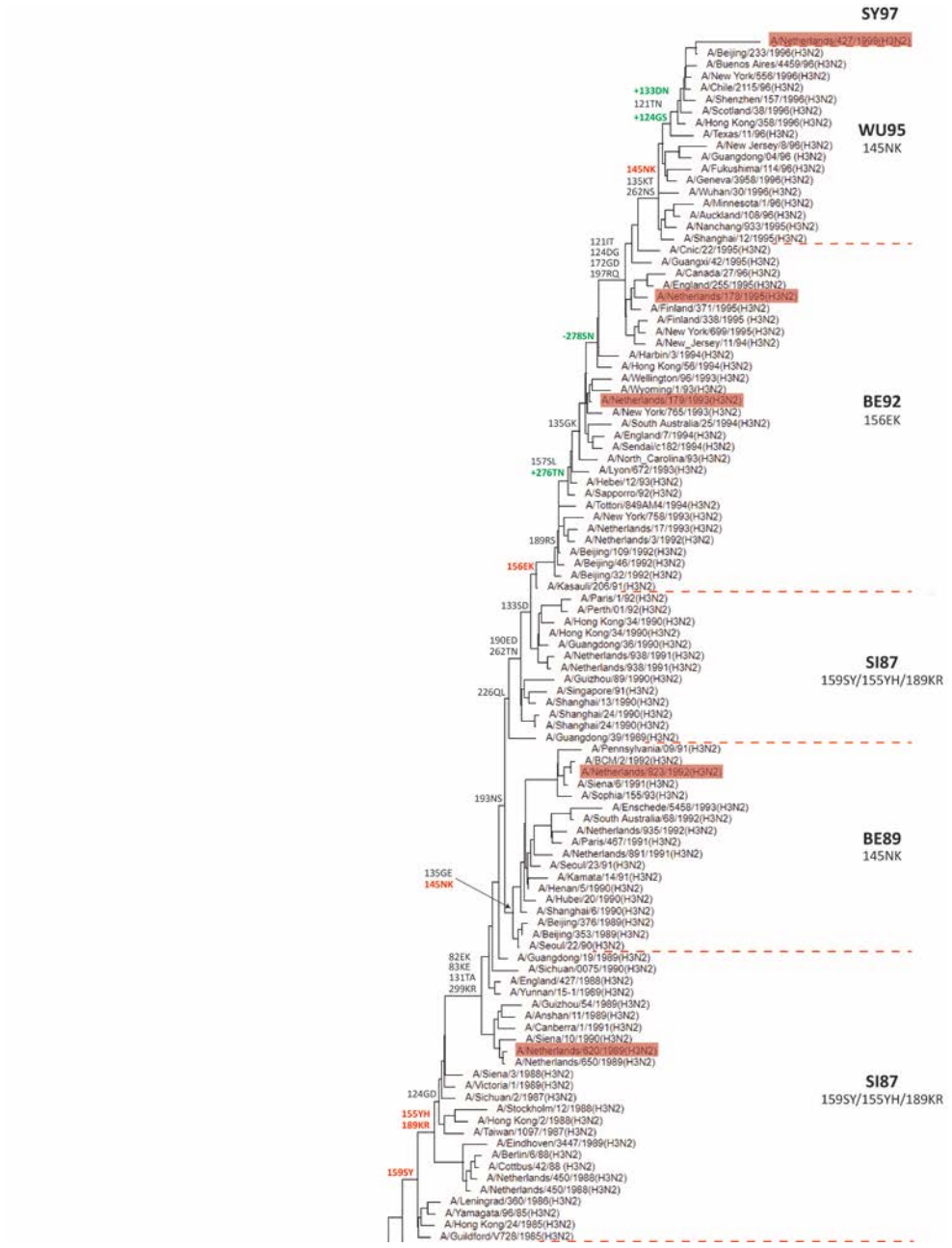
SY97
A/Netherlands/427/1999(H3N2)
A/Beijing/233/1996(H3N2)
A/Buenos Aires/4459/96(H3N2)
A/New York/556/1996(H3N2)
A/Chile/2115/96(H3N2)
A/Shenzhen/157/1996(H3N2)
A/Scotland/38/1996(H3N2)
A/Hong Kong/358/1996(H3N2)
A/Texas/11/96(H3N2)
A/New Jersey/8/96(H3N2)
A/Guangdong/04/96 (H3N2)
A/Fukushima/114/96(H3N2)
A/Geneva/3958/1996(H3N2)
A/Wuhan/30/1996(H3N2)
A/Minnesota/1/96(H3N2)
A/Auckland/108/96(H3N2)
A/Nanchang/933/1995(H3N2)
A/Shanghai/12/1995(H3N2)
+133DN
121TN
+124GS
WU95
145NK
145NK
135KT
262NS
121IT
124DG
172GD
197RQ
A/Cnic/22/1995(H3N2)
A/Guangxi/42/1995(H3N2)
A/Canada/27/96(H3N2)
A/England/255/1995(H3N2)
A/Netherlands/179/1995(H3N2)
A/Finland/371/1995(H3N2)
A/Finland/338/1995 (H3N2)
A/New York/699/1995(H3N2)
A/New_Jersey/11/94(H3N2)
-278SN
A/Harbin/3/1994(H3N2)
A/Hong Kong/56/1994(H3N2)
A/Wellington/96/1993(H3N2)
A/Wyoming/1/93(H3N2)
A/Netherlands/179/1993(H3N2)
BE92
156EK
135GK
A/New York/765/1993(H3N2)
A/South Australia/25/1994(H3N2)
A/England/7/1994(H3N2)
A/Sendai/c182/1994(H3N2)
A/North_Carolina/93(H3N2)
157SL
+276TN
A/Lyon/672/1993(H3N2)
A/Hebei/12/93(H3N2)
A/Sapporo/92(H3N2)
A/Totori/849A/M4/1994(H3N2)
A/New York/758/1993(H3N2)
A/Netherlands/17/1993(H3N2)
189RS
A/Netherlands/3/1992(H3N2)
A/Beijing/109/1992(H3N2)
A/Beijing/46/1992(H3N2)
156EK
A/Beijing/32/1992(H3N2)
A/Kasauli/206/91(H3N2)
A/Paris/1/92(H3N2)
133SD
A/Perth/01/92(H3N2)
A/Hong Kong/34/1990(H3N2)
A/Hong Kong/34/1990(H3N2)
190ED
262TN
A/Guangdong/36/1990(H3N2)
A/Netherlands/938/1991(H3N2)
A/Netherlands/938/1991(H3N2)
SI87
159SY/155YH/189KR
A/Guizhou/89/1990(H3N2)
226QL
A/Singapore/91(H3N2)
A/Shanghai/13/1990(H3N2)
A/Shanghai/24/1990(H3N2)
A/Shanghai/24/1990(H3N2)
A/Guangdong/39/1989(H3N2)
A/Pennsylvania/09/91(H3N2)
A/BCH/2/1992(H3N2)
A/Netherlands/823/1992(H3N2)
A/Siena/6/1991(H3N2)
193NS
A/Sophia/155/93(H3N2)
A/Enschede/5458/1993(H3N2)
A/South Australia/68/1992(H3N2)
A/Netherlands/935/1992(H3N2)
A/Paris/467/1991(H3N2)
BE89
145NK
A/Netherlands/891/1991(H3N2)
A/Seoul/23/91(H3N2)
135GE
145NK
A/Kamata/14/91(H3N2)
A/Henan/5/1990(H3N2)
A/Hubei/20/1990(H3N2)
A/Shanghai/6/1990(H3N2)
A/Beijing/376/1989(H3N2)
A/Beijing/353/1989(H3N2)
A/Seoul/22/90(H3N2)
A/Guangdong/19/1989(H3N2)
82EK
83KE
131TA
299KR
A/Sichuan/0075/1990(H3N2)
A/England/427/1988(H3N2)
A/Yunnan/15-1/1989(H3N2)
A/Guizhou/54/1989(H3N2)
A/Anshan/11/1989(H3N2)
A/Canberra/1/1991(H3N2)
A/Siena/10/1990(H3N2)
A/Netherlands/620/1989(H3N2)
A/Netherlands/650/1989(H3N2)
A/Siena/3/1988(H3N2)
A/Victoria/1/1989(H3N2)
A/Sichuan/2/1987(H3N2)
SI87
159SY/155YH/189KR
124GD
A/Stockholm/12/1988(H3N2)
155YH
189KR
A/Hong Kong/2/1988(H3N2)
A/Taiwan/1097/1987(H3N2)
A/Eindhoven/3447/1989(H3N2)
A/Berlin/6/88(H3N2)
159SY
A/Cottbus/42/88 (H3N2)
A/Netherlands/450/1988(H3N2)
A/Netherlands/450/1988(H3N2)
A/Leningrad/360/1986(H3N2)
A/Yamagata/96/85(H3N2)
A/Hong Kong/24/1985(H3N2)
A/Guildford/V728/1985(H3N2)

Table 1. Clsuter transition and accessory postitions changes (percentage) from cluster VI75 to SY97

	Cluster transition positions (aa position)														Accessory positions					
	145		155		156		158		159		189		193		133		190		226	
Cluster (nr of seq)	**aa**	**%**	**aa**	**%**	**aa**	**%**	**aa**	**%**	**aa**	**%**	**aa**	**%**	**aa**	**%**	**aa**	**%**	**aa**	**%**	**aa**	**%**
VI75 (35)	**N**	**94**	**Y**	**100**	**K**	**100**	**G**	**100**	**S**	**100**	**189QK**	**100**	**193ND**	**100**	**N**	**100**	**E**	**100**	**L**	**100**
	K	**6**																		
TX77 (21)	**N**	**100**	**Y**	**100**	**K**	**100**	**158GE**	**100**	**S**	**100**	**K**	**100**	**N**	**95**	**N**	**95**	**E**	**100**	**L**	**100**
													K	**5**	**D**	**5**				
BK79 (186)	**N**	**86**	**Y**	**100**	**156KE**	**88**	**E**	**100**	**S**	**100**	**K**	**100**	**N**	**95**	**133NS**	**96**	**E**	**100**	**L**	**98**
	K	**13**			**K**	**9**							**K**	**5**	**N**	**3**				
SI87 (210)	**N**	**92**	**155YH**	**83**	**E**	**75**	**E**	**98**	**159SY**	**91**	**189KR**	**83**	**N**	**93**	**S**	**98**	**E**	**100**	**L**	**96**
	K	**7**	**Y**	**17**	**K**	**22**			**H**	**4**	**K**	**17**	**K**	**7**	**N**	**2**			**Q**	**4**
BE89 (230)	**145NK**	**100**	**H**	**100**	**E**	**90**	**E**	**59**	**Y**	**99**	**R**	**98**	**193KS**	**90**	**S**	**90**	**E**	**100**	**L**	**100**
					K	**7**	**D**	**41**					**K**	**4**	**N**	**10**				
SI87 TOP (16)	**N**	**100**	**H**	**100**	**E**	**31**	**E**	**94**	**Y**	**100**	**R**	**100**	**S**	**100**	**D**	**50**	**190ED**	**88**	**226LQ**	**88**
					K	**69**									**S**	**44**	**D**	**13**	**L**	**13**
BE92 (625)	**N**	**88**	**H**	**100**	**156EK**	**99**	**E**	**97**	**Y**	**99**	**189RS**	**98**	**S**	**97**	**133SD**	**98**	**D**	**98**	**L**	**51**
	K	**12**					**D**	**2**					**R**	**3**					**I**	**26**
																			Q	**22**
WU95 (387)	**145NK**	**100**	**H**	**100**	**K**	**99**	**E**	**98**	**Y**	**99**	**S**	**100**	**S**	**94**	**D**	**54**	**D**	**91**	**V**	**76**
													R	**5**	**N**	**46**	**V**	**6**	**I**	**22**
SY97 (1818)	**K**	**99**	**H**	**96**	**156KQ**	**99**	**158EK**	**97**	**Y**	**97**	**S**	**99**	**S**	**99**	**133DN**	**99**	**D**	**99**	**V**	**94**
			T	**4**					**N**	**2**					**D**	**1**			**I**	**6**

Cluster transition mutation along trunk of phylogenetic tree of Figure 2

Cluster transition mutation on branch (no change along trunk) of Figure 2

Accessory mutation along trunk of Figure 2 without effect on antigenicity

We selected cluster transition SI87 to BE92 for further analysis. The effect of the individual mutations on receptor binding was examined in the background of SI87 (Figure 4A, forward mutations) and BE92 (Figure 4B, backward mutations). All four forward mutations increased binding to glycophorin A and fetuin but decreased binding to the other three receptors. As was already observed above for the cluster transition mutations (Figure 2), the backward mutations did not give a consistent pattern of binding effects that are opposite to the direction of the corresponding forward mutations. Clearly, the binding effects of single substitutions are context-dependent. The cumulative binding effects on receptor binding by consecutive introduction of mutations 193NS, 190ED and 133SD is

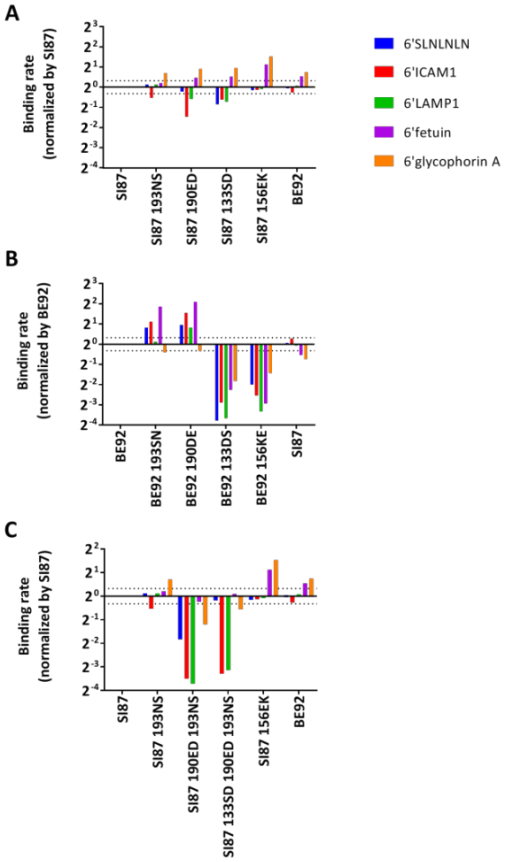

Figure 4. Effect of accessory or compensatory mutations in SI87 and BE92 on virus binding. (A) Initial binding rates of viruses containing mutations (193NS, 190ED, 133SD and 156EK) in the background of SI87 (panel A), and the corresponding backward mutations (193SN, 190DE, 133DS and 156KE) in the background of BE92 are plotted for different receptors normalized to SI87 or BE92 respectively. (C) Initial binding rates of viruses containing cumulative mutations (193NS, 193NS+190ED, 193NS+190ED+133SD) in the background of SI87 are plotted for different receptors normalized to SI87 (absolute binding rates are indicated in Fig S1A.)

shown in Figure 4C. The negative effects of mutations 193NS, 190ED and 133SD on binding to 6'SLNLNLN, ICAM1and LAMP1 are cumulative in general. The positive effects of the single mutations on binding to glycophorin A and fetuin (Figure 5A) are not cumulative but collectively result in a slightly negative effect on binding to glycophorin A. We therefore conclude that, for cluster transition SI87 to BE92, a proposed mechanism (7) in which the initial escape from antibodies is accomplished by increased receptor binding, is not supported by our results.

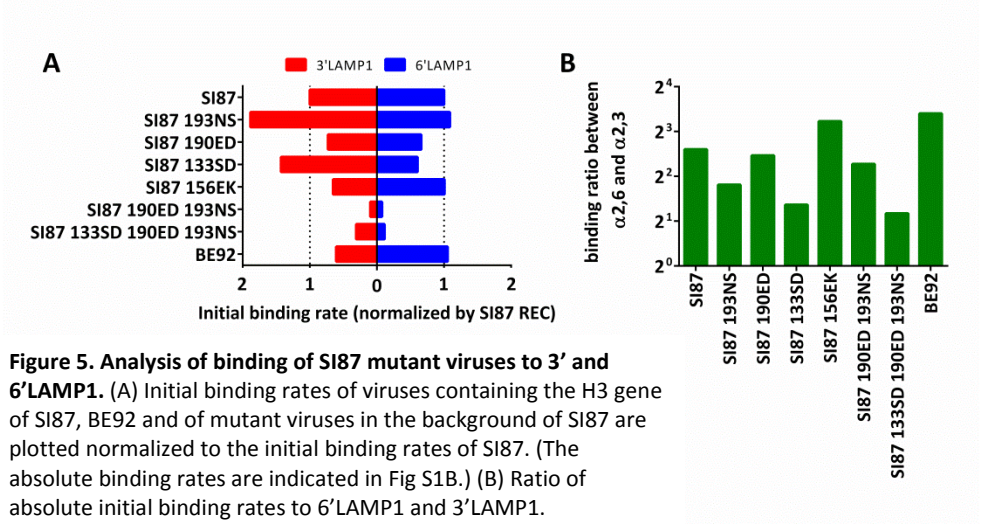

Figure 5. Analysis of binding of SI87 mutant viruses to 3' and 6'LAMP1. (A) Initial binding rates of viruses containing the H3 gene of SI87, BE92 and of mutant viruses in the background of SI87 are plotted normalized to the initial binding rates of SI87. (The absolute binding rates are indicated in Fig S1B.) (B) Ratio of absolute initial binding rates to 6'LAMP1 and 3'LAMP1.

Another selective force for the acquirement of substitutions 193NS, 190ED and 133SD could be ongoing adaptation to human receptors. The effect of individual or cumulative mutations in the background of SI87 is plotted, in the same way as in Figure. 1, in Figure 5A and 5B. Together, mutations 193NS, 190ED and 133SD resulted in a decreased binding rate to α2,3-linked SIAs although this was not simply caused by the additive effects of the individual mutations. Possibly, the negative effect of mutations 193NS, 190ED and 133SD on binding to different glycoproteins carrying human-type receptors created a background that is permissive for the introduction of cluster transition mutation 156EK.

In Figure 6, we plotted the absolute binding rates of a large set of mutants on the previously constructed antigenic map (6) to visualize potential correlations between binding rate and antigenic distance. The effects on binding rate to an N-linked (LAMP1) and an O-linked glycoprotein (Glycophorin A) are compared. For neither receptor a clear correlation between antigenic distance and binding rate was observed. However, the changes in binding rate are relatively small when comparing the three cluster determinants (SI87, BE89 and BE92) and the cluster transition mutations (highlighted in yellow). The effects of many of the potential compensatory mutations are larger but forward and backward effects are not consistently of opposite direction. Remarkably, the effects on Glycophorin A and LAMP1 differ for many of the mutants.

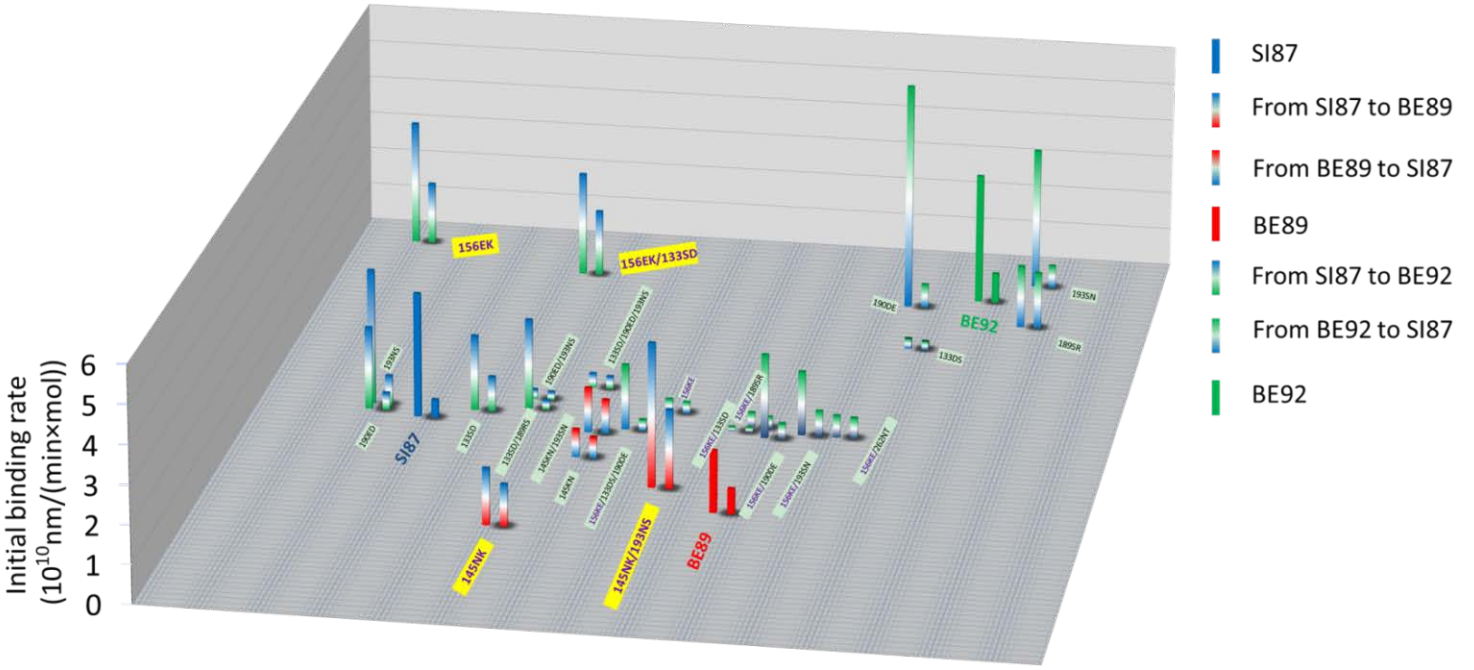

Figure 6. 3D plot of virus binding to 6'LAMP1 and 6'glycophorin A in relation to antigenic distance between the SI87, BE89 and BE92 clusters. Antigenic distance between SI87, BE89 and BE92 consensus viruses is plotted on the floor of the 3D map based on (6). The binding rates are indicated by the bar graphs (in 10^{10} nm/min.mol). Antigenic cluster determining viruses are color-coded (SI87, blue; BE89, red; BE92, green). Viruses with forward and backward mutations are color-coded by gradient colours from top (color of antigenic cluster in which the mutation was made) to bottom (color of the destiny antigenic cluster). For example, forward mutations in the background of SI87 towards BE92 are labelled by gradient colour from blue to green (top to bottom). Vice versa, the backward mutations in the background of BE92 towards SI87 are labelled from green to blue (top to bottom). The bars with and without the grey shading underneath indicate the binding levels to 6'glycophorin A and 6'LAMP1, respectively. All bars are labelled by text boxes indicating the mutations. The cluster transition mutations are indicated in purple. Yellow boxes indicate cluster transition mutations from SI87 to BE89 or BE92.

DISCUSSION

Since its introduction in the human population, the antigenic evolution of seasonal IAV H3N2 has proceeded by punctuated transitions from one antigenic cluster to the next (6). In this study we analyzed the receptor-binding properties of H3N2 viruses from 1968 until 2002 and of several mutant variants thereof, with the aim to analyze to what extent transition from one antigenic cluster to another was accompanied with changes in the receptor-binding properties of these viruses. Our results indicate that until 1997 only relatively small changes in H3N2 virus binding rate to glycoproteins that we selected to represent mucins (glycophorin A) or densely sialylated N-linked transmembrane proteins (LAMP1, ICAM1) have occurred between the different antigenic clusters. Cluster-transition mutations were shown to have either positive or negative effects on the receptor binding rate. These effects strongly depended on the genetic background in which they were introduced. Some antigenically-neutral (accessory) amino acid substitutions were introduced along the evolutionary track from SI87 to BE92, just preceding the introduction of the antigenic cluster transition mutation. They had additive negative effects on receptor binding and we speculate that these accessory mutations created the genetic background that favored the selection of the antigenic cluster transition mutation. Determination of the selective forces that drive the selection of cluster transition and accessory mutations will help to understand the pathways of antigenic change.

Studies concerning changes in binding avidity and specificity often focus on the binding to epithelial cell surface receptors supporting virus entry. Nevertheless, changes in binding rates that occur during antigenic evolution will also affect the potential to escape from decoy receptors present on mucins in respiratory mucus. Interestingly, many of the mutations tested in this study have differential effects on binding to mucus-like receptors (glycophorin A) versus cell surface-like receptors (ICAM1 and Lamp1). Such differences may highlight slight deviations from the optimal binding balance required for infection and transmission and as such reveal critical steps in the antigenic and genetic evolution of IAVs. By using cell culture expressed glycoproteins as receptor probes we have ample opportunities for further tailoring these proteins to specific demands.

Antigenic change is mostly dependent on amino acid substitutions at only seven positions near the HA receptor binding site. These cluster transition mutations may disturb the precisely tuned virus binding rate and specificity for a diverse spectrum of SIA receptors attached to soluble decoy proteins or present at functional virus entry sites. Accessory substitutions, that hardly affect antigenicity, might be selected for compensating the potentially detrimental effects of cluster transition mutations. Their selection upon the acquirement of a cluster transition mutation shapes the extended side-branches of antigenic clusters and their high frequency complicates a systematic analysis. In this paper

we have focused on cluster transition mutations and on the smaller group of accessory mutations that were introduced along the trunk of the phylogenetic HA tree (Figure 2) and are mostly maintained for longer periods in several consecutive antigenic clusters. In contrast to several accessory mutations, the cluster transition mutations have a relatively limited effect on virus binding rate, thereby arguing against the hypothesis that accessory mutations are mostly selected for restoring binding rates.

An alternative hypothesis (7), in which more gradual antigenic change is initially driven by the favorable selection for binding rate enhancing mutations, is clearly not universally applicable. It is strongly contradicted by the negative effects of mutations 193NS, 190ED and 133SD on binding rate (Figure 3C) prior to introduction of cluster transition mutation 156KE. An ongoing genetic drift towards human-type α2,6-linked receptor usage was observed for the consecutive antigenic clusters (Figure 4B), but is clearly not caused by mutations 193NS, 190ED and 133SD, which decrease the ratio of the α2,6/α2,3 binding rate (Figure 4D). Strikingly, cluster transition mutations 156KE (BE92) and 145NK (BE89 and WU95) have been selected on many independent occasions already long before the antigenic cluster became solidly established (quantified in Table 1). Positive selection of an antibody-evasive mutation like 156KE, in an immune host, will likely be followed by negative selection due to non-favorable effects in non-immune hosts in the early phase of an epidemic. When the non-favorable effects are small, as might be the case for 156KE, the mutation may pop up regularly and occur more frequently in time as seen for the last phase of the SI87 cluster (Table 1, SI87 TOP). Antigenicity of two consecutive antigenic clusters can be switched back and forth in vitro by mutating the cluster transition position (3, 6). In contrast, reverse mutations at positions causing changes in binding rate do not consistently give this mirrored pattern, as was dramatically demonstrated by the large negative effect of the 156EK back-substitution in BE92. Thus, binding rate reducing mutations 193NS/190ED/133SD may have created a favorable setting for selection of binding rate enhancing mutation 156EK.

What drives the selection of the accessory mutations is not known. Mutation 190ED (first introduced in A/Shanghai/24/1990) might have been selected in response to the directly preceding selection of the highly remarkable substitution 226LQ (A/Guangdong/39/1989). 226Q remained dominant in the last years of the SI87 cluster but gradually disappeared in the following antigenic cluster (Table 1). The reverse mutation 226QL, is one of the two hallmark substitutions, together with 228GS, that determines a switch from avian to human receptor specificity (19) and was already present in the earliest human H3N2 isolates in 1968 (20). In contrast, 190ED is one of the two substitutions determining a switch from avian to human receptor specificity for H1N1 viruses but is only first introduced in (and maintained since) 1990 in H3N2. Also in H3N2 it is in close contact with the SIA moiety of the sialoside receptor (21, 22) but only limited evidence for its

contribution to α2,6 SIA-specific binding has been reported (23). We speculate that these mutations compensate each other's effect on α2,3/α2,6 SIA-binding specificity.

Our results do not indicate a clear correlation between changes in virus-receptor binding and in antigenicity, as has been reported previously (24) for the N145K cluster transition mutation that occurred between 1992 and 1995 (BE92 to WU95 cluster transition). While the increased binding resulting from this cluster transition mutation is in agreement with the model proposed by Hensley at al., (7) in which increased HA-receptor binding avidity drives antigenic drift by the subsequent selection of accessory mutations, our results indicate that accessory mutations may also precede or even be required for the selection of an antigenic cluster transition mutation (SI87 to BE92 cluster transition). Selection of antigenic cluster transition mutations may thus be driven via different processes. Furthermore, it is plausible that also mutations in NA may drive selection of mutations in HA, including cluster transition mutations. Possibly, for each antigenic cluster transition, the determining mutations may have been selected via different selective processes, which may make it quite difficult to predict upcoming antigenic changes.

REFERENCES

1. Stohr K. Influenza--WHO cares. The Lancet Infectious diseases. 2002 Sep;2(9):517.
2. Akazawa M, Sindelar JL, Paltiel AD. Economic costs of influenza-related work absenteeism. Value in health : the journal of the International Society for Pharmacoeconomics and Outcomes Research. 2003 Mar-Apr;6(2):107-15.
3. Smith DJ, Lapedes AS, de Jong JC, Bestebroer TM, Rimmelzwaan GF, Osterhaus AD, et al. Mapping the antigenic and genetic evolution of influenza virus. Science. 2004 Jul 16;305(5682):371-6.
4. Bedford T, Suchard MA, Lemey P, Dudas G, Gregory V, Hay AJ, et al. Integrating influenza antigenic dynamics with molecular evolution. eLife. 2014;3:e01914.
5. Wiley DC, Wilson IA, Skehel JJ. Structural identification of the antibody-binding sites of Hong Kong influenza haemagglutinin and their involvement in antigenic variation. Nature. 1981 Jan 29;289(5796):373-8.
6. Koel BF, Burke DF, Bestebroer TM, van der Vliet S, Zondag GC, Vervaet G, et al. Substitutions near the receptor binding site determine major antigenic change during influenza virus evolution. Science. 2013 Nov 22;342(6161):976-9.
7. Hensley SE, Das SR, Bailey AL, Schmidt LM, Hickman HD, Jayaraman A, et al. Hemagglutinin receptor binding avidity drives influenza A virus antigenic drift. Science. 2009 Oct 30;326(5953):734-6.
8. Linderman SL, Hensley SE. Antibodies with 'Original Antigenic Sin' Properties Are Valuable Components of Secondary Immune Responses to Influenza Viruses. PLoS pathogens. 2016 Aug;12(8):e1005806.
9. Li Y, Myers JL, Bostick DL, Sullivan CB, Madara J, Linderman SL, et al. Immune history shapes specificity of pandemic H1N1 influenza antibody responses. The Journal of experimental medicine. 2013 Jul 29;210(8):1493-500.
10. Rogers GN, Paulson JC. Receptor determinants of human and animal influenza virus isolates: differences in receptor specificity of the H3 hemagglutinin based on species of origin. Virology. 1983 Jun;127(2):361-73.
11. Rogers GN, Pritchett TJ, Lane JL, Paulson JC. Differential sensitivity of human, avian, and equine influenza A viruses to a glycoprotein inhibitor of infection: selection of receptor specific variants. Virology. 1983 Dec;131(2):394-408.
12. Ito T, Couceiro JN, Kelm S, Baum LG, Krauss S, Castrucci MR, et al. Molecular basis for the generation in pigs of influenza A viruses with pandemic potential. Journal of virology. 1998 Sep;72(9):7367-73.
13. Tomita M, Marchesi VT. Amino-acid sequence and oligosaccharide attachment sites of human erythrocyte glycophorin. Proceedings of the National Academy of Sciences of the United States of America. 1975 Aug;72(8):2964-8.
14. Pisano A, Redmond JW, Williams KL, Gooley AA. Glycosylation sites identified by solid-phase Edman degradation: O-linked glycosylation motifs on human glycophorin A. Glycobiology. 1993 Oct;3(5):429-35.
15. Hanisch FG. O-glycosylation of the mucin type. Biological chemistry. 2001 Feb;382(2):143-9.
16. Casasnovas JM, Stehle T, Liu JH, Wang JH, Springer TA. A dimeric crystal structure for the N-terminal two domains of intercellular adhesion molecule-1. Proceedings of the National Academy of Sciences of the United States of America. 1998 Apr 14;95(8):4134-9.
17. de Vries E, de Vries RP, Wienholts MJ, Floris CE, Jacobs MS, van den Heuvel A, et al. Influenza A virus entry into cells lacking sialylated N-glycans. Proceedings of the National Academy of Sciences of the United States of America. 2012 May 8;109(19):7457-62.
18. Chu VC, Whittaker GR. Influenza virus entry and infection require host cell N-linked glycoprotein. Proceedings of the National Academy of Sciences of the United States of America. 2004 Dec 28;101(52):18153-8.

19. Vines A, Wells K, Matrosovich M, Castrucci MR, Ito T, Kawaoka Y. The role of influenza A virus hemagglutinin residues 226 and 228 in receptor specificity and host range restriction. Journal of virology. 1998 Sep;72(9):7626-31.
20. Matrosovich M, Tuzikov A, Bovin N, Gambaryan A, Klimov A, Castrucci MR, et al. Early alterations of the receptor-binding properties of H1, H2, and H3 avian influenza virus hemagglutinins after their introduction into mammals. Journal of virology. 2000 Sep;74(18):8502-12.
21. Ha Y, Stevens DJ, Skehel JJ, Wiley DC. X-ray structure of the hemagglutinin of a potential H3 avian progenitor of the 1968 Hong Kong pandemic influenza virus. Virology. 2003 May 10;309(2):209-18.
22. Yang H, Carney PJ, Chang JC, Guo Z, Villanueva JM, Stevens J. Structure and receptor binding preferences of recombinant human A(H3N2) virus hemagglutinins. Virology. 2015 Mar;477:18-31.
23. Lin YP, Xiong X, Wharton SA, Martin SR, Coombs PJ, Vachieri SG, et al. Evolution of the receptor binding properties of the influenza A(H3N2) hemagglutinin. Proceedings of the National Academy of Sciences of the United States of America. 2012 Dec 26;109(52):21474-9.
24. Li Y, Bostick DL, Sullivan CB, Myers JL, Griesemer SB, Stgeorge K, et al. Single hemagglutinin mutations that alter both antigenicity and receptor binding avidity influence influenza virus antigenic clustering. Journal of virology. 2013 Sep;87(17):9904-10.
25. de Vries E, Tscherne DM, Wienholts MJ, Cobos-Jimenez V, Scholte F, Garcia-Sastre A, et al. Dissection of the influenza A virus endocytic routes reveals macropinocytosis as an alternative entry pathway. PLoS Pathog. 2011 Mar;7(3):e1001329.
26. Dai M, Guo H, Dortmans JC, Dekkers J, Nordholm J, Daniels R, et al. Identification of Residues That Affect Oligomerization and/or Enzymatic Activity of Influenza Virus H5N1 Neuraminidase Proteins. Journal of virology. 2016 Oct 15;90(20):9457-70.

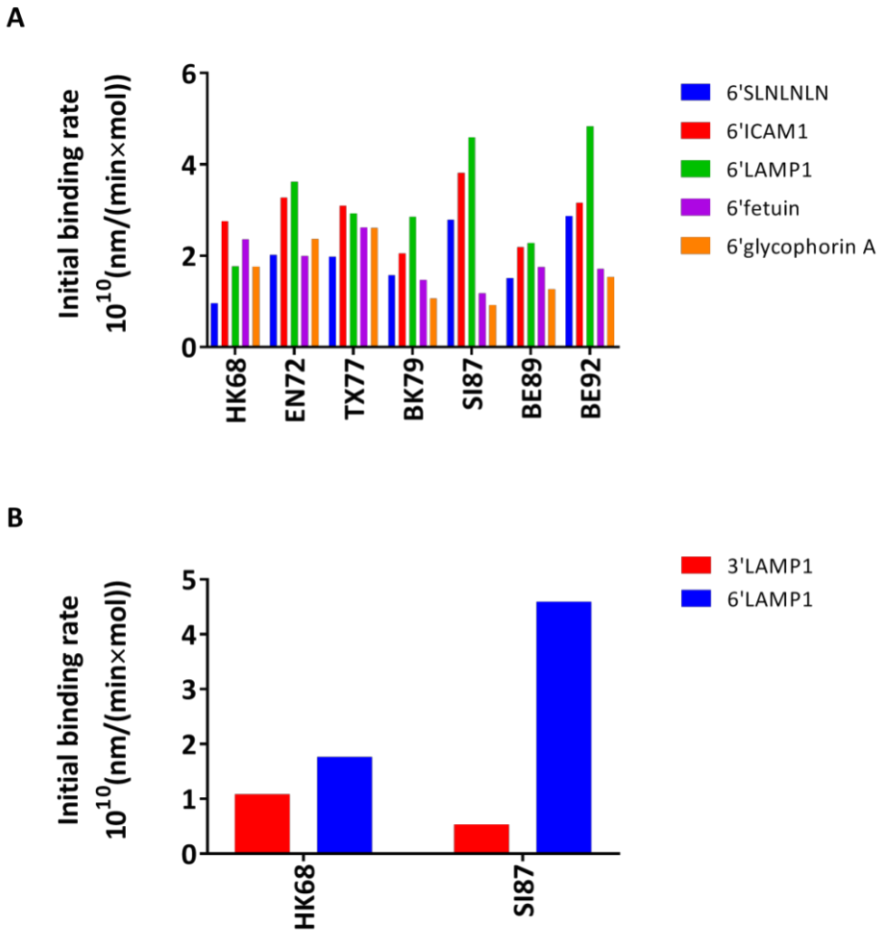

Supplementary Figure 1. Absolute initial binding rates of wild type viruses. (A) Initial binding rates to 6'glycans or 6'glycoproteins. (B) Initial binding rates to 3' and 6'LAMP1.

Chapter 5

Rapid Emergence of Highly Pathogenic Avian Influenza Subtypes from a Subtype H5N1 Hemagglutinin Variant

Erik de Vries, Hongbo Guo*, Meiling Dai*, Peter J.M. Rottier, Frank J.M. van Kuppeveld, and Cornelis A.M. de Haan

Virology Division, Department of Infectious Diseases & Immunology, Faculty of Veterinary Medicine, Utrecht University, Yalelaan 1, 3584CL Utrecht, the Netherlands

*These authors contributed equally

Emerg Infect Dis. 2015;21:842–6.

ABSTRACT

In 2014, novel highly pathogenic avian influenza A H5N2, H5N5, H5N6, and H5N8 viruses caused outbreaks in Asia, Europe, and North America. The H5 genes of these viruses form a monophyletic group that evolved from a clade 2.3.4 H5N1 variant. This rapid emergence of new H5Nx combinations is unprecedented in the H5N1 evolutionary history.

A highly pathogenic avian influenza (HPAI) A(H5N1) virus (A/goose/Guangdong/1/1996) was first detected in China in 1996. Multiple clades, defined by phylogenetic characterization of the H5 hemagglutinin (HA) (1), have evolved and spread across Asia, Africa, and Europe, causing enormous losses to the poultry industry. A total of 694 human infections (death rate 58%) were recorded during 2003–2014 (2).

During the evolution of HPAI H5N1 viruses, reassortment events involving the 6 internal gene segments have often been detected (reviewed in [3]), but novel subtypes (i.e., combinations of HPAI H5 with other N subtypes) have rarely been isolated. In 2014, a novel highly virulent reassortant HPAI H5N6 virus (4) caused multiple outbreaks in Southeast Asia and 1 lethal human infection, which led the Food and Agricultural Organization of the United Nations to issue a warning (5). Outbreaks of novel HPAI H5N8 virus in South Korea (6,7), China (8), and Japan raised further concern, and in November 2014, this subtype emerged outside Eastern Asia, causing outbreaks in poultry farms in Germany, the Netherlands, the United Kingdom, Canada, and the United States.

THE STUDY

To determine the evolutionary history of the HA proteins of these novel HPAI subtypes, we collected all HPAI H5 coding region sequences for all subtypes, except H5N1, and then aligned them with 850 H5N1 HA sequences representing all HPAI H5N1 clades (selected from ≈5,000 total sequences) and constructed a phylogenetic tree (Figure 1). Reassortment events leading to the generation of novel H5Nx subtypes are almost uniquely restricted to a single branch of the tree; the branch contains all isolates of the recent HPAI H5N2, H5N5, H5N6, and H5N8 outbreaks. The only other H5Nx reassortants that have been identified are a limited number of H5N2 subtype isolates that are present in 5 other branches of the tree.

A more detailed analysis (Figure 2) revealed that the monophyletic H5 clade harboring all the recent novel H5Nx reassortants evolved from early members of H5N1 clade 2.3.4 (a group of highly similar H5N1 viruses isolated in China in 2005). On January 12, 2015, the World Health Organization recommended designation of the novel H5 clade as 2.3.4.4 in anticipation of a revised H5 nomenclature (11). A previously described (12) H5N5 virus (A/duck/Guangdong/wy24/2008) is the first detected reassortant subtype within this clade; the donor of the NA segment of this virus could not clearly be identified (13). Subsequent reassortment events between viruses harboring an HA segment originally derived from the novel H5N5 viruses and a range of other avian influenza viruses have generated the H5N2, H5N6, and H5N8 subtypes.

The HA protein of A/wild duck/Hunan/211/2005, a member of H5N1 clade 2.3.4, is highly similar to that of other clade 2.3.4 members, differing from the HA of the earliest known

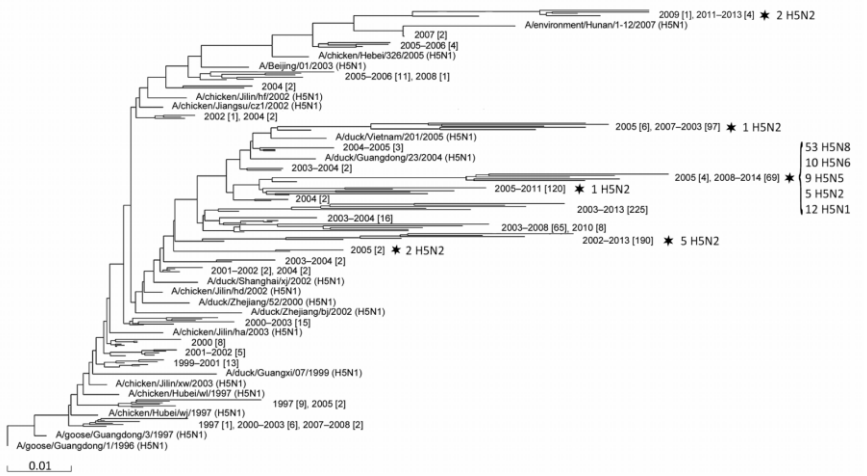

Figure 1. Phylogenetic tree showing the evolutionary history of the hemagglutinin (HA) proteins of novel highly pathogenic avian influenza (HPAI) H5 HA subtype viruses. By using MUSCLE (9), we aligned the coding region sequences for 89 HPAI H5 HA subtype viruses, excluding H5N1, with those for 850 H5N1 HA viruses representing all HPAI H5N1 clades (1); the 89 H5 HA sequences were identified in the NCBI Influenza Virus Resource (10) and the GISAID EpiFlu Database (http://www.gisaid.org). A phylogenetic tree was constructed by using the PHYLIP Neighbor Joining algorithm using the F84 distance matrix (http://www.ncbi.nlm.nih.gov/genomes/FLU/DatasetExplorer/fluPage.cgi?pageInclude=References.inc#PHYLIP). The number of sequences present in a branch is indicated between brackets. Stars indicate the branches that contain subtypes other than H5N1. The genotypes (H5N2, H5N5, H5N6, and H5N8) and their numbers of occurrence in a particular branch are indicated at right. Scale bar indicates evolutionary distance (nucleotide substitutions per site). Details for GISAID-derived sequences are shown in the Table.

H5N5 descendant (A/duck/Guangdong/wy24/2008, clade 2.3.4.4) at only 12 aa positions. Seven amino acid substitutions are subsequently maintained in all descending viruses: K86R, T160A, N187D, K222Q, S227R, N244H, and A267T. Substitutions K222Q and S227R are unique to clade 2.3.4.4 and have not been observed previously in any HPAI H5N1 viruses.

Within the subtree shown in Figure 2, the H5N2 viruses are present in 2 branches. N2 of A/duck/Jiangsu/m234/2012 was derived from an H11N2 virus (14); the N2 of the other viruses in this branch were derived from an avian H3N2 virus (15). In addition, 12 H5N1 reassortants were found to be spread over different branches of the subtree (Figure 2). The N1 proteins of these reassortants are derived from different H5N1 viruses that descended from H5 clade 2.3.2. Whereas the N1 of 8 identical isolates from Vietnam (A/Muscovy duck/Vietnam/LBM631/2014) is highly similar to the N1 of clade 2.3.2.1b virus A/barn swallow/Hong Kong/1161/2010 (1), the N1 of A/duck/eastern China/108/2008 is highly similar to the N1 of clade 2.3.2.1c virus A/duck/Hunan/8/2008 (1), suggesting that independent reassortment events have taken place.

The H5N8 and the H5N6 viruses have segregated into 2 branches. Analysis of the N6 proteins (data not shown) indicates that the H5N6 viruses (all from southern China) are the result 2 independent reassortment events with avian H6N6 strains. Unfortunately, sequences from the recent H5N6 outbreaks in Vietnam (5) are not yet present in the databases. The 2 different H5N8 virus clusters most likely evolved from a single H5N8 reassortant virus (A/duck/Jiangsu/k1203/2010) that was isolated in China in 2010 (13).

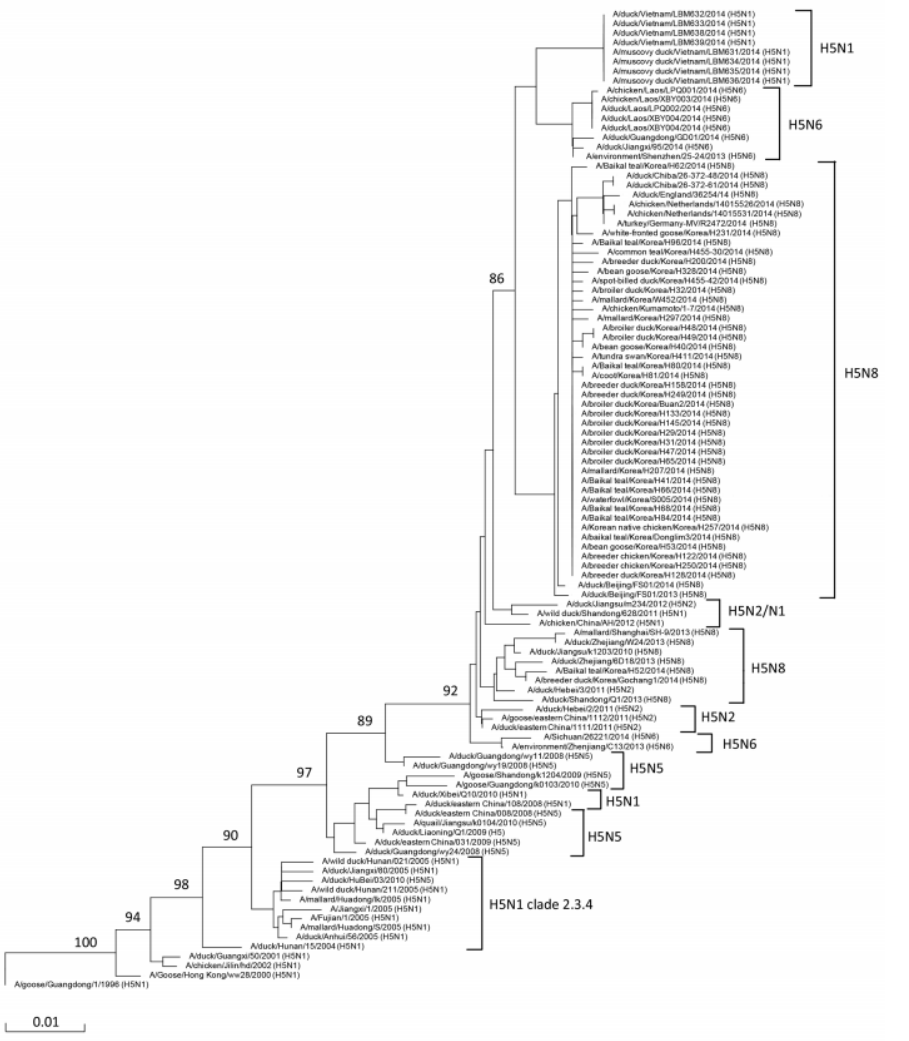

Figure 2. Hemagglutinin protein tree (neighbor-joining, point accepted mutation distance matrix model) of subtypes present in branch descending from highly pathogenic avian influenza A(H5N1) cluster 2.3.4 (see Figure 1). MUSCLE (9) was used to align protein sequences. Subtype group positions are indicated at right. Bootstrap values (n = 1,000) at key nodes are indicated. Scale bar indicates evolutionary distance (nucleotide substitutions per site).

Table. Details for GISAID-derived sequences of the hemagglutinin genome segment of various influenza A(H5) subtype viruses descended from a highly pathogenic avian A(H5N1) virus hemagglutinin variant*

Segment ID	Country	Collection date	Isolate name	Originating/submitting laboratory
EPI544756	Germany	2014 Nov 04	A/turkey/Germany-MV/R2472/2014	Friedrich-Loeffler-Institut
EPI530063	China	2013 Dec 02	A/environment/Shenzhen/25–24/2013	BGI-Shenzhen
EPI533583	China	2014 Apr 21	A/Sichuan/26221/2014	WHO Chinese National Influenza Center
EPI548623	Netherlands	2014 Nov 15	A/chicken/Netherlands/14015531/2014	Central Veterinary Institute
EPI547678	Netherlands	2014 Nov 14	A/Chicken/Netherlands/14015526/2014	Central Veterinary Institute
EPI530054	China	2014 Jan 10	A/duck/Jiangxi/95/2014	BGI-Shenzhen
EPI548493	Japan	2014 Nov 18	A/duck/Chiba/26–372–61/2014	National Institute of Animal Health
EPI548485	Japan	2014 Nov 18	A/duck/Chiba/26–372–48/2014	National Institute of Animal Health
EPI547673	UK	2014 Nov 14	A/duck/England/36254/14	Animal and Plant Health Agency
EPI543002	China	2014 Jan 20	A/duck/Beijing/FS01/2014	Institute of Microbiology, Chinese Academy of Sciences
EPI542617	China	2013 Nov 10	A/duck/Beijing/FS01/2013	Institute of Microbiology, Chinese Academy of Sciences
EPI431456	China	2011 Dec 07	A/duck/Hebei/3/2011	Institute of Microbiology, Chinese Academy of Sciences
EPI431448	China	2011 Dec 01	A/duck/Hebei/2/2011	Institute of Microbiology, Chinese Academy of Sciences

*The GISAID EpiFlu Database is available at http://www.gisaid.org. BGI, Beijing Genomics Institute; ID, identification; UK, United Kingdom; WHO, World Health Organization.

Both clusters were identified in Korea in 2014, whereas members of the most evolved cluster were detected later in 2014 in Japan, Germany, the Netherlands, and the United Kingdom.

CONCLUSION

Since 1996, reassortment events involving H5N1 HPAI viruses have, as far as detected, only rarely led to the generation of new H5Nx subtypes. The 2008 generation of an H5N5 reassortant virus (prototype A/duck/Guangdong/wy/24/2008) represents the creation of a new HPAI virus that has led to the generation of a range of novel H5Nx reassortants that acquired novel NA proteins (H5N2, H5N6, and H5N8). The H5N6 reassortant became of particular concern after spreading over a wide geographic area in Southeast Asia and causing a fatal human infection in China (5). Meanwhile, the H5N8 subtype spread to Europe in November 2014, resulting in large economic losses in the poultry industry. On the basis of reports from the World Organisation for Animal Health, H5N8 and H5N2 viruses were detected in Canada and the United States in December 2014.

In this study, we exclusively focused on the unique occurrence of new HA–NA combinations. Recent publications have already described the reassortment events of the internal gene segments of several of the viruses mentioned above (6–8,11–14). In contrast to novel HA–NA combinations, novel constellations of internal gene segments are far from unique and have frequently been observed for HPAI H5N1 viruses (3). Our analysis

indicates that new HPAI viruses have emerged that carry H5 proteins capable of matching with multiple NA subtypes. Whether the formation of new HA–NA combinations confers a selective advantage that contributed to the emergence of these novel subtypes is not known and requires elaborate research. However, the balance between HA (receptor binding) and NA (receptor cleavage) protein activities is known to be critical to cell entry and host tropism and may be an important factor that lead to the emergence of new HA–NA combinations. In contrast to HPAI H5N1, the novel clade 2.3.4.4 viruses, excluding H5N6 viruses, have not caused human infections. However, it is unknown to what extent the repeated acquisition of a new NA proteins could enhance the rate of evolution of the HA protein. Obviously such changes could further affect host and tissue specificity, potentially having serious consequences. Therefore, surveillance is required to monitor further spread, evolution, and potential changes in host range.

ACKNOWLEDGMENT

We gratefully acknowledge the authors and originating and submitting laboratories of the sequences from the GISAID EpiFlu Database, on which part of this research is based. All submitters of data may be contacted directly via the GISAID website (http://www.gisaid.org).

REFERENCES

1. World Health Organization/World Organisation for Animal Health/Food and Agriculture Organization (WHO/OIE/FAO). Revised and updated nomenclature for highly pathogenic avian influenza A (H5N1) viruses. Influenza Other Respir Viruses. 2014;8:384–8.
2. World Health Organization. Cumulative number of confirmed human cases for avian influenza A(H5N1) reported to WHO, 2003–2015 [cited 2015 Jan 19]. http://www.who.int/influenza/human_animal_interface/EN_GIP_20150106CumulativeNumberH5N1cases.pdf?ua=1
3. Lei F, Shi W. Prospective of genomics in revealing transmission, reassortment and evolution of wildlife-borne avian influenza A (H5N1) viruses. Curr Genomics. 2011;12:466–74.
4. Qi X, Cui L, Yu H, Ge Y, Tang F. Whole-genome sequence of a reassortant H5N6 avian influenza virus isolated from a live poultry market in China, 2013. Genome Announc. 2014;2:e00706–14.
5. FAO warns of new strain of avian influenza virus. Vet Rec. 2014;175:343.
6. Ku KB, Park EH, Yum J, Kim JA, Oh SK, Seo SH. Highly pathogenic avian influenza A(H5N8) virus from waterfowl, South Korea, 2014. Emerg Infect Dis. 2014;20:1587–8.
7. Lee YJ, Kang HM, Lee EK, Song BM, Jeong J, Kwon YK, Novel reassortant influenza A(H5N8) viruses, South Korea, 2014. Emerg Infect Dis. 2014;20:1087–9.
8. Wu H, Peng X, Xu L, Jin C, Cheng L, Lu X, Novel reassortant influenza A(H5N8) viruses in domestic ducks, eastern China. Emerg Infect Dis. 2014;20:1315–8.
9. Edgar RC. MUSCLE: multiple sequence alignment with high accuracy and high throughput. Nucleic Acids Res. 2004;32:1792–7.
10. Bao Y, Bolotov P, Dernovoy D, Kiryutin B, Zaslavsky L, Tatusova T, The influenza virus resource at the National Center for Biotechnology Information. J Virol. 2008;82:596–601.
11. World Health Organization. Evolution of the influenza A(H5) haemagglutinin: WHO/OIE/FAO H5 Working Group reports a new clade designated 2.3.4.4 [cited 2015 Jan 19]. http://www.who.int/influenza/gisrs_laboratory/h5_nomenclature_clade2344/en/
12. Liu CG, Liu M, Liu F, Lv R, Liu DF, Qu LD, Emerging multiple reassortant H5N5 avian influenza viruses in ducks, China, 2008. Vet Microbiol. 2013;167:296–306.
13. Zhao K, Gu M, Zhong L, Duan Z, Zhang Y, Zhu Y, Characterization of three H5N5 and one H5N8 highly pathogenic avian influenza viruses in China.Vet Microbiol. 2013;163:351–7.
14. Gu M, Huang J, Chen Y, Chen J, Wang X, Liu X. Genome sequence of a natural reassortant H5N2 avian influenza virus from domestic mallard ducks in eastern China. J Virol. 2012;86:12463–4 .
15. Zhao G, Gu X, Lu X, Pan J, Duan Z, Zhao K, Novel reassortant highly pathogenic H5N2 avian influenza viruses in poultry in China. PLoS ONE. 2012;7:e46183 .

Chapter 6

Highly Pathogenic Influenza A(H5Nx) Viruses with Altered H5 Receptor-Binding Specificity

Hongbo Guo[1]*, Erik de Vries[1]*, Ryan McBride[2], Jojanneke Dekkers[1], Kim M. Bouwman[3], Corwin Nycholat[2], M. Helene Verheije[3], James C. Paulson[2], Frank J.M. van Kuppeveld[1], and Cornelis A.M. de Haan[1]

1 Virology Division, Department of Infectious Diseases & Immunology, Faculty of Veterinary Medicine, Utrecht University, Utrecht, The Netherlands

2 Departments of Cell and Molecular Biology, Chemical Physiology, and Immunology and Microbial Science, The Scripps Research Institute, La Jolla, California, USA

3 Department of Pathobiology, Faculty of Veterinary Medicine, Utrecht University, Utrecht, The Netherlands

* These authors contributed equally

Emerg Infect Dis 23: 220-231.

ABSTRACT

The emergence and intercontinental spread of highly pathogenic clade 2.3.4.4 H5Nx avian influenza A virus subtypes is unprecedented. H5N8 and H5N2 genotypes have caused huge damage to the poultry industry in Europe and North America and lethal human infections by the H5N6 genotype have occurred in Asia. Knowledge on the evolution of receptor-binding specificity of these viruses, which may affect host range, is urgently required. We now show that their emergence is accompanied by a change in receptor-binding specificity. In contrast to the ancestral clade 2.3.4 H5 proteins, the novel clade 2.3.4.4 H5 proteins bind to fucosylated sialosides due to substitutions K222Q and S227R that are unique for highly pathogenic H5 proteins. North American clade 2.3.4.4 isolates have only retained the K222Q substitution but still bind fucosylated sialosides. The altered receptor-binding specificity of the clade 2.3.4.4 H5 proteins may have contributed to the emergence and spread of the H5Nx viruses.

INTRODUCTION

Highly pathogenic (HP) H5N1 avian influenza A viruses (IAVs) cause huge economic losses in the poultry industry and may cause zoonotic infections. Recently, a novel HP IAV H5 clade 2.3.4.4 has emerged (1-4) demonstrating an unprecedented intercontinental spread. Whereas HP IAVs previously detected in poultry in the Americas are thought to have descended from American low pathogenic IAVs (5), clade 2.3.4.4 viruses were the first HP H5 IAVs of the A/goose/Guangdong/1/1996-lineage to appear in North America(2-4) in the winter of 2014-2015. The emergence of these novel viruses resulted in the culling of more than 7 million turkeys and 42 million chickens in the USA alone (6). In Asia, thirteen (mostly lethal) cases of human infection with clade 2.3.4.4 H5N6 viruses have been reported. The emergence of new IAV genotypes carrying a clade 2.3.4.4 hemagglutinin (HA) that infect poultry and humans emphasizes the need for a detailed characterization of their molecular properties.

IAVs are subtyped according to their envelope glycoproteins HA and neuraminidase (NA). Sixteen HA and nine NA subtypes are found in aquatic birds constituting the animal IAV reservoir. IAVs of the H5 or H7 subtype occasionally acquire a multibasic cleavage site in their HA (7) resulting in a HP phenotype. In general, HP H5 IAVs are of the N1 subtype (H5N1). In contrast, the novel HP H5 clade 2.3.4.4 viruses have teamed up with different NA subtypes, including N1, N2, N3, N5, N6 and N8 (1, 8-16)

HA proteins bind to sialoside receptors on the host cell surface. Avian and human IAVs prefer binding to sialic acids linked to a penultimate galactose via an α2-3- or α2-6-linkage, respectively (17). Type and number of internal monosaccharides and their linkages determine IAV receptor fine-specificity (18, 19). NA removes sialic acids from glycans, allowing IAV particles to be released from the cell surface after assembly and from decoy receptors e.g. in mucus. The balance between the activities of the HA and NA proteins is of critical importance for optimal viral fitness, tropism, and transmission (20).

A change in HA receptor-binding properties may affect virus host-range, within-host viral properties and have contributed to the remarkable spread of the clade 2.3.4.4 viruses. While a recent study (21) reported enhanced avidity of HP H5N6 viruses for human-type receptors, recombinant clade 2.3.4.4 H5 proteins from North American isolates exhibit a strict avian receptor-binding preference (22). Here the receptor-binding properties of clade 2.3.4.4 H5 proteins from a European H5N8 virus were compared to an early ancestral clade 2.3.4 H5 protein from a H5N1 virus. The clade 2.3.4.4 H5 proteins were shown to differ in their receptor-binding properties from their parental H5 protein in their ability to bind fucosylated sialoside receptors. Amino acid changes at positions 222 and 227, which are not found in other HP H5 proteins, are responsible for the differences in receptor-binding properties.

MATERIALS AND METHODS

Genes, expression vectors, protein expression and purification. Codon-optimized H5-encoding cDNAs (Genscript USA) of H5N1 A/wild duck/Hunan/211/2005 (GenBank: EU329186.1) and H5N8 A/chicken/Netherlands/14015526/2014 (GiSAID number EPI_ISL_167905) were cloned in pCD5 expression vectors flanked by signal peptide-, GCN4- isoleucine-zipper trimerizaton motif-, and Strep-tag II-encoding sequences, mutagenized when indicated, expressed and purified as described previously (23).

HA receptor-binding assays. Binding of HA to fetuin and transferrin (Sigma), and to glycan arrays was assessed similarly as described previously (23). Biolayer interferometry was performed with the Octet QK (ForteBio) using in-house synthesized saccharides NeuAcα2-3Galβ1-4GlcNAcβ1-3Galβ1-4GlcNAc (3'SLNLN), NeuAcα2-6Galβ1-4GlcNAcβ1-3Galβ1-4GlcNAc (6'SLNLN), NeuAcα2-3Galβ1-4(Fucα1-3)GlcNAc (3'SLe^X), and NeuAcα2-6Galβ1-4GlcNAc (3'SLN) coupled to LC-LC-biotin. Streptavidin sensors were loaded with 0.1 µM glycan for 15 min. Association of HA proteins (0.2 µg/ul) was assessed in the presence of StrepMAB-Classic (IBA) at a 2:1 molar ratio. Binding of HA to tissues was performed as described (24), except that H5 proteins were precomplexed with StrepMAB-Classic-HRP (IBA) and Goat anti-mouse IgG (H+L)-HRP (Invitrogen). Immunohistochemistry with 3'SLe^X-specific antibody KM93 (25) (EMD Millipore) in a 1:500 dilution was performed using standard procedures, including antigen retrieval (26) on an avian intestinal tissue microarray (27).

Modelling. The crystal structure of the H5 protein from A/Vietnam/1194/2004 (H5N1) in complex with 3'SLe^X (PDB Accession number 3ZNM (28) was used as a template for modelling the structures of A/wild duck/Hunan/211/2005 and A/chicken/Netherlands/14015526/2014 using SWISS-MODEL (29). Subsequent energy minimizations were not necessary as inspection of the modelled structure by GROMOS revealed no unfavourable energy interactions. Superpositioning of the Cα-backbone atoms of residues lining the receptor-binding site (RBS) of either A/wild duck/Hunan/211/2005 (H5N1) or A/chicken/Netherlands/14015526/2014 (H5N8) with A/Vietnam/1194/2004 (H5N1) demonstrated that the root mean square deviation of the superpositioned atoms was smaller than 0.2 Å in both cases. Molecular interactions were further examined using the Swiss-Pdb Viewer (30).

RESULTS

Receptor-binding properties of different H5 proteins.

We compared the receptor-binding properties of an H5 protein derived of an early clade 2.3.4 H5N1 isolate (A/wild duck/Hunan/211/2005) with a clade 2.3.4.4 isolate (H5N8 A/chicken/Netherlands/14015526/2014) detected in Europe (referred to as H5N1$_{2.3.4}$

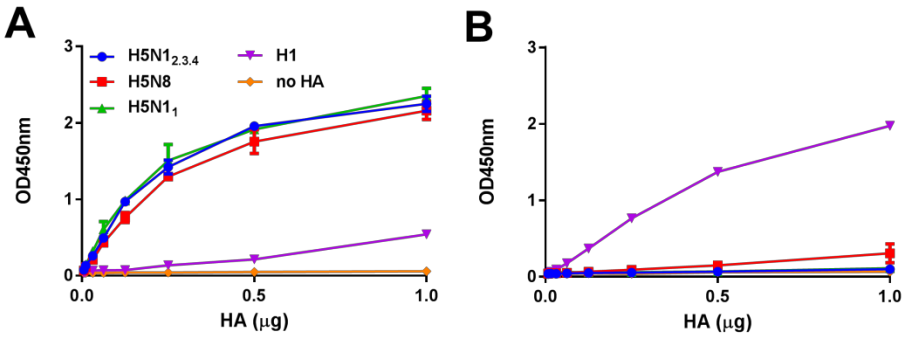

Figure 1. Binding of influenza A virus hemagglutinins to A) fetuin and B) transferrin. Limiting dilutions of soluble H5 trimers complexed with horseradish peroxidase–conjugated antibodies were used in a fetuin- or transferrin-binding assay. Optical density at 450 nm (OD_{450}) corresponds to binding of HA to glycoproteins. HA, hemagglutinin; $H5N1_{2.3.4}$, novel H5N1 virus clade 2.3.4; $H5N1_1$, H5N1 virus clade 1. Representative experiments performed in triplicate are shown. Standard deviations are indicated. The curves were statistically compared by determining EC50 values by non-linear regression analysis using Graphpad Prism software. Two-tailed t test showed these values to significantly differ between $H5N1_{2.3.4}$ and H5N8 for binding to transferrin (P=0.0007), but not to fetuin.

and H5N8 HA proteins, respectively) using recombinant soluble HA proteins (23). The H5 proteins were analysed for their binding to fetuin and transferrin (Fig. 1A and B). Fetuin contains α2-3- and α2-6-linked sialiosides in a 2:1 ratio (31, 32), while transferrin only contains α2-6-linked sialosides (33). As controls we used a clade 1 H5 protein (H5N1 A/Viet Nam/1203/2004; referred to as $H5N1_1$) and an H1 protein of a human seasonal H1N1 virus (A/Kentucky/UR06-0258/2007; referred to as H1) with known receptor-binding properties (23, 26). All H5 proteins efficiently bound fetuin, whereas only H5N8 HA showed limited binding to transferrin, indicating that $H5N1_{2.3.4}$ and H5N8 HA proteins prefer binding to α2-3-linked sialic acids similarly as $H5N1_1$ HA (26). The H1 protein bound fetuin to a lower extent than the H5 proteins, and bound transferrin, in agreement with this protein preferentially binding α2-6-linked sialosides (23).

Receptor fine-specificity of the $H5N1_{2.3.4}$ and H5N8 HA proteins was determined using glycan array analysis. The H5 proteins bound to a range of mono- and bi-antennary α2-3-linked glycan structures corresponding to N- and O-linked sialosides (Fig. 2 and results not shown). Both proteins did not bind to α2-6-linked sialosides (results not shown). The specificity of the $H5N1_{2.3.4}$ HA protein was similar to that of its early $H5N1_1$ ancestor (26) (supplementary Fig.S1). However, glycan array analysis revealed a fucosylation-specific change in receptor fine-specificity for the H5N8 protein. In Fig. 2 we compared the binding to two sets of α2-3-linked sialosides that only differ in the absence (glycans 1-9; red bars) or presence (glycans 11-19; blue bars) of fucose at the GlcNAc of lactosamine repeats (Fig. 3). The $H5N1_{2.3.4}$ HA protein only bound to one fucosylated glycan (nr 13, 6-sulfo 3'Sialyl

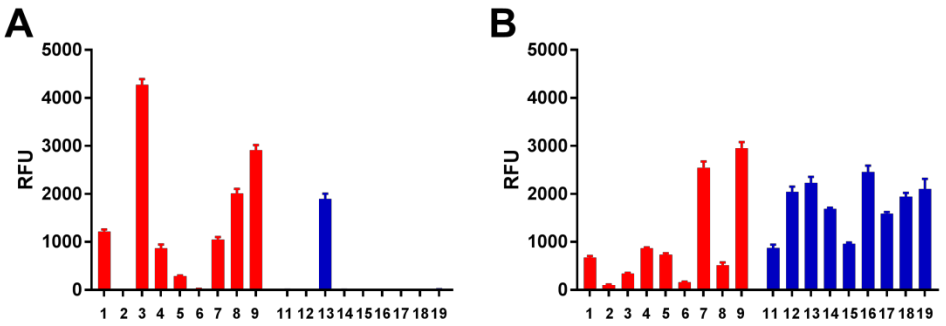

Figure 2. Glycan array analysis of recombinant H5 proteins of influenza A viruses. A) Wild-type $H5N1_{2.3.4}$ (KS) and B) H5N8 (QR) H5 proteins were applied to the glycan array precomplexed with StrepMAB-classic (IBA GmbH, Göttingen, Germany) and fluorescent secondary antibodies. Letters in parentheses indicate amino acids at positions 222 and 227. Binding of hemagglutinins is indicated in relative fluorescence units (RFU). Binding is shown to sialylated glycans present in the array for nonfucosylated (glycans 1–9; red bars) and fucosylated (glycans 11–19; blue bars) forms. Glycan numbers indicated on the x-axes correspond to glycan structures shown in Figure 3. $H5N1_{2.3.4}$, novel H5N1 virus clade 2.3.4. Means of 6 independent replicates are graphed, standard errors of the means are indicated.

Lewis X [6S-3'SLe^X]). In contrast, the H5N8 HA protein bound well to all α1-3- as well as the single α1-4-fucosylated glycan (nr 15). We also analysed binding of these proteins to different glycans using biolayer interferometry (Fig. 4). While $H5N1_{2.3.4}$ and the H5N8 HA proteins displayed similar binding properties towards 3'SLNLN, 6'SLNLN and 3'SLN, they clearly differed in their binding to 3'SLe^X, in agreement with the glycan array analysis (Fig 2).

Phylogenetic analysis of clade 2.3.4.4 H5 proteins.

To identify the residues responsible for these differences in receptor binding, we mapped the amino acid substitutions occurring along the trunk of a HA protein phylogenetic tree (Fig. 5). Clade 2.3.4.4 viruses first emerged in 2008 (34). Eight amino acid substitutions, still maintained in the recently emerging clade 2.3.4.4 viruses, characterize the transition from the most closely related clade 2.3.4 ancestor (A/wild duck/Hunan/211/2005 (H5N1)). The number of occurrences of these amino acid substitutions in a set of 2562 HAs from HP H5N1 viruses isolated between 1996 and 2015 (excluding clade 2.3.4.4 viruses) is listed in the insert in Fig. 5. Interestingly, substitutions K222Q and S227R (H3 numbering used here, corresponding to K218Q and S223R in H5 numbering), which have hardly occurred before (0.08 and 0.9 % respectively), happen in the RBS. In the course of further evolution a glycosylation site at the head domain at position 160 is lost and two other unique substitutions (K193N, T193D) occur in the vicinity of the RBS. The Ser residue at position 227 present in $H5N1_{2.3.4}$ HA protein is observed again in late clade 2.3.4.4 H5-containing viruses that have been detected in North America.

Receptor-binding properties of mutant H5 proteins.

The amino acid substitutions in H5N8 HA mentioned above were introduced into the $H5N1_{2.3.4}$ HA protein and analysed for their effects on receptor binding. Substitutions T160A or S227R did not affect fetuin binding (Fig. 6A), while K222Q reduced binding

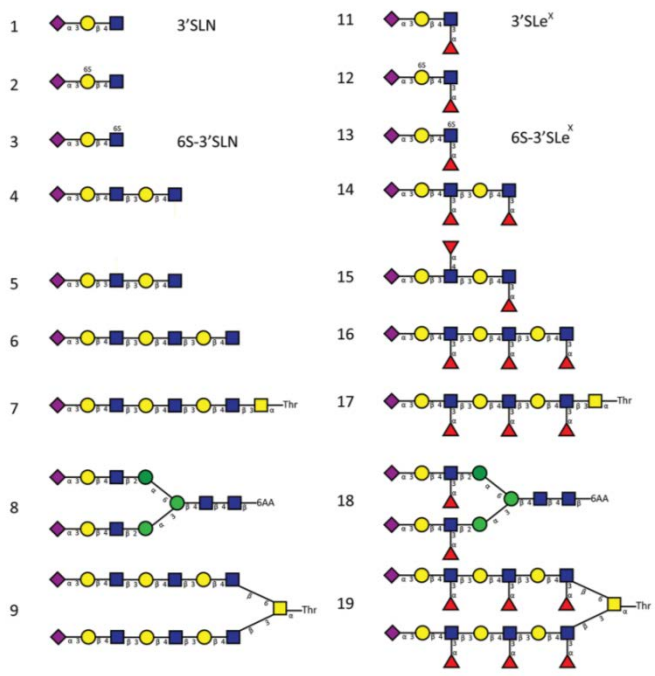

Figure 3. Glycan structures of influenza A viruses. Structures are shown for sialylated glycans present in the array in nonfucosylated (glycans 1–9) and fucosylated (glycans 11–19) forms and binding by hemagglutinins is shown in Figures 2 and 7. Glycans 1 and 11 correspond to 3'SLN (nonfucosylated glycan) and $3'SLe^X$ (fucosylated form of 3'SLN), respectively. Similarly, glycans 3 and 13 correspond to 6-O-sulfo 3'SLN (6S-3'SLN) and 6-O-sulfo $3'SLe^X$ (6S-$3'SLe^X$), respectively. Blue squares, N-acetylglucosamine; yellow circles, galactose; green circles, mannose; purple diamonds, sialic acid; red triangles, fucose. $H5N1_{2.3.4}$, novel H5N1 virus clade 2.3.4.

approximately twofold. Reduction of binding was not observed when substitution K222Q was combined with S227R. Introduction of additional substitutions at position 160, 193 and 199 in the order in which they occurred during evolution of clade 2.3.4.4 HAs did not affect fetuin binding. The receptor fine-specificity of these proteins was studied by glycan array analysis. Substitution T160A did not change receptor fine-specificity (Supplementary Fig S1). In comparison to the wildtype $H5N1_{2.3.4}$ protein (Fig. 2A), substitution K222Q (Fig. 7A) strongly decreased binding whereas substitution S227R (Fig. 7B) had a more specific negative effect. In contrast, when combined substitutions K222Q and S227R (Fig. 7C) enhanced binding to the glycans bound by the wildtype $H5N1_{2.3.4}$ HA (Fig. 2A) and, importantly, resulted in additional binding of fucosylated glycans that are also bound by the H5N8 protein (Fig. 2B). Additional introduction of the mutations found at position 160, 193 and 199 in the background of the Q222- and R227-containing $H5N1_{2.3.4}$ HA protein did not affect the receptor fine-specificity (Supplementary Fig. S1). We conclude that the combination of substitutions K222Q and S227R, already present in

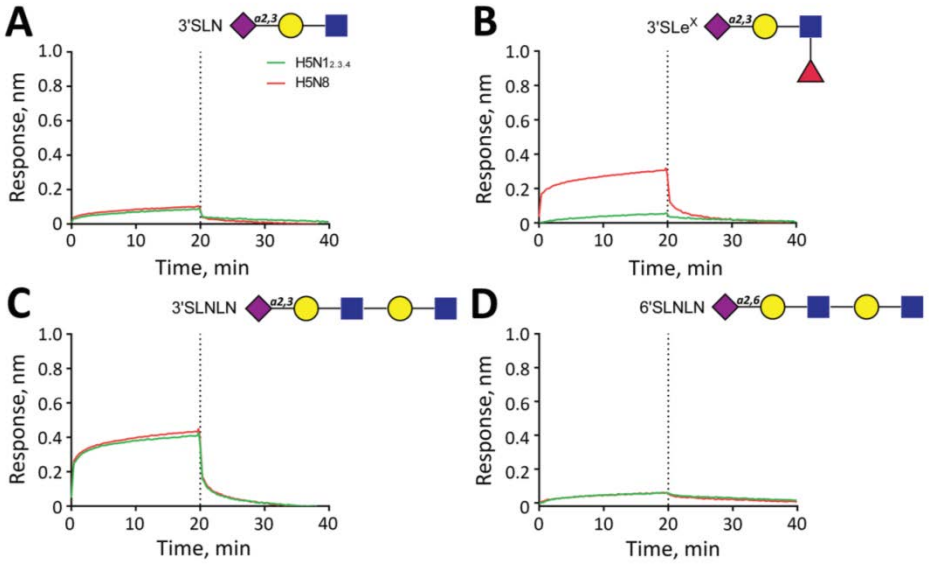

Figure 4. Analysis of binding of influenza A virus H5N1$_{2.3.4}$ and H5N8 hemagglutinins to sialylated glycans by using biolayer interferometry. A) 3'SLN, B) 3'SLe^X, C) 3'SLNLN, D) 6'SLNLN. After complexing biotinylated glycans with streptavidin sensors, association and subsequent dissociation of H5 proteins complexed with StrepMAB-classic (IBA GmbH, Göttingen, Germany) was determined. Blue squares, N-acetylglucosamine; yellow circles, galactose; purple diamonds, sialic acid; red triangles, fucose. The dotted lines at the 20-min time points distinguish the association and dissociation phases. H5N1$_{2.3.4}$, novel H5N1 virus clade 2.3.4.

the earliest clade 2.3.4.4 H5Nx viruses (Fig. 5), is largely responsible for the different receptor-binding properties of the H5N1$_{2.3.4}$ and the H5N8 HAs.

The branch of clade 2.3.4.4 H5 proteins that harbours the Taiwanese and North American viruses contains reverse substitution R227S (Fig. 5). We studied to what extent the residues at position 222 and 227 affects receptor-binding in the background of the H5N8 protein. Substitutions R227S and/or Q222K hardly affected fetuin binding (Fig. 6B). On the glycan array, the R227S substitution did not affect the binding of the H5N8 HA protein to fucosylated sialosides (Fig. 7E) whereas the Q222K substitution, alone or in combination with R227S, abolished binding of fucosylated receptors (Fig. 7D and F). We conclude that the identity of residue 222 is of crucial importance for binding of fucosylated sialosides regardless of the background of the HP H5 protein. However, while R227 is required for binding of fucosylated sialosides in clade 2.3.4 H5, this is not the case for clade 2.3.4.4 proteins.

Modelling of amino acid substitutions in the H5 structure.

We analysed the interaction of the H5N1$_{2.3.4}$ and the H5N8 HA proteins with a fucosylated and sialylated tetrasaccharide (3'SLe^X; Fig. 3, nr 11) by modelling on the

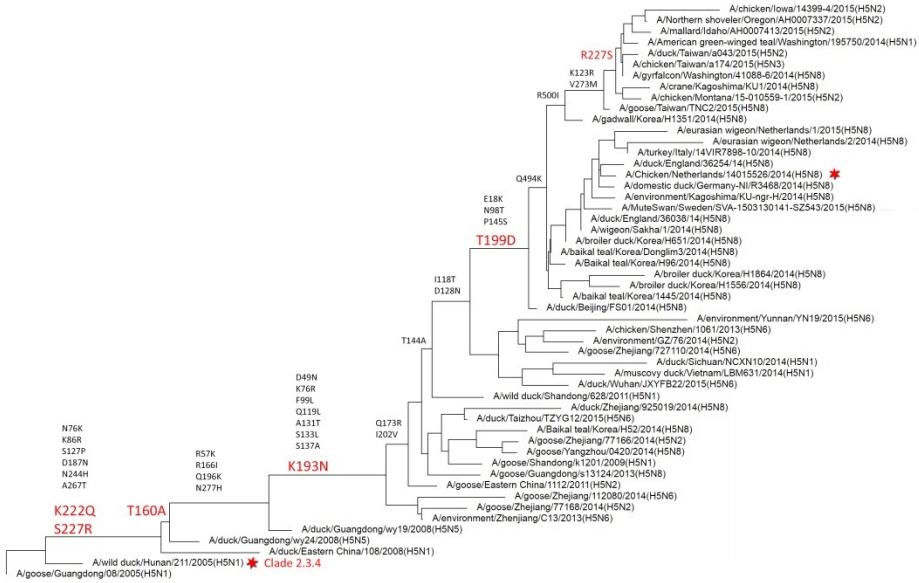

Figure 5. Phylogenetic analysis of influenza A virus clade 2.3.4.4 H5 proteins. A 362-aa full-length hemagglutinin (HA) sequence for H5 clade 2.3.4.4 was obtained from GenBank and the GISAID database (http://platform.gisaid.org). An HA protein tree was constructed by using the PHYLIP neighbor-joining algorithm (https://ugene.net/wiki/display/UUOUM/PHYLIP+Neighbor-Joining) and the F84 distance matrix. This tree was used to construct a guide tree with 52 HA sequences representing all branches of the tree. These sequences were used to construct a summary tree of similar topology as the guide tree. Items above the branches indicate key residues that differ between different branches. Items in red above the branches indicate mutations introduced in this study. The HA protein tree is rooted by an early clade 2.3.4 isolate (A/goose/Guangdong/08). $H5N1_{2.3.4}$ and H5N8 HA proteins used in this study are indicated by red stars. $H5N1_{2.3.4}$, novel H5N1 virus clade 2.3.4.

structure of a clade 1 HP H5 protein ($H5N1_1$ A/Vietnam/1194/2004) that was co-crystalized with $3'SLe^X$ (28). Fig. 8 displays the $3'SLe^X$ ligand and the important parts of the RBS (190-helix, 130-loop and 220-loop). Poor binding of the $H5N1_1$ A/Vietnam/1194/2004 HA protein to $3'SLe^X$ was explained (28) by steric hindrance between Lys at position 222 and the fucose (Fig. 8A). This steric hindrance is maintained in $H5N1_{2.3.4}$ HA protein but is lost after the K222Q substitution in H5N8 HA protein (Fig. 8B and C). The effects of the amino acid 227 on binding of fucosylated sialosides may result from the possibility to form a hydrogen bond between the 220-loop and the amino-terminal end of the 190-helix via the side chains of R227 and N186, thereby influencing the flexibility of the RBS. At two positions that differ between the $H5N1_{2.3.4}$ and the H5N8 HA proteins (S137A and S185P) we observed changes in the potential to form hydrogen bonds between important elements of the RBS as indicated in Fig. 8. Such changes may affect the interaction of HA with the sialic acid-containing glycans and may explain the back-ground-dependent effect of the residue at position 227.

Binding of H5 proteins to avian tissues

We studied binding of the $H5N1_{2.3.4}$ and the H5N8 to avian tissues that differ in the presence of fucosylated sialosides. An antibody to $3'SLe^X$ bound strongly to the epithelial cells of chicken trachea, but not to duck intestinal tissue (Fig. 9A), in agreement with previous findings (35). Removal of sialic acids by VCNA abolished binding. Tissue derived

Table 1. Amino acids in hemagglutinins from 2,562 highly pathogenic influenza A(H5N1) viruses isolated during 19962015 (excluding clade 2.3.4.4 viruses)

Position and amino acid	No. occurrences	Position and amino acid	No. occurrences	Position and amino acid	No. occurrences
18K	119	128N	276	196K	183
49N	301	131T	49	199D	0
57K	481	133L	1,029	202V	75
76K	16	137A	545	222Q	2
76R	0	144A	4	227R	23
86R	5	145S	1,873	244H	316
98T	32	160A	1,467	267T	1,805
99L	57	166I	160	273M	10
118T	1	173R	67	277H	1
119L	0	187N	117	494K	0
123R	40	193N	4	500I	0
127P	329				

from another Anseriformes species (Greylag/Canada goose) also did not display $3'SLe^X$, while differential staining results were obtained for the intestinal tissues of different Galliformes species (Table 1). The different H5 proteins efficiently bound chicken trachea (Fig. 9B and C) and duck intestines that do not display $3'SLe^X$-containing glycans. Staining of duck tissues by the $H5N1_{2.3.4}$ HA protein was less intense than for the H5N8 HA protein. We conclude that the presence of $3'SLe^X$ -containing sialosides may affect the binding of H5N8 HA protein to avian tissues but is not essential.

DISCUSSION

Clade 2.3.4.4 H5Nx viruses have displayed an unprecedented worldwide spread. Notably, gene reassortments with other IAV genotypes have generated a range of clade 2.3.4.4 viruses containing different NA subtypes, even though they harbour an H5 protein that hitherto was almost exclusively associated with members of a monophyletic clade of N1 proteins descending from early HP H5N1 isolates. We now show that the emergence of clade 2.3.4.4 H5Nx viruses is accompanied with a change in HA receptor-binding specificity. Altered receptor-binding properties may affect the balance between HA and NA, allow the virus to team up with different NA subtypes, and may result in altered host range and thereby spreading.

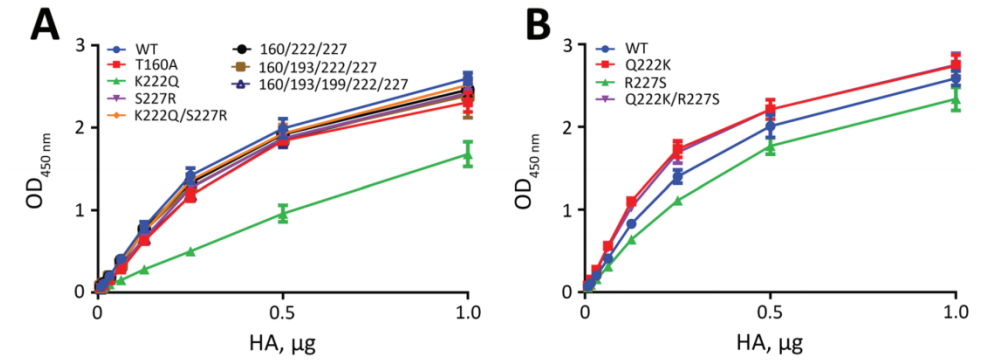

Figure 6. Binding of influenza A virus mutant H5N1$_{2.3.4}$ HA (A) and H5N8 HA (B) to fetuin. Binding was assayed as described in the legend to Figure 1. Mutated residues are indicated. 160/222/227, 160/193/222/227, and 160/193/199/222/227 refer to T160A/K222Q/S227R, T160A/K193N/K222Q/S227R and T160A/K193N/T199D/K222Q/S227R substitutions in H5N1$_{2.3.4}$ HA, respectively. Optical density at 450nm (OD_{450}) corresponds to binding of HA to glycoproteins. WT, wild-type; HA, hemagglutinin. H5N1$_{2.3.4}$, novel H5N1 virus clade 2.3.4. Representative experiments performed in triplicate are graphed. Standard deviations are shown. Curves were statistically compared by determining the EC50 values by non-linear regression analysis using Graphpad Prism software. One-way ANOVA followed by Tukey's multiple comparisons test showed these values to significantly differ between WT and K222Q (A; P<0.0001) and between WT and the three mutant proteins shown in B (P<0.003).

Clade 2.3.4.4 HA from a European H5N8 virus efficiently binds fucosylated sialosides, in contrast to an HA from the ancestral clade 2.3.4 (this study) and older HP H5N1 HAs (27, 36). We have shown that amino acid substitutions K222Q and S227R in the RBS of early clade 2.3.4.4 HAs are required for this change in receptor-binding specificity. HA residues K222 and S227 are extremely conserved among all clades of HP H5N1 viruses, the double substitution K222Q/S227R only being introduced at the root of clade 2.3.4.4 (Fig. 5). Structural analysis of a clade 1 HA indicates that the close proximity of the conserved K222 side-chain and the fucose-moiety of 3'SLe^X most likely destabilizes their interaction (28). Modelling indicates that such a clash is still present in H5N1$_{2.3.4}$, but absent in H5N8 HA proteins carrying Q222 and R227 residues (Fig. 8).

Surprisingly, introduction of K222Q into H5N1$_{2.3.4}$ HA, which removes the clash with the fucose-moiety (28), in itself does not enable binding to fucosylated receptors (Fig. 7). Additional introduction of an arginine at position 227 (double-substitution K222Q/S227R) in H5N1$_{2.3.4}$ HA was, however, sufficient to obtain a glycan array-binding profile nearly identical to that of H5N8 HA. Substitution S227R may result in the 220-loop interacting with the conserved loop at the N-terminus of the 190-helix via two hydrogen bonds between R227 and N186 (Fig. 8C). This interaction, potentially limiting mobility of the 220-loop, may contribute to stabilize the RBS in a conformation that enables binding of fucosylated receptors. Strikingly, R227 was required for binding of fucosylated sialosides in the background of the H5N1$_{2.3.4}$, but not the H5N8 HA protein (Fig. 7). In agreement herewith, HA proteins of the Taiwanese/North American branch of clade 2.3.4.4 viruses,

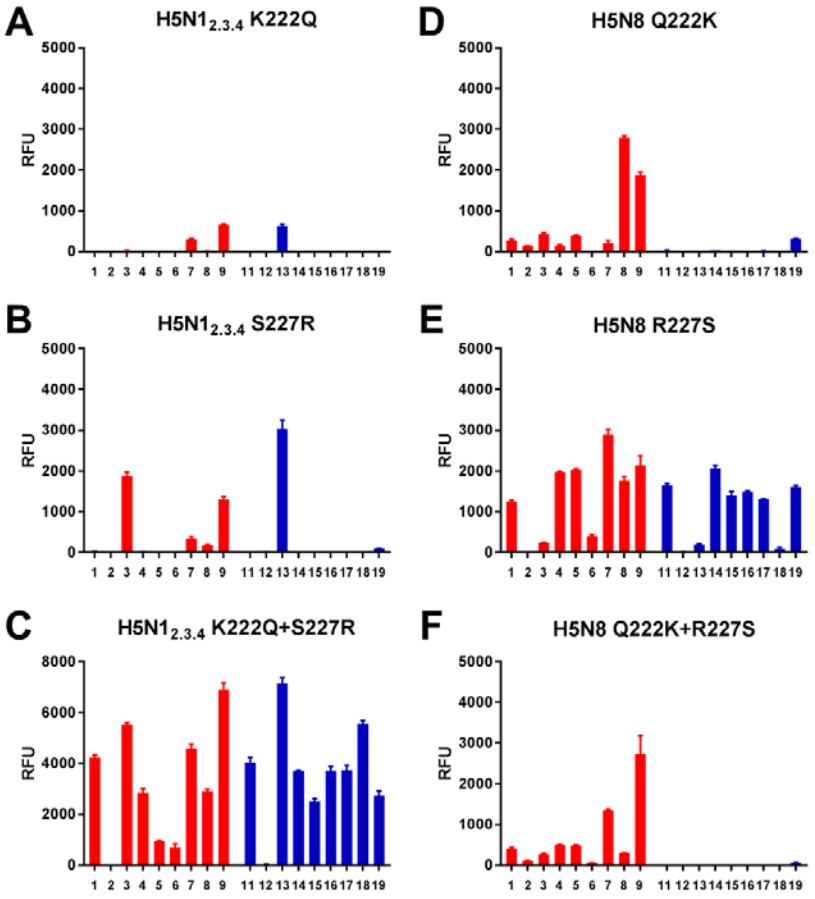

Figure 7. Glycan array analysis of influenza A virus mutant H5 proteins. A) mutant H5N1$_{2.3.4}$ K222Q (QS); B) mutant H5N1$_{2.3.4}$ S227R (KR); C) mutant H5N1$_{2.3.4}$ K222Q/S227R (QR); D) H5N8 Q222K (KR); E) R227S (QS); F) Q227R/R227S (KS). Proteins were applied to the glycan array as detailed in the legend to Figure 2. Letters in parentheses indicate amino acids at positions 222 and 227. Binding of hemagglutinins is indicated in relative fluorescence units (RFU). Binding is shown to sialylated glycans present in the array in nonfucosylated (glycans 1–9; red bars) and fucosylated (glycans 11–19; blue bars) forms. Glycan numbers indicated on the x-axes correspond to glycan structures shown in Figure 3. H5N1$_{2.3.4}$, novel H5N1 virus clade 2.3.4. Means of 6 independent replicates are graphed, standard errors of the means are indicated. Statistical analysis of the fucosylated glycan-binding profiles normalized for binding to the corresponding nonfucosylated glycans using Graphpad Prism software (One way ANOVA followed by Sidak's multiple comparisons test) showed significant differences ($P<0.05$) in the binding profiles between H5N1$_{2.3.4}$ and H5N8 (shown in Fig. 2) and between H5N1$_{2.3.4}$ (Fig. 2A) and mutant H5N1$_{2.3.4}$ K222Q/S227R (Fig. 7C). In addition, significant differences in the binding profiles were observed between H5N8 (Fig. 2B) and mutants thereof carrying the Q222K substitution (Fig. 7D and F). Other mutations did not significantly affect the normalized fucosylated glycan-binding profile when compared to their parental wild-type protein.

which obtained reverse substitution R227S (Fig. 5), also efficiently bind fucosylated receptors (22).

Analysis of all HA sequences available in Genbank of all avian genotypes shows that the frequency of occurrence of Q222 and R227 is, depending on the genotype, zero or extremely low. As an exception, Q222 is highly conserved in H7 and H10 genotypes and R227 is the dominant amino acid in H6 and H13 genotypes. The combination Q222/R227 occurs in a single clade of low pathogenic (LP) H5N2 viruses represented by A/chicken/Ibaraki/1/05 (H5N2) (37) which was shown to be able to bind to fucosylated receptors, and for which residues 222 and 227 were shown to be important (38). The contribution of the individual residues at these positions for receptor-binding was, however, not evaluated. The Japanese isolates of this clade originate from Central American H5N2 viruses (37). Intercontinental transfer of avian influenza viruses is a very rare event, drawing a remarkable parallel between two viral clades (HP H5Nx and LP H5N2), both of which have acquired the ability to bind fucosylated receptors and managed to spread intercontinentally. Like HP H5Nx, LP H5N2 might be spread by wild birds although the possibility could not be ruled out that a virus or vaccine was illegally introduced into Japan from Central America (39).

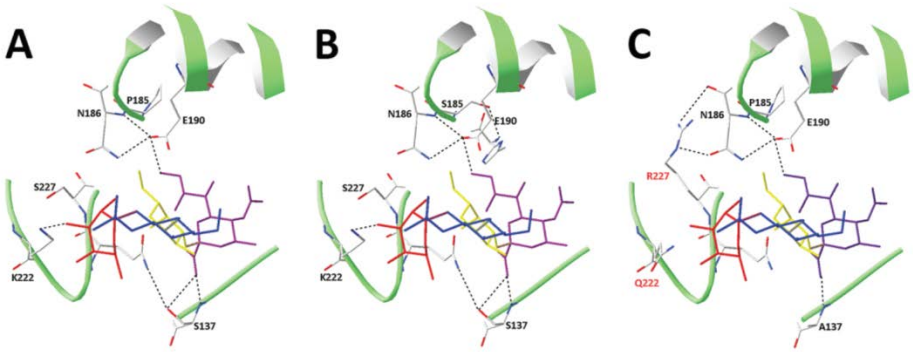

Figure 8. Structural models of influenza A virus H5 proteins complexed with 3'SLe^X. A) Clade 1 H5 ($H5N1_1$ of A/Vietnam/1194/2004) complexed with 3'SLe^X (PDB 3ZNM0 (29). B) $H5N1_{2.3.4}$ and C) H5N8 hemagglutinins were modeled into the structure shown in panel A as detailed in Materials and Methods. Key amino acids are indicated and shown in a stick representation. C (gray), O (red), and N (blue) in the side chains are colored. SIA, Gal, GlcNAc, and Fuc moieties of 3'SLe^X are shown in purple, yellow, blue, and red, respectively. Hydrogen bonds are indicated by dotted lines. $H5N1_{2.3.4}$, novel H5N1 virus clade 2.3.4; $H5N1_1$, H5N1 virus clade 1.

The ability of some LP avian IAVs to bind to fucosylated receptors of the 3'SLe^X type has been considered a poultry-specific adaptation (19, 35, 36, 38, 40) although extensive studies on sufficient numbers of isolates across the complete range of HA genotypes are lacking. Except for LP H7 viruses, that all efficiently bound 6S-3'SLe^X, irrespective of their host species (41), duck viruses were suggested to bind poorly to 3'SLe^X type receptors (19,

36, 38, 40, 42). However, adaptation to binding of 3'SLe^X type receptors has never been reported in HP H5N1 viruses isolated from poultry, while a recent study showed poor binding of HP H5 and HP7 viruses to 3'SLe^X (43). In another study, binding of a few avian IAVs to fucosylated receptors correlated with their binding to α2-6-linked sialosides (40). However, here we found only very weak binding of H5N8 HA to 2-6-specific transferrin (Fig. 1B) and no measurable binding to α2-6-linked sialosides on the glycan array (data not shown) or by biolayer interferometry (Fig. 4). Also HA proteins of the Taiwanese/North American branch of clade 2.3.4.4 viruses did not bind α2-6-linked sialosides (22). These results therefore do not support the hypothesis that increased binding to fucosylated receptors enhances the propensity of avian IAVs to evolve into binding α2-6-linked sialoside receptors.

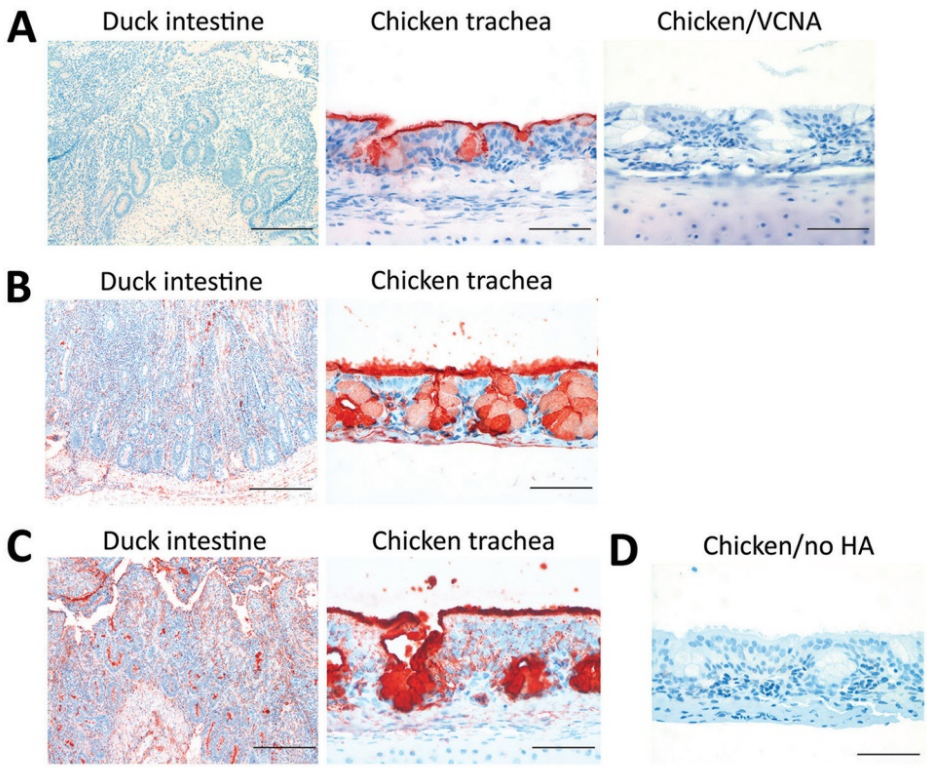

Figure 9. Histochemical analysis of binding of influenza A virus H5 proteins to avian tissues. A) Duck intestine and chicken trachea tissues stained with an antibody specific for 3'SLe^X (anti-3'SLe^X). Tissue sections treated with Vibrio cholerae neuraminidase (VCNA) before immunostaining were used as controls. Scale bars indicate 200 µm in left panel and 50 µm in center and right panels. B, C) Duck intestine and chicken trachea tissues incubated with H5 proteins H5N1$_{2.3.4}$ and H5N8 after precomplexing with horseradish peroxidase (HRP)–conjugated antibodies. Scale bars indicate 200 µm in left panel and 50 µm in right panel. D) Chicken trachea tissues incubated with HRPconjugated antibodies against H5N1$_{2.3.4}$ (no hemagglutinin [HA]) were used as a negative control. H5N1$_{2.3.4}$, novel H5N1 virus clade 2.3.4. Scale bar indicates 50 µm.

Clade 2.3.4.4 viruses are generally considered to have evolved in and being spread by wild birds and ducks prior to introduction into poultry. Phylogenetic analyses based on HA sequences (i.e. Fig.4) have shown the evolvement into several branches/subclades often harbouring multiple H5Nx genotypes. Substitutions K222Q and S227R were present in the earliest H5N5 isolates (A/duck/Guangdong/wy24/2008) and have been maintained in all branches except the above mentioned Taiwanese/North American branch of clade 2.3.4.4 viruses, which obtained reverse substitution R227S. This strongly suggests that the capacity to bind to 3'SLe^X-type receptors has arisen in wild birds. The potential role of altered receptor specificity in extended host-range and the contribution to the rapid world-wide spread is still unknown. The presence of 3'SLe^X type receptors on intestinal epithelial cells varies between different avian species (Table 1)(35) and does not appear to be required for infection of these birds, but their presence in other tissues and species requires further investigation. Apart from determining host-range, altered receptor specificity may also influence other factors involved in spreading like virus titers, shedding and pathogenesis in infected birds.

Table 2. Detection of 3'SLe^X in intestine of avian hosts of influenza A(H5Nx) virus clade 2.3.4.4 subtypes*

Order	Family	Common name	3'SLe^X staining of intestine[a]	H5Nx infection[b]
Galliformes	*Phasianidae*	Chicken	+	H5N8/H5N6/H5N2
Galliformes	*Phasianidae*	Turkey	-+	H5N8/H5N6
Galliformes	*Phasianidae*	Quail	-	H5N8
Galliformes	*Phasianidae*	Pheasant	+	H5N2
Galliformes	*Phasianidae*	Partridge	-	N.D.
Galliformes	*Numididae*	Guinea fowl	+	H5N8
Anseriformes	*Anatidae*	Mallard duck	-	H5N8/H5N6/H5N2
Anseriformes	*Anatidae*	Teal	N.T	H5N8/H5N6
Anseriformes	*Anatidae*	Swan	N.T.	H5N8
Anseriformes	*Anatidae*	Greylag/Canada goose	-	H5N8/H5N6
Columbiformes	*Columbidae*	Pigeon	++	H5N6
Falconiformes	*Falconidae*	Gyrfalcon	N.T.	H5N8
Gruiformes	*Gruidae*	Crane	N.T.	H5N8
Strigiformes	*Strigidae*	Snowy owl	N.T.	H5N2
Acipitriformes	*Accipitridae*	Cooper's hawk/Bald eagle	N.T.	H5N2/H5N8

*ND, not detected; NT, not tested; SLe, sialyl Lewis; –, no visible staining; -+, few cells weakly stained; +, intense staining of cells; ++, intense staining of many cells.

†Subtypes identified in different bird species on the basis of data from GenBank and GISAID (http://platform.gisaid.org).

Outbreaks of clade 2.3.4.4 viruses in poultry may very well have contributed to enhanced spreading (44-46) but adaptations in HA leading to the evolvement of poultry-specific clades have not yet been detected in HA-based phylogenetic analyses. Reassortments of the six internal gene segments are continuously associated with the further evolution of H5Nx viruses but the potential contribution of the internal gene constellation to (poultry-specific) spreading remains to be determined. Of particular interest are the recent outbreaks of H5N6 in poultry and ducks in South-East Asia that may have driven non-avian infections including 13, mostly lethal, human cases (47). Although enhanced avidity of

these H5N6 viruses for human-type receptors (carrying α2-6-linked sialosides) has been reported (21), the amino acid combination Q222/R227, which also all H5N6 viruses harbour in their HA, is unlikely to be responsible and other amino acid substitutions which have been shown to contribute to binding of α2-6-linked sialosides by HP H5N1 viruses have also not been detected in H5N6 (48, 49). Two clades of H5N6 viruses have been revealed by phylogenetic analysis (50), one harbouring an NA protein with a truncated stem and the other a full length stem. Truncation of the stem has been considered as a poultry-specific NA adaptation. Both H5N6 clades appear to have acquired their N6 segment in independent events from H6N6 viruses (50), one of which already contained the stem deletion. Also, both clades have caused infections in wild birds, poultry and humans and evidence for species-specific adaptions in NA is lacking.

A longstanding paradigm in IAV biology is the requirement for an optimal balance between HA binding and NA cleavage. HA binding displays a clear receptor fine-specificity but substrate fine-specificity of NAs has hardly been investigated. A recent report showed that all neuraminidase genotypes (only N4 was not tested) display relatively poor digestion of fucosylated receptors (43). Possibly due to the tight binding of such receptors by clade 2.3.4.4 viruses, the N1 neuraminidase of HP H5 viruses may have lost an unknown advantage over other NA genotypes in creating an optimal HA/NA balance, leading to the remarkable success of novel H5Nx reassortants within this clade.

ACKNOWLEDGMENT

This study was supported by the Dutch Ministry of Economic Affairs, Agriculture, and Innovation (Castellum Project Zoonotic Avian Influenza); National Institutes of Health grant AI114730 (J.C.P.); and a grant from the Kuang Hua Educational Foundation (J.C.P.). Synthetic glycans used for biolayer interferometry were provided by the Consortium for Functional Glycomics (grant no. GM62116). H.G. is supported by a grant from the Chinese Scholarship Council.

REFERENCES

1. de Vries E, Guo H, Dai M, Rottier PJ, van Kuppeveld FJ, de Haan CA. Rapid Emergence of Highly Pathogenic Avian Influenza Subtypes from a Subtype H5N1 Hemagglutinin Variant. Emerging infectious diseases. 2015 May;21(5):842-6.
2. Saito T, Tanikawa T, Uchida Y, Takemae N, Kanehira K, Tsunekuni R. Intracontinental and intercontinental dissemination of Asian H5 highly pathogenic avian influenza virus (clade 2.3.4.4) in the winter of 2014-2015. Reviews in medical virology. 2015 Nov;25(6):388-405.
3. Ip HS, Torchetti MK, Crespo R, Kohrs P, DeBruyn P, Mansfield KG, et al. Novel Eurasian highly pathogenic avian influenza A H5 viruses in wild birds, Washington, USA, 2014. Emerging infectious diseases. 2015 May;21(5):886-90.
4. Pasick J, Berhane Y, Joseph T, Bowes V, Hisanaga T, Handel K, et al. Reassortant highly pathogenic influenza A H5N2 virus containing gene segments related to Eurasian H5N8 in British Columbia, Canada, 2014. Scientific reports. 2015;5:9484.
5. Swayne DE. High pathogenicity avian influenza in the Americas. In: Swayne DE, editor. Avian Influenza. Oxford, UK: Blackwell; 2009. p. 191-216.
6. https://www.aphis.usda.gov/animal_health/downloads/animal_diseases/ai/hpai-preparedness-and-response-plan-2015.pdf.
7. Bottcher-Friebertshauser E, Garten W, Matrosovich M, Klenk HD. The hemagglutinin: a determinant of pathogenicity. Current topics in microbiology and immunology. 2014;385:3-34.
8. Wu H, Peng X, Xu L, Jin C, Cheng L, Lu X, et al. Novel reassortant influenza A(H5N8) viruses in domestic ducks, eastern China. Emerging infectious diseases. 2014 Aug;20(8):1315-8.
9. Lee YJ, Kang HM, Lee EK, Song BM, Jeong J, Kwon YK, et al. Novel reassortant influenza A(H5N8) viruses, South Korea, 2014. Emerging infectious diseases. 2014 Jun;20(6):1087-9.
10. Ku KB, Park EH, Yum J, Kim JA, Oh SK, Seo SH. Highly pathogenic avian influenza A(H5N8) virus from waterfowl, South Korea, 2014. Emerging infectious diseases. 2014 Sep;20(9):1587-8.
11. FAO warns of new strain of avian influenza virus. The Veterinary record. 2014 Oct 11;175(14):343.
12. Liu CG, Liu M, Liu F, Lv R, Liu DF, Qu LD, et al. Emerging multiple reassortant H5N5 avian influenza viruses in ducks, China, 2008. Veterinary microbiology. 2013 Dec 27;167(3-4):296-306.
13. Qi X, Cui L, Yu H, Ge Y, Tang F. Whole-Genome Sequence of a Reassortant H5N6 Avian Influenza Virus Isolated from a Live Poultry Market in China, 2013. Genome announcements. 2014;2(5).
14. Zhao K, Gu M, Zhong L, Duan Z, Zhang Y, Zhu Y, et al. Characterization of three H5N5 and one H5N8 highly pathogenic avian influenza viruses in China. Veterinary microbiology. 2013 May 3;163(3-4):351-7.
15. World Health Organization. Evolution of the influenza A(H5) haemagglutinin: WHO/OIE/FAO H5 Working Group reports a new clade designated 2.3.4.4 [cited 2015 Jan 19].
16. Gu M, Huang J, Chen Y, Chen J, Wang X, Liu X, et al. Genome sequence of a natural reassortant H5N2 avian influenza virus from domestic mallard ducks in eastern China. Journal of virology. 2012 Nov;86(22):12463-4.
17. Connor RJ, Kawaoka Y, Webster RG, Paulson JC. Receptor specificity in human, avian, and equine H2 and H3 influenza virus isolates. Virology. 1994 Nov 15;205(1):17-23.
18. Paulson JC, de Vries RP. H5N1 receptor specificity as a factor in pandemic risk. Virus research. 2013 Dec 5;178(1):99-113.
19. Gambaryan A, Yamnikova S, Lvov D, Tuzikov A, Chinarev A, Pazynina G, et al. Receptor specificity of influenza viruses from birds and mammals: new data on involvement of the inner fragments of the carbohydrate chain. Virology. 2005 Apr 10;334(2):276-83.
20. Wagner R, Matrosovich M, Klenk HD. Functional balance between haemagglutinin and neuraminidase in influenza virus infections. Reviews in medical virology. 2002 May-Jun;12(3):159-66.

21. Sun H, Pu J, Wei Y, Sun Y, Hu J, Liu L, et al. Highly pathogenic avian influenza H5N6 viruses exhibit enhanced affinity for human type sialic acid receptor and in-contact transmission in model ferrets. Journal of virology. 2016 Apr 27.
22. Yang H, Carney PJ, Mishin VP, Guo Z, Chang JC, Wentworth DE, et al. The molecular characterizations of surface proteins hemagglutinin and neuraminidase from recent H5Nx avian influenza viruses. Journal of virology. 2016 Apr 6.
23. de Vries RP, de Vries E, Moore KS, Rigter A, Rottier PJ, de Haan CA. Only two residues are responsible for the dramatic difference in receptor binding between swine and new pandemic H1 hemagglutinin. The Journal of biological chemistry. 2011 Feb 18;286(7):5868-75.
24. Dortmans JC, Dekkers J, Wickramasinghe IN, Verheije MH, Rottier PJ, van Kuppeveld FJ, et al. Adaptation of novel H7N9 influenza A virus to human receptors. Scientific reports. 2013;3:3058.
25. Dohi T, Nemoto T, Ohta S, Shitara K, Hanai N, Nudelman E, et al. Different binding properties of three monoclonal antibodies to sialyl Le(x) glycolipids in a gastric cancer cell line and normal stomach tissue. Anticancer research. 1993 Sep-Oct;13(5A):1277-82.
26. Wickramasinghe IN, de Vries RP, Grone A, de Haan CA, Verheije MH. Binding of avian coronavirus spike proteins to host factors reflects virus tropism and pathogenicity. Journal of virology. 2011 Sep;85(17):8903-12.
27. Wickramasinghe IN, de Vries RP, Eggert AM, Wandee N, de Haan CA, Grone A, et al. Host tissue and glycan binding specificities of avian viral attachment proteins using novel avian tissue microarrays. PloS one. 2015;10(6):e0128893.
28. Xiong X, Tuzikov A, Coombs PJ, Martin SR, Walker PA, Gamblin SJ, et al. Recognition of sulphated and fucosylated receptor sialosides by A/Vietnam/1194/2004 (H5N1) influenza virus. Virus research. 2013 Dec 5;178(1):12-4.
29. Guex N, Peitsch MC. SWISS-MODEL and the Swiss-PdbViewer: an environment for comparative protein modeling. Electrophoresis. 1997 Dec;18(15):2714-23.
30. Schwede T, Kopp J, Guex N, Peitsch MC. SWISS-MODEL: An automated protein homology-modeling server. Nucleic acids research. 2003 Jul 1;31(13):3381-5.
31. Baenziger JU, Fiete D. Structure of the complex oligosaccharides of fetuin. The Journal of biological chemistry. 1979 Feb 10;254(3):789-95.
32. Spiro RG, Bhoyroo VD. Structure of the O-glycosidically linked carbohydrate units of fetuin. The Journal of biological chemistry. 1974 Sep 25;249(18):5704-17.
33. Spik G, Bayard B, Fournet B, Strecker G, Bouquelet S, Montreuil J. Studies on glycoconjugates. LXIV. Complete structure of two carbohydrate units of human serotransferrin. FEBS letters. 1975 Feb 15;50(3):296-9.
34. Smith GJ, Donis RO, World Health Organization/World Organisation for Animal HF, Agriculture Organization HEWG. Nomenclature updates resulting from the evolution of avian influenza A(H5) virus clades 2.1.3.2a, 2.2.1, and 2.3.4 during 2013-2014. Influenza and other respiratory viruses. 2015 Sep;9(5):271-6.
35. Hiono T, Okamatsu M, Nishihara S, Takase-Yoden S, Sakoda Y, Kida H. A chicken influenza virus recognizes fucosylated alpha2,3 sialoglycan receptors on the epithelial cells lining upper respiratory tracts of chickens. Virology. 2014 May;456-457:131-8.
36. Gambaryan A, Tuzikov A, Pazynina G, Bovin N, Balish A, Klimov A. Evolution of the receptor binding phenotype of influenza A (H5) viruses. Virology. 2006 Jan 20;344(2):432-8.
37. Okamatsu M, Saito T, Yamamoto Y, Mase M, Tsuduku S, Nakamura K, et al. Low pathogenicity H5N2 avian influenza outbreak in Japan during the 2005-2006. Veterinary microbiology. 2007 Sep 20;124(1-2):35-46.
38. Hiono T, Okamatsu M, Igarashi M, McBride R, de Vries RP, Peng W, et al. Amino acid residues at positions 222 and 227 of the hemagglutinin together with the neuraminidase determine binding of H5 avian influenza viruses to sialyl Lewis X. Archives of virology. 2016 Feb;161(2):307-16.

39. Sugiura K, Yamamoto M, Nishida T, Tsukamoto D, Saito T, Onodera T. Recent outbreaks of avian influenza in Japan. Revue scientifique et technique. 2009 Dec;28(3):1005-13.
40. Gambaryan AS, Tuzikov AB, Pazynina GV, Desheva JA, Bovin NV, Matrosovich MN, et al. 6-sulfo sialyl Lewis X is the common receptor determinant recognized by H5, H6, H7 and H9 influenza viruses of terrestrial poultry. Virology journal. 2008;5:85.
41. Gambaryan AS, Matrosovich TY, Philipp J, Munster VJ, Fouchier RA, Cattoli G, et al. Receptor-binding profiles of H7 subtype influenza viruses in different host species. Journal of virology. 2012 Apr;86(8):4370-9.
42. Gambaryan AS, Tuzikov AB, Pazynina GV, Webster RG, Matrosovich MN, Bovin NV. H5N1 chicken influenza viruses display a high binding affinity for Neu5Acalpha2-3Galbeta1-4(6-HSO3)GlcNAc-containing receptors. Virology. 2004 Sep 1;326(2):310-6.
43. Heider A, Mochalova L, Harder T, Tuzikov A, Bovin N, Wolff T, et al. Alterations in hemagglutinin receptor-binding specificity accompany the emergence of highly pathogenic avian influenza viruses. Journal of virology. 2015 May;89(10):5395-405.
44. Fang S, Bai T, Yang L, Wang X, Peng B, Liu H, et al. Sustained live poultry market surveillance contributes to early warnings for human infection with avian influenza viruses. Emerging microbes & infections. 2016;5(8):e79.
45. Yuan R, Wang Z, Kang Y, Wu J, Zou L, Liang L, et al. Continuing Reassortant of H5N6 Subtype Highly Pathogenic Avian Influenza Virus in Guangdong. Frontiers in microbiology. 2016;7:520.
46. Bi Y, Mei K, Shi W, Liu D, Yu X, Gao Z, et al. Two novel reassortants of avian influenza A (H5N6) virus in China. The Journal of general virology. 2015 May;96(Pt 5):975-81.
47. Shen YY, Ke CW, Li Q, Yuan RY, Xiang D, Jia WX, et al. Novel Reassortant Avian Influenza A(H5N6) Viruses in Humans, Guangdong, China, 2015. Emerging infectious diseases. 2016 Aug;22(8):1507-9.
48. Herfst S, Schrauwen EJ, Linster M, Chutinimitkul S, de Wit E, Munster VJ, et al. Airborne transmission of influenza A/H5N1 virus between ferrets. Science. 2012 Jun 22;336(6088):1534-41.
49. Imai M, Watanabe T, Hatta M, Das SC, Ozawa M, Shinya K, et al. Experimental adaptation of an influenza H5 HA confers respiratory droplet transmission to a reassortant H5 HA/H1N1 virus in ferrets. Nature. 2012 Jun 21;486(7403):420-8.
50. Bi Y, Liu H, Xiong C, Di L, Shi W, Li M, et al. Novel avian influenza A (H5N6) viruses isolated in migratory waterfowl before the first human case reported in China, 2014. Scientific reports. 2016;6:29888.

Chapter 7

General discussion

Influenza A viruses (IAVs) cause annual epidemics, periodic pandemics, and enzootic infections of different hosts species. The impact on human and animal health continues to be huge (1-3). New pandemic threats, for instance from H5Nx and H7N9 viruses (4-7), remain on the lure and the economic losses are considerable. The continuous, and mostly unpredictable, evolution of IAVs poses a major challenge to annual vaccine efficacy and maintains a status where new pandemics or enzootic infections can appear out of the blue.

In this thesis we have focused on IAV's two viral envelope glycoproteins that play a key role in establishing a new infection. Hemagglutinin (HA) and neuraminidase (NA) are, on the one hand, main players in viral immune evasion (2, 3, 8)and, on the other hand determining factors in pandemic and enzootic potential (1-3). HA and NA interact with sialic acids (SIA) receptors that are omni-present on animal cell surfaces (9-11). HA binds to SIA by its receptor binding site (RBS), which ultimately results in endocytic uptake of the virions (12). On the contrary, NA is a receptor destroying enzyme by cleaving sialic acids (13, 14). Besides being used as a functional entry receptor on host cells, SIA receptors are also abundantly present on proteins in the mucus layer that covers epithelial cells (15). These function as decoy receptors, a feature that is counteracted by viral NA activity.

Bio-layer interferometry (BLI) is a technique that allowed us to study the interactions between IAV particles and its SIA receptor repertoire in real-time. Our aim was to develop quantitative methods that can reveal insight into IAV receptor binding dynamics under model conditions that, albeit simplified, represent the complex receptor landscape encountered by IAV during *in vivo* infection. Here we discuss the relevance of our findings in connection to *in vivo* IAV infection and evolution.

I. Respiratory epithelium: the *in vivo* landscape of IAV infection

In humans, IAVs infect epithelial cells of the respiratory tract (2, 3, 16). The major cell types of the respiratory epithelium are ciliated and non-ciliated columnar cells, goblet cells, and basal cells (17) (Figure 1). Basal cells serve as stem cells for renewal of the epithelium. Goblet cells are specialized, non-ciliated columnar cells that secrete mucus which forms a visco-elastic gel of about 2 to 20 μm thickness (18-20) that covers the underlaying, much less viscous, periciliary layer (PCL) (21). Ciliary beating of ciliated cells, sweeps the mucus out of the lungs, carrying with it the debris that has become stuck to it. Cilia are 0.2 to 0.3 μm in diameter and range from 6 to 7 μm in length in the upper airways, to 4 μm in the smaller airways (22, 23). The distance between two cilia is, on average, around 200nm (Figure 2) (24).

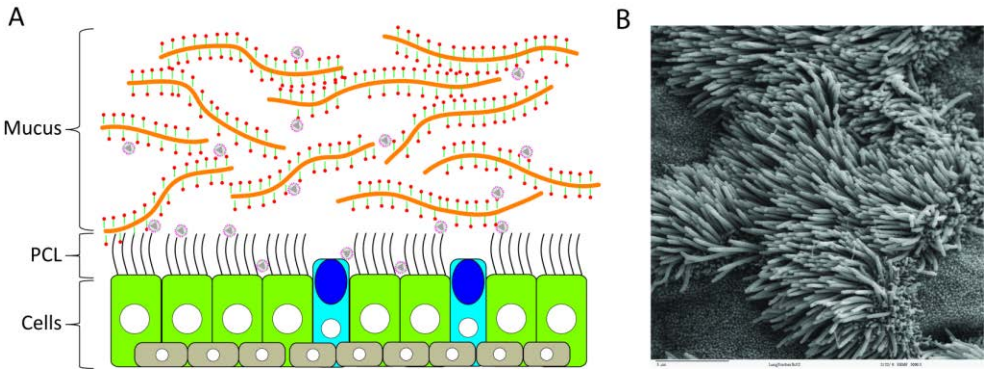

Figure 1A. Schematic representation of the epithelial cells. The respiratory epithelium contains three major cell types, which are ciliated cells (green), goblet cells (blue), and basal cells (grey). The mucus secreted by the goblet cells forms a viscoelastic blanket over the tops of the cilia.
Figure 1B. Respiratory epithelium with ciliated and non-ciliated cells.

The PCL and the mucus layer present a formidable barrier for IAV to transverse, because of their extremely high content of densely sialylated mucins (25, 26). Soluble mucins constitute ~1% (w/w) of the watery (~98%) mucus layer and 50 to 90% of their mass consists of, mostly O-linked, carbohydrates (27, 28). This implies that the *in vivo* concentration of soluble mucins by far exceeds the minimal concentrations required to dissolve IAV-receptor complexes as shown in **Chapter 3**. Soluble mucins form, by polymerization, large, elongated, assemblies (up to 2.10^4 kDa) giving the mucus layer a mesh-like appearance with pore sizes up to 500nm in width (29). Membrane-spanning mucins and tethered muco-polysaccharides covering the cilia protrude far into the narrow (~200nm) space l between cilia, creating a microenvironment from which soluble mucins as well as beads larger than 40 nm were shown to be excluded (30). As cilia can almost certainly not be infected because of their internal tubulin structures, IAV particles (~100nm diameter) first need to travel to the cell membrane at the base of the cilia. So how do they achieve this? It has been shown that NA activity enables IAV to traverse the mucus layer (31, 32), presumably by counteracting binding to mucin decoy receptors. We consider NA activity-driven virus particle rolling (**Chapter 2**) as a mechanism that can provide directionality and even traction to particle migration over elongated mucin tracks, by following a receptor concentration gradient created by NA activity. Directional virus movement on fetuin-coated glass slides has recently been observed using live microscopy (33). Especially for traversing the PCL, traction is likely to be crucial to support migration through the tight inter-ciliar mesh into which 40nm beads cannot penetrate by diffusion (30). Despite this difficult access to the entry sites, human IAVs were shown to efficiently infect ciliated cells as well as goblet cells (34-36), both expressing α2,6-linked SIAs and small amounts of α2,3-linked SIAs (17, 37). Inaccessibility for soluble mucins, that

otherwise will efficiently elute IAVs from a receptor-coated surface (**Chapter 3**), may very well lend a major advantage to using the well-hidden entry sites at the ciliar base.

In the absence of mucin-driven virus elution, maturation of virus binding (discussed in paragraph IIa below) will occur more readily and may promote the clustering of signaling receptors that was shown to trigger downstream signaling events leading to endocytic uptake (38-43). It is not yet clear, which cell surface glycoproteins function as functional IAV uptake receptors that can initiate endocytosis. Possible candidates are proteins that carry glycan assemblies that could support faster binding maturation, like a cluster of short O-linked glycans (as observed for glycophorin A, **Chapter** 3) or N-glycans with branched and extended LacNAc antennae (44). Glycomic analysis of the human respiratory tract identified (45) heterogeneous mixtures of bi-, tri-, and tetra-antennary N-glycans with varying numbers of N-acetyllactosamine repeats as well as sialylated core-1 and core-2 O-glycans but they have not been mapped to specific proteins or cell types yet.

Classically, NA activity was primarily considered to be required for the release of nascent virus particles. Clinical isolates of IAVs appear to bud from the plasma membrane into two types of virus particles, spherical and filamentous. The long (up to 10 μm, (46)) filamentous particles, containing the genome segments in their extreme tips, appear very fragile and are particularly observed when still attached to the infected cell (47). They may therefore function to breach to mucus layer, which might be required for host-to-host transmission or to facilitate cell-to-cell spread. Newly budded spherical particles on the other hand, may move over their de-sialylated cell of origin to neighbouring cells by using the overlaying sialylated mucus layer as a track that supports virus rolling.

II. IAV-receptor interaction: A delicately balanced and dynamic process

A paradigm in IAV biology and evolution is the maintenance of an optimal, but poorly defined, functional balance between HA, NA and their receptors (48-50). In other words, NA enzymatic activity and specificity need to match HA binding affinity and specificity. This balance involves the establishment of a new infection but also needs to support efficient release of virus particles at the end of the infection cycle. The essential player, besides HA and NA, is the wide spectrum of sialoside receptors that are differentially distributed of over decoy and functional receptors. These are bound and cleaved to a variable extent by different HAs and NAs (51).

IAV-receptor interaction is a highly dynamic process by nature. The use of BLI, employing a tailor-made glycoprotein receptor toolkit, allowed us to study the simultaneous contribution of NA and HA to virus particle binding to specifically coated receptor surfaces, in presence or absence of decoy receptors. It revealed novel mechanistic insights into a tight, but highly dynamic interaction and enabled quantitative determination of virus

binding rates (**Chapter 2 and 3**). The gained knowledge and resources were further employed to study changes in IAV-receptor binding associated with antigenic evolution (**Chapter 4**) or virus reassortment (**Chapter 5 and 6**).

IIa. A model for the dynamic interaction between IAV and its receptors

The highly dynamic interaction between IAV and its receptors is founded on two principles. (I), a very low avidity of the individual HA-SIA interaction (K_D in the low mM range) and (II), the multivalent interaction between virus and receptor surface. The initial binding rate (see **IIb** below) depends on virus and receptor concentration and on the K_D of the concerning individual HA-SIA interaction. The latter is, practically spoken, undeterminable in most cases. We have found that the NA active site also contributes to the initial binding rate, in a negative correlation with its catalytic activity (**Chapter 2**). Subsequent binding events, leading to tight polyvalent binding, are independent of virus concentration but will be affected by receptor density, diversity and distribution. The high K_D of individual interactions results in their rapid dissociation but, as this does not occur simultaneously, the virus remains attached. However, the released binding site becomes available for binding of soluble competitors (**Chapter 3**). This happens iteratively and leads to rapid elution of virus by antibodies but also, at physiologically relevant concentrations, by mucin decoy receptors. Obviously, receptor density on the decoy protein and the HA/NA balance for the receptors involved will be a determining factor for elution efficiciency. Unbound receptors are vulnerable to cleavage by NA, thereby reducing the SIA content of the receptor surface. Importantly, this drives rolling of virus particles over receptor-coated surfaces (**Chapter 2 and 3**). Whether the dissociation of an individual interaction leads to immediate cleavage by NA, thereby inducing rolling, remains to be determined. It will require the translocation of a neighboring NA to the just-released SIA. Alternatively, virus particles may be bound in a “wobbly” state. Dissociation of an interaction on one side of the interaction surface may allow an association at the other side of the interaction surface, thereby causing a small translocation of the particle. NA activity logically will speed up this process by decreasing the number of available free SIAs in the vicinity of the particle. The speed of rolling will depend on NA catalytic rate and the association and dissociation rate constants (k_{on} and k_{off}) of individual HA-SIA interactions. Receptor diversity (different k_{on}, k_{off} and NA susceptibility) and density on a cell surface could influence the track that is followed. Virus particle morphology and flexibility may also be an important factors for its translocation capacity. We speculate that the observed reduction of virus motility in time, denoted as virus binding maturation, is caused by the formation of multiple interactions with an HA trimer. In such a conFigureuration, at least on interaction will be maintained most of the time leading to a much less “wobbly” state of the virus particle. This in turn might promote the rapid accumulation of HA trimers having multiple receptor interactions. Biologically important implications of rolling and

maturation have been discussed above (**I**). Recently, directional IAV particle motion on fetuin-coated glass slides was observed by using total internal reflection microscopy. Particles moved at two different velocities, both requiring NA activity (33).

IIb. Quantification of virus binding: the relevance to in vivo binding

BLI has recently found its way into the lab for quantification of virus binding. For IAV, attempts focused on determination of the virus-receptor dissociation constant (Kd) (52-55). End-point (60 min) binding levels were used for plotting fractional virus binding saturation (f) against receptor density. The Hill equation (describing cooperative binding) was employed to derive an apparent Kd (Kd = ([virus](1-f))/f)) at every receptor density. However, the Hill equation does not reflect a physically possible reaction scheme for highly multivalent interactions (56) and variation of receptor density is not gradual but dictated by the fixed grid of the high affinity binding probes on the particular BLI biosensors (**Chapter 2**). In practice, virus dissociation was not observed, even at very low receptor loading levels. Thus, low virus-binding levels do not result from equilibrium binding, but rather from reduced maximal virus loading levels at low receptor densities. *In vivo*, virus binding will rapidly be followed by the crucial step of infection: virus entry. We therefore consider the initial virus binding rate v^{obs} as the most relevant parameter for quantitative analysis of virus binding (**Chapter 2**).

IIc. Biotinylated glycoproteins: a tailor-made toolkit mimicking natural IAV receptors

Membrane-spanning glycoproteins are natural probes for studying virus-receptor interactions in contrast to the often used synthetic glycans and the poorly glycosylated serum proteins fetuin and transferin. Trans-membrane glycoproteins densely covered with N-linked glycans (LAMP-1, ICAM-1) were used to mimic IAV cell surface receptors whereas Glycophorin A (1 N-linked and 16 O-linked glycosylation sites on a fifty amino acid stretch (57, 58)) was used to mimic mucin decoy receptors A major advantage of building a biotinylated glycoprotein receptor expression toolkit is its versatility towards further expansion (other proteins) and refinement of receptor specificity patterns in order to provides us with a large receptor repertoire, closely mimicking the receptors found in vivo. The latter we have started by genetic modification (removal of glycosylation sites), expression in specific cell lines (e.g. CHO cells which exclusively attach α2,3-linked SIAs (59)) or overexpression of sialyltransferases ST3GALI, ST3GALIV and ST6GALI resulting in over-production of specific SIA linkage types on the expressed glycoproteins (60) (**Chapter 2 and 3**).

IId. The HA/NA balance: quantification by BLI

The importance of a functional HA/NA balance, though still poorly defined, has been supported by a range of in vivo and in vitro experiments (48, 50, 61-72). However,

conclusions were often drawn by correlating the individually determined properties of HA and NA. BLI was recently used (73) to determine the binding curves of virus particles in presence of NA activity in an attempt to directly quantify the HA/NA balance. We used a similar assay, and developed an additional assay that specifically determines the NA activity-driven self-elution rate of receptor-bound virus particles (**Chapter 2**). The latter assay is essential for the analysis of viruses with a relatively high NA activity which in the first-mentioned assay give only very limited binding. It provides approaches for quantification of a receptor-specific HA/NA balance. Virus rolling and the observed NA activity-driven changes in particle morphology (**Chapter 2**) are complicating kinetic factors that are also expected to occur in the first assay. However, they are better recorded by the self-elution assay and should not be ignored in a quantitative interpretation of the results. Glycoprotein receptors like LAMP-1 are superior, to for instance synthetic glycans, for the determination of the HA/NA balance as very little maturation is observed after short binding times (**Chapter 3**). As a note of caution for interpreting results, we point to our results in **Chapter 2** that show how the HA/NA balance can be tuned by NA particle incorporation levels, in addition to its intrinsic activity. Finally, like HA, NA protein affects the HA/NA balance by displaying receptor fine specificity (74). In **Chapter 2** we used BLI to show that PR8 virus particles could bind (non-)fucosylated synthetic glycans to the same extent, but strongly differed in the ability to cleave these receptors.

IIe. The difference between virus-receptor binding and HA protein-receptor binding

The receptor specificity of a particular virus strain is often inferred from studies using recombinant HA proteins and methods like glycan array analysis. Such methods are very sensitive for the detection of effects of single amino acid substitutions but may not quantitatively reflect changes in binding rates for the corresponding viruses (75-79). However, determination of receptor binding of virus particles by employing endpoint assays has often been suggested to suffer from high aspecific binding levels. In **Chapter 2** we showed that single amino acid substitution E190D in HA, reported to be responsible for the acquirement of human receptor binding properties (80-83), resulted in an absolute switch in binding preference from α2,3- to α2,6-linked SIAs when using recombinant soluble HA proteins **(Chapter 2)**. Binding rate analysis of the corresponding viruses by BLI, showed this switch to be far from absolute. Apparently, the antibody-induced complexation of HA proteins required for glycan array analysis (only multivalent binding is strong enough to be detected) results in artificial assemblies that do not properly reflect virus particles. BLI provides a background-free method for determination of genuine binding rates.

III. Virus evolution and antigenic drift: changing virus receptor interactions

IIIa. Antigenic drift and the role of receptor binding

IAVs are evolutionarily dynamic viruses (84, 85). Mutations that change amino acids in the antigenic portions of the surface glycoproteins HA and NA may produce selective advantages for viral strains by allowing them to evade (preexisting) immunity (1-3, 8). This is the basis for the antigenic drift observed for human IAVs, which has been documented in detail for H3N2 (86). Antigenic drift proceeds by clearly punctuated steps, called antigenic cluster transitions, urging the regular vaccine updates. During 34 years of H3N2 evolution since 1968, they were caused by mutations at only seven positions adjacent to the HA receptor binding site (the cluster transition mutations) (87). Other mutations may compensate for potential negative effects of cluster transition mutations on virus binding. In **Chapter 4**, we used BLI to show that 9 consecutive cluster transitions (HK68 until SY97 spanning 29 years) resulted in minor changes in receptor binding rate. Also, the individual antigenic cluster transition mutations themselves only moderately increased or decreased binding. In contrast, for a cluster transition that was investigated in more detail (cluster transition SI87 to BE92 that occurred around 1992), three non-cluster transition mutations (193NS, 190ED and 133SD) appeared to have caused a large negative effect on binding rate. These mutations were introduced immediately prior to the cluster transition mutation (156EK) but did not affect antigenicity. Cluster transition mutation 156EK was further remarkable in a sense that viruses carrying this particular mutation had been isolated regularly over the preceding 10 years. However, only its introduction into the background of mutations 193NS, 190ED and 133SD has led to the establishment of a novel antigenic cluster where all prior occurrences of this cluster transition mutation were mapped to short dead-end branches of a phylogenetic tree, suggesting they possessed a reduced viral fitness. In principle, an antigenic cluster transition mutation will be selected in a background that sufficiently compensates for the potential negative effects on virus fitness by the cluster transition mutation itself. However, in the face of increasing herd immunity, the positive selective effect of antigenic change caused by the cluster transition mutation will progressively lower the requirement for a strong compensatory effect of an already existing background. In other words, there will be more time to acquire compensatory mutations afterwards.

An alternative model for the evolutionary mechanism of IAV antigenic drift proposes that modulation of receptor binding avidity is the primary driver of antigenic change (88). The initial selection, in immune individuals, of mutations that increase binding avidity, would provide an escape mechanism from antibodies that block receptor binding. These mutations, as well as subsequent mutations selected in naïve individuals for restoring binding avidity, will result in gradual antigenic change. Clearly, consecutive mutations 193NS, 190ED and 133SD do not support such a mechanism as none of them increases

binding avidity. Further studies will be required to determine the selective advantages of these mutations and their potential involvement in the generation of antigenic change. In this perspective, it will be worthwhile to extensively investigate the effects of mutations 193NS, 190ED and 133SD, as well as mutations following upon the introduction of cluster transition mutation 156EK, for their precise effect on HA/NA/receptor balance by using our established set of BLI assays and glycoproteins representing the natural receptor repertoire. This will require their analysis in the background of their cognate NA.

IIIb. Emergence of reassortant viruses in relation to receptor binding

Apart from causing or facilitating antigenic change, mutations in HA and NA can provide other selective advantages due to their effect on the interactions with sialoside receptors. For instance, viruses may acquire the capacity for better infection of, or improved fitness in, an expanded avian host species range. Mutations in HA and NA may result in an improved HA/NA balance for the novel host receptor repertoire. Besides mutations in HA or NA, reassortment events resulting in the acquirement of novel HA and NA combinations can be involved. A striking example is the recent emergence of a wide range of reassortant IAVs that all carry an H5 segment that is a descendant from the highly pathogenic (HP) H5N1 virus that first appeared in 1996 in Hong Kong (89-91). Since 2005, a monophyletic clade (clade 2.3.4.4) of this HP H5 segment has been involved in an unprecedented number of reassortments, giving rise to the so-called group of H5Nx viruses because of the involvement of a number of different NA genotypes (92-100). Members of this H5Nx group have spread around the world at a pace that was never seen before. Their spread has been attributed to migrating wild birds from which source it rapidly has spread further to poultry (101, 102). Only for H5N6 occasional infections of humans have been reported (103). The remarkable “reassortment-prone” evolution of the clade 2.3.4.4 H5 proteins and associated world-wide spread were reason to us for an analysis of their binding properties.

In **Chapter 5 and 6**, we showed that emergence of HP clade 2.3.4.4 H5Nx viruses is accompanied by a change in HA receptor-binding specificity. In comparison to the ancestral 2.3.4 clade, the earliest H5 proteins (H5N5 from 2005) from clade 2.3.4.4 had acquired two substitutions (K222Q and S227R) in the RBS that have not occurred before in HP H5 proteins. These mutations resulted in increased binding to a fucosylated sialoside structure that is better known as the Sialyl-LewisX (SLe^X) antigen (104, 105). The SLe^X antigen is characterized by fucosylation of the N-acetylglucosamine moiety of the terminal lactosamine repeat. The ability of some low pathogenic avian IAVs to bind to SLe^X has been considered a poultry-specific adaptation (105-108) although extensive studies on sufficient numbers of isolates across the complete range of HA genotypes are lacking. Phylogenetic analysis of H5Nx viruses **(Chapter 5 and 6)**, however, indicates that the

ability to bind SLe^X has arisen in wild birds. Binding profiles of parental clade 2.3.4 and novel clade 2.3.4.4 H5 proteins to tissues of different avian species did not correlate with the presence of fucosylated sialosides as determined by immunohistochemistry **(Chapter 6).** The selective advantage of clade 2.3.4.4 H5N1 viruses to obtain altered receptor binding properties still remains to be established.

It might be argued that an altered binding avidity and specificity needs be accompanied by compensatory changes in NA activity to prevent disturbance of the HA/NA balance. Possibly, because of tight binding of SLe^X by clade 2.3.4.4 viruses, the N1 of highly pathogenic H5 viruses might have lost a yet unknown advantage over other NA genotypes in creating an optimal HA/NA balance. This may have led to the appearance of many novel H5Nx viruses by reassortment which is normally very rare for HP H5 clades. Most NA proteins appear relatively poor in cleavage of fucosylated receptors ((109) and **Chapter 2**) but it has not yet been investigated whether this holds true for the specific NA proteins of different genotypes that have recently reassorted to form the H5Nx group of IAVs. We hypothesize that the altered receptor binding properties of the novel clade 2.3.4.4 H5 protein somehow has contributed to emergence of novel H5Nx subtype viruses and to the unprecedented intercontinental spread of these novel viruses via wild birds (100). These studies **(Chapter 5 and 6)** also indicate the importance of analyzing the receptor-binding and cleavage fine specificity of newly emerging IAVs. As the receptor binding and cleavage properties are not directly predictable from the primary HA and NA sequences, it is advisable to additionally perform phenotypic analyses of the HA and NA proteins, preferably using both recombinant proteins as well as (recombinant) virus particles.

IV. Future perspectives and applicability

The BLI based assays described in this thesis give insight into the real-time kinetics of IAV-receptor interactions. We can now quantify the HA/NA balance by descriptive parameters, using a precisely tunable receptor repertoire. Mechanistic features like virus particle rolling and binding maturation have been discovered. Still, many questions remain and further development of assays is required. Ultimately, one would like to be able to determine the individual kinetic rate and binding constants of an HA/NA pair for a particular receptor, and use them to correctly predict the kinetics of virus-cell interaction in relation to the specific HA/NA pair. Here we address a few other issues that need to be explored in the near future.

IVa. Analysis of virus binding to membrane-embedded receptors

Like traditional extra-cellular cargo molecules destined for endocytic uptake, receptor-bound viruses may float over the cell surface by lateral diffusion of the receptor in a fluidic plasma membrane. It may lead to receptor clustering and signaling (38, 110, 111),

resulting in endocytic uptake (112). Virus rolling and binding maturation may affect this process. IAV particles were shown to become immobilized at the plasma membrane followed by *de novo* formation of clathrin-coated pits and endocytosis (41). However, prior Mmotility of IAVs on the cell surface is hard to measure.

Binding of IAV to static receptor surfaces ignores a potential role of receptor mobility and clustering. This could be studied by coating sensors with receptor-harboring vesicles. Even more useful, but challenging, will be the application of cell-based BLI assays using sensors coated with fixed or living cells. Cell-based BLI assays which monitor signal transduction in living cells induced by antibody binding to the epidermal growth factor receptor were recently developed(113). Rearrangements in the cytoskeleton induced upon antibody binding were readily detected. Virus binding to cells may result in considerable changes in light reflection and could possibly be detected by BLI. This would mimic the natural situation of virus binding to glycoproteins embedded in a fluid membrane. Additionally, such assays may provide insight into signaling resulting in cytoskeletal rearrangements induced upon virus binding (114).

IVb Application of BLI-based methods for antigenic cartography

Hemagglutination inhibition (HI) assays are routinely used to quantify antibodies (Ab) that inhibit agglutination of red blood cells (RBCs) (115) and, for instance, to detect and quantify antigenic change (87, 116-118). Hemagglutination titers are commonly used for standardization of virus particle numbers in such assays [ref] as well as many virus-receptor binding assays. However, hemagglutination titers intrinsically depend on the interaction of a particular HA with the SIAs present on a particular RBC. Such titers therefore reflect, in addition to virus particle number, virus-receptor binding avidity and specificity. Also, glycosylation and sialylation patterns of RBCs differ, to an unknown extent, between species and individuals (119, 120) which will affect HI titers (121). BLI provides, in high throughput, quantification of HA-specific Ab titers by elution of virus particles that are pre-loaded to a standard level on selected receptors. BLI-based and HI-based antigenic maps should be compared for their correlation with functional antigenicity as determined by the inhibition of infection by specific antisera.

IVc The role of mucus in IAV infection in relation to zoonotic transfer and COPD.

IAV requires NA activity in order to traverse the mucus layer overlaying epithelial cells before infection can occur (31, 32). The inhibitory effects of mucus decoy receptors can be quantified using BLI. Mucin glycosylation and sialylation patterns vary significantly between species (122-124), and thus are likely to influence IAV host species specificity. These differences may form an important part of the barrier that prevents zoonotic transmission. Also, increased IAV infection has been associated with respiratory diseases

like COPD, including asthma (125). Especially children with a respiratory disease have more severe problems associated with IAV infection. Some studies showed that in these patients, the severity of airway infection is related to glycosylation changes on mucins (126, 127). BLI assays will allow comparative studies on the effects of mucus, from patients or different species, on virus binding rates in relation to infection and zoonotic transfer.

IVd Assessing the role of NA in virus binding

BLI allowed to dissect the highly intertwined functions of HA and NA. Whereas HA-dependent virus-receptor surface interaction directs NA activity to that surface, NA itself can also contribute to the initial binding rate. This may occur via the catalytic site, in case of NAs with a low cleavage rate (128, 129), or via the enigmatic 2nd SIA-binding site (130-133). BLI could identify the binding rate contribution via the NA active site, which occurs in competition with active site-binding NA inhibitors (**Chapter 2**), and could be applied for recent H3N2 viruses that display severely reduced HA binding avidity to the SIA receptors. Their N2 acquired high binding avidity for SIA receptors and displayed reduced enzymatic activity (129, 134). The 2nd SIA-binding site, which is only conserved in avian IAVs (131, 135), increases the activity of soluble NA tetramers (131), but its function in the context of a virus particle remains unclear. BLI seems well suited to analyze and quantify the contribution of the 2nd SIA-binding site to virus binding rate. However, the lack of competitors binding to the 2nd SIA-binding site and the simultaneous contribution of HA to virus binding requires novel approaches to be developed.

IVe Application of BLI for the analysis of antiviral drugs

The use of anti-viral, NA-inhibiting, drugs has led to the selection of drug resistant IAVs with mutations in NA (136). The half-maximal inhibitory concentration is commonly determined by using a soluble, monovalent, NA substrate (137). However, *in vivo* inhibitor sensitivity is likely to be affected by the corresponding HA protein. For instance, NA inhibitors displayed stronger effects on virus infectivity in the presence of decoy receptors to which the HA protein could bind (31). Thus, to determine the inhibitor sensitivity of a particular isolate, the functionality of HA and decoy receptors needs to be taken into account. Infection assays are being employed to this purpose (138, 139) but do not allow high throughput approaches and suffer from cell line specific issues. BLI allows quantification of the inhibition of NA activity-driven self-elution of virus particles in the presence of mucus. Preliminary results indicate that IC50s differ considerably between viruses harboring the same NA (unpublished). The obtained IC50 values need to be correlated to the inhibitory effects of the NA inhibitors during *in vivo* (experimental) virus infections. In addition, BLI can be used for screening compounds that interfere with HA-receptor binding, similarly as we demonstrated for antibodies and mucus.

Ultimately, virus particle phenotypes as determined by the different BLI assays, need to be correlated to the characteristics of virus *in vivo* infections. For instance, we need to determine the extent to which the balance between HA and NA reflects the abilities of a virus to infect a certain host species. This will enable the screening of emerging IAVs and may allow us to predict the danger that they pose to humans or other potential host species. As an intermediate step, the infection of primary liquid-to-air epithelial cells, harvested from different host species, and covered by a mucus layer may present a useful model system.

REFERENCES

1. Taubenberger JK, Kash JC. Influenza virus evolution, host adaptation, and pandemic formation. Cell host & microbe. 2010 Jun 25;7(6):440-51.
2. Palese P SM. Orthomyxoviridae: the viruses and their replication. In: Knipe DM HP, editor. Fields virology. 5th ed. Philadelphia, PA.: Lippincott Williams & Wilkins; 2007.
3. Wright PF NG, Kawaoka Y. Orthomyxoviruses. In: Knipe DM HP, editor. Fields virology. 5th ed. Philadelphia, PA.: Lippincott Williams & Wilkins; 2007. p. 1691–740.
4. Watanabe T, Watanabe S, Maher EA, Neumann G, Kawaoka Y. Pandemic potential of avian influenza A (H7N9) viruses. Trends in microbiology. 2014 Nov;22(11):623-31.
5. Barr IG. Assessing the potential pandemic risk of recent avian influenza viruses. The European respiratory journal. 2017 Mar;49(3).
6. Zhang Q, Shi J, Deng G, Guo J, Zeng X, He X, et al. H7N9 influenza viruses are transmissible in ferrets by respiratory droplet. Science. 2013 Jul 26;341(6144):410-4.
7. Russell CA, Fonville JM, Brown AE, Burke DF, Smith DL, James SL, et al. The potential for respiratory droplet-transmissible A/H5N1 influenza virus to evolve in a mammalian host. Science. 2012 Jun 22;336(6088):1541-7.
8. Doherty PC, Turner SJ, Webby RG, Thomas PG. Influenza and the challenge for immunology. Nature immunology. 2006 May;7(5):449-55.
9. Gamblin SJ, Skehel JJ. Influenza hemagglutinin and neuraminidase membrane glycoproteins. The Journal of biological chemistry. 2010 Sep 10;285(37):28403-9.
10. Chen X, Varki A. Advances in the biology and chemistry of sialic acids. ACS chemical biology. 2010 Feb 19;5(2):163-76.
11. Tiralongo J. Introduction to Sialic Acid Structure, Occurrence, Biosynthesis and Function. In: Joe Tiralongo IM-D, editor. Sialobiology: Structure, Biosynthesis and Function Sialic Acid Glycoconjugates in Health and Disease: Bentham Science Publishers; 2013. p. 76-114.
12. Wilson IA, Skehel JJ, Wiley DC. Structure of the haemagglutinin membrane glycoprotein of influenza virus at 3 A resolution. Nature. 1981 Jan 29;289(5796):366-73.
13. Shtyrya YA, Mochalova LV, Bovin NV. Influenza virus neuraminidase: structure and function. Acta naturae. 2009 Jul;1(2):26-32.
14. Varghese JN, McKimm-Breschkin JL, Caldwell JB, Kortt AA, Colman PM. The structure of the complex between influenza virus neuraminidase and sialic acid, the viral receptor. Proteins. 1992 Nov;14(3):327-32.
15. Zanin M, Baviskar P, Webster R, Webby R. The Interaction between Respiratory Pathogens and Mucus. Cell host & microbe. 2016 Feb 10;19(2):159-68.
16. Taubenberger JK, Morens DM. The pathology of influenza virus infections. Annual review of pathology. 2008;3:499-522.
17. Alberts B, Wilson JH, Hunt T. Molecular biology of the cell. 5th ed. New York: Garland Science; 2008.
18. Rubin BK. Physiology of airway mucus clearance. Respiratory care. 2002 Jul;47(7):761-8.
19. Nicod LP. Lung Defenses. In: SINGH SK, editor. Human Respiratory Viral Infections. New York; 2014.
20. Widdicombe J. Relationships among the composition of mucus, epithelial lining liquid, and adhesion of microorganisms. American journal of respiratory and critical care medicine. 1995 Jun;151(6):2088-92; discussion 92-3.
21. Schwab U, Leigh M, Ribeiro C, Yankaskas J, Burns K, Gilligan P, et al. Patterns of epithelial cell invasion by different species of the Burkholderia cepacia complex in well-differentiated human airway epithelia. Infection and immunity. 2002 Aug;70(8):4547-55.
22. Thorley AJ, Tetley TD. Pulmonary epithelium, cigarette smoke, and chronic obstructive pulmonary disease. International journal of chronic obstructive pulmonary disease. 2007;2(4):409-28.

23. Tilley AE, Walters MS, Shaykhiev R, Crystal RG. Cilia dysfunction in lung disease. Annual review of physiology. 2015;77:379-406.
24. Howard L. In: LungTrachea2a, editor. http://remfdartmouthedu/images/mammalianLungSEM/source/12html; 2004.
25. Kaliner M, Marom Z, Patow C, Shelhamer J. Human respiratory mucus. The Journal of allergy and clinical immunology. 1984 Mar;73(3):318-23.
26. Knowles MR, Boucher RC. Mucus clearance as a primary innate defense mechanism for mammalian airways. The Journal of clinical investigation. 2002 Mar;109(5):571-7.
27. Jeffery PK, Li D. Airway mucosa: secretory cells, mucus and mucin genes. The European respiratory journal : official journal of the European Society for Clinical Respiratory Physiology. 1997 Jul;10(7):1655-62.
28. Lamblin G, Roussel P. Airway mucins and their role in defence against micro-organisms. Respiratory medicine. 1993 Aug;87(6):421-6.
29. Michelle R. Dawson DG. Mucosal barriers. In: Muro S, editor. Drug Delivery Across Physiological Barriers: CRC press Taylor & Fransis Group; 2016.
30. Button B, Cai LH, Ehre C, Kesimer M, Hill DB, Sheehan JK, et al. A periciliary brush promotes the lung health by separating the mucus layer from airway epithelia. Science. 2012 Aug 24;337(6097):937-41.
31. Cohen M, Zhang XQ, Senaati HP, Chen HW, Varki NM, Schooley RT, et al. Influenza A penetrates host mucus by cleaving sialic acids with neuraminidase. Virology journal. 2013 Nov 22;10:321.
32. Yang X, Steukers L, Forier K, Xiong R, Braeckmans K, Van Reeth K, et al. A beneficiary role for neuraminidase in influenza virus penetration through the respiratory mucus. PloS one. 2014;9(10):e110026.
33. Sakai T, Nishimura SI, Naito T, Saito M. Influenza A virus hemagglutinin and neuraminidase act as novel motile machinery. Scientific reports. 2017 Mar 27;7:45043.
34. Zeng H, Goldsmith CS, Maines TR, Belser JA, Gustin KM, Pekosz A, et al. Tropism and infectivity of influenza virus, including highly pathogenic avian H5N1 virus, in ferret tracheal differentiated primary epithelial cell cultures. Journal of virology. 2013 Mar;87(5):2597-607.
35. Matrosovich MN, Matrosovich TY, Gray T, Roberts NA, Klenk HD. Human and avian influenza viruses target different cell types in cultures of human airway epithelium. Proceedings of the National Academy of Sciences of the United States of America. 2004 Mar 30;101(13):4620-4.
36. Ibricevic A, Pekosz A, Walter MJ, Newby C, Battaile JT, Brown EG, et al. Influenza virus receptor specificity and cell tropism in mouse and human airway epithelial cells. Journal of virology. 2006 Aug;80(15):7469-80.
37. Baum LG, Paulson JC. Sialyloligosaccharides of the respiratory epithelium in the selection of human influenza virus receptor specificity. Acta histochemica Supplementband. 1990;40:35-8.
38. Boulant S, Stanifer M, Lozach PY. Dynamics of virus-receptor interactions in virus binding, signaling, and endocytosis. Viruses. 2015 Jun 02;7(6):2794-815.
39. de Graaf M, Fouchier RA. Role of receptor binding specificity in influenza A virus transmission and pathogenesis. The EMBO journal. 2014 Apr 16;33(8):823-41.
40. de Vries E, de Vries RP, Wienholts MJ, Floris CE, Jacobs MS, van den Heuvel A, et al. Influenza A virus entry into cells lacking sialylated N-glycans. Proceedings of the National Academy of Sciences of the United States of America. 2012 May 8;109(19):7457-62.
41. Rust MJ, Lakadamyali M, Zhang F, Zhuang X. Assembly of endocytic machinery around individual influenza viruses during viral entry. Nature structural & molecular biology. 2004 Jun;11(6):567-73.
42. Skehel JJ, Wiley DC. Receptor binding and membrane fusion in virus entry: the influenza hemagglutinin. Annual review of biochemistry. 2000;69:531-69.

43. Matlin KS, Reggio H, Helenius A, Simons K. Infectious entry pathway of influenza virus in a canine kidney cell line. The Journal of cell biology. 1981 Dec;91(3 Pt 1):601-13.
44. Peng W, de Vries RP, Grant OC, Thompson AJ, McBride R, Tsogtbaatar B, et al. Recent H3N2 Viruses Have Evolved Specificity for Extended, Branched Human-type Receptors, Conferring Potential for Increased Avidity. Cell host & microbe. 2017 Jan 11;21(1):23-34.
45. Walther T, Karamanska R, Chan RW, Chan MC, Jia N, Air G, et al. Glycomic analysis of human respiratory tract tissues and correlation with influenza virus infection. PLoS pathogens. 2013 Mar;9(3):e1003223.
46. Badham MD, Rossman JS. Filamentous Influenza Viruses. Current clinical microbiology reports. 2016 Sep;3(3):155-61.
47. Calder LJ, Wasilewski S, Berriman JA, Rosenthal PB. Structural organization of a filamentous influenza A virus. Proceedings of the National Academy of Sciences of the United States of America. 2010 Jun 08;107(23):10685-90.
48. Wagner R, Matrosovich M, Klenk HD. Functional balance between haemagglutinin and neuraminidase in influenza virus infections. Reviews in medical virology. 2002 May-Jun;12(3):159-66.
49. Yen HL, Liang CH, Wu CY, Forrest HL, Ferguson A, Choy KT, et al. Hemagglutinin-neuraminidase balance confers respiratory-droplet transmissibility of the pandemic H1N1 influenza virus in ferrets. Proceedings of the National Academy of Sciences of the United States of America. 2011 Aug 23;108(34):14264-9.
50. Xu R, Zhu X, McBride R, Nycholat CM, Yu W, Paulson JC, et al. Functional balance of the hemagglutinin and neuraminidase activities accompanies the emergence of the 2009 H1N1 influenza pandemic. Journal of virology. 2012 Sep;86(17):9221-32.
51. Suzuki Y, Ito T, Suzuki T, Holland RE, Jr., Chambers TM, Kiso M, et al. Sialic acid species as a determinant of the host range of influenza A viruses. Journal of virology. 2000 Dec;74(24):11825-31.
52. Lin YP, Xiong X, Wharton SA, Martin SR, Coombs PJ, Vachieri SG, et al. Evolution of the receptor binding properties of the influenza A(H3N2) hemagglutinin. Proceedings of the National Academy of Sciences of the United States of America. 2012 Dec 26;109(52):21474-9.
53. Vachieri SG, Xiong X, Collins PJ, Walker PA, Martin SR, Haire LF, et al. Receptor binding by H10 influenza viruses. Nature. 2014 Jul 24;511(7510):475-7.
54. Xiong X, Coombs PJ, Martin SR, Liu J, Xiao H, McCauley JW, et al. Receptor binding by a ferret-transmissible H5 avian influenza virus. Nature. 2013 May 16;497(7449):392-6.
55. Xiong X, Martin SR, Haire LF, Wharton SA, Daniels RS, Bennett MS, et al. Receptor binding by an H7N9 influenza virus from humans. Nature. 2013 Jul 25;499(7459):496-9.
56. Weiss JN. The Hill equation revisited: uses and misuses. FASEB journal : official publication of the Federation of American Societies for Experimental Biology. 1997 Sep;11(11):835-41.
57. Tomita M, Marchesi VT. Amino-acid sequence and oligosaccharide attachment sites of human erythrocyte glycophorin. Proceedings of the National Academy of Sciences of the United States of America. 1975 Aug;72(8):2964-8.
58. Pisano A, Redmond JW, Williams KL, Gooley AA. Glycosylation sites identified by solid-phase Edman degradation: O-linked glycosylation motifs on human glycophorin A. Glycobiology. 1993 Oct;3(5):429-35.
59. North SJ, Huang HH, Sundaram S, Jang-Lee J, Etienne AT, Trollope A, et al. Glycomics profiling of Chinese hamster ovary cell glycosylation mutants reveals N-glycans of a novel size and complexity. The Journal of biological chemistry. 2010 Feb 19;285(8):5759-75.
60. Tiralongo IM-D. Sialobiology: Structure, Biosynthesis and Function Sialic Acid Glycoconjugates in Health and Disease; 2013.
61. Schrauwen EJ, Fouchier RA. Host adaptation and transmission of influenza A viruses in mammals. Emerging microbes & infections. 2014 Feb;3(2):e9.

62. Baum LG, Paulson JC. The N2 neuraminidase of human influenza virus has acquired a substrate specificity complementary to the hemagglutinin receptor specificity. Virology. 1991 Jan;180(1):10-5.
63. Mochalova L, Kurova V, Shtyrya Y, Korchagina E, Gambaryan A, Belyanchikov I, et al. Oligosaccharide specificity of influenza H1N1 virus neuraminidases. Archives of virology. 2007;152(11):2047-57.
64. Suzuki T, Horiike G, Yamazaki Y, Kawabe K, Masuda H, Miyamoto D, et al. Swine influenza virus strains recognize sialylsugar chains containing the molecular species of sialic acid predominantly present in the swine tracheal epithelium. FEBS letters. 1997 Mar 10;404(2-3):192-6.
65. Rudneva IA, Sklyanskaya EI, Barulina OS, Yamnikova SS, Kovaleva VP, Tsvetkova IV, et al. Phenotypic expression of HA-NA combinations in human-avian influenza A virus reassortants. Archives of virology. 1996;141(6):1091-9.
66. Kaverin NV, Gambaryan AS, Bovin NV, Rudneva IA, Shilov AA, Khodova OM, et al. Postreassortment changes in influenza A virus hemagglutinin restoring HA-NA functional match. Virology. 1998 May 10;244(2):315-21.
67. Gubareva LV, Robinson MJ, Bethell RC, Webster RG. Catalytic and framework mutations in the neuraminidase active site of influenza viruses that are resistant to 4-guanidino-Neu5Ac2en. Journal of virology. 1997 May;71(5):3385-90.
68. Tai CY, Escarpe PA, Sidwell RW, Williams MA, Lew W, Wu H, et al. Characterization of human influenza virus variants selected in vitro in the presence of the neuraminidase inhibitor GS 4071. Antimicrobial agents and chemotherapy. 1998 Dec;42(12):3234-41.
69. McKimm-Breschkin JL, Blick TJ, Sahasrabudhe A, Tiong T, Marshall D, Hart GJ, et al. Generation and characterization of variants of NWS/G70C influenza virus after in vitro passage in 4-amino-Neu5Ac2en and 4-guanidino-Neu5Ac2en. Antimicrobial agents and chemotherapy. 1996 Jan;40(1):40-6.
70. Bantia S, Ghate AA, Ananth SL, Babu YS, Air GM, Walsh GM. Generation and characterization of a mutant of influenza A virus selected with the neuraminidase inhibitor BCX-140. Antimicrobial agents and chemotherapy. 1998 Apr;42(4):801-7.
71. Blick TJ, Sahasrabudhe A, McDonald M, Owens IJ, Morley PJ, Fenton RJ, et al. The interaction of neuraminidase and hemagglutinin mutations in influenza virus in resistance to 4-guanidino-Neu5Ac2en. Virology. 1998 Jun 20;246(1):95-103.
72. Hughes MT, Matrosovich M, Rodgers ME, McGregor M, Kawaoka Y. Influenza A viruses lacking sialidase activity can undergo multiple cycles of replication in cell culture, eggs, or mice. Journal of virology. 2000 Jun;74(11):5206-12.
73. Benton DJ, Martin SR, Wharton SA, McCauley JW. Biophysical measurement of the balance of influenza a hemagglutinin and neuraminidase activities. The Journal of biological chemistry. 2015 Mar 6;290(10):6516-21.
74. Gulati S, Lasanajak Y, Smith DF, Cummings RD, Air GM. Glycan array analysis of influenza H1N1 binding and release. Cancer biomarkers : section A of Disease markers. 2014 Jan 01;14(1):43-53.
75. Xu R, de Vries RP, Zhu X, Nycholat CM, McBride R, Yu W, et al. Preferential recognition of avian-like receptors in human influenza A H7N9 viruses. Science. 2013 Dec 06;342(6163):1230-5.
76. Dortmans JC, Dekkers J, Wickramasinghe IN, Verheije MH, Rottier PJ, van Kuppeveld FJ, et al. Adaptation of novel H7N9 influenza A virus to human receptors. Scientific reports. 2013 Oct 28;3:3058.
77. Watanabe T, Kiso M, Fukuyama S, Nakajima N, Imai M, Yamada S, et al. Characterization of H7N9 influenza A viruses isolated from humans. Nature. 2013 Sep 26;501(7468):551-5.

78. de Vries RP, de Vries E, Moore KS, Rigter A, Rottier PJ, de Haan CA. Only two residues are responsible for the dramatic difference in receptor binding between swine and new pandemic H1 hemagglutinin. The Journal of biological chemistry. 2011 Feb 18;286(7):5868-75.
79. Childs RA, Palma AS, Wharton S, Matrosovich T, Liu Y, Chai W, et al. Receptor-binding specificity of pandemic influenza A (H1N1) 2009 virus determined by carbohydrate microarray. Nature biotechnology. 2009 Sep;27(9):797-9.
80. Glaser L, Stevens J, Zamarin D, Wilson IA, Garcia-Sastre A, Tumpey TM, et al. A single amino acid substitution in 1918 influenza virus hemagglutinin changes receptor binding specificity. Journal of virology. 2005 Sep;79(17):11533-6.
81. Tumpey TM, Maines TR, Van Hoeven N, Glaser L, Solorzano A, Pappas C, et al. A two-amino acid change in the hemagglutinin of the 1918 influenza virus abolishes transmission. Science. 2007 Feb 02;315(5812):655-9.
82. Stevens J, Blixt O, Glaser L, Taubenberger JK, Palese P, Paulson JC, et al. Glycan microarray analysis of the hemagglutinins from modern and pandemic influenza viruses reveals different receptor specificities. Journal of molecular biology. 2006 Feb 3;355(5):1143-55.
83. Stevens J, Blixt O, Tumpey TM, Taubenberger JK, Paulson JC, Wilson IA. Structure and receptor specificity of the hemagglutinin from an H5N1 influenza virus. Science. 2006 Apr 21;312(5772):404-10.
84. Rejmanek D, Hosseini PR, Mazet JA, Daszak P, Goldstein T. Evolutionary Dynamics and Global Diversity of Influenza A Virus. Journal of virology. 2015 Nov;89(21):10993-1001.
85. Chen R, Holmes EC. Avian influenza virus exhibits rapid evolutionary dynamics. Molecular biology and evolution. 2006 Dec;23(12):2336-41.
86. Smith DJ, Lapedes AS, de Jong JC, Bestebroer TM, Rimmelzwaan GF, Osterhaus AD, et al. Mapping the antigenic and genetic evolution of influenza virus. Science. 2004 Jul 16;305(5682):371-6.
87. Koel BF, Burke DF, Bestebroer TM, van der Vliet S, Zondag GC, Vervaet G, et al. Substitutions near the receptor binding site determine major antigenic change during influenza virus evolution. Science. 2013 Nov 22;342(6161):976-9.
88. Hensley SE, Das SR, Bailey AL, Schmidt LM, Hickman HD, Jayaraman A, et al. Hemagglutinin receptor binding avidity drives influenza A virus antigenic drift. Science. 2009 Oct 30;326(5953):734-6.
89. World Health Organization/World Organisation for Animal HF, Agriculture Organization HNEWG. Revised and updated nomenclature for highly pathogenic avian influenza A (H5N1) viruses. Influenza and other respiratory viruses. 2014 May;8(3):384-8.
90. Saito T, Tanikawa T, Uchida Y, Takemae N, Kanehira K, Tsunekuni R. Intracontinental and intercontinental dissemination of Asian H5 highly pathogenic avian influenza virus (clade 2.3.4.4) in the winter of 2014-2015. Reviews in medical virology. 2015 Nov;25(6):388-405.
91. Ip HS, Torchetti MK, Crespo R, Kohrs P, DeBruyn P, Mansfield KG, et al. Novel Eurasian highly pathogenic avian influenza A H5 viruses in wild birds, Washington, USA, 2014. Emerging infectious diseases. 2015 May;21(5):886-90.
92. Wu H, Peng X, Xu L, Jin C, Cheng L, Lu X, et al. Novel reassortant influenza A(H5N8) viruses in domestic ducks, eastern China. Emerging infectious diseases. 2014 Aug;20(8):1315-8.
93. Kang HM, Lee EK, Song BM, Jeong J, Choi JG, Moon OK, et al. Novel reassortant influenza A(H5N8) viruses among inoculated domestic and wild ducks, South Korea, 2014. Emerging infectious diseases. 2015 Feb;21(2):298-304.
94. Lee YJ, Kang HM, Lee EK, Song BM, Jeong J, Kwon YK, et al. Novel reassortant influenza A(H5N8) viruses, South Korea, 2014. Emerging infectious diseases. 2014 Jun;20(6):1087-9.
95. Song Y, Cui J, Song H, Ye J, Zhao Z, Wu S, et al. New reassortant H5N8 highly pathogenic avian influenza virus from waterfowl in Southern China. Frontiers in microbiology. 2015;6:1170.
96. Ku KB, Park EH, Yum J, Kim JA, Oh SK, Seo SH. Highly pathogenic avian influenza A(H5N8) virus from waterfowl, South Korea, 2014. Emerging infectious diseases. 2014 Sep;20(9):1587-8.

97. Liu CG, Liu M, Liu F, Lv R, Liu DF, Qu LD, et al. Emerging multiple reassortant H5N5 avian influenza viruses in ducks, China, 2008. Veterinary microbiology. 2013 Dec 27;167(3-4):296-306.
98. Qi X, Cui L, Yu H, Ge Y, Tang F. Whole-Genome Sequence of a Reassortant H5N6 Avian Influenza Virus Isolated from a Live Poultry Market in China, 2013. Genome announcements. 2014 Sep 11;2(5).
99. Zhao K, Gu M, Zhong L, Duan Z, Zhang Y, Zhu Y, et al. Characterization of three H5N5 and one H5N8 highly pathogenic avian influenza viruses in China. Veterinary microbiology. 2013 May 3;163(3-4):351-7.
100. Role for migratory wild birds in the global spread of avian influenza H5N8. Science. 2016 Oct 14;354(6309):213-7.
101. Wong FY, Phommachanh P, Kalpravidh W, Chanthavisouk C, Gilbert J, Bingham J, et al. Reassortant highly pathogenic influenza A(H5N6) virus in Laos. Emerging infectious diseases. 2015 Mar;21(3):511-6.
102. Wu H, Lu R, Peng X, Xu L, Cheng L, Lu X, et al. Novel reassortant highly pathogenic H5N6 avian influenza viruses in poultry in China. Infection, genetics and evolution : journal of molecular epidemiology and evolutionary genetics in infectious diseases. 2015 Apr;31:64-7.
103. WHO. Human infection with avian influenza A(H5N6) virus – China. 2016 [cited; Available from: http://www.who.int/csr/don/4-january-2016-avian-influenza-china/en/
104. Wickramasinghe IN, de Vries RP, Eggert AM, Wandee N, de Haan CA, Grone A, et al. Host tissue and glycan binding specificities of avian viral attachment proteins using novel avian tissue microarrays. PloS one. 2015;10(6):e0128893.
105. Gambaryan A, Tuzikov A, Pazynina G, Bovin N, Balish A, Klimov A. Evolution of the receptor binding phenotype of influenza A (H5) viruses. Virology. 2006 Jan 20;344(2):432-8.
106. Gambaryan A, Yamnikova S, Lvov D, Tuzikov A, Chinarev A, Pazynina G, et al. Receptor specificity of influenza viruses from birds and mammals: new data on involvement of the inner fragments of the carbohydrate chain. Virology. 2005 Apr 10;334(2):276-83.
107. Hiono T, Okamatsu M, Nishihara S, Takase-Yoden S, Sakoda Y, Kida H. A chicken influenza virus recognizes fucosylated alpha2,3 sialoglycan receptors on the epithelial cells lining upper respiratory tracts of chickens. Virology. 2014 May;456-457:131-8.
108. Hiono T, Okamatsu M, Igarashi M, McBride R, de Vries RP, Peng W, et al. Amino acid residues at positions 222 and 227 of the hemagglutinin together with the neuraminidase determine binding of H5 avian influenza viruses to sialyl Lewis X. Archives of virology. 2016 Feb;161(2):307-16.
109. Heider A, Mochalova L, Harder T, Tuzikov A, Bovin N, Wolff T, et al. Alterations in hemagglutinin receptor-binding specificity accompany the emergence of highly pathogenic avian influenza viruses. Journal of virology. 2015 May;89(10):5395-405.
110. Ewers H, Smith AE, Sbalzarini IF, Lilie H, Koumoutsakos P, Helenius A. Single-particle tracking of murine polyoma virus-like particles on live cells and artificial membranes. Proceedings of the National Academy of Sciences of the United States of America. 2005 Oct 18;102(42):15110-5.
111. Grove J, Marsh M. The cell biology of receptor-mediated virus entry. The Journal of cell biology. 2011 Dec 26;195(7):1071-82.
112. Ehrlich M, Boll W, Van Oijen A, Hariharan R, Chandran K, Nibert ML, et al. Endocytosis by random initiation and stabilization of clathrin-coated pits. Cell. 2004 Sep 03;118(5):591-605.
113. Verzijl D, Riedl T, Parren P, Gerritsen AF. A novel label-free cell-based assay technology using biolayer interferometry. Biosensors & bioelectronics. 2017 Jan 15;87:388-95.
114. Taylor MP, Koyuncu OO, Enquist LW. Subversion of the actin cytoskeleton during viral infection. Nature reviews Microbiology. 2011 Jun;9(6):427-39.
115. Summary analysis of 2010 survey of National Influenza Centres in the WHO Global Influenza Surveillance Network. Releve epidemiologique hebdomadaire. 2011 Apr 22;86(17):166-9.

116. Garten RJ, Davis CT, Russell CA, Shu B, Lindstrom S, Balish A, et al. Antigenic and genetic characteristics of swine-origin 2009 A(H1N1) influenza viruses circulating in humans. Science. 2009 Jul 10;325(5937):197-201.
117. Both GW, Sleigh MJ, Cox NJ, Kendal AP. Antigenic drift in influenza virus H3 hemagglutinin from 1968 to 1980: multiple evolutionary pathways and sequential amino acid changes at key antigenic sites. Journal of virology. 1983 Oct;48(1):52-60.
118. Koel BF, Mogling R, Chutinimitkul S, Fraaij PL, Burke DF, van der Vliet S, et al. Identification of amino acid substitutions supporting antigenic change of influenza A(H1N1)pdm09 viruses. Journal of virology. 2015 Apr;89(7):3763-75.
119. Aich U, Beckley N, Shriver Z, Raman R, Viswanathan K, Hobbie S, et al. Glycomics-based analysis of chicken red blood cells provides insight into the selectivity of the viral agglutination assay. The FEBS journal. 2011 May;278(10):1699-712.
120. Cohen M, Hurtado-Ziola N, Varki A. ABO blood group glycans modulate sialic acid recognition on erythrocytes. Blood. 2009 Oct 22;114(17):3668-76.
121. Ovsyannikova IG, White SJ, Albrecht RA, Garcia-Sastre A, Poland GA. Turkey versus guinea pig red blood cells: hemagglutination differences alter hemagglutination inhibition responses against influenza A/H1N1. Viral immunology. 2014 May;27(4):174-8.
122. Zalewska A, Zwierz K, Zolkowski K, Gindzienski A. Structure and biosynthesis of human salivary mucins. Acta biochimica Polonica. 2000;47(4):1067-79.
123. Klein A, Carnoy C, Wieruszeski JM, Strecker G, Strang AM, van Halbeek H, et al. The broad diversity of neutral and sialylated oligosaccharides derived from human salivary mucins. Biochemistry. 1992 Jul 07;31(26):6152-65.
124. Gerken TA, Jentoft N. Structure and dynamics of porcine submaxillary mucin as determined by natural abundance carbon-13 NMR spectroscopy. Biochemistry. 1987 Jul 28;26(15):4689-99.
125. Yeganeh B, Rezaei Moghadam A, Tran AT, Rahim MN, Ande SR, Hashemi M, et al. Asthma and influenza virus infection:focusing on cell death and stress pathways in influenza virus replication. Iranian journal of allergy, asthma, and immunology. 2013 Mar;12(1):1-17.
126. Davril M, Degroote S, Humbert P, Galabert C, Dumur V, Lafitte JJ, et al. The sialylation of bronchial mucins secreted by patients suffering from cystic fibrosis or from chronic bronchitis is related to the severity of airway infection. Glycobiology. 1999 Mar;9(3):311-21.
127. Cheng PW, Boat TF, Cranfill K, Yankaskas JR, Boucher RC. Increased sulfation of glycoconjugates by cultured nasal epithelial cells from patients with cystic fibrosis. The Journal of clinical investigation. 1989 Jul;84(1):68-72.
128. Laver WG, Colman PM, Webster RG, Hinshaw VS, Air GM. Influenza virus neuraminidase with hemagglutinin activity. Virology. 1984 Sep;137(2):314-23.
129. Lin YP, Gregory V, Collins P, Kloess J, Wharton S, Cattle N, et al. Neuraminidase receptor binding variants of human influenza A(H3N2) viruses resulting from substitution of aspartic acid 151 in the catalytic site: a role in virus attachment? Journal of virology. 2010 Jul;84(13):6769-81.
130. Dai M, McBride R, Dortmans JC, Peng W, Bakkers MJ, de Groot RJ, et al. Mutation of the Second Sialic Acid-Binding Site, Resulting in Reduced Neuraminidase Activity, Preceded the Emergence of H7N9 Influenza A Virus. Journal of virology. 2017 May 1;91(9).
131. Uhlendorff J, Matrosovich T, Klenk HD, Matrosovich M. Functional significance of the hemadsorption activity of influenza virus neuraminidase and its alteration in pandemic viruses. Archives of virology. 2009;154(6):945-57.
132. Webster RG, Air GM, Metzger DW, Colman PM, Varghese JN, Baker AT, et al. Antigenic structure and variation in an influenza virus N9 neuraminidase. Journal of virology. 1987 Sep;61(9):2910-6.

133. Varghese JN, Colman PM, van Donkelaar A, Blick TJ, Sahasrabudhe A, McKimm-Breschkin JL. Structural evidence for a second sialic acid binding site in avian influenza virus neuraminidases. Proceedings of the National Academy of Sciences of the United States of America. 1997 Oct 28;94(22):11808-12.
134. Zhu X, McBride R, Nycholat CM, Yu W, Paulson JC, Wilson IA. Influenza virus neuraminidases with reduced enzymatic activity that avidly bind sialic Acid receptors. Journal of virology. 2012 Dec;86(24):13371-83.
135. Gambaryan AS, Matrosovich MN. What adaptive changes in hemagglutinin and neuraminidase are necessary for emergence of pandemic influenza virus from its avian precursor? Biochemistry Biokhimiia. 2015 Jul;80(7):872-80.
136. Fiore AE, Fry A, Shay D, Gubareva L, Bresee JS, Uyeki TM. Antiviral agents for the treatment and chemoprophylaxis of influenza --- recommendations of the Advisory Committee on Immunization Practices (ACIP). MMWR Recommendations and reports : Morbidity and mortality weekly report Recommendations and reports. 2011 Jan 21;60(1):1-24.
137. Kinchington D, Schinazi, Raymond F. Antiviral Methods and Protocols. 2000.
138. Su CY, Wang SY, Shie JJ, Jeng KS, Temperton NJ, Fang JM, et al. In vitro evaluation of neuraminidase inhibitors using the neuraminidase-dependent release assay of hemagglutinin-pseudotyped viruses. Antiviral research. 2008 Sep;79(3):199-205.
139. Charyasriwong S, Watanabe K, Rahmasari R, Matsunaga A, Haruyama T, Kobayashi N. In vitro evaluation of synergistic inhibitory effects of neuraminidase inhibitors and methylglyoxal against influenza virus infection. Archives of medical research. 2015 Jan;46(1):8-16.

Summary in English

Influenza A viruses (IAVs) are pathogens of birds and mammals, including humans. They cause a huge economic burden and major public health problems. IAV belongs to the *Orthomyxoviridae* family. They are enveloped viruses containing negative-sense, segmented RNA genomes. IAVs are classified further into different subtypes according to the particular combination of hemagglutinin (HA) and neuraminidase (NA) surface glycoproteins that they contain. Sixteen HA (H1-16) and nine NA (N1-9) subtypes have been identified, all of which are found in viruses from aquatic birds. IAVs from aquatic birds may adapt to other host species, including domestic poultry and different mammals.

All IAVs recognize terminal sialic acids (SIAs) as receptor. HA is responsible for binding to SIA receptors, whereas NA cleaves SIA receptors. The linkage type of SIA to the penultimate residue is an important determinant of host specificity. Avian viruses prefer to bind α2,3-linked SIA, whereas human viruses preferentially bind to α2,6-linked SIA. Similarly, the NA specificity for α2,3 and α2,6-linked SIAs depends on IAV target hosts, even though most NAs retained activity against α2,3-linked SIAs. In addition, the type and number of internal monosaccharides and their linkages are important for HA and NA receptor fine specificity.

HA binding, NA cleavage and the HA/NA balance are of great importance in IAV entry, replication, release and transmission. In this thesis we aimed to develop real-time binding analysis methodology for studying the dynamics of IAV-receptor interactions. The method enabled us to study HA and NA activity independently as well as the balance between the two and was applied to investigate the interactions between IAV and both functional and decoy receptors. Furthermore, we aimed to analyze the correlation between antigenic drift and virus-receptor binding and the extent to which the emergence of novel highly pathogenic (HP) H5Nx viruses was accompanied with changes in virus receptor binding properties.

In **Chapter 2**, we established kinetic and label-free methodology to study virus-receptor interactions based on biolayer (BLI). To this end, BLI biosensors coated with synthetic sialylated glycans or specifically engineered glycoproteins were used for studying binding and release of a set of model IAVs. Viruses differing in their HA or NA were used to systematically address the effect of changes in HA or NA activity and specificity on binding and release kinetics. We propose that the observed initial binding rate (v^{obs}) is the most relevant virus binding parameter. In addition, we identified a contribution of NA to the initial binding rate and showed that NA activity is dramatically dependent on substrate binding by HA. In the absence of NA activity, viruses were dynamically, but irreversibly attached to the receptor-coated sensors. Virus particles were rolling over the receptor-coated surface and appeared to undergo morphological changes driven by NA activity. Based on these observations, we propose that the HA/NA balance is a crucial determinant of viral fitness by enabling migration through mucus layers and over cell surfaces.

In **Chapter 3**, we further studied how viruses interact with functional and decoy receptors using BLI. To this end, we not only used synthetic glycans, but also developed a set of biotinylated glycoprotein receptors differing in the number and type of their glycan side chains. In addition, we analyzed the effects of mucus samples or antibodies on virus-receptor dynamics. Based on our results, we conclude that v^{obs} depends on receptor density on the biosensor and on glycoproteins. Self-elution of virus particles was shown to depend on the number of virus particles attached to the sensor and on the receptor density. Both antibodies and mucus decoy receptors were shown to interfere with the virus-receptor interactions. Strikingly, virus self-elution and elution driven by mucus or antibodies decreased upon increased virus-receptor binding times indicating virus binding to become much tighter with time. We refer to this process as maturation of virus binding. Maturation of virus binding is proposed to result from multiple HA protomers in the HA trimer interacting with sialisodes, thereby reducing access of neuraminidase and competitors to receptors and HA proteins.

Antigenic cluster transitions during H3N2 evolution are caused by mutations at only seven positions adjacent to the HA receptor binding site (referred to as antigenic cluster transition mutations). Other, accessory, mutations may compensate for potential negative effects of cluster transition mutations on virus binding. In **Chapter 4**, we used BLI to show that three cluster transitions resulted in only very limited changes in receptor binding. In contrast, individual antigenic cluster transition mutations increased or decreased binding. Potential compensatory effects on receptor binding were observed for some of the accessory mutations, suggesting that accessory mutations may function in limiting the changes in receptor binding properties during antigenic cluster transitions. The effects of forward mutations, introduced in the old antigenic cluster, were not always opposite to the effects of the corresponding backward mutations the new cluster. Thus, the effect of a specific mutation is affected by the background in which it was made. Identification of the order in which the mutations occurred by phylogenetic analysis revealed that some accessory mutations that affected receptor binding preceded the cluster transition mutation, suggesting that they may have driven or permitted the cluster transition.

In 2014 novel HP H5 viruses, containing different NA subtypes (referred to as H5Nx viruses), emerged and displayed unprecedented intercontinental spread. In **Chapter 5**, we determined the evolutionary history of the HA proteins of these novel HP subtypes and showed that these H5 genes form a monophyletic group that evolved from a clade 2.3.4 H5N1 variant. In **Chapter 6**, we studied the extent to which unique substitutions observed in these H5 proteins (designated clade 2.3.4.4 H5 proteins) affected receptor binding. The novel viruses displayed altered binding characteristics in being able to bind fucosylated receptors resulting from -for HP H5 unique- substitutions at positions 222 and 227 in the RBS. We hypothesize that the altered receptor-binding specificity of clade 2.3.4.4 H5

proteins has contributed to their ability to team up with different NA subtypes and their unprecedented emergence and spread.

Finally, in **Chapter 7**, the main findings described in this thesis are discussed and placed in a broader perspective.

Samenvatting-Nederlands

Influenza A virussen (IAV) zijn pathogenen voor vogels en zoogdieren, waaronder mensen. Ze veroorzaken grote economische- en gezondheidsschade. IAV horen tot de familie *Orthomyxoviridae*. Deze virussen bevatten een enveloppe en een gesegmenteerd RNA genoom van negatieve polariteit. IAV worden onderverdeeld in verschillende subtypes aan de hand van de specifieke combinatie van de hemagglutinine (HA) en neuraminidase (NA) oppervlakte-eiwitten die ze bevatten. Er zijn zestien HA (H1-16) en negen NA (N1-9) subtypes geïdentificeerd, die allemaal gevonden worden in virussen voorkomend in wilde watervogels. IAV van watervogels kunnen zich aanpassen aan andere gastheerspecies, waaronder pluimvee en verschillende zoogdieren.

Alle IAV herkennen terminale siaalzuursuikers (SIA) als receptor. HA zorgt voor de binding aan SIA-receptoren, terwijl NA deze receptoren klieft. Het type binding van SIA aan het op een na laatste suikerresidu bepaalt in hoge mate de gastheerspecificiteit van IAV. Vogelvirussen prefereren binding aan α2,3-gekoppelde SIA, terwijl humane virussen bij voorkeur binden aan α2,6-gekoppelde SIA. Ook de voorkeur van NA voor α2,3- en α2,6-gekoppelde SIA hangt af van de gastheerspecificiteit van IAV, hoewel de meeste NA eiwitten het vermogen om α2,3-gekoppelde SIA te klieven behouden hebben. Daarnaast zijn ook het type en aantal van de interne suikers en hun koppelingen van belang voor de exacte receptorspecificiteit van HA en NA.

Binding door HA, klieving door NA en de balans tussen HA en NA zijn belangrijk voor het binnendringen van IAV in cellen, replicatie, vrijkomen van virusdeeltjes en transmissie. In dit proefschrift hadden we tot doel om een bindingsmethode te ontwikkelen waarmee we de dynamica van IAV-receptor interacties in real-time kunnen meten. Deze methode gaf ons de mogelijkheid om de activiteit van HA en NA onafhankelijk van elkaar, alsmede de balans tussen de twee, te onderzoeken. We hebben de methode gebruikt om zowel de interacties van IAV met functionele als niet-functionele receptoren te onderzoeken. Bovendien hadden we tot doel om de correlatie tussen antigene veranderingen in HA en receptor binding te onderzoeken. Daarnaast hebben we onderzocht in hoeverre het ontstaan van nieuwe hoog pathogene (HP) H5Nx virussen gepaard ging met veranderingen in de receptor-bindende eigenschappen van het virus.

In **Hoofdstuk 2** hebben we een kinetische, labelings-vrije, methode ontwikkeld om interacties tussen virussen en receptoren te kunnen meten gebaseerd op “biolayer interferometry” (BLI). Hiertoe werden BLI biosensoren gecoat met synthetische gesialyleerde glycanen of met specifiek-gemanipuleerde glycoproteïnen en gebruikt om binding aan, en vrijkomen van, een set modelvirussen te onderzoeken. Virussen die verschillen in hun HA of NA werden gebruikt om systematisch te onderzoeken hoe veranderingen in de specificiteit van HA of NA de kinetiek van binding en vrijkomen beïnvloeden. We stellen voor dat de gemeten initiële bindingssnelheid (v^{obs}) de meest relevante parameter is voor virusbinding. Daarnaast vonden we een bijdrage van NA aan

de initiële bindingssnelheid en lieten we zien dat klieving door NA in hoge mate afhankelijk is van binding door HA aan de receptoren. In de afwezigheid van NA activiteit waren virussen dynamisch, maar irreversibel, gebonden aan de receptor-bevattende sensoren. De virusdeeltjes rolden over het receptor-bevattende oppervlak en leken een morfologische verandering te ondergaan die gedreven werd door NA activiteit. Gebaseerd op deze observaties, stellen we voor dat de balans tussen HA en NA van cruciaal belang is voor de virale "fitness" door migratie door de mucus en over het celoppervlak mogelijk te maken.

In **Hoofdstuk 3** hebben we vervolgens bestudeerd hoe virussen interacteren met functionele en niet-functionele receptoren door middel van BLI. Daartoe hebben we niet alleen gebruik gemaakt van synthetische glycanen, maar hebben we ook een set gebiotinyleerde glycoproteïnen gemaakt, die verschillen in het aantal en type van hun suikerzijketens. Bovendien hebben we bestudeerd hoe mucus preparaten en antilichamen de dynamica van virus-receptor interacties beïnvloeden. Gebaseerd op onze resultaten, concluderen we dat de v^{obs} afhangt van de receptordichtheid op de biosensor en op de glycoproteïnen. Zelf-elutie van viruspartikels was afhankelijk van het aantal virusdeeltjes gebonden aan de sensor en van de receptordichtheid. Zowel antilichamen als niet-functionele receptor bevattend mucus konden interfereren met de virus-receptor binding. Opvallend genoeg, nam zowel de zelf-elutie als de elutie gedreven door mucus of antilichamen af met toenemende virus-receptor bindingstijden, wat aangeeft dat de bindingsterkte van het virus toeneemt in de tijd. We noemen dit proces rijping van virusbinding. We stellen voor dat rijping van virusbinding ontstaat doordat meerdere HA protomeren in de HA trimeer binden aan de SIA-bevattende receptoren, waardoor de toegang van neuraminidase en moleculen die competeren met de binding van HA aan receptoren ernstig gereduceerd wordt.

Overgang van H3N2 virus van het ene naar het andere antigeen cluster wordt veroorzaakt door mutaties op slechts zeven posities dicht bij de receptorbindingsplaats (antigene cluster overgangsmutaties genaamd). Andere accessoire mutaties kunnen mogelijk compenseren voor de potentiele negatieve effecten van antigene cluster overgangsmutaties op virus binding. In **Hoofdstuk 4** hebben we BLI gebruikt om te laten zien dat drie antigene cluster overgangen slechts een beperkt effect hadden op receptorbinding. In tegenstelling hiermee, hadden de individuele cluster overgangsmutaties een positief of negatief effect op binding. Sommige van de bijbehorende accessoire mutaties hadden een compenserend effect op de receptorbinding, wat mogelijk aangeeft dat deze mutaties de veranderingen in receptorbinding tijdens antigene cluster overgangen kunnen beperken. Het effect van voorwaartse mutaties in een "oud" antigeen cluster was niet altijd tegenovergesteld van het effect van de tegenovergestelde mutaties in het nieuwe antigene cluster. Het effect van een specifieke mutatie hangt dus af van de achtergrond waarin deze is gemaakt.

Opheldering van de volgorde waarin de mutaties plaatsvonden door fylogenetische analyse liet zien dat sommige accessoire mutaties, die receptorbinding beïnvloeden, voorafgingen aan de cluster overgangsmutatie, wat suggereert dat deze mutaties de cluster overgangen mogelijk maakten of deze zelfs induceerden.

In 2014 doken nieuwe HP H5 virussen op, die verschillende NA subtypes bevatten (H5Nx virussen genaamd) en die een ongekende intercontinentale verspreiding vertoonden. In **Hoofdstuk 5** hebben we de evolutionaire geschiedenis van de HA eiwitten van deze nieuwe HP subtypes bepaald en laten we zien dat de H5 genen afstammen van een monofylogenetische groep die evolueerde uit H5N1 groep 2.3.4. In **Hoofdstuk 6** hebben we onderzocht in hoeverre unieke veranderingen in deze H5 eiwitten (behorend tot H5 groep 2.3.4.4) van invloed waren op receptorbinding. De nieuwe virussen vertoonden veranderde bindingseigenschappen doordat ze in staat waren om gefucosyleerde receptoren te binden door -voor HP H5 unieke- mutaties op positie 222 en 227 in de receptorbindingsplaats. We hypothetiseren dat de veranderde bindingspecificiteit van de groep 2.3.4.4 H5 eiwitten heeft bijgedragen aan het vermogen van deze virussen om samen te gaan met verschillende NA subtypes en aan hun ongekende opkomst en verspreiding.

Uiteindelijk hebben we de belangrijkste bevindingen beschreven in dit proefschrift bediscussieerd en in een breder perspectief geplaatst in **Hoofdstuk 7**.

中文概述

A 型流感病毒（Influenza A virus，IAV）是能感染鸟类和哺乳动物（包括人类）的病原微生物。流感的流行会造成巨大的经济负担和严重的公共卫生问题。IAV 属于正黏病毒科，包含着分节段的 RNA 基因组。病毒表面有血凝素（hemaggltuinin，HA）和神经氨酸酶（neuraminidase，NA）根据这两种糖蛋白的不同亚型，可将 IAV 分为不同类型。其中，在流感的天然宿主水生鸟类中分离鉴定出 16 种 HA（H1-16）和 9 种 NA（N1-9）。这些来自于水生鸟类的流感病毒可以适应新的宿主，如家禽和哺乳动物等。

所有的流感病毒都识别唾液酸（sialic acids，SIAs）为受体。HA 主要负责与唾液酸受体进行结合，而 NA 负责切割唾液酸受体。SIAs 唾液酸作为最末端的糖基，可与次末端的糖基以不同形式的构象进行连接，从而决定病毒的宿主特异性。禽流感病毒倾向于与 α2,3 构象的唾液酸结合，而人流感病毒倾向于 α2,6 构象的唾液酸结合。虽然 NA 保留了其切割 α2,3 唾液酸的特性，但也有针对 α2,3/α2,6 构象唾液酸的宿主特异性差异。另外，糖链中内部的寡糖结构和数量以及构象也对 HA 和 NA 与受体的特异性结合产生影响。

HA 与受体的结合，NA 对受体的切割，以及 HA 与 NA 之间的平衡关系对 IAV 的入侵、复制、释放和传播都有重要作用。在本论文中，我们建立了一种新型动力学的实时监测方法来研究 HA 和 NA 独立的活性和两者间的平衡关系，并应用此方法进一步对 IAV 与功能和非功能受体之间的动态相互作用进行分析。我们还深入分析阐释了抗原漂移与病毒受体之间的关系，研究了新发的高致病性禽流感的受体结合改变。

在**第二章**中，我们阐述了用新型动力学方法研究病毒受体的结合。该方法基于生物膜干扰技术（biolayer interferometry，BLI），无需对分子或者病毒进行标记。为了实现这一目标，我们将含有 SIAs 唾液酸的合成糖或者特异性修饰了的糖蛋白附着在生物感应器上，以此建立一系列的流感病毒结合与释放的模型。将具有不同 HA 和 NA 的流感病毒进行系统化的研究，从而分析 HA 或者 NA 的活性和特异性影响病毒受体结合和释放的动态过程。我们设定病毒受体的初始结合律（v^{obs}）作为最具参考价值的研究参数。这个技术也可以用来阐述 NA 对病毒与受体结合的影响，展示病毒中 NA 的切割活性依赖于 HA 与受体的结合。当 NA 的活性被抑制的时候，病毒与受体的结合为不可逆的反应。病毒可以在受体表面进行滚动，也可以发生形态变化，

这种变化是通过 NA 的切割活性实现的。基于以上结果，我们认为：病毒穿过细胞表面的黏液层从而到达细胞表面这一过程中，HA 和 NA 的平衡是重要决定因素。

在**第三章**中，我们进一步通过 BLI 技术研究了病毒与功能性和非功能性受体之间的相互作用。我们不仅利用合成糖作为受体，而且还研制了一系列新型的生物素化的糖蛋白作为受体。这些糖蛋白具有不同数量和类型的糖基侧链。我们分析了粘液样品以及抗体对病毒受体之间动态相互作用的影响。基于已获得的结果，我们认为 v^{obs} 依赖于受体的类型，以及在生物探针表面的密度。具体地说，病毒从受体表面的解离通过 NA 进行，这一过程依赖于病毒颗粒在受体表面的数量以及受体在生物探针的密度。抗体和粘液非功能性受体都能干扰病毒和受体相互作用。当病毒与受体的结合时间增长，病毒 NA 介导的自我解离和粘液/抗体介导的解离作用会降低。这一现象说明当结合时间增长之后，病毒与受体的结合会更加紧密。我们将这一现象定义为病毒与受体结合成熟。病毒结合的成熟是由于多个 HA 的原聚体与含有唾液酸的糖进行结合，从而限制了 NA 与受体的集合，也限制了结合抑制物对 HA 与受体的结合。

在 H3N2 流感病毒的进化过程中，抗原群体簇的改变是由靠近 HA 受体结合位点的 7 个氨基酸的突变引起的。其他突变可能补充辅助这 7 个氨基酸突变引起的对病毒结合的负面影响。在**第四章**中，我们应用 BLI 来研究三个抗原簇突变对病毒结合的影响。这些潜在的、在受体结合方面的影响也在非抗原簇突变中发现。这一结果说明非抗原簇的决定性突变可能对受体结合特性的改变有限制作用。这些进化方向一致的突变并不总能具有相应反向突变的负面作用。因此，一个特定突变的作用是受到背景基因组影响的。根据系统进化的影响，我们排列出突变出现的顺序，并根据这些突变的顺序进行研究。研究发现有一例非簇转化突变出现在簇转化突变之前，这说明这个突变能够引发或者允许抗原簇改变。

2014 年，新型的高致病性 H5 禽流感病毒出现，并展示出了空前的跨洲际传播的特性。这类病毒具有不同的 NA 亚型，可以叫做 H5Nx 病毒。在**第五章**中，我们研究了这类 H5 病毒 HA 蛋白的进化历史，结果显示这类病毒是从分支 2.3.4 H5 的病毒变异株进化来的。在**第六章**中，我们研究了特异性的氨基酸突变多大程度上可以影响 H5 蛋白的受体结合活性。这些新发病毒确实显现出已改变的病毒结合特性，它们可以结合岩藻糖化的糖受体。这一改变是由 HA 蛋白上 222 和 227 位点的改变导致

的。我们推断这种分支 2.3.4.4 的 H5 病毒改变了的受体结合特异性有助于该病毒与其他不同 NA 亚型进行结合，这是引起史无前例的跨洲际出现和传播的原因。

在**第七章**中，我们从更广泛的视角对主要研究方向进行了讨论。

Acknowledgements

I am taking this great opportunity to express my gratitude to everyone who supported me throughout my PhD period.

My deep gratitude goes first to my promoter, **Frank van Kuppeveld**, who gave me the opportunity to pursue my PhD in the Netherlands. I am very grateful for your aspiring guidance. I have benefited a lot from our monthly work meetings. You have taught me how to do the research, how to present my data, how to do the scientific writing and so on. Thanks a lot for all your supervision and support!

My sincere appreciation extends to my co-promotors, **Xander de Haan** and **Erik de Vries**. As my daily supervisors, you taught me by action how to do the scientific research, from setting up an experiment with proper controls, to designing and performing complicated and sophisticated experiments, to collecting and analyzing experimental data, and to presenting the data and writing the scientific articles with logic and precision. This PhD thesis would have never been possible without all of your input and effort. **Xander**, your dedication to the research and your enthusiastic about the research inspire me. I appreciate your supervision and all the effort you have made to support and help me. I have benefited a lot from having a supportive co-promotor like you. Thank you very much and all my best wishes for your career and families. **Erik**, your words have magic. Your way of describing virus-receptor interaction always help me create a vivid and interesting imagination in my mind. You taught me the practical skills in the lab, trained me in troubleshooting and scientific thinking, and helped me to give presentation and write papers step by step. I have learned lots of things from you, not only in science field but also about Dutch culture, history and geography. Thank you very much for your supervision and encouragement. I hope you will have complete recovery soon.

I would like to thank **Rauol**, who gave me invaluably constructive suggestions in my research. Also, you showed me the Dutch culture and taught me how to go ice-skating. **Peter, Herman,** and **Berend Jan,** thank you so much for your help and great advices.

During my PhD study, I received enormous supports from my friends and colleagues in the lab. **Meiling,** thank you very much for your companion. We spent plenty of time together during these four years. I will never forget your infectious laugh and your positive attitude. I wish you have a very happy life and bright future. **Wenjuan**, you are a very optimistic and hard-working person. Thank you very much for your help and support. I enjoy talking to you and sharing opinions with you. I wish you can successfully get your PhD with a big success and have many publications. **Floor van der Vegt**, it has been joyful time working with you. You are very funny and made tons of hilarious jokes. You are highly motivated for your work. Thanks a lot for your companion and the fun you brought to me. I really appreciate your help for the experiments.

Many thanks for the master students, **Anne**, **Adinda**, **Tim** and **Keanu.** Thank you very much for your hard work during the internship! I wish all of you have a very bright future.

I would like to thank **Floor Peters, Jojanneke** and **Jos**, who helped me a lot when I just came into the lab. **Erhard** and **Malta**, thanks for your help in the lab.

I also want to thank our collaborators, **Ron Fouchier**, **James Paulson**, **Ryan McBride**, **Corwin Nycholat**, **Geert Jan Boons**, **Jack Li**, **Helene Verheije** and **Kim Bouwman**, who provided us a great deal of good data, performed excellent experiments, and offered us very useful materials.

Erion and **Maryam**, my graceful and elegant paranymphs, thank you very much for supporting me during the defense and helping me organize the reception and party. **Erion**, you are a beautiful princess in the lab. Your home-made Korean food is amazing. Thank you for your kindness and sharing; I enjoyed every talk we had. **Maryam,** I was so lucky to become your officemate. Thank you for all the experience and knowledge you shared with me, which helped me a lot live in the Netherlands.

Nancy and **Arno,** thanks a lot for your help! Without your quick and kind response to the ordering and your technical support, my work in the lab would have been less efficient.

I would like to thank all my officemates, **Qiushi, Huihui, Floor, Maryam, Chunhua** and **Wenjuan** for all the happy and funny hours we had together. **Qiushi,** thank you very much for sharing with me several useful information. **Chunhua,** I am grateful for all the encouraging and inspiring conversations we had.

Huihui, we spent most of unforgettable time in and outside the lab. You are like an angel to me. I remembered clearly the first day I came to the Netherlands. You cooked for me and showed me how to do grocery shopping here. Thank you for all the experience and knowledge you shared with me, which helped me a lot to start and continue my work and life and helped me to get through my darkest time in the Netherlands. All my best wishes for you!

I would like to thank **Wentao**, **Yifei**, **Shan** and **Chunyan**, my sweet Chinese colleagues. **Wentao,** you are like a big brother for us. You work hard and dedicate to your research. I wish you achieve your career goal successfully. **Yifei**, you are a very talented person and you are highly motivated for your research. I wish you successfully get your PhD with very high impact publications. **Shan** and **Chunyan,** you are very kind and sweet girls. I had lots of fun talking to you. I wish you have a happy life during your stay in the Netherlands.

I would also like to thank our lunch/movie group members, **Brenda**, **Esther**, **Erion**, **Fiona**, **Floor**, **Huib**, **Linda**, **Lisa** and **Maryam, Malta**. It will be always my good memory of sharing

French Fries and different culture. It was very joyful time for me to see movies together with all of you. Thank you, **Floor** and **Linda,** for organizing the Sinterklaas party. It was a very special moment. Thank you, **Sinterklaas**, I really like the gifts you gave to me.

My colleagues from virology division, it was great to work together with you, sharing ideas and helping each other. I would like to thank my PhD fellows, **Christine, Cristina, Erion, Huib, Jim, Linda, Lisa, Lucian, Mark, Qian, Qiushi,** and **Ruben**, and my post-docs fellows, **Esther, Fiona, Hendrik, Hilde, Ivy, Jeroen, Martijn, Matthijn and Rachel.** My tenichician fellows

Anja and **Clasien,** thank you for helping me and giving me advices. **Rosita** and **Mariella,** thank you for arranging my VISA application and my accommodation.

The four years life in the Netherlands will have never been so colorful and exciting without my dearest friends. Thanks for bringing me so many joyful moments and wonderful experience. **Jiefei**, I was so lucky to meet you and Huihui in the Netherlands. I admire your attitude towards life. I enjoyed your "black" Chinese-Western combined cooking recipe. I enjoyed the journey we went to Italy together. I enjoyed the movie and dinner time. I wish you have a very happy life. **Xiaoyan,** it was the destiny to meet you on the way to the Uithof. You were my traveling companion every day. We shared our daily life, experience and thoughts. You brought me enormous amount of positive energy. Thank you, **Xiaoyan** and **Jiakun**, for your support all the time. I wish you have a perfect life and future. **Fenghua**, my dear fitness companion, thank you for all the support and encouragement. We achieved a lot during the last two years. I wish we can continue doing exercise in that way and keep ourselves fit forever.

I want to sincerely thank the **Chinese scholarship council (CSC)**, who financially supported me and provided me with such a great chance to study abroad for four years. 我要向中国留学基金委（CSC）以及中国驻荷兰大使馆教育处致以诚挚的感谢，感谢对我在荷兰学习期间的资助和帮助。

在此，我要感谢在荷兰的朋友们，谢谢你们给了我精神鼓励和支持。**戴美玲**，**刘晓晨**，**张浩**，**杨欣**，**刘芳**，**娄博**和**王朝文**，感谢你们让我刚到荷兰就有到了家的感觉；**李文涛**师兄，**张渭东**师兄，**郎一飞**，**李泽世**，**杜文娟**，**赵珊**，**王春燕**，**李春华**老师，**余瑞松**老师和**罗锐**老师，谢谢你们在工作上的帮助和生活中的支持。

To my friends who I met in Rotterdam, **Yijin**, **Xinying**, **Wanlu**, **Xulei**, **Yuebang**, **Wenhui**, **Yingying** & **Zhanmin**, **Guoying** & **Ying**, **Li Shan**, **Li Meng**, **Buyun**, **Xiaonan & Changbo**, **Ruoyu**, **Danli**, **Gao Wen**, **Gao Ya**, **Wen Bei** & **Liu Fan**, **Liqin** & **Haobo**, **Ping Zhen**, **Xiaolei**,

Changbin, **Wu Bin**, **Huang Ling & Tongwei**, **Kuikui**, **Guannan**, **Yu Xue** *et al*. Wish you all the best!

感谢我的硕士导师，**刘胜旺**研究员，谢谢您在硕士研究期间对我的指导和关心，感谢您对我出国求学的支持和鼓励。感谢**韩宗玺**老师，**邵昱昊**老师以及**各位老师们**和**师兄师姐师弟师妹们**对我的照顾和鼓励。感谢山东农业大学**刘思当**教授对我的关心和支持。

感谢我的父母和公公婆婆，是您们的关心和支持让我一直追求着自己的梦想走下去。感谢所有在国内的亲戚和朋友们对我的鼓励和关心。

Last but not least, to my beloved husband, **Wenshi**, thank you for your enormous love and support. You are the one who is always supporting and encouraging me. Thank you for taking really good care of me. All the best wishes for our bright future!

Curriculum Vitae

Hongbo Guo was born on February 02, 1988, in Qingdao, Shandong Province, China. She grew up and attended primary, middle and high school in her hometown. In 2006, she moved to Tai'an in western Shandong Province to start her Bachelor study in Veterinary medicine at Shandong Agricultural University. In 2010, she started her master study at Graduate School of Chinese Academy of Agricultural Science (CAAS), Beijing, China. One year later, she formally started her master research training at Harbin Veterinary Research Institute, CAAS. Under the supervision of Prof. dr. Shengwang Liu, she finished her thesis book, entitled "Isolation, characterization and biology property analysis of Pigeon Paramyxovirus-1 Viruses (PPMV-1s)". In 2013, with the support of China Scholarship Council, she got an opportunity to start her Ph.D. study at the department of Infectious diseases and Immunology, Utrecht Univerisity, the Netherlands. Under the supervision of Prof. dr. Frank van Kuppeveld, Dr. Xander de Haan and Dr. Erik de Vries, she focused on dynamics and Specificity of Influenza A Virus-Receptor Interactions.

List of Publications

1. J.Baggen, D.L.Hurdiss, G.Zocher, N.Mistry, R.W.Roberts, J. J.Slager, **H.Guo**, A.L.W.van Vliet, M.Wahedi, K.Benschop, E.Duizer, C.A.M.de Haan, E.de Vries, J.M.Casasnovas, R.J.de Groot, N.Arnberg, T.Stehle, N.A.Ranson, H.J.Thibaut and F.J.M.van Kuppeveld. Role of enhanced receptor engagement in the evolution of a pandemic acute hemorrhagic conjunctivitis virus. Proceedings of the National Academy of Sciences of the United States of America 115 (2), 397 (2018)

2. W.Zhang, M.van Eijk, **H.Guo**, A.van Dijk, O.B.Bleijerveld, M.H.Verheije, G.Wang, H.P.Haagsman and E.J.Veldhuizen. Expression and characterization of recombinant chicken mannose binding lectin. Immunobiology 222 (3), 518 (2017)

3. C.Li, W.Li, E.Lucio de Esesarte, **H.Guo**, P.van den Elzen, E.Aarts, E.van den Born, P.J.M.Rottier and B.J.Bosch. Cell attachment domains of the PEDV spike protein are key targets of neutralizing antibodies. Journal of virology 91 (12), (2017)

4. **H.Guo***, E.de Vries*, R.McBride, J.Dekkers, W.Peng, K.M.Bouwman, C.Nycholat, M.H.Verheije, J.C.Paulson, F.J.M.van Kuppeveld and C.A.M.de Haan. Highly Pathogenic Influenza A(H5Nx) Viruses with Altered H5 Receptor-Binding Specificity. Emerging infectious diseases 23 (2), 220 (2017) (*co-1st author)

5. M.Dai, **H.Guo**, J.C.Dortmans, J.Dekkers, J.Nordholm, R.Daniels, F.J.M.van Kuppeveld, E.de Vries and C.A.M.de Haan. Identification of Residues That Affect Oligomerization and/or Enzymatic Activity of Influenza Virus H5N1 Neuraminidase Proteins. Journal of virology 90 (20), 9457 (2016)

6. J.Baggen, H.J.Thibaut, J.Staring, L.T.Jae, Y.Liu, **H.Guo**, J.J.Slager, J.W.de Bruin, A.L.van Vliet, V.A.Blomen, P.Overduin, J.Sheng, C.A.M.de Haan, E.de Vries, A.Meijer, M.G.Rossmann, T.R.Brummelkamp and F.J.M.van Kuppeveld. Enterovirus D68 receptor requirements unveiled by haploid genetics. Proceedings of the National Academy of Sciences of the United States of America 113 (5), 1399 (2016)

7. E.de Vries, **H.Guo***, M.Dai*, P.J.Rottier, F.J.M.van Kuppeveld and C.A.M.de Haan. Rapid Emergence of Highly Pathogenic Avian Influenza Subtypes from a Subtype H5N1 Hemagglutinin Variant. Emerging infectious diseases 21 (5), 842 (2015) (*co-2nd author)

8. S.Liu, Q.Xu, Z.Han, X.Liu, H.Li, **H.Guo**, N.Sun, Y.Shao and X.Kong. Origin and characteristics of the recombinant novel avian infectious bronchitis coronavirus isolate ck/CH/LJL/111054. Infection, genetics and evolution. 23, 189 (2014)

9. **H.Guo**, X.Liu, Y.Xu, Z.Han, Y.Shao, X.Kong and S.Liu. A comparative study of pigeons and chickens experimentally infected with PPMV-1 to determine antigenic relationships between PPMV-1 and NDV strains. Veterinary microbiology 168 (1), 88 (2014)

10. X.Liu, H.Ma, Q.Xu, N.Sun, Z.Han, C.Sun, **H.Guo**, Y.Shao, X.Kong and S.Liu, Characterization of a recombinant coronavirus infectious bronchitis virus with distinct S1 subunits of spike and nucleocapsid genes and a 3' untranslated region. Veterinary microbiology 162 (2-4), 429 (2013)

11. **H.Guo**, X.Liu, Z.Han, Y.Shao, J.Chen, S.Zhao, X.Kong and S.Liu. Phylogenetic analysis and comparison of eight strains of pigeon paramyxovirus type 1 (PPMV-1) isolated in China between 2010 and 2012. Archives of virology 158 (6), 1121 (2013)

12. H.Ma, Y.Shao, C.Sun, Z.Han, X.Liu, **H.Guo**, X.Liu, X.Kong and S.Liu. Genetic diversity of avian infectious bronchitis coronavirus in recent years in China. Avian diseases 56 (1), 15 (2012)

Manuscripts in Preparation

13. **H.Guo**, H.Rabouw, A.Slomp, M.Dai, F.van der Vegt, R.McBride, J.C.Paulson, R.J.de Groot, F.J.van Kuppeveld, E.de Vries*, C.A.M.de Haan*. Dissecting the complexity of influenza A virus binding kinetics by biolayer interferometry allows assessment of HA/NA balance, the contribution of NA to virus binding and virus rolling over surfaces.

14. **H.Guo**, W.Du, F.van der Vegt, J.Li, G.J.Boons, F.J.Mvan Kuppeveld, E.de Vries*, C.A.M.de Haan*. Novel aspects of the dynamics of influenza A virus interaction revealed by biolayer interferometry.

15. **H.Guo***, W.Du*, F.van der Vegt, J.Li, G.J.Boons, F.J.M.van Kuppeveld, R. Fouchier, E.de Vries, C.A.M.de Haan. Human H3N2 influenza A viruses of consecutive antigenic clusters maintain similar receptor binding properties by the combined effects of individual amino acid substitutions. (*co-1st author)